

AFFDL-TR-78-206
VOLUME I

FASTENER HOLE QUALITY

Structures Design Department
General Dynamics Fort Worth Division
Fort Worth, Texas 76101

December 1978

Technical Report AFFDL-TR-78-206, Volume I
Final Report June 1976 - October 1978

Approved for Public Release; Distribution Unlimited

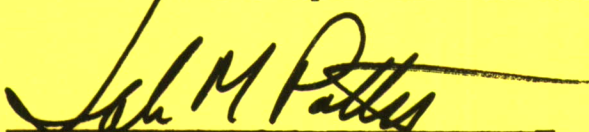
AIR FORCE FLIGHT DYNAMICS LABORATORY
AIR FORCE WRIGHT AERONAUTICAL LABORATORIES
AIR FORCE SYSTEMS COMMAND
WRIGHT-PATTERSON AIR FORCE BASE, OHIO 45433

NOTICE

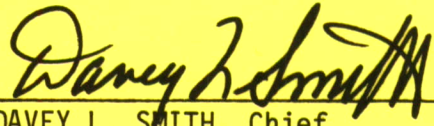
When Government drawings, specifications, or other data are used for any purpose other than in connection with a definitely related Government procurement operation, the United States Government thereby incurs no responsibility nor any obligation whatsoever; and the fact that the government may have formulated, furnished, or in any way supplied the said drawings, specifications, or other data, is not to be regarded by implication or otherwise as in any manner licensing the holder or any other person or corporation, or conveying any rights or permission to manufacture, use, or sell any patented invention that may in any way be related thereto.

This report has been reviewed by the Information Office (OI) and is releasable to the National Technical Information Service (NTIS). At NTIS, it will be available to the general public, including foreign nations.

This technical report has been reviewed and is approved for publication.

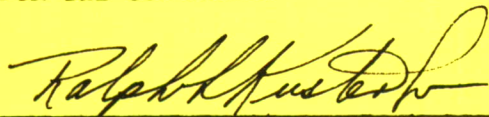


JOHN M. POTTER
Project Engineer
Fatigue, Fracture & Reliability Gp
Structural Integrity Branch



DAVEY L. SMITH, Chief
Structural Integrity Branch
Structures & Dynamics Division

FOR THE COMMANDER



RALPH L. KUSTER, JR., Colonel, USAF
Chief, Structures & Dynamics Division

"If your address has changed, if you wish to be removed from our mailing list, or if the addressee is no longer employed by your organization please notify AFFDL/FBE, W-PAFB, OH 45433 to help us maintain a current mailing list".

Copies of this report should not be returned unless return is required by security considerations, contractual obligations, or notice on a specific document.

Unclassified

SECURITY CLASSIFICATION OF THIS PAGE (When Data Entered)

REPORT DOCUMENTATION PAGE		READ INSTRUCTIONS BEFORE COMPLETING FORM
1. REPORT NUMBER AFFDL-TR-78-206, Vol. I	2. GOVT ACCESSION NO.	3. RECIPIENT'S CATALOG NUMBER
4. TITLE (and Subtitle) FASTENER HOLE QUALITY		5. TYPE OF REPORT & PERIOD COVERED Final Technical Report June 1976 - October 1978
		6. PERFORMING ORG. REPORT NUMBER FZM 6809
7. AUTHOR(s) P.J. Noronha, S.P. Henslee, D.E. Gordon, Z.R. Wolanski, and B.G.W. Yee		8. CONTRACT OR GRANT NUMBER(s) F33615-76-C-3113
9. PERFORMING ORGANIZATION NAME AND ADDRESS General Dynamics Corporation Fort Worth Division Fort Worth, Texas 76101		10. PROGRAM ELEMENT, PROJECT, TASK AREA & WORK UNIT NUMBERS 486U0223
11. CONTROLLING OFFICE NAME AND ADDRESS Air Force Flight Dynamics Laboratory (FB) Air Force Wright Aeronautical Laboratories Wright-Patterson Air Force Base, Ohio 45433		12. REPORT DATE December 8, 1978
		13. NUMBER OF PAGES 165
14. MONITORING AGENCY NAME & ADDRESS (if different from Controlling Office)		15. SECURITY CLASS. (of this report) Unclassified
		15a. DECLASSIFICATION/DOWNGRADING SCHEDULE
16. DISTRIBUTION STATEMENT (of this Report) Approved for public release; distribution unlimited.		
17. DISTRIBUTION STATEMENT (of the abstract entered in Block 20, if different from Report)		
18. SUPPLEMENTARY NOTES		
19. KEY WORDS (Continue on reverse side if necessary and identify by block number) Equivalent initial flaw size, fastener hole quality, clearance fit, transition fit, F-16 randomized spectrum, B-1 spectrum, axial scratch mismatch, localized yielding, improved drilling, improved assembly.		
20. ABSTRACT (Continue on reverse side if necessary and identify by block number) This report describes the development of the equivalent initial flaw size concept as a potential design tool and the generation of equivalent initial flaw size data as a function of several manufacturing and design variables. Several factors or mechanisms that strongly affected the fatigue behavior of fastener holes have been identified and corrected to achieve a 100% improvement in fatigue life. Some of these improvements are being implemented in the F-16 production program and the improved drilling will be implemented in the C5A-H Mod. Program.		

FOREWORD

This final technical report covers all the work performed under Air Force Contract F33615-76-C-3113 entitled "Fastener Hole Quality". The work was performed during the period from June 1976 to October 1978. This project was accomplished under the technical direction of Mr. John M. Potter of the Fatigue, Fracture and Reliability Group, Structural Integrity Branch, Structures Division, Air Force Flight Dynamics Laboratory, Wright-Patterson Air Force Base, Ohio. This program has as its overall objective to establish and determine the equivalent initial flaw size (EIFS) in fastener holes to support USAF Damage Tolerance and Durability Requirements as stated in MIL-A-83444 and MIL-A-008866 (B), respectively, and to establish the criteria for fastener hole quality with respect to structural performance.

This program was performed in the Materials Research Laboratory, Materials Technology Section, Structures and Design Department of the Fort Worth Division, General Dynamics Corporation. The program was managed by Dr. P. J. Noronha with valuable participation and technical support by Mr. S. P. Henslee, Mr. D. E. Gordon, and Dr. J. C. Couchman of Materials Research Laboratory; Mr. Z. R. Wolanski and W. S. Margolis of Metallurgical Laboratory; Mr. L. J. Backof of Manufacturing Technology and Support; Mr. G. Hales of the Fracture and Fatigue Group; and Mr. G. R. Arnett of Central Data System Center. This program was under the overall supervision of Dr. B. G. W. Yee as management focal point interface.

This final program report was submitted by the authors on November 6, 1978.

TABLE OF CONTENTS

<u>SECTION</u>	<u>PAGE</u>
I INTRODUCTION	1
II PROGRAM OBJECTIVES AND TECHNICAL APPROACH	3
2.1 Material Selection and Specimen Fabrication	5
2.2 Nondestructive Inspection	9
2.3 Specimen Testing/Load Histories/Test Plan	9
2.4 Fractography	10
2.5 Crack Growth Analysis	10
2.6 Equivalent Initial Flaw Size Concept	10
III TASK I NO-LOAD TRANSFER RESULTS	16
3.1 Fighter Spectrum	16
3.1.1 Clearance-Fit Fastener Holes	16
3.1.2 Transition-Fit Fastener Holes	21
3.2 Bomber Spectrum	21
3.2.1 Clearance-Fit Fastener Holes	21
3.2.2 Transition-Fit Fastener Holes	29
3.2.3 Comparison of Hole Classes	29
3.3 NDE Results	29
3.3.1 Eddy Current	29
3.3.2 Dial Bore Gauge	39
3.3.3 Rotary Proficorder	39
3.3.4 Linear Proficorder	39
3.3.5 Ultrasonics	53
3.4 SEM Investigation	53
3.5 Improved Drilling	60
3.6 Comparison of Results	60
IV Task II LOW-LOAD TRANSFER RESULTS	72
4.1 Fighter Spectrum	72
4.2 Bomber Spectrum	72
4.3 NDE	77
4.3.1 Eddy Current	77
4.3.2 Rotary Attachment to Proficorder Plus Dial Bore Gauge	80

TABLE OF CONTENTS (CONTINUED)

<u>SECTION</u>	<u>PAGE</u>
4.4 SEM Analysis	84
4.5 Comparison of Results	90
V TASK III FASTENER HOLE QUALITY IMPROVEMENTS	92
5.1 Definition & Identification of Hole Quality	92
5.2 Low-Load Transfer Results	94
5.2.1 Fighter Spectrum Results	97
5.2.2 Bomber Spectrum Results	97
5.2.3 Improved Drilling and Assembly	97
5.2.4 Comparison of Results	107
VI TASK IV EXTENSION TO STEEL AND TITANIUM	108
6.1 Steel	108
6.2 Titanium	110
VII TASK V EXTENSION TO COLD-WORKED AND TAPER-LOK HOLES	117
7.1 Cold-Worked Holes	117
7.2 Taper-Lok Holes	122
VIII CONCLUSIONS AND OBSERVATIONS	125
IX RECOMMENDATIONS	130
APPENDIX A-NDE TECHNIQUES	131
APPENDIX B-EQUIVALENT INITIAL FLAW SIZE CONCEPT	145
REFERENCES	152

LIST OF FIGURES

<u>Figure</u>		<u>Page</u>
2-1	Flow Chart Showing Technical Approach	4
2-2	No-Load Transfer Specimen Geometry	6
2-3	Low-Load Transfer Specimen Geometry	7
2-4	Winslow Spacematic Drilling Equipment	8
2-5	Schematic Showing Fatigue Lives of Two Fastener Holes Having Different EIFS	12
2-6	Crack Growth Curves for Properly Drilled and Reamed Fastener Holes	14
2-7	Selection of a Single Analytical Curve for a Sample of Fractographic Crack Growth Histories	15
3-1	EIFS for Drilled and Drilled and Reamed Holes	19
3-2	Crack Depth at One Life for Drilled and Drilled and Reamed Holes	20
3-3	EIFS for Improperly and Properly Drilled Holes	22
3-4	Crack Depth at One Life for Properly and Improperly Drilled Holes	23
3-5	EIFS Distributions for Properly and Improperly Drilled and Reamed Holes	24
3-6	Crack Depth at One Life for Properly and Improperly Drilled and Reamed Holes	25
3-7	EIFS Distributions for Fighter and Bomber Load Histories	26

LIST OF FIGURES (CONT'D)

<u>Figure</u>		<u>Page</u>
3-8	EIFS for Properly and Improperly Drilled Holes	27
3-9	Crack Depth at One Life for Properly and Improperly Drilled Holes	28
3-10	EIFS Distributions for Properly and Improperly Drilled and Reamed Holes	30
3-11	Crack Depth at One Life for Properly and Improperly Drilled and Reamed Holes	31
3-12	Crack Depth at One Life for Drilled and Drilled and Reamed Holes	32
3-13	Crack Depth at Two Lives for Drilled and Drilled and Reamed Holes	33
3-14	Eddy Current Signal Amplitude Versus EIFS	34
3-15	Maximum Eddy Current Amplitude Versus EIFS, Drilled and Reamed Holes	35
3-16	Maximum Eddy Current Amplitude Versus EIFS, Improperly Drilled and Drilled and Reamed Holes	36
3-17	Correlation of Eddy Current Inspection to EIFS	37
3-18	Correlation of Inspection to Hole Quality (large EIFS)	38
3-19	Effect of Hole Out-of-Roundness on the Eddy Current Amplitude	41
3-20	Eddy Current Amplitude as a Function of Out-of-Roundness Measured with a Dial Bore Gage	42
3-21	Effect of Surface Roughness in Fastener Holes on the Eddy Current Signal	43
3-22	Dimensional Tolerance Parameter Versus EIFS for Drilled Holes, Fighter Load History	44

LIST OF FIGURES (CONT'D)

<u>Figure</u>		<u>Page</u>
3-23	Dimensional Tolerance Parameter Versus EIFS for Drilled and Reamed Holes, Fighter Load History	45
3-24	Dimensional Tolerance Parameter Versus EIFS for Drilled Holes, Bomber Load History	46
3-25	Dimensional Tolerance Parameter Versus EIFS for Drilled and Reamed Holes, Bomber Load History	47
3-26	Final Depth Crack Vs. Average Hole Diameter for Holes Drilled by Winslow Technique.	48
3-27	Typical Properties of Conventional and Improved Drilling	49
3-28	Linear Proficorder Scans Showing Total Surface Profile for Two Quackenbush Properly Drilled Holes	50
3-29	Linear Proficorder Scans Showing Total Surface Profile for Two Winslow Improperly Drilled Holes	51
3-30	Surface Roughness as a Function of Crack Depth	52
3-31	Eddy Current and Linear Proficorder Trace (Specimen QPF-10; Wide Groove at the 3:00 orientation)	54
3-32	Reflected Ultrasonic Signal Amplitude Versus EIFS	55
3-33	Reflected Ultrasonic Waveforms Showing the Effect of a Double-Drilled Hole on the Reflected Waveform	56
3-34	Morphology of a Scratch - Properly Drilled Fastener Hole (Large EIFS)	57
3-35	Fatigue Crack Initiating from a Scratch in a Drilled and Reamed Fastener Hole	58

LIST OF FIGURES (CONT'D)

<u>Figure</u>		<u>Page</u>
3-36	Morphology of a Crack Initiating from a Point Source, Improved Drilling Fastener Hole (Small EIFS)	59
3-37	EIFS for Conventionally Drilled and Improved Drilled Holes	61
3-38	Crack Depth at One Life for Conventionally and Improved Drilled Holes	62
3-39	Crack Depth at 1.5 Lives	63
3-40	Behavior of Fatigue Crack Initiating at Point Source	66
3-41	Crack Front Morphology Due to Point Source Initiation	67
3-42	Behavior of Fatigue Crack Initiating from a Scratch	68
3-43	Initiation of a Line Source Yielding a Single Plane Crack	69
4-1	Cumulative Probability of EIFS for Drilled and Reamed Fastener Holes	73
4-2	Cumulative Probability of Fatigue Crack Depths at One Life	74
4-3	Effect of Hole Fabrication Process on EIFS Distributions	75
4-4	Cumulative Probabilities of Fatigue Crack Depths at One Life	76
4-5	Effect of Stress Level on EIFS Distribution	78
4-6	Effect of Stress Level on Crack Size Distribution	79

LIST OF FIGURES (CONT'D)

<u>Figure</u>		<u>Page</u>
4-7	Resolution of 0.025-inch-Deep Fatigue Crack	81
4-8	Sensitivity of Eddy Current to Surface Defects	82
4-9	Typical Eddy Current Scans of Conventional and Improved Drilling Fastener Holes	83
4-10	Comparison of Roundness for Conventional and Improved Drilling	85
4-11	Polar Plots Showing (a) a scratch 2.25 mils deep x 8.0 mils wide and (b) a scratch .9 mils deep	86
4-12	Maximum Diameter Versus EIFS	87
4-13	SEM Micrograph Showing Fatigue Crack Initiation from Faying Surface Near Fastener Hole for a Transition-Fit Hole (100X)	88
4-14	SEM Micrograph Showing "Near Corner" Crack Initiation at Faying Surface for a Transition-Fit Hole (43x)	89
5-1	Effect of Flaw Shape Size on EIFS	94
5-2	Coalescence of Multiple Cracks to Form a Single Large Crack	95
5-3	EIFS for Properly and Improperly Drilled 15%-Load Transfer Specimens	98
5-4	EIFS Distributions for Conventional and Improved Drilling Fighter Load History, and 15%-Load Transfer	99
5-5	Effect of Hole Fabrication Process on EIFS Distributions	100
5-6	Cumulative Probabilities of Fatigue Crack Depths at One Life	101

LIST OF FIGURES (CONT'D)

<u>Figure</u>		<u>Page</u>
5-7	Cumulative Probabilities Showing Fatigue Enhancement of Fastener Holes	103
5-8	Cumulative Probabilities for Fatigue Crack Depths at One Life Showing Durability of Each Process	104
5-9	Effect of Max. Fighter Spectrum Stress Level on EIFS Distribution for Improved Drilling of Load Transfer Specimens	105
5-10	Effect of Maximum Spectrum Stress on EIFS Distribution	106
6-1	No-Load Transfer Specimen for Task IV Material AF 1410 Steel	109
6-2	EIFS for Drilled and Reamed No-Load Steel Specimens	112
6-3	No-Load Transfer Specimen for Task IV	113
6-4	EIFS for Drilled and Reamed Titanium Specimens	116
7-1	Final Crack Length Vs. Permanent Deformation for Cold-Worked Holes	119
7-2	Final Crack Depth Vs. Permanent Deformation for Cold-Worked Holes	120
7-3	Crack Growth as a Function of Fatigue Cycling in No-Load Transfer Cold-Worked Holes	123
8-1	Ninety Percentile Crack Growth Behavior for Conventionally Drilled and Reamed, Conventionally Drilled and Improved Drilling of Fastener Holes	128
8-2	Ninety Percentile Crack Growth Behavior for Conventional Drilling and Assembly and Improved Drilling and Assembly	129

LIST OF TABLES

<u>Table</u>	<u>Page</u>
2-1 Crack Growth Analysis Variables	11
3-1 Summary of Test Conditions	17
3-2 Depth of Largest Flaws from Polar Plots for No-Load Transfer Drilled Specimens	40
3-3 Cumulative Probability Results for Task I No-Load Transfer, Fighter Spectrum	64
3-4 Cumulative Probability Results for Task I No-Load Transfer, Bomber Spectrum	71
4-1 Summary of Results	91
6-1 Final Crack Depths for AF 1410 Steel No-Load Transfer Specimens (Fighter Load Sequence)	111
6-2 Final Crack Depths for Ti 6Al-4V No-Load Transfer Specimens (Baseline Stress = 82.5 KSI)	114
6-3 EIFS and Hole Diameters for Ti 6Al-4V No-Load Transfer Specimens	115
7-1 Final Crack Sizes for Cole-Worked Holes	118
7-2 Results of Residual Stress Measurements	121
7-3 Primary Crack After Two Lives for 7475-T7351 Al Taper-Lok No-Load Transfer Specimen, Baseline Stress + 45 KSI, Fighter Spectrum	124

SECTION I

INTRODUCTION

Fastener holes are regions of high stress concentration and provide the primary locations for initiation and growth of fatigue cracks in metallic aircraft structures (Reference 1). This phenomenon is largely responsible for limiting the durability and economic life of such structures. Durability design procedures incorporating fracture mechanic analysis methodologies to account for the effect of fatigue cracks appear in literature (Reference 2).

The fatigue behavior of a sample of supposedly identical fastener holes is extremely variable, indicating that material, manufacturing, and assembly quality influence the initiation and growth of cracks. Only recently have investigations into the effects of manufacturing parameters on fatigue life of fastener holes been pursued. Koster et al. (Reference 3) investigated tapered fastener systems; Moore (Reference 4) reported on straight-shank and interference-fit fastened joints. The majority of previous studies were done using nonproduction equipment to prepare the specimens and fastener holes. This program is a comprehensive investigation of the effect of manufacturing and assembly procedures employed in aircraft production on the fatigue behavior of fastener holes.

The program initially consisted of five separate tasks. In Task I, the influence of manufacturing quality on the fatigue behavior of straight-shank drilled and drilled and reamed holes in aluminum was investigated for a no-load transfer condition. Task II extended the investigation of fatigue behavior dependence on manufacturing and assembly procedures to the low-load transfer condition. The objective of Task III was to improve the life of low-load transfer specimens by elimination of the most detrimental fatigue mechanisms established in Tasks I and II. The first three tasks comprise a comprehensive investigation of the straight-shank-fastened joints typical of aluminum air frame structure.

A limited investigation of interference systems, i.e., cold-worked and taper-lok holes in aluminum, was performed in Task IV. The fatigue behavior of straight-shank fastener holes in high-strength steel and titanium was analysed in Task V.

"Production hole quality", a term encompassing all manufacturing and assembly parameters affecting fatigue behavior, was correlated to the life of fastener holes using the Equivalent Initial Flaw Size Concept (EIFS) defined in MIL-A-83444. As a result of the extensive data base accumulated during the course of this program, substantial improvements in the EIFS analytical methodologies were realized. Appendix B contains a comprehensive description of the EIFS concept, its application to the evaluation of hole quality. It also describes how the EIFS approach may be applied to the initial design of fastener holes to ensure on a quantitative basis a durable airframe structure.

SECTION II

PROGRAM OBJECTIVES AND TECHNICAL APPROACH

The primary objective of this program was to establish the cause of variation in fatigue life of metallic structure containing fastener holes and to provide methods for controlling the life of individual fastener holes during their manufacture. In order to provide a quantitative basis for correlation of the fatigue life to the manufactured quality, a fracture mechanics approach for life prediction was employed.

The technical approach selected for this program is shown in Figure 2-1. Fastener holes were fabricated in coupon test specimens by use of hand-held automatic processes and tooling representative of that used in actual production. These fastener holes were then totally characterized by five state-of-the-art nondestructive inspection (NDI) techniques. Following this surface/dimensional characterization, straight-shank, protruding-head fasteners were installed and the coupons were fatigue tested. Realistic crack growth data was ensured through fatigue testing with an F-16 or a bomber load history.

Upon completion of coupon fatigue testing, the crack growth behavior, i.e., crack growth curves, was established for each fatigue crack. These crack growth curves were analytically back-tracked to establish the equivalent initial flaw size (EIFS), a fictitious size of a flaw existing at the time of manufacture within the fastener hole. These flaws ideally grow from the application of the first load and follow the analytical crack growth curve.

The EIFS and NDI results, having been established for each specimen tested, were compared. Correlations were to provide an inspection-based means by which the EIFS could be monitored during manufacture. This objective was revised so the fatigue life of structure containing holes could be extended through procedural control of hole production techniques. EIFS distributions were obtained for the various processes, allowing relative evaluation of those processes to be performed accurately or with a minimum amount of effort.

Those processes found to produce the best hole quality, i.e., the longest fatigue lives, were introduced and implemented in production. At this time these changes are producing manufactured fastener holes at no increase in cost with a substantial increase in the durability of aluminum aircraft structure.

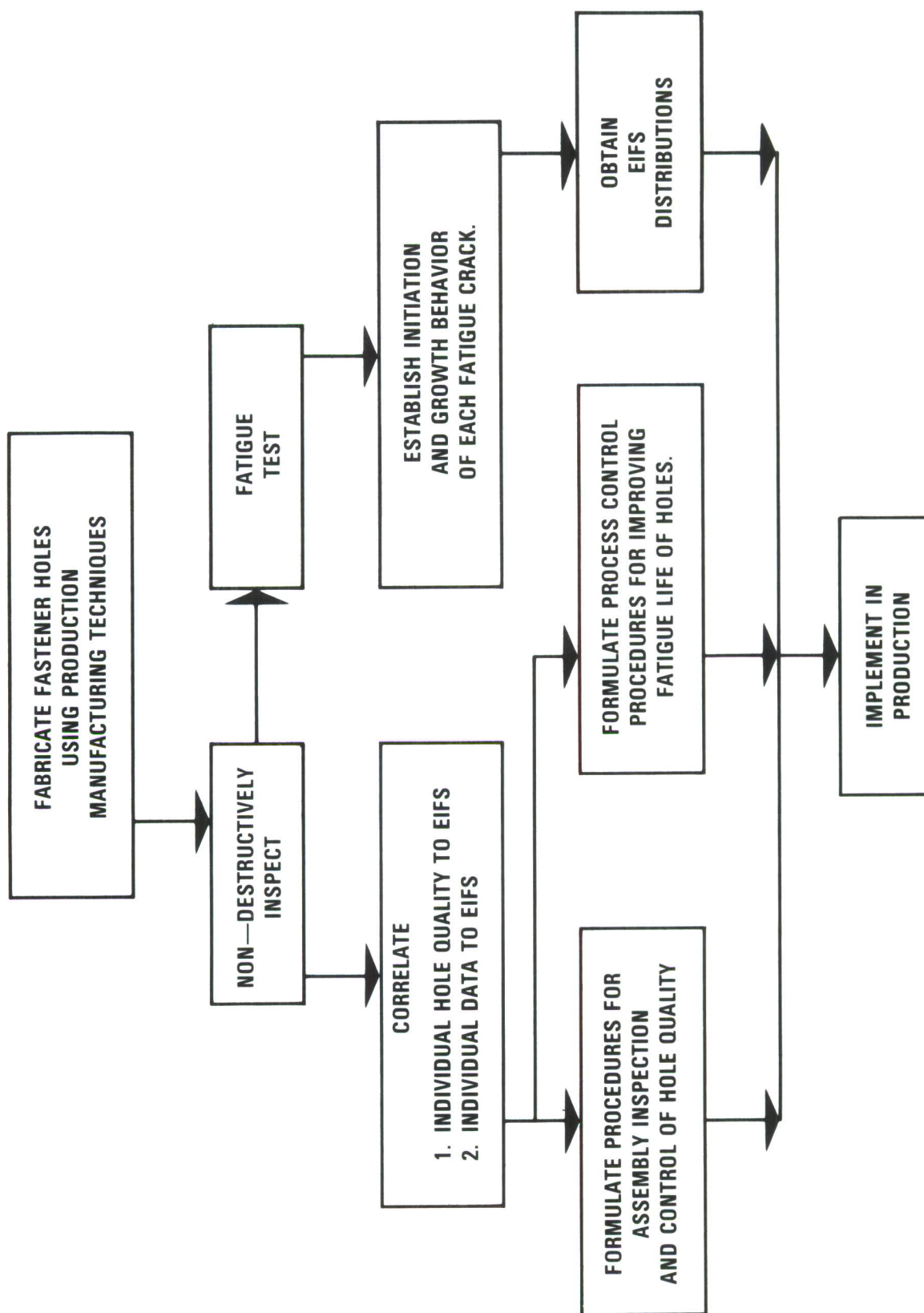


Figure 2-1 Flow Chart Showing Technical Approach

2.1 MATERIAL SELECTION AND SPECIMEN FABRICATION

The material selected for Tasks I, II and III was 7475-T7351 aluminum. This alloy is extensively used in fracture and durability critical areas of the F-16, such as the lower wing skins. Coupon specimens were fabricated from three lots of production stock. Mechanical properties were obtained for each lot to assure that F-16 production specifications were equalled or exceeded.

Specimens were designed for two conditions: no-load transfer, (Task I) and low-load transfer (Tasks II and III). The no-load transfer specimens, Figure 2-2, are a standard dog-bone configuration with a reduced mid-section and constant width and thickness in the gage areas. Single fastener holes were drilled in these specimens and filled with straight-shank, protruding-head NAS 6204-7 fasteners. These fasteners were used throughout the program. Both nut and head ends of the fasteners received steel washers.

The low-load transfer specimens, Figure 2-3, were designed to achieve 15% load transfer. This level of load transfer and design approach is representative of the F-16 lower wing skin. The reversed double dog-bone geometry closely follows MIL-STD-1312 standard load-transfer specimens. Both fastener holes in this specimen geometry were nominally a 0.250-in. diameter, as were those in no-load transfer specimen.

Two hole-manufacturing methods were employed to produce the fastener holes in Tasks I and II. Both hole preparation techniques were hand-held automatic equipment producing different classes of holes. Clearance fit holes of 0.250-in. - 0.253-in. diameter were produced by use of the Winslow Spacematic Model HS-1, Figure 2-4. The Spacematic is pneumatically driven with pneumatic over hydraulic pressure for feed rate control and retraction. This is a single-step drilling process.

Transition fit holes of 0.2500-in. - 0.2507-in. diameter were produced by a two-step drill and ream process using the Quackenbush QDA-100. This unit is pneumatically powered with feed rate mechanically controlled. Both Spacematic and Quackenbush units require tooling to accurately control hole location. The tooling used in this study was representative of that used on the F-16 production line, as well as those operators of the drilling equipment.

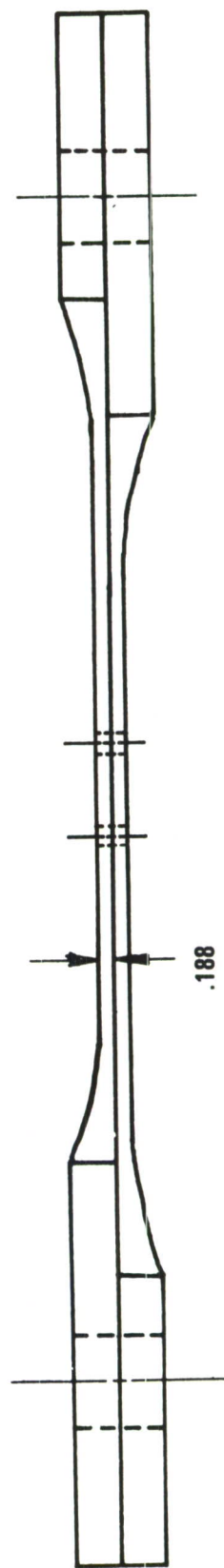
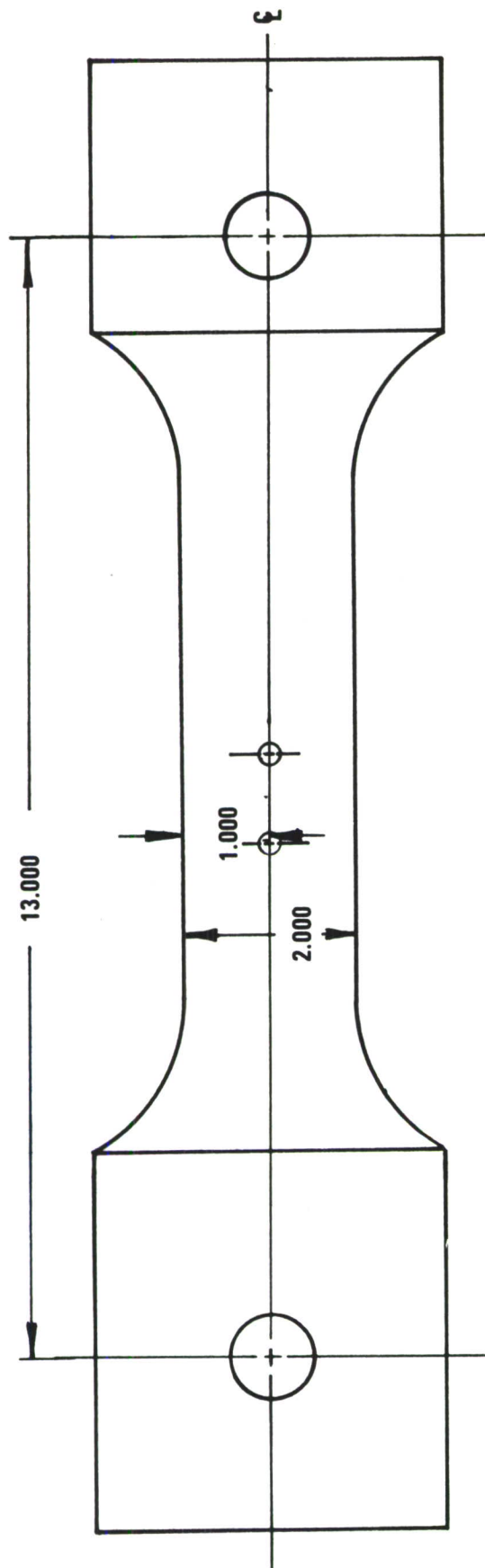


Figure 2-3 Low-Load Transfer Specimen Geometry

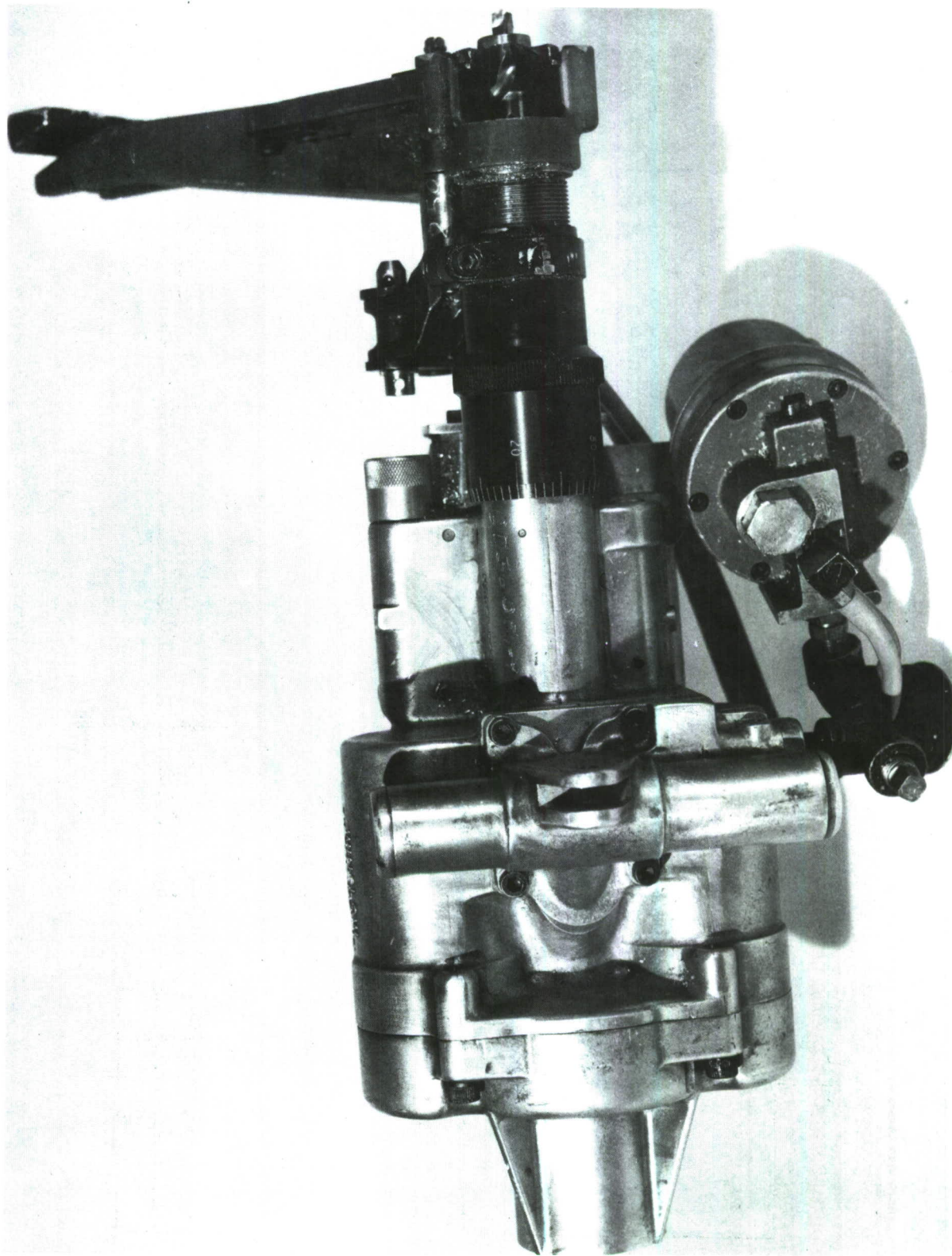


Figure 2-4 Winslow Spacematic Drilling Equipment

In order to better evaluate these two conventional processes, a variable was introduced in the manufacturing state of the fastener holes - improper drilling or drilling and reaming. Improper or abusive techniques were process deviations that would not generally be observed or tolerated on a production line. The processes included the use of intentionally dulled cutters, inadequate pneumatic line pressure, presence of titanium or steel chips, and extremely dirty cutting tools, i.e., built-up edges. The purpose of the improper techniques was to bring out rogue flaws or gross geometrical discontinuities.

2.2 NON-DESTRUCTIVE INSPECTION

Surface integrity and non destructive techniques were used to characterize every hole subjected to cyclic loading. The techniques used were:

- (1) Eddy Current
- (2) Ultrasonics
- (3) Rotary Proficorder (Dial Bore Gauge)
- (4) Linear Proficorder
- (5) Rubber Cast

The techniques utilized were those having the potential of being used in the production environment with demonstrated quantitative and repeatability measurements.

Comparisons were made between NDI parameters as measured by the different inspection techniques and EIFS. Correlations were attempted in order to identify holes with poor fatigue life from NDI data. A master list was developed to record the NDI reading for each technique, the specimen number, the fastener hole number, angular position, and depth from the surface.

2.3 SPECIMEN TESTING/LOAD HISTORIES/TEST PLAN

The fatigue testing of all coupon specimens was performed using six servo-controlled, hydraulically actuated, closed-loop-feedback load frames. Representative results were assured through the use of computer-generated loads spectra, which were independently controlled at each load frame. Real-time strip-chart recorders allowed computer command signals to be followed to within a $\pm 1.0\%$ accuracy.

Spectrum testing was performed using either a fighter or bomber spectra. The fighter load history used was the F-16 400-hour block randomized wing-root bending spectrum. This load history was a preliminary development spectrum and is more severe relative to the actual F-16 durability load history. Testing was carried out for two equivalent lives for the fighter, or 16,000 flight hours. The bomber load history used was the B-1 or AMAVS (Advanced Metallic Air Vehicular Structure) spectra, developed at General Dynamics Fort Worth Division. An equivalent of three lives, or 3840 flights, was the point at which testing was truncated.

2.4 FRACTOGRAPHY

Following fatigue testing the largest crack in each coupon was exposed by application of a tensile overload. Crack growth behavior of these cracks was then determined using optical fractographic techniques. Crack growth curves were established from the maximum crack length to below 0.005 inch for all specimens. This means of producing crack growth histories was very accurate and reproduceable, yielding consistent empirical results.

2.5 CRACK GROWTH ANALYSIS

On completion of fatigue testing a data generation-synthesis task was initiated. First crack growth analyses were produced to match as closely as possible the empirical crack growth behavior of the fastest growing crack of each test series. This analysis was performed in an iterative manner using an in-house computer routine (CGR, Crack Growth Rate). The crack growth analyses routine makes use of the Forman crack growth equation in conjunction with the Wheeler retardation model. Best fits to the empirical data were achieved by varying the amount of retardation. Other variables of importance are listed in Table 2-1. The ability to analytically fit empirical crack growth data in a concise and regular manner produced several desirable results, the most obvious of which was the consistency of the Equivalent Initial Flaw Size data, to be presented later.

2.6 EQUIVALENT INITIAL FLAW SIZE CONCEPT

The fatigue behavior of every specimen tested in this program was quantified using the Equivalent Initial Flaw Size (EIFS) approach. The EIFS method, specified in MIL-STD-83444A (Reference 5), is a means of measuring and possibly characterizing the economic life of structures having fastener holes. As shown in Figure 2-5

Table 2-1 CRACK GROWTH ANALYSIS VARIABLES

- 1. CRACK GROWTH EQUATIONS: FORMAN**
- 2. CRACK GROWTH MODEL: WHEELER RETARDATION MODEL**
- 3. THRESHOLD STRESS INTENSITY: 0.0 ksi $\sqrt{\text{in.}}$**
- 4. ENVIRONMENT: LABORATORY AIR**
- 5. SPECIMEN DIMENSIONS: 0.375 INCHES THICK BY 1.5 INCHES WIDE**
- 6. HOLE DIAMETER: 0.25 INCHES**
- 7. DEFECT CONFIGURATION: BOLT HOLE CRACK. (CORNER AND IMBEDDED)**
- 8. ASPECT RATIO: 0.5**

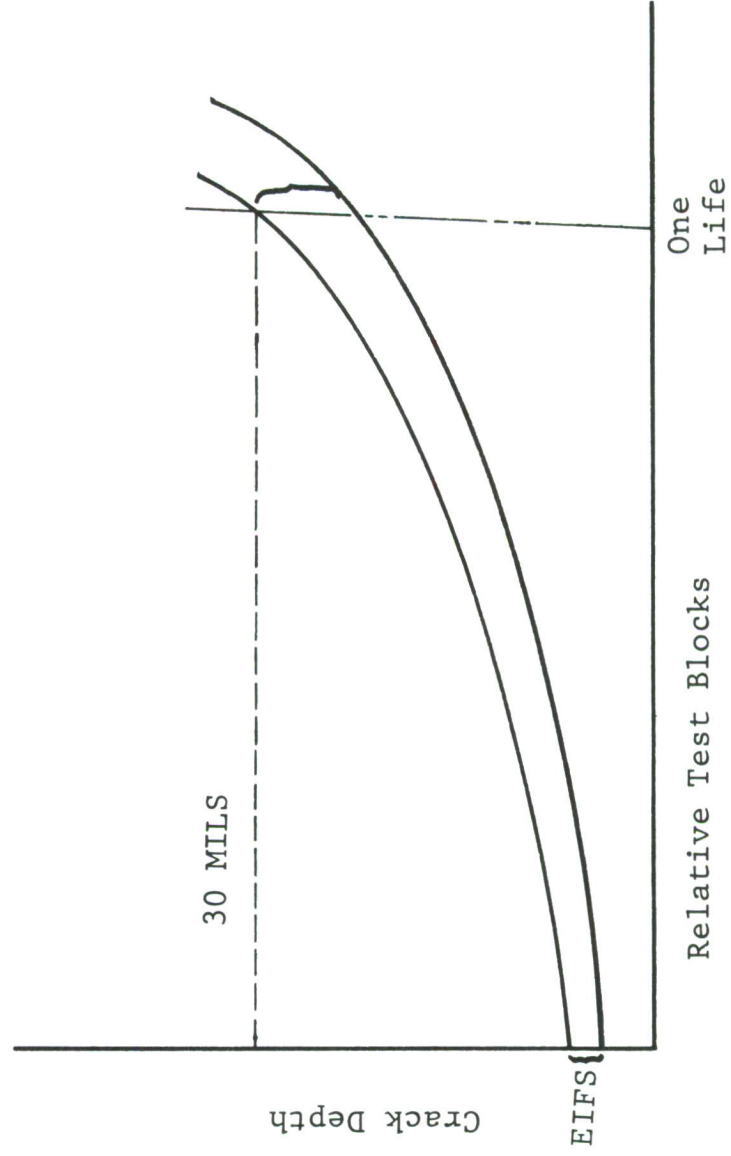


Figure 2-5 Schematic Showing Fatigue Lives of Two Fastener Holes Having Different EIFS

the EIFS is that pseudo fatigue crack assumed to be present in a fastener hole at time zero, or prior to putting a structure into service. Under the spectrum fatigue loading encountered, the fatigue crack exhibits the crack growth behavior shown. The economic limit is described as that service life duration required for the crack to reach a depth of 0.030 inch.

Fatigue crack depth at the end of one life is directly proportional to the EIFS of a fastener hole as shown in Figure 2-5. A population of fastener holes possesses a range of EIFS values that will govern the final crack depths at the end of the design service life of the structure.

The EIFS for the largest fatigue crack in each specimen tested was established by matching the fractographic crack growth data to an analytical curve. Typically, fractographic methods are not able to track crack growth histories below crack depths of 0.001 - 0.01 inch. The lower limit is dependent on the amount of wear occurring at the crack tip, which obscures fatigue striation bands. EIFS values obtained in this program were characteristically in the range of 0.0001 - 0.005 inch. As a result, the analytical curves had to be regressed to smaller initial crack dimensions.

EIFS values were obtained for each fatigue crack in a sample of specimens using a single analytical curve, described below. All specimens in a sample were tested with either a fighter or a bomber load history at one selected maximum spectrum stress level. The behavior of fatigue cracks obtained for any given sample should scatter in the growth rate as well as the time to crack initiation. Typical behavior showing the amount of scatter is seen in Figure 2-6 for drilled and reamed fastener holes. The five specimens whose fractographic curves are plotted indicate the range of crack growth behavior occurring for 38 specimen tested.

Selection of a simple analytical curve for determination of individual EIFS values for each specimen was made using well-defined criteria. An analytical curve was grown so as to define a conservative bound, as seen in Figure 2-7, to the fastest growing crack in a sample of specimens, over as large a range of crack depth as possible. The EIFS for each specimen was obtained by matching the analytical crack growth to each fractographic crack growth history using regression analysis to obtain the best fit. The analytical and fractographic curves were matched between crack depths of 0.01 - 0.05 inch. The crack depth value of the analytical curve, corresponding to time zero for each fractographic crack growth history, was the EIFS value for that fastener hole. An EIFS value was obtained for every specimen in a sample.

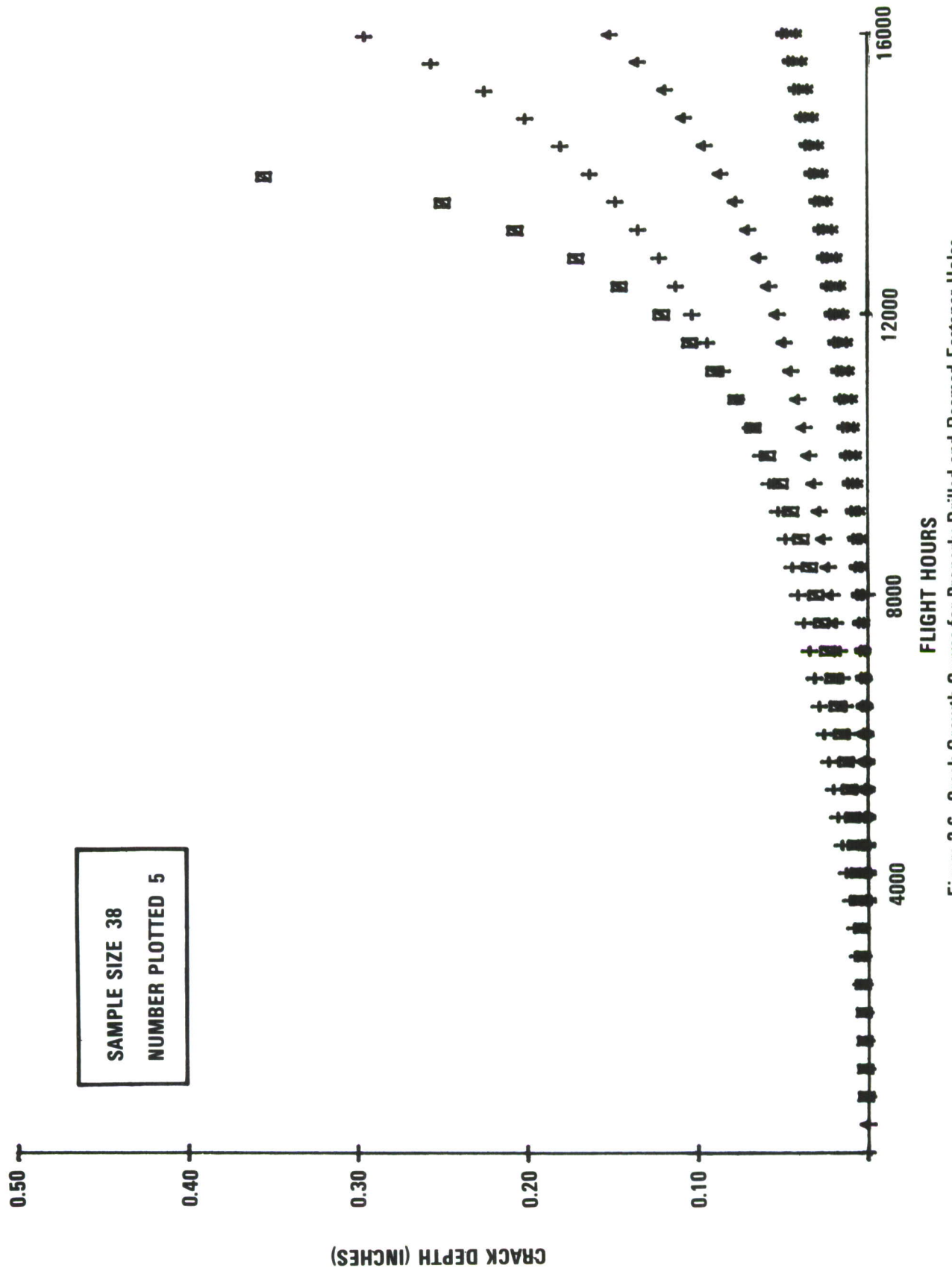


Figure 2-6 Crack Growth Curves for Properly Drilled and Reamed Fastener Holes

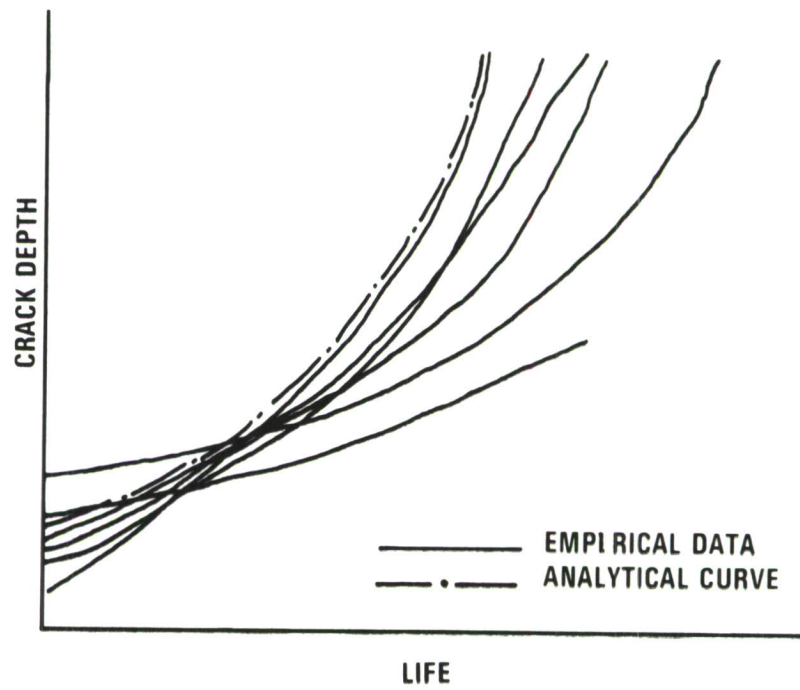


Figure 2-7 Selection of a Single Analytical Curve for a Sample of Fractographic Crack Growth Histories

SECTION III

TASK I NO-LOAD TRANSFER RESULTS

The overall objectives of this task were the investigation of the effects of hole quality on fatigue performance using no-load transfer specimens with filled fastener holes. Surface-integrity and non-destructive techniques were used to completely characterize every fastener hole prior to subjection to cyclic loading, thus allowing the potential of each technique for automated inspection and characterization to be evaluated.

A total of 200 specimens were fabricated and fatigue tested in this task. Hole fabrication processes and load histories employed for fatigue testing are shown in Table 3-1. The specimens were evenly divided between fighter and bomber load histories and the hole fabrication process respectively.

The results of coupon fatigue listing for all tasks will be presented as cumulative probability versus equivalent initial flaw size or crack depth at a given life interval. This is a means of data representation for an entire test condition and should be interpreted as shown in the following examples. If the mean EIFS value for a given test condition is 0.0005 inch, then 50% of all the EIFS values will be equal to or less than this value. On the other hand, a 99% cumulative probability for an EIFS of 0.001 inch would imply that 99% of the EIFS values would be equal to or less than 0.001 inch. If this structure contained 100 holes, then only 1%, or 1 hole, would have an EIFS greater than 0.001 inch.

3.1 FIGHTER SPECTRUM

3.1.1 Clearance-Fit Fastener Holes

Results presented for the no-load transfer condition reflect general trends observed throughout the data collection phase. Cumulative distributions for both EIFS and crack depths will tend to be lower for the clearance-fit fastener hole with respect to transition-fit fastener holes. This trend is shown in Figures 3-1 and 3-2, where the EIFS and crack depths at one life are plotted for drilled clearance-fit fastener holes, and drilled and reamed transition-fit fastener holes. Note that in both cases the mean, or 50-percentile values are greater for the transition-fit fastener holes.

Table 3-1 SUMMARY OF TEST CONDITIONS

ALLOY: 7475—T7351 ALUMINUM. HOLE DIAMETER: 0.250 INCHES NOMINAL. MAXIMUM SPECTRUM: (i) FIGHTER = 34 ksi STRESS (GROSS): (ii) BOMBER = 33 ksi (BASELINE WITH EXCEPTIONS NOTED)					
CLASS OF FASTENER HOLE FATIGUE TEST CONFIGURATION	CLEARANCE FIT SPACEMATIC DRILL		TRANSITION FIT QUACKENBUSH DRILL AND REAM		
	FIGHTER	BOMBER	FIGHTER	BOMBER	
TASK I A (CONVENTIONAL EQUIPMENT) NO—LOAD TRANSFER	38 PROPERLY FABRICATED	37 PROPERLY FABRICATED	38 PROPERLY FABRICATED	37 PROPERLY FABRICATED	
	13 IMPROPERLY FABRICATED	12 IMPROPERLY FABRICATED	13 IMPROPERLY FABRICATED	12 IMPROPERLY FABRICATED	
TASK I B (MODIFIED EQUIPMENT) NO—LOAD TRANSFER	30 PROPERLY FABRICATED	—	—	—	
TASK II (CONVENTIONAL EQUIPMENT) 15% LOAD TRANSFER	38 PROPERLY FABRICATED	37 PROPERLY FABRICATED	38 PROPERLY FABRICATED	37 PROPERLY FABRICATED	
	13 IMPROPERLY FABRICATED				
TASK III (MODIFIED EQUIPMENT) 15% LOAD TRANSFER	30 PROPERLY FABRICATED	30 PROPERLY FABRICATED			
	10 PROPERLY FABRICATED (120% OF BASELINE STRESS)	10 PROPERLY FABRICATED (120% OF BASELINE STRESS)			
	10 PROPERLY FABRICATED (90% OF BASELINE STRESS)	10 PROPERLY FABRICATED (90% OF BASELINE STRESS)			

Table 3-1 SUMMARY OF TEST CONDITIONS (Cont'd)

ALLOY (i) 7475—T7351 ALUMINUM (ii) AF—1410 STEEL (iii) 6—4 ANNEALED TITANIUM TEST SPECTRUM: FIGHTER LOAD HISTORY HOLE DIAMETER: 0.250 INCHES NOMINAL				
CLASS OF FASTENERS HOLE FATIGUE TEST CONDITION	TRANSITION FIT QUACKENBUSH DRILL AND REAM	COLD WORKED	TAPER—LOK	
TASK IV A NO—LOAD TRANSFER (STEEL)	30 PROPERLY FABRICATED	—	—	
TASK IV B NO—LOAD TRANSFER (TITANIUM)	30 PROPERLY FABRICATED	—	—	
TASK V NO—LOAD TRANSFER (ALUMINUM)	—	30 PROPERLY FABRICATED	30 PROPERLY FABRICATED	

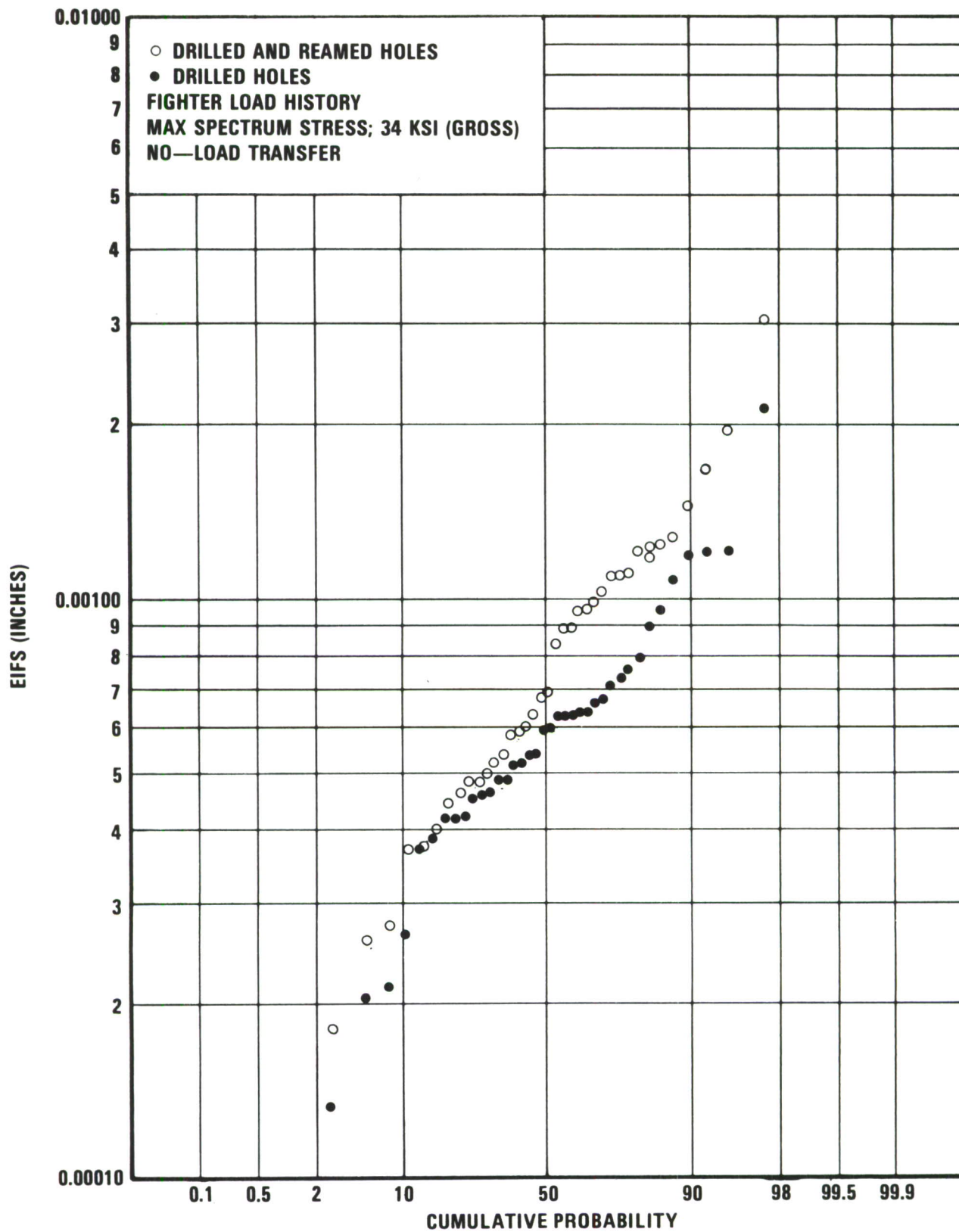


Figure 3-1 EIFS for Drilled and Drilled and Reamed Holes

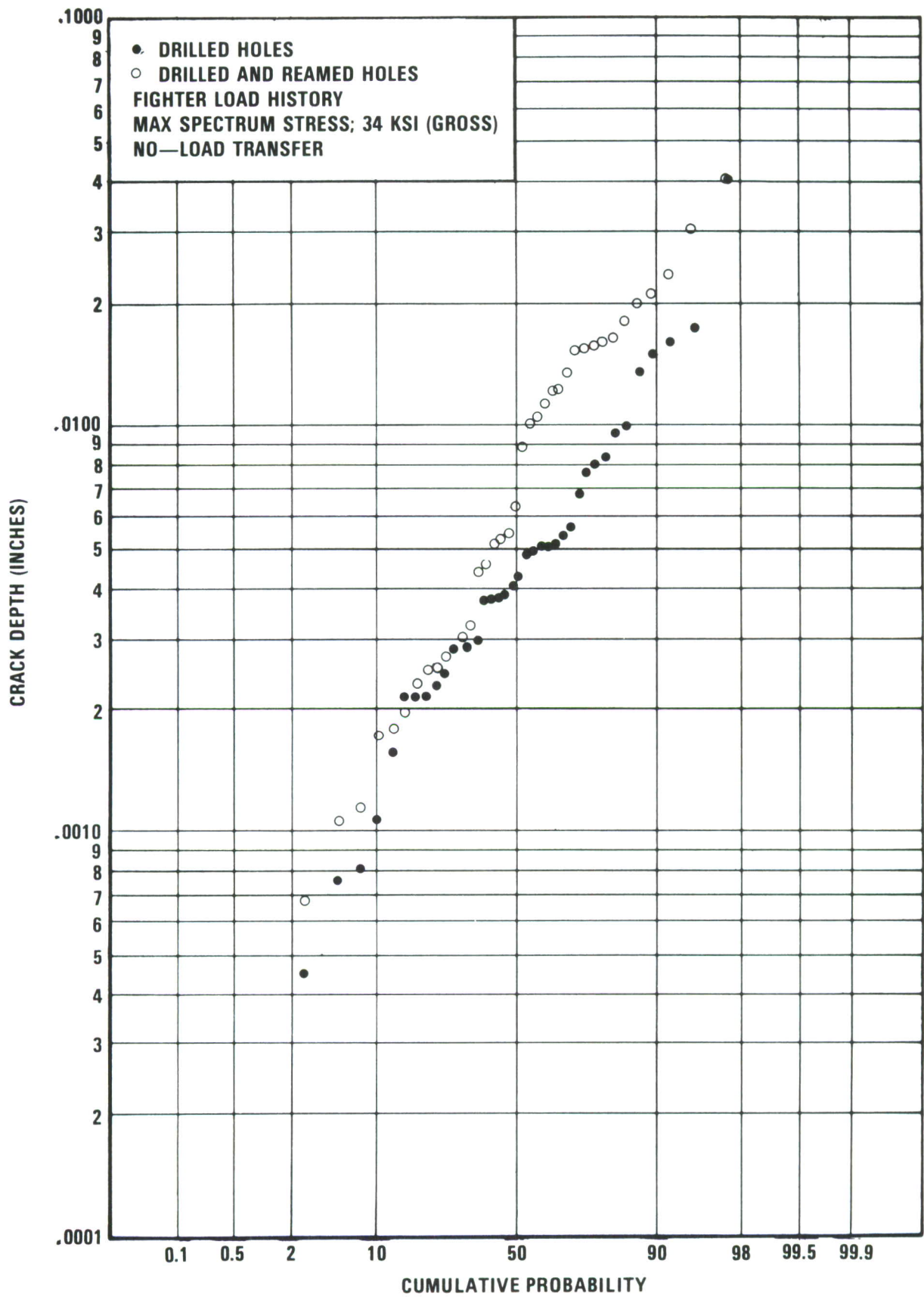


Figure 3-2 Crack Depth at One Life for Drilled and Drilled and Reamed Holes

The effect of improperly or abusively drilled fastener holes is shown in Figures 3-3 and 3-4. In both cases, the mean EIFS and crack depth values for the improperly drilled fastener holes lie at twice that of the properly drilled fastener holes. The upper-extreme values approach each other, making two implications. First, the worst-case properly drilled fastener hole is no better than the worst-case improperly drilled hole. Second, the fatigue-crack initiating mechanism for both extreme cases is possibly the same.

3.1.2 Transition-Fit Fastener Holes

The transition-fit fastener holes, as previously mentioned, were fabricated using a two-step drill and ream operation. These fastener holes behaved approximately the same, as shown in Figures 3-1 and 3-2, in fatigue as the clearance-fit fastener holes.

The behavior of transition-fit fastener holes produced using proper and improper techniques are shown in Figures 3-5 and 3-6. Both EIFS and crack depth at one life show essentially no difference between the proper and improper techniques. It is also noted that the slopes for both proper and improper techniques are the same, implying that the same width distributions apply to both procedures.

3.2 BOMBER SPECTRUM

3.2.1 Clearance-Fit Fastener Holes

Coupon fatigue testing was conducted under both the F-16 fighter and B-1 bomber spectra, as previously mentioned. The EIFS distributions for clearance-fit fastener holes using these two spectra are shown in Figure 3-7. Differences occurring in the slopes reflect the relative sizes of the distributions. Thus the EIFS values are stress sensitive and spectrum dependent. Lower EIFS values for those specimens tested using the bomber spectrum should not be considered to be of better "quality" than those specimens tested with the fighter spectrum.

The EIFS and crack depth values are compared for properly and improperly drilled clearance-fit fastener holes in Figures 3-8 and 3-9 respectively. A slightly lower EIFS distribution is observed for the properly drilled fastener hole compared to the improperly drilled fastener hole. The distributions are more widely separated in Figure 3-9 for the crack depths at one life. This behavior is slightly anomalous compared to other similar data, as for example in Figures 3-3 and 3-4, where the crack depth and EIFS distribu-

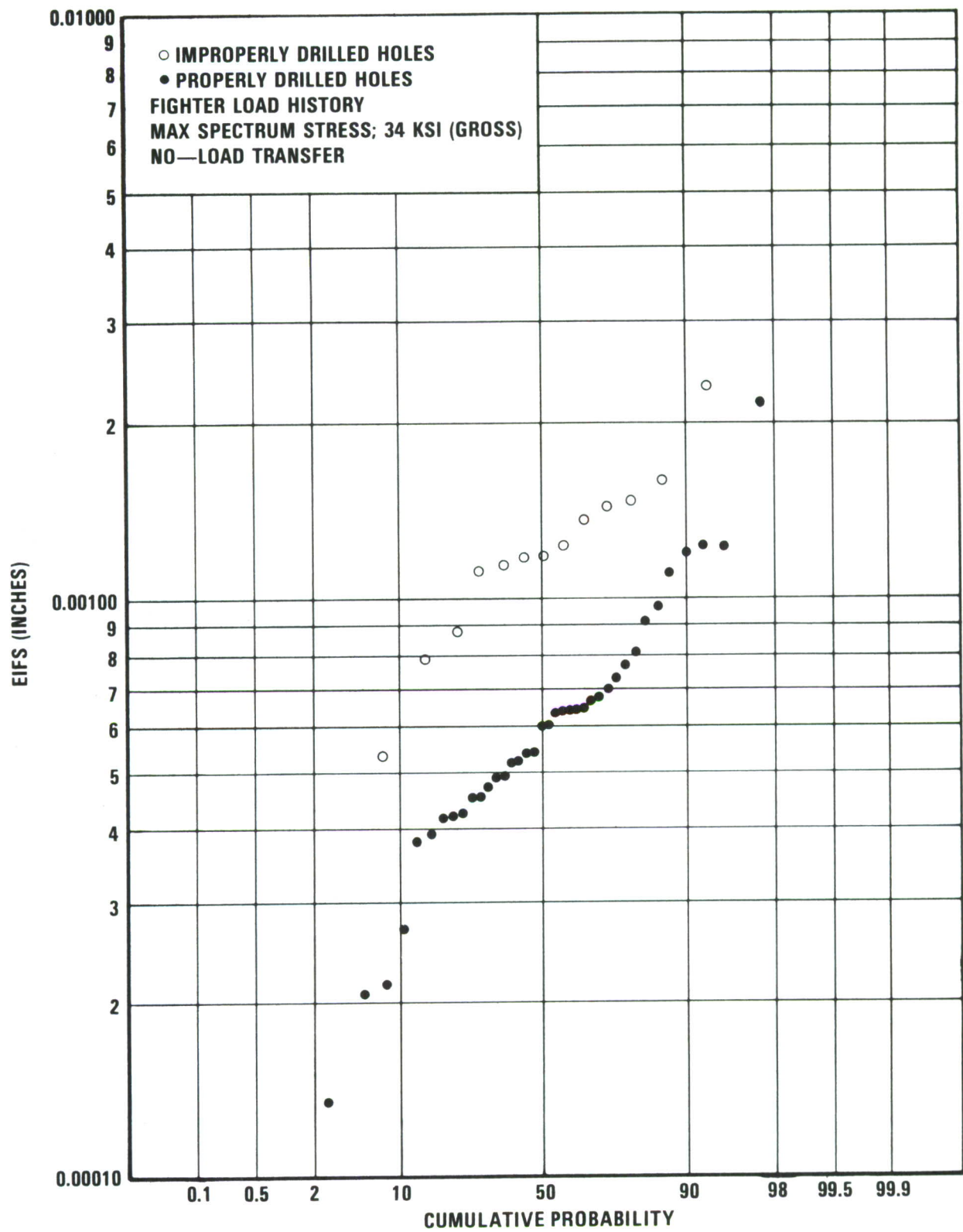


Figure 3-3 EIFS for Improperly and Properly Drilled Holes

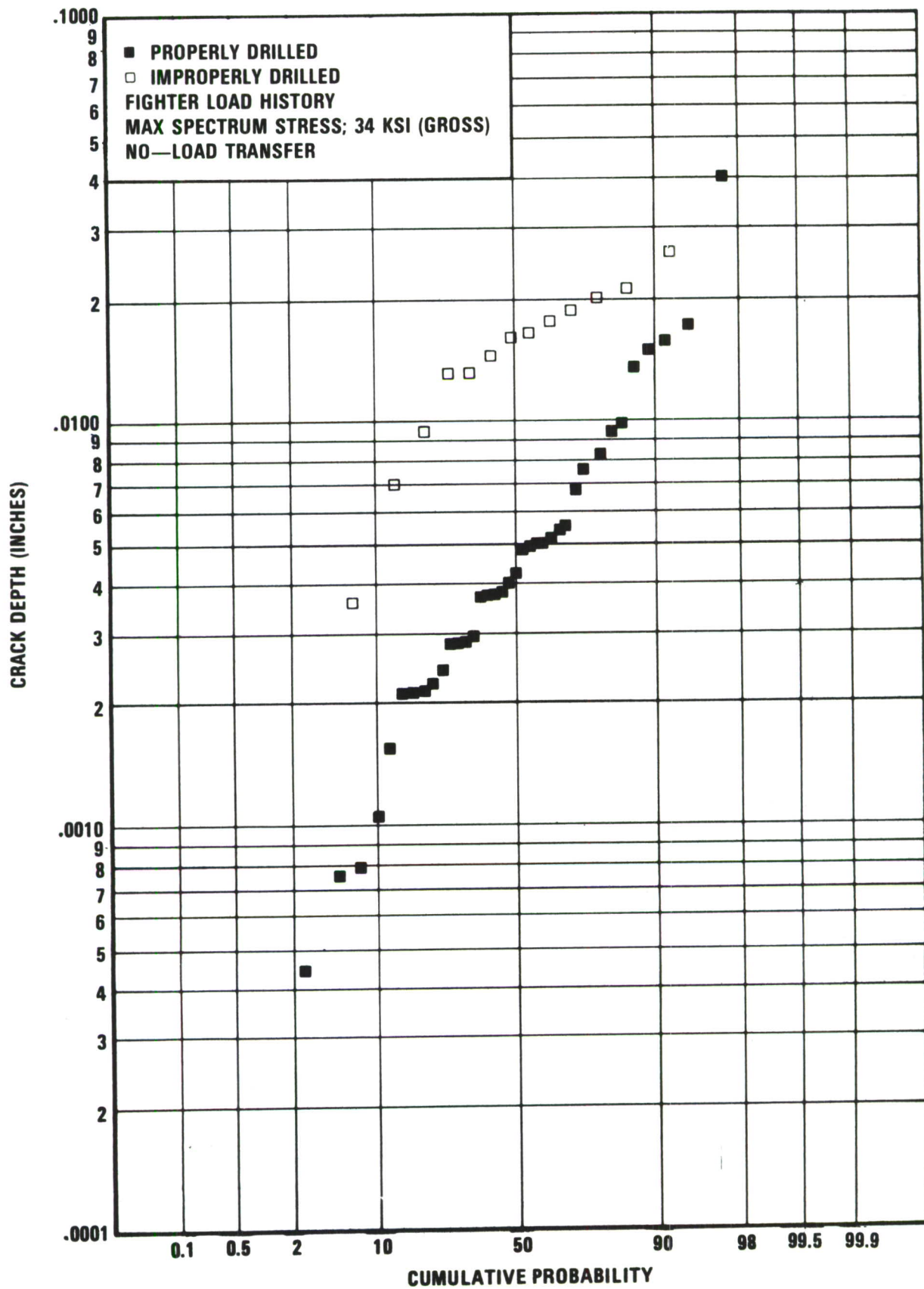


Figure 3-4 Crack Depth at One Life for Properly and Improperly Drilled Holes

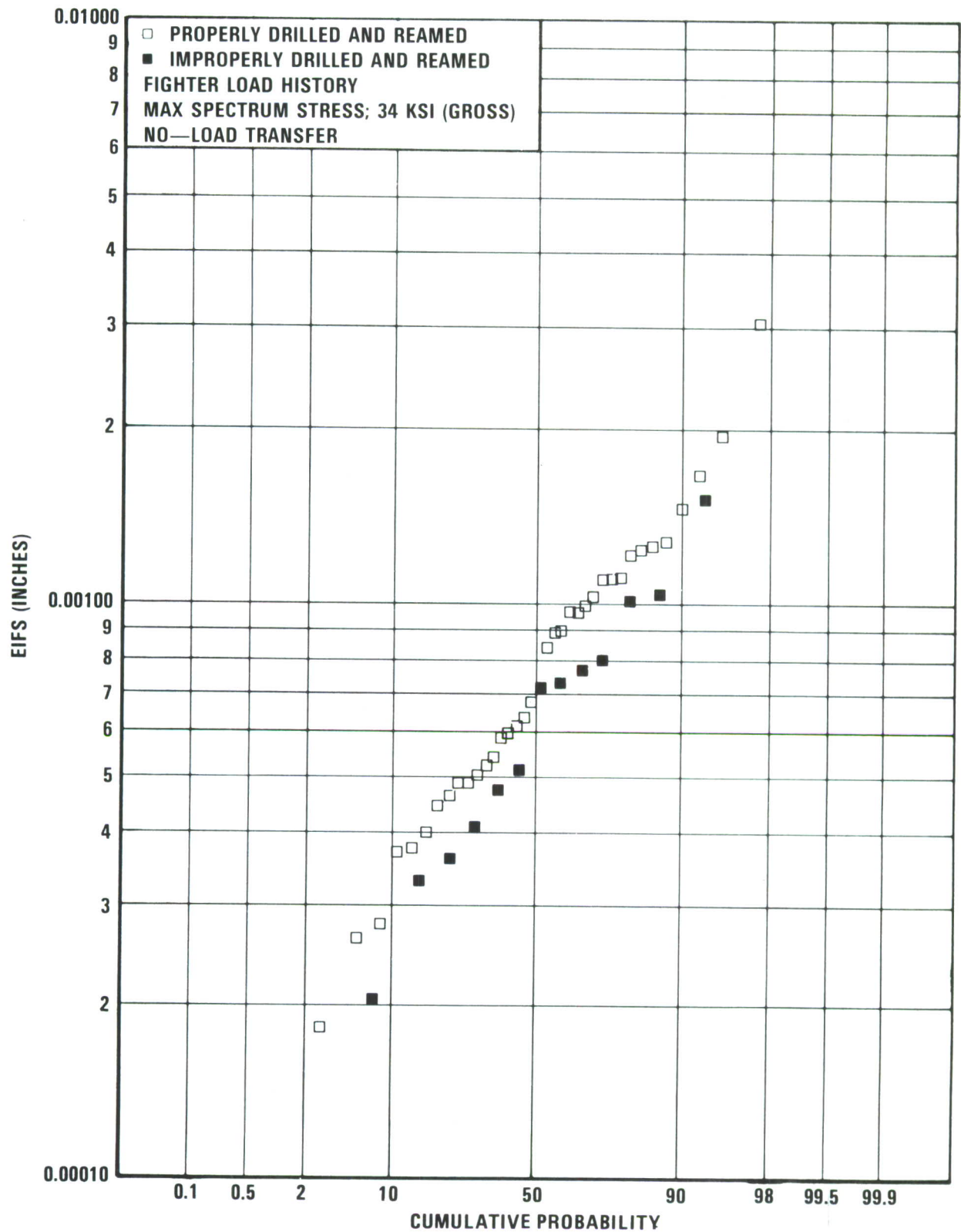


Figure 3-5 EIFS Distributions for Properly and Improperly Drilled and Reamed Holes

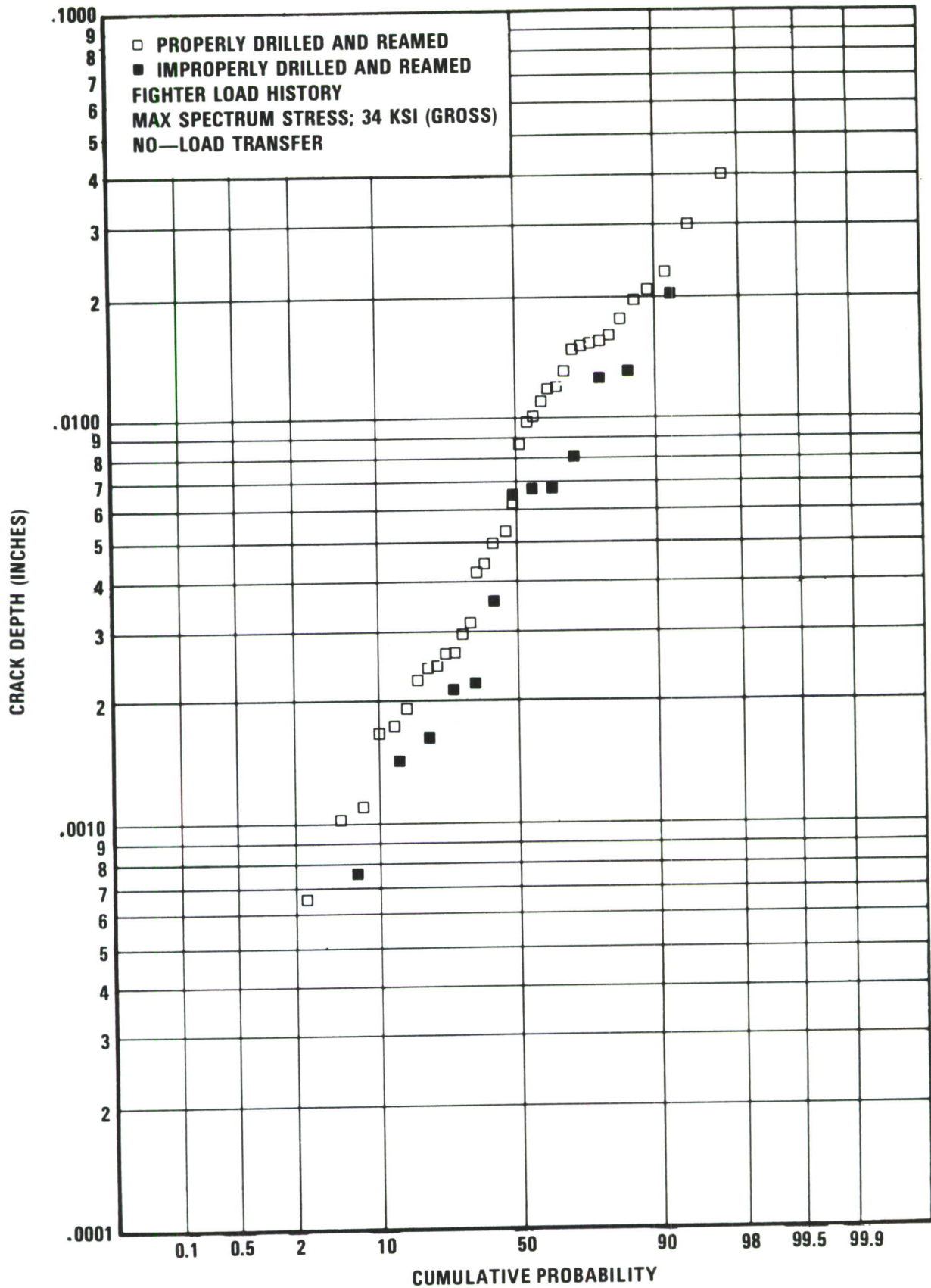


Figure 3-6 Crack Depth at One Life for Properly and Improperly Drilled and Reamed Holes



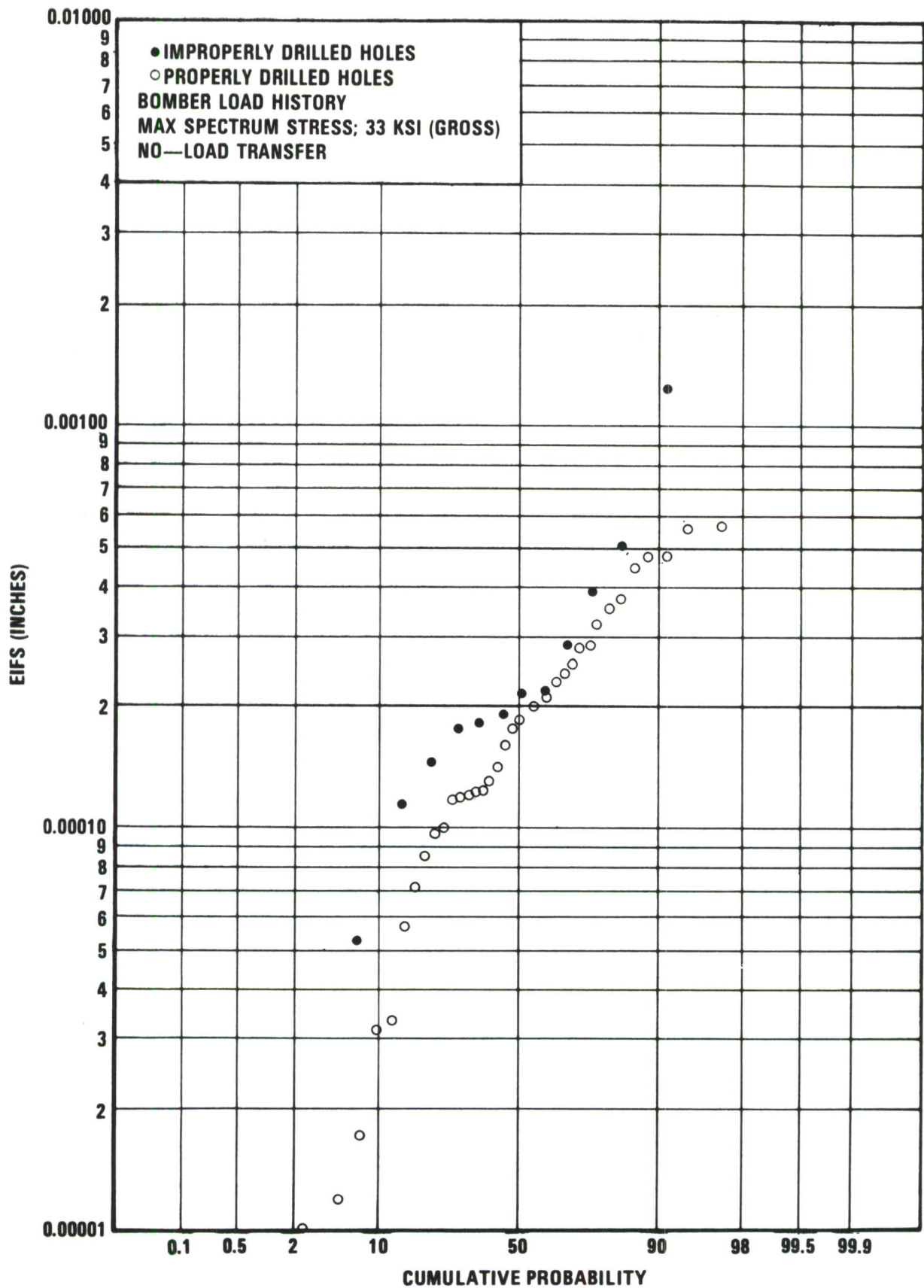


Figure 3-8 EIFS for Properly and Improperly Drilled Holes

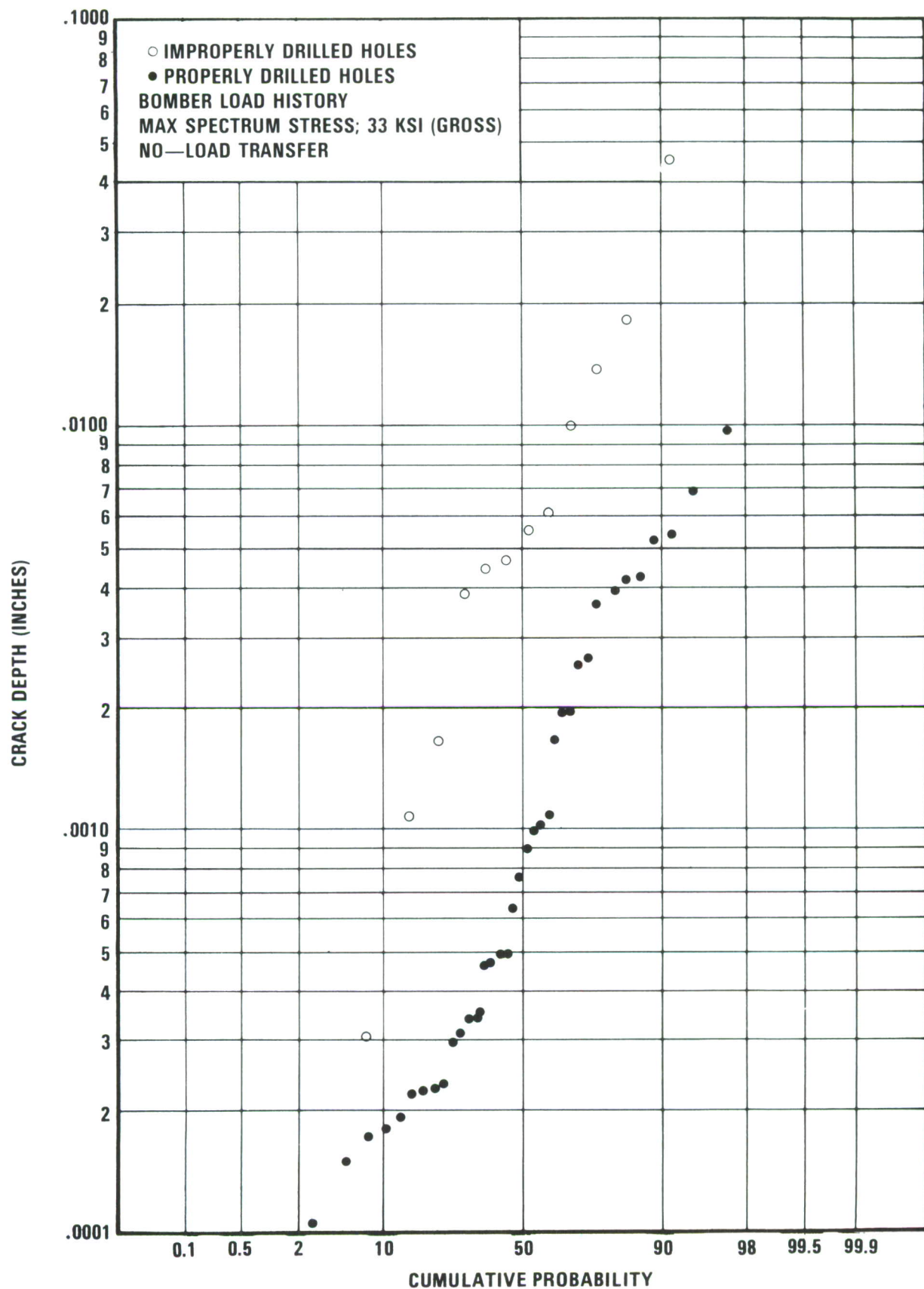


Figure 3-9 Crack Depth at One Life for Properly and Improperly Drilled Holes

tions show similar behavior. Such uniform behavior was observed throughout this investigation.

3.2.2 Transition-Fit Fastener Holes

Figures 3-10 and 3-11 show EIFS and crack depth distributions respectively for proper and improperly drilled and reamed fastener holes fatigue tested with the bomber spectrum. The distributions for the proper and improper processes are nearly identical. These results are not unexpected when compared to the behavior of the transition-fit fastener holes tested using the fighter spectrum. In comparison the mean crack depth at one life is approximately the same value for transition-and clearance-fit holes. The extremal values, or the durability critical holes, which are of the most importance structurally, tend to spread. Thus, the transition-fit crack depths, as shown in Figure 3-12, at cumulative probabilities of 98% show values approaching twice those of the clearance fit holes. Magnification of this tendency is seen in Figure 3-13, where transition-fit crack depths at two lives are approximately three times those values for clearance-fit fastener holes.

3.3 NDE RESULTS (TASK I)

All specimens in Task I were examined by five NDE techniques. From these results, correlations were attempted between parameters such as dimensional tolerance parameter, maximum eddy-current amplitude at critical orientations, etc., as a function of equivalent initial flaw size (EIFS).

3.3.1 Eddy Current

Eddy current scans were taken of all fastener holes in Task I. Orientation of the specimens with respect to the eddy current probe was documented. Shown in Figures 3-14, 3-15, and 3-16 are plots of the maximum eddy-current amplitude versus EIFS. Little or no correlation was found between the two parameters. The only set of specimens where some correlation was obtained was for the improperly drilled fastener holes. In this case, gross discontinuities were often present, which caused large eddy current signals. An example of an eddy current scan from a hole with a large vertical scratch is shown in Figure 3-17. However, in many cases, the primary fatigue crack origins were due to shallow vertical scratches that were undetected with eddy current, Figure 3-18.

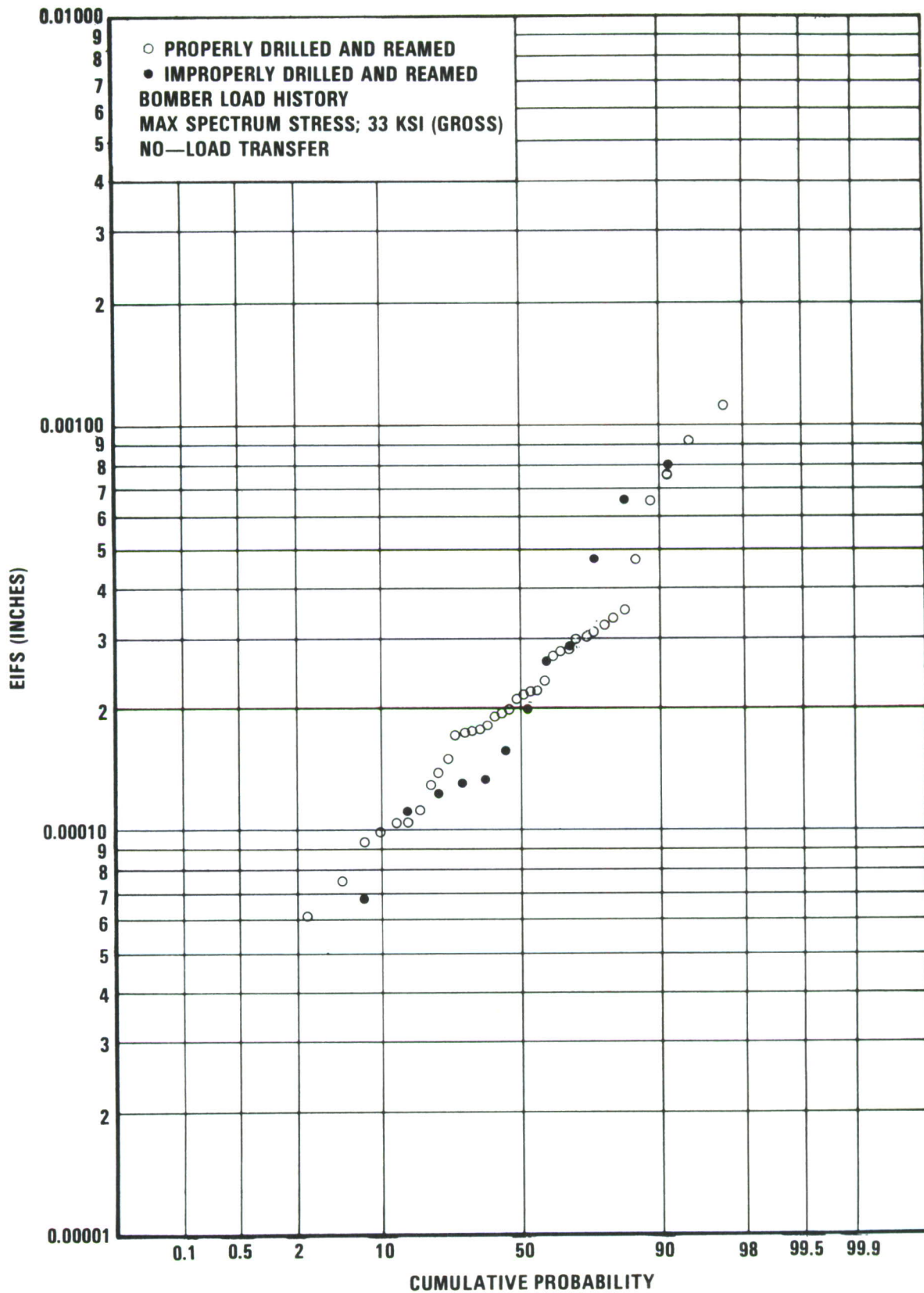


Figure 3-10 EIFS Distributions for Properly and Improperly Drilled and Reamed Holes

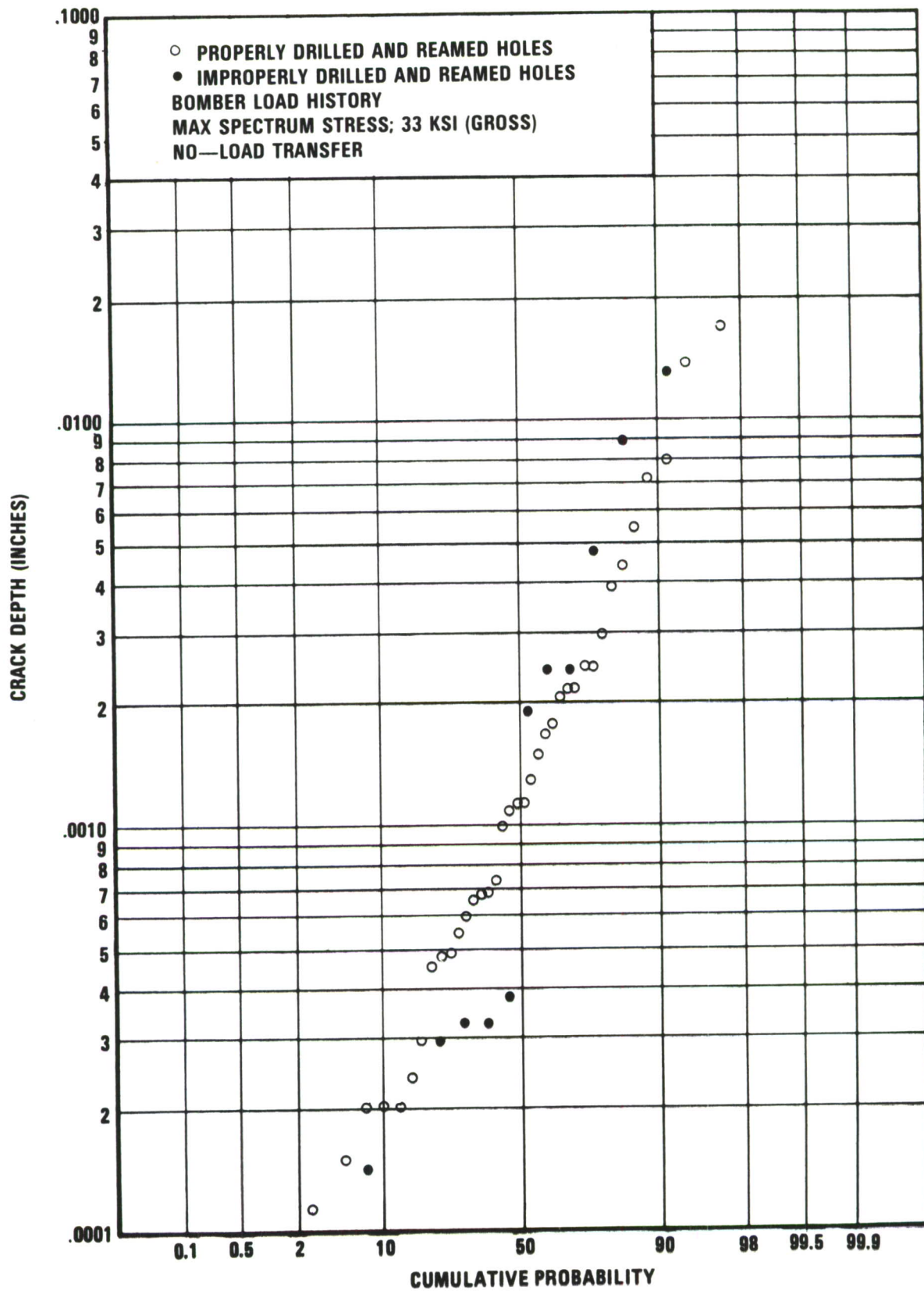


Figure 3-11 Crack Depth at One Life for Properly and Improperly Drilled and Reamed Holes

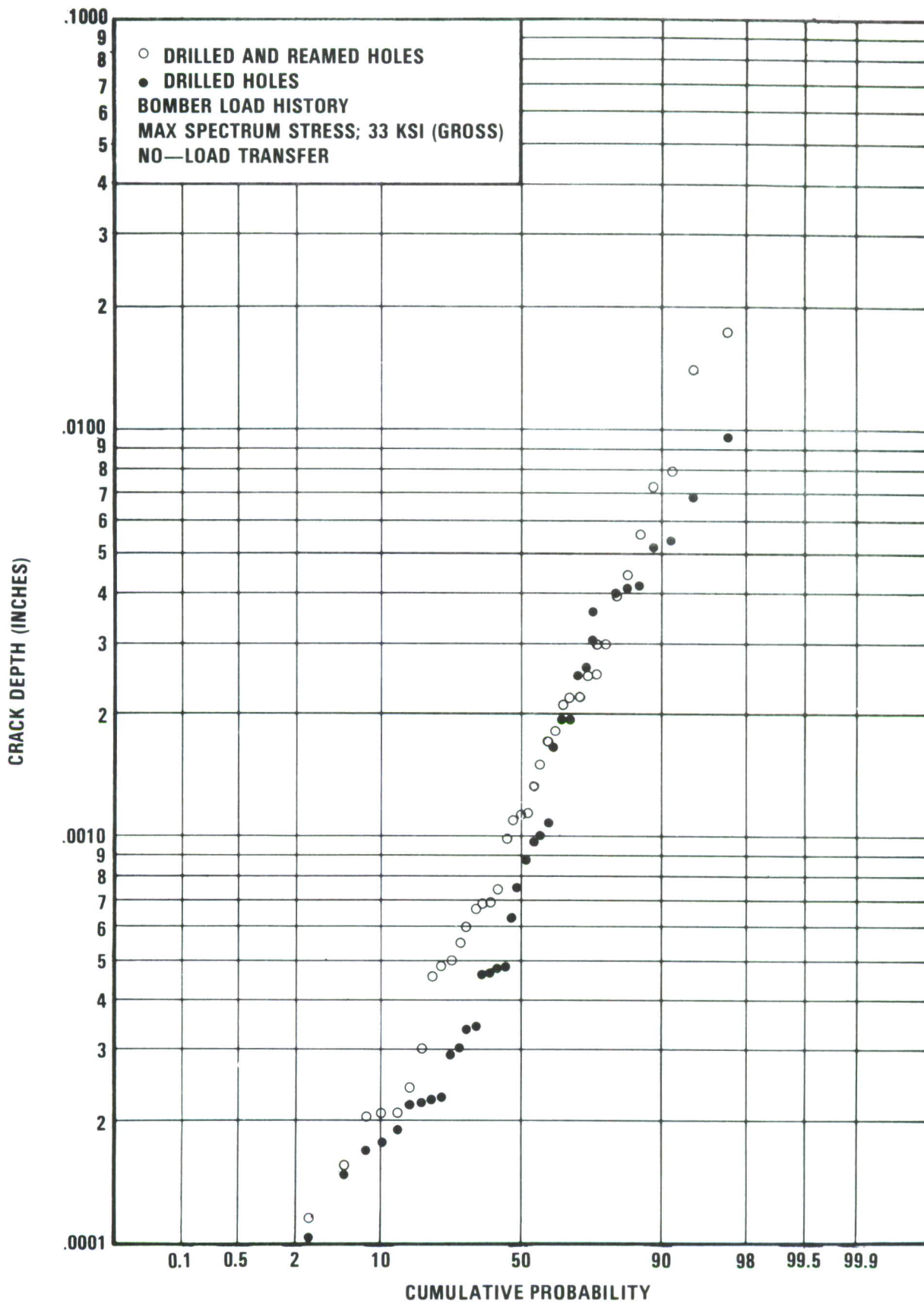


Figure 3-12 Crack Depth at One Life for Drilled and Drilled and Reamed Holes

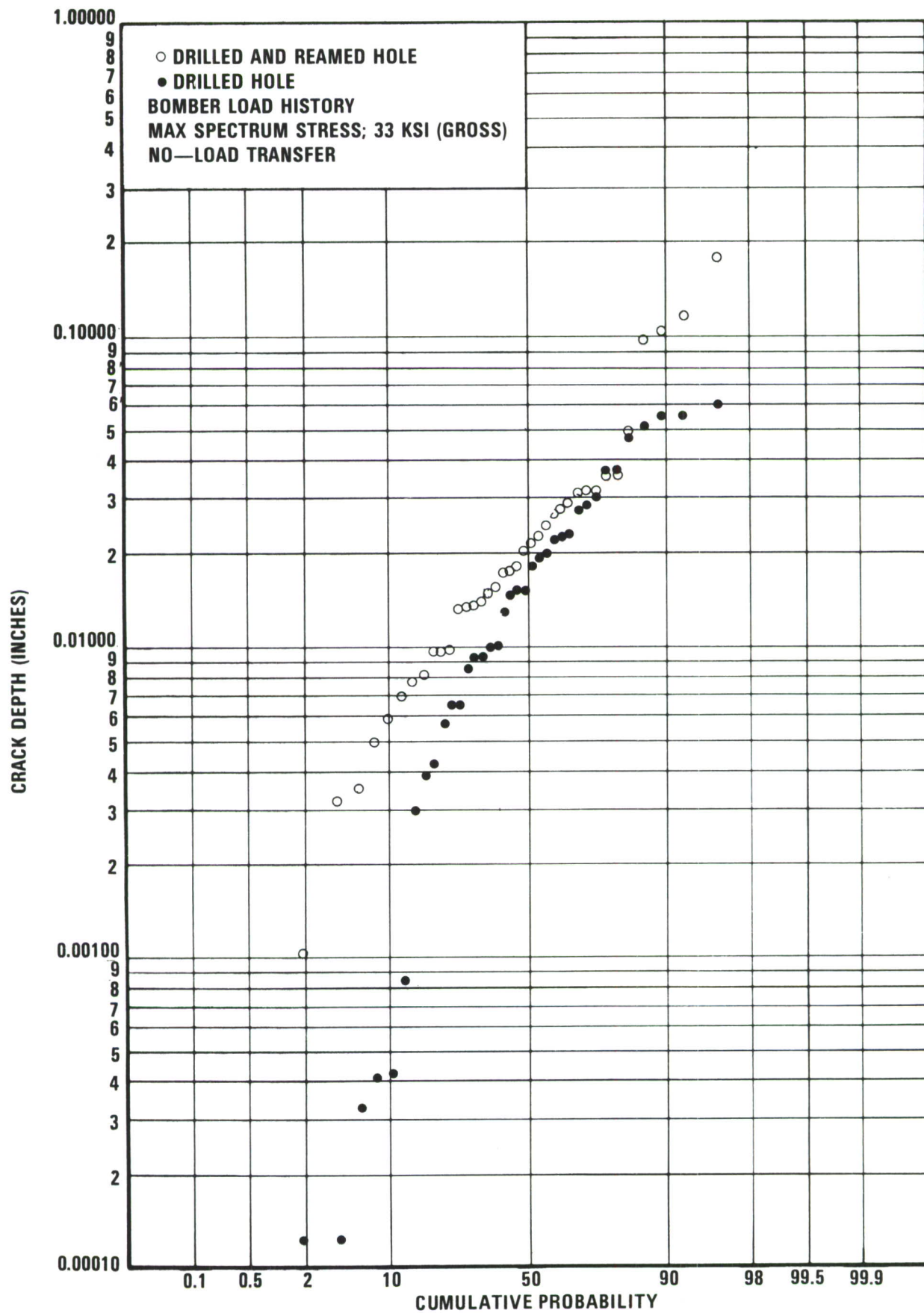
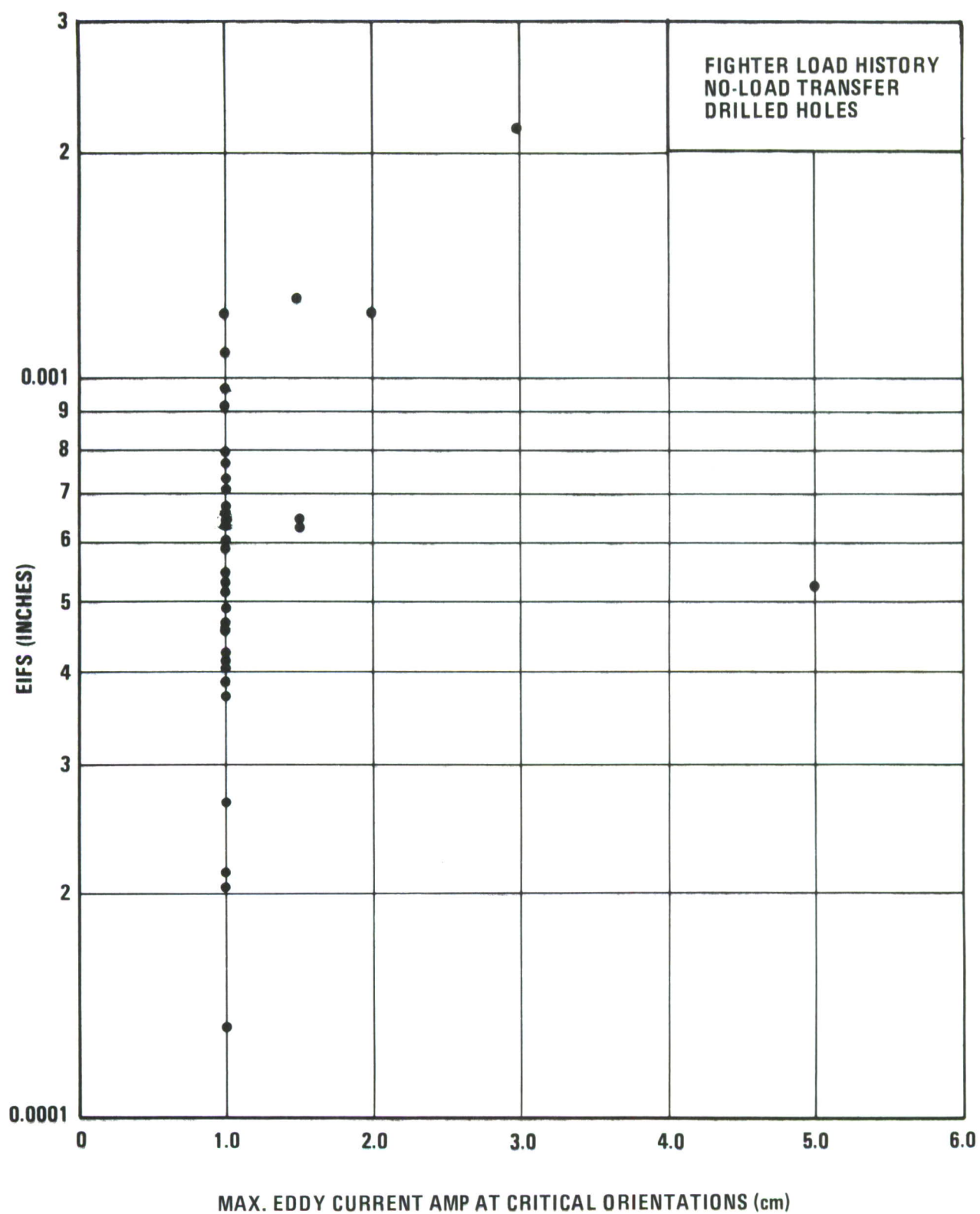


Figure 3-13 Crack Depth at Two Lives for Drilled and Drilled and Reamed Holes



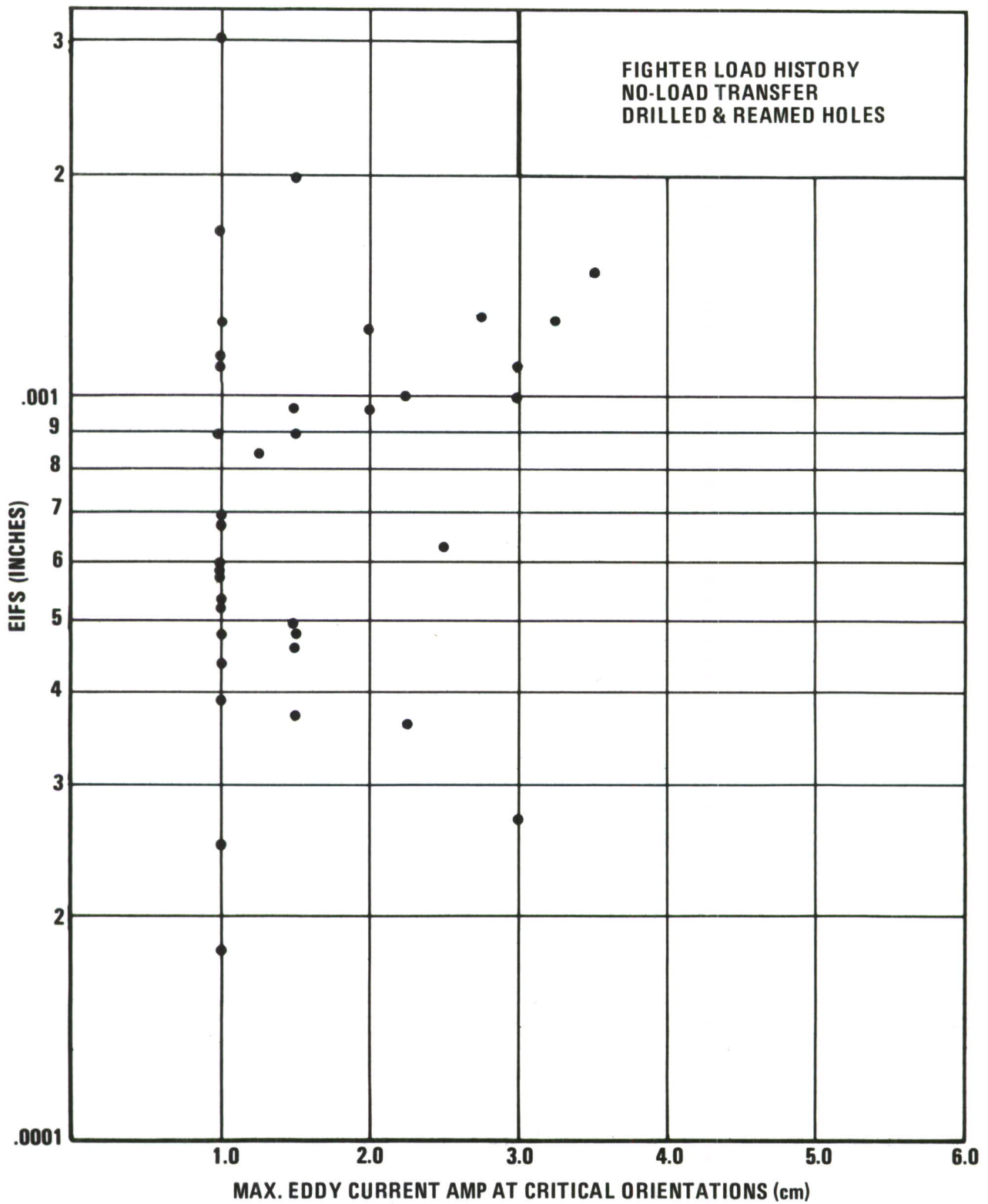


Figure 3-15 Maximum Eddy Current Amplitude versus EIFS, Drilled and Reamed Holes

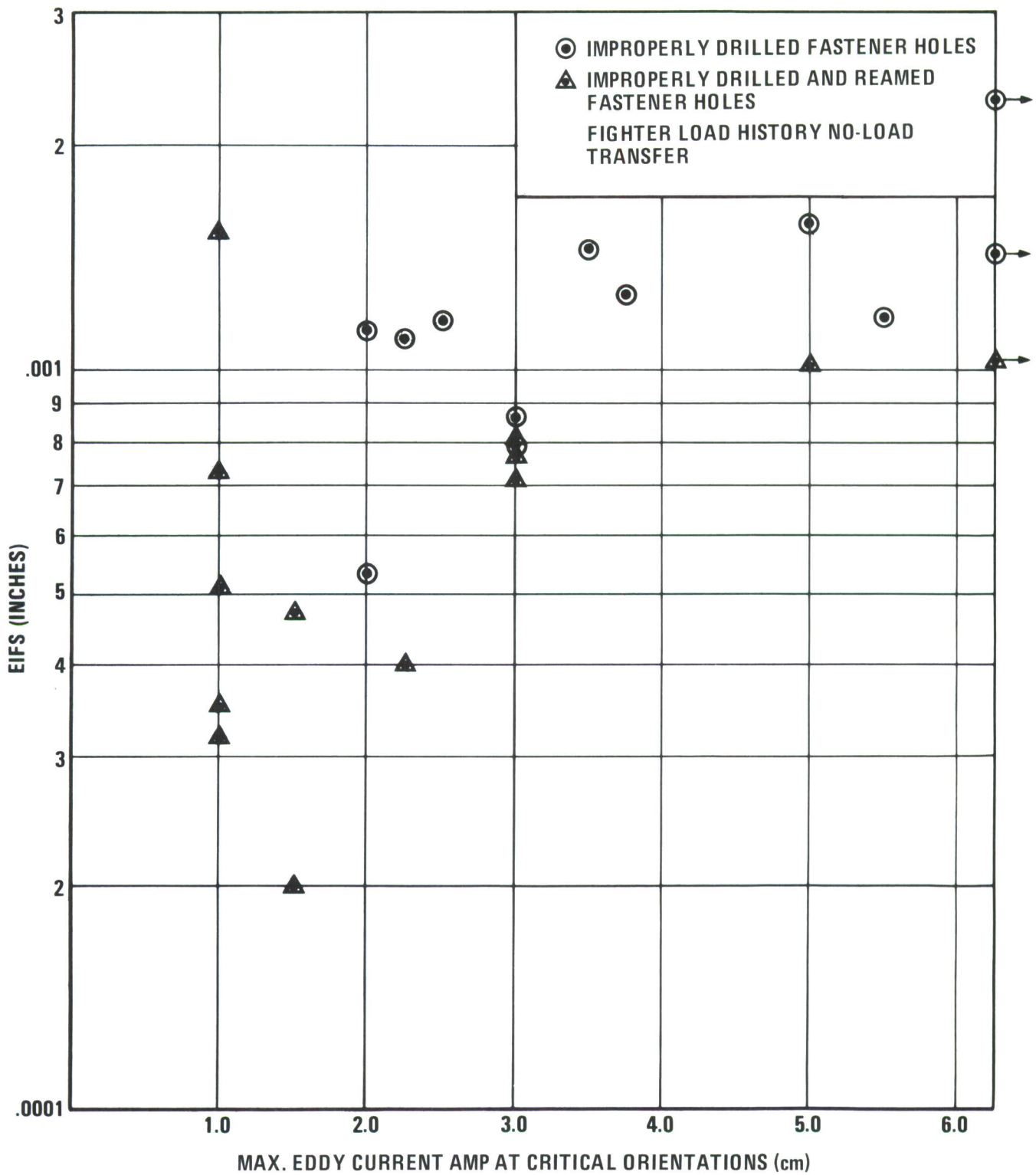
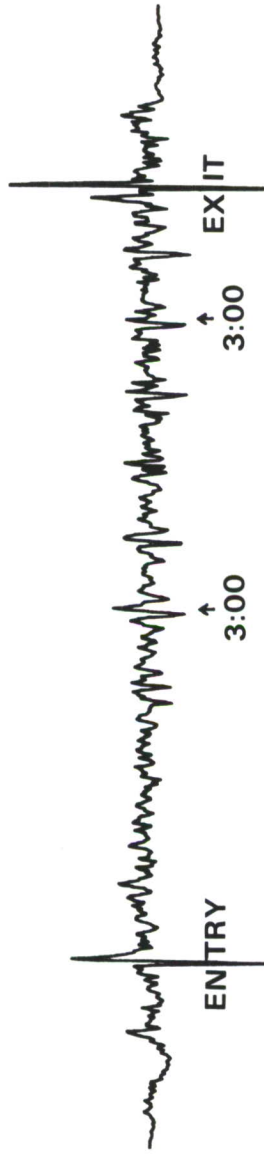
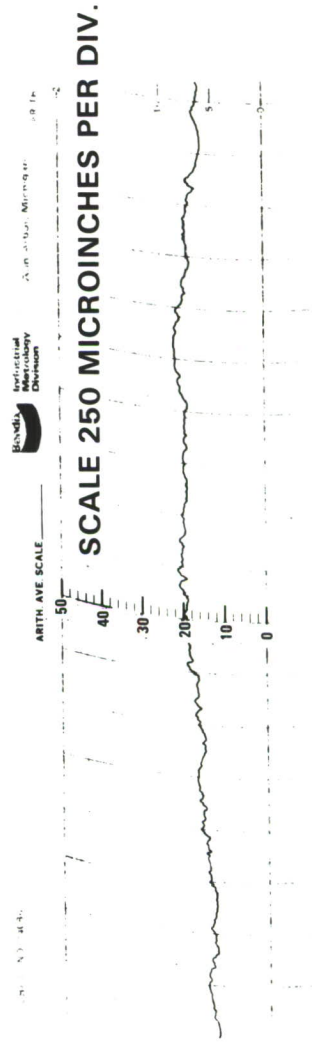


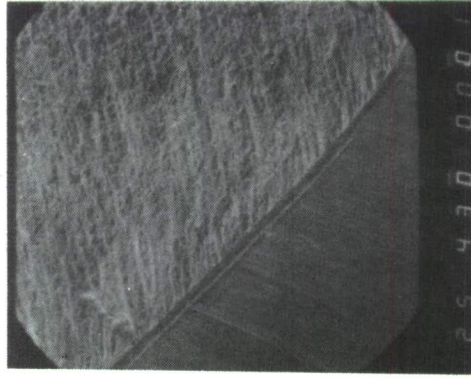
Figure 3-16 Maximum Eddy Current Amplitude versus EIFS, Improperly Drilled and Drilled and Reamed Holes



EDDY CURRENT SCAN SHOWING A VERTICAL SCRATCH

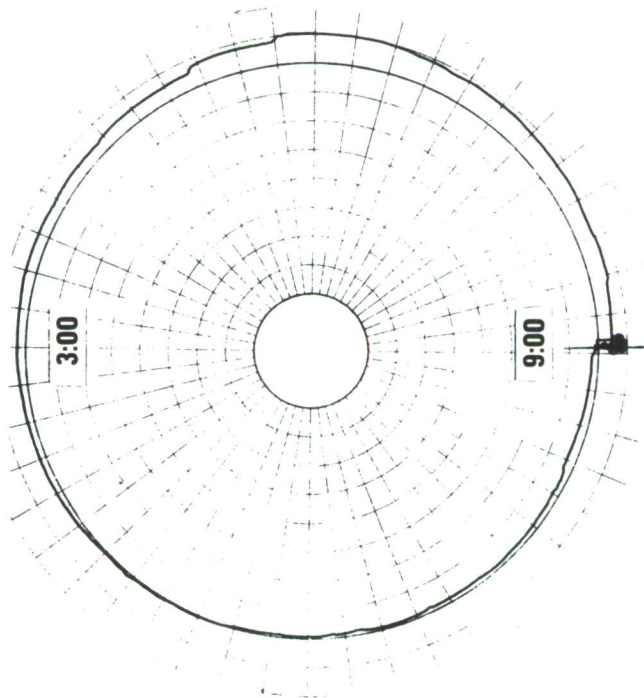
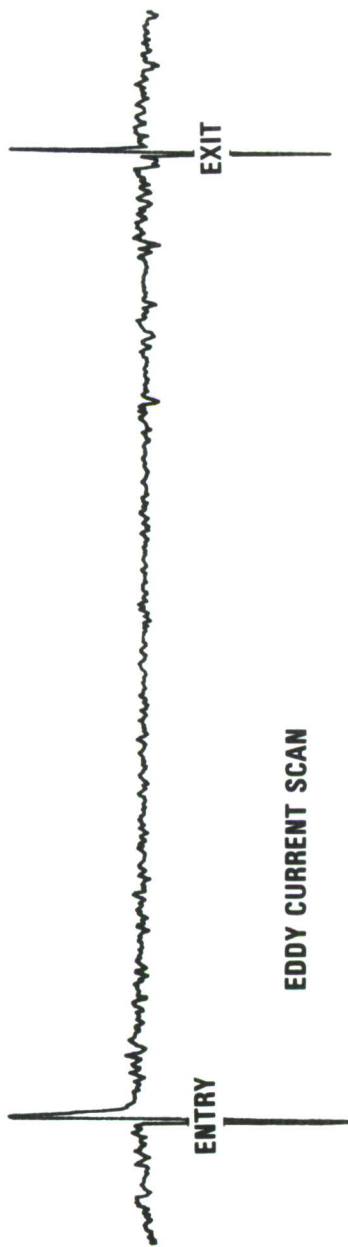


LINEAR PROFILOMETER TRACE AT 3:00 OCLOCK

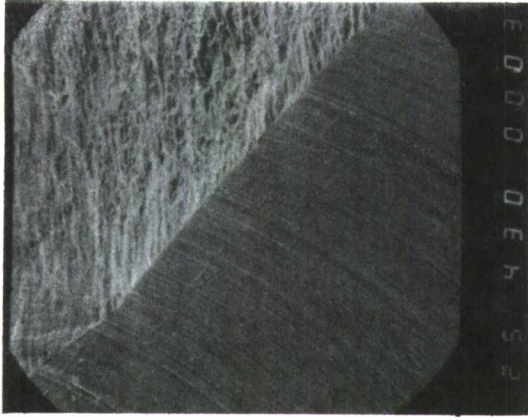


SEM PHOTOGRAPH OF
PRIMARY FATIGUE CRACK
ORIGIN. 43X.

Figure 3-17 Correlation of Eddy Current Inspection to EIFS



**POLAR PLOT SHOWING UNIFORMITY OF HOLE SURFACE.
250 MICROINCHES PER DIVISION**



**SEM PHOTOGRAPH OF PRIMARY
FATIGUE CRACK ORIGIN. 43X**



**LINEAR PROFILOMETER TRACE AT 3:00 ORIENTATION.
250 MICROINCHES PER DIVISION**

C1 Figure 3-18 Correlation of Inspection to Hole Quality (Large EIFS)

Variations in hole dimensions, such as out-of-roundness (OOR) and tapering, can be monitored with eddy current measurements if lift-off effects are not minimized. Eddy current amplitudes were found to correlate with hole OOR. The effect of OOR on the eddy current amplitude can be observed in Figure 3-19. A corresponding plot of eddy current amplitude as a function of OOR, as measured with a dial bore gauge, is shown in Figure 3-20. A larger hole out-of-roundness produces more lift-off, thus causing a larger-amplitude eddy-current signal.

In a manner similar to that used for monitoring out-of-roundness, eddy current techniques can also be used to monitor surface finish in fastener holes, Figure 3-21. If lift-off is not completely minimized, the eddy current signal is more sensitive to a rougher surface, thus causing a larger amplitude signal.

3.3.2 Dial Bore Gauge

From the dial bore gauge readings, a dimensional tolerance parameter was derived for correlation to the EIFS of the fastener holes. Again, no correlation was obtained between these two parameters for no-load transfer specimens, Figures 3-22, 3-23, 3-24, and 3-25. No correlation was obtained between diameters measured and final crack depth. This data is shown in Figure 3-26 for holes drilled by the Winslow technique.

3.3.3 Rotary Proficorder

Polar plots were obtained on all Task I specimens from scans taken with the rotary attachment to a Bendix proficorder. In general, the drilled holes showed larger surface irregularities than the reamed holes. Again, no direct correlation could be obtained from polar plots and EIFS, Table 3-2. The total surface profile of the improved drilled holes indicated better hole quality compared to conventionally drilled holes, Figure 3-27.

3.3.4 Linear Proficorder

Typical linear proficorder traces of no-load transfer specimens are shown in Figure 3-28. Some of the holes showed large gross defects, such as those in Figure 3-29. However, little or no

**Table 3-2 DEPTH OF LARGEST FLAWS FROM POLAR PLOTS FOR NO-LOAD TRANSFER
DRILLED SPECIMENS**

<u>SPECIMEN NO.</u>	<u>DEPTH OF LARGEST FLAW AT THE CRITICAL ORIENTATIONS FROM POLAR PLOTS (μ IN.)*</u>	<u>NO-LOAD TRANSFER SPECIMEN FIGHTER LOAD SEQUENCE EIFS (IN.)</u>
WPF-7	≤ 100	.00121
8	100	.000907
9	100	.00109
10	100	.000631
11	100	.00216
12	100	.000605
13	100	.000665
14	100	.000732
15	100	.00205
16	100	.00122
17	100	.000599
18	100	.000798
19	100	.000643
20	100	.000460
21	100	.00122
22	100	.000638
23	125	.000762
24	100	.000521
25	100	.000676
26	100	.000418
27	100	.000372
28	100	.000396
29	100	.000542
30	100	.000424
31	100	.000537
32	100	.000712
33	100	.000467
34	100	.000635
35	250	.000642
36	100	.000418
37	100	.000457
38	100	.000518
39	100	.000489
40	100	.000489
41	100	.000265
42	100	.000132
43	≤ 100	.000214

*Inspection Resolution Limited to 100 μ In.

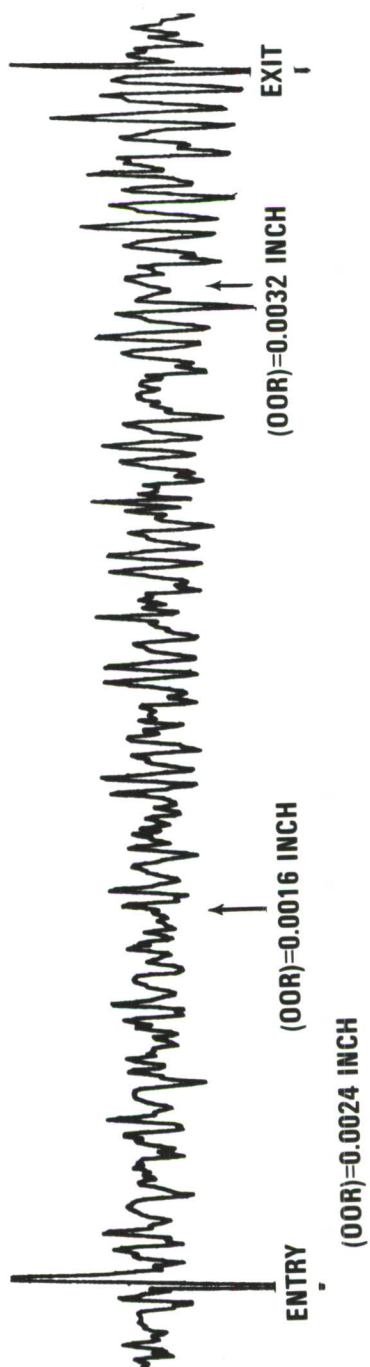
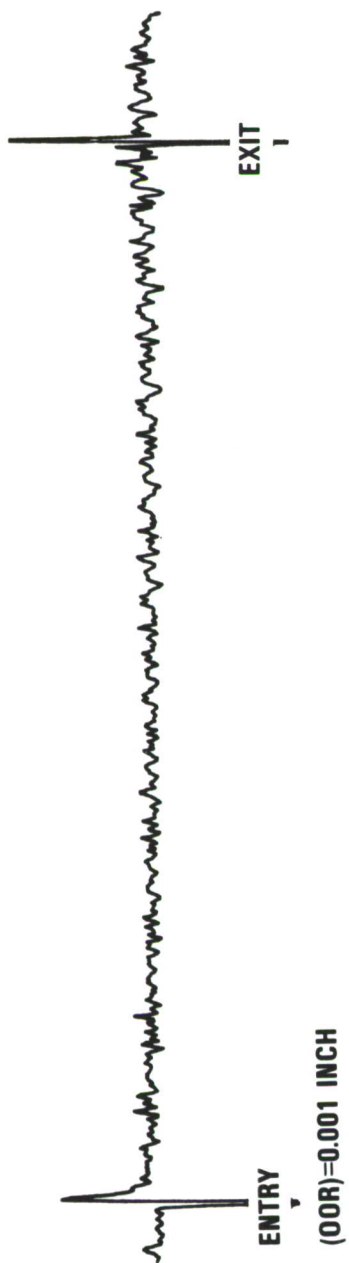
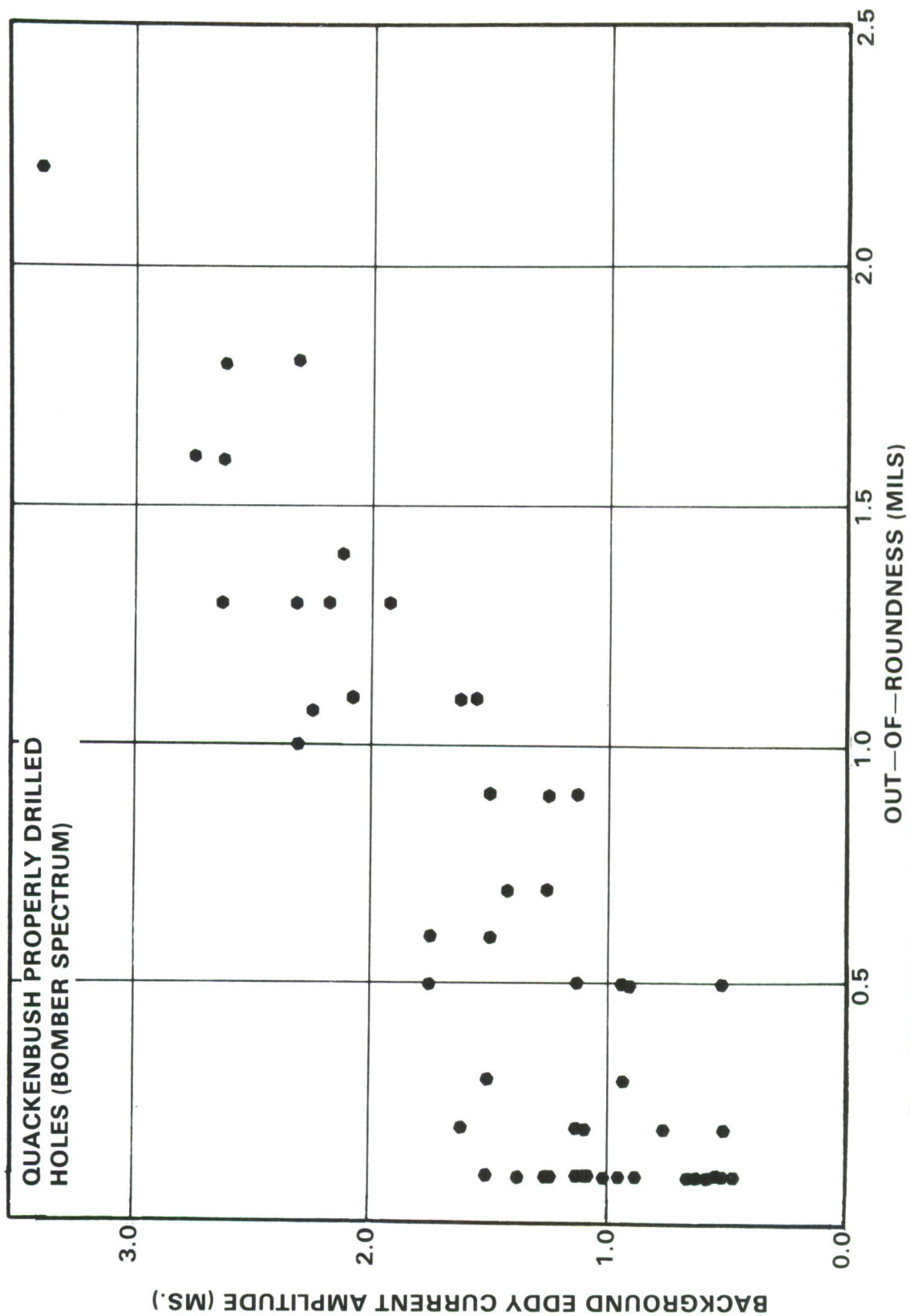


Figure 3-19 Effect of Hole Out-of-Roundness on the Eddy Current Amplitude



ENTRY



ENTRY



ENTRY



Figure 3-21 Effect of Surface Roughness in Fastener Holes on the Eddy Current Signal

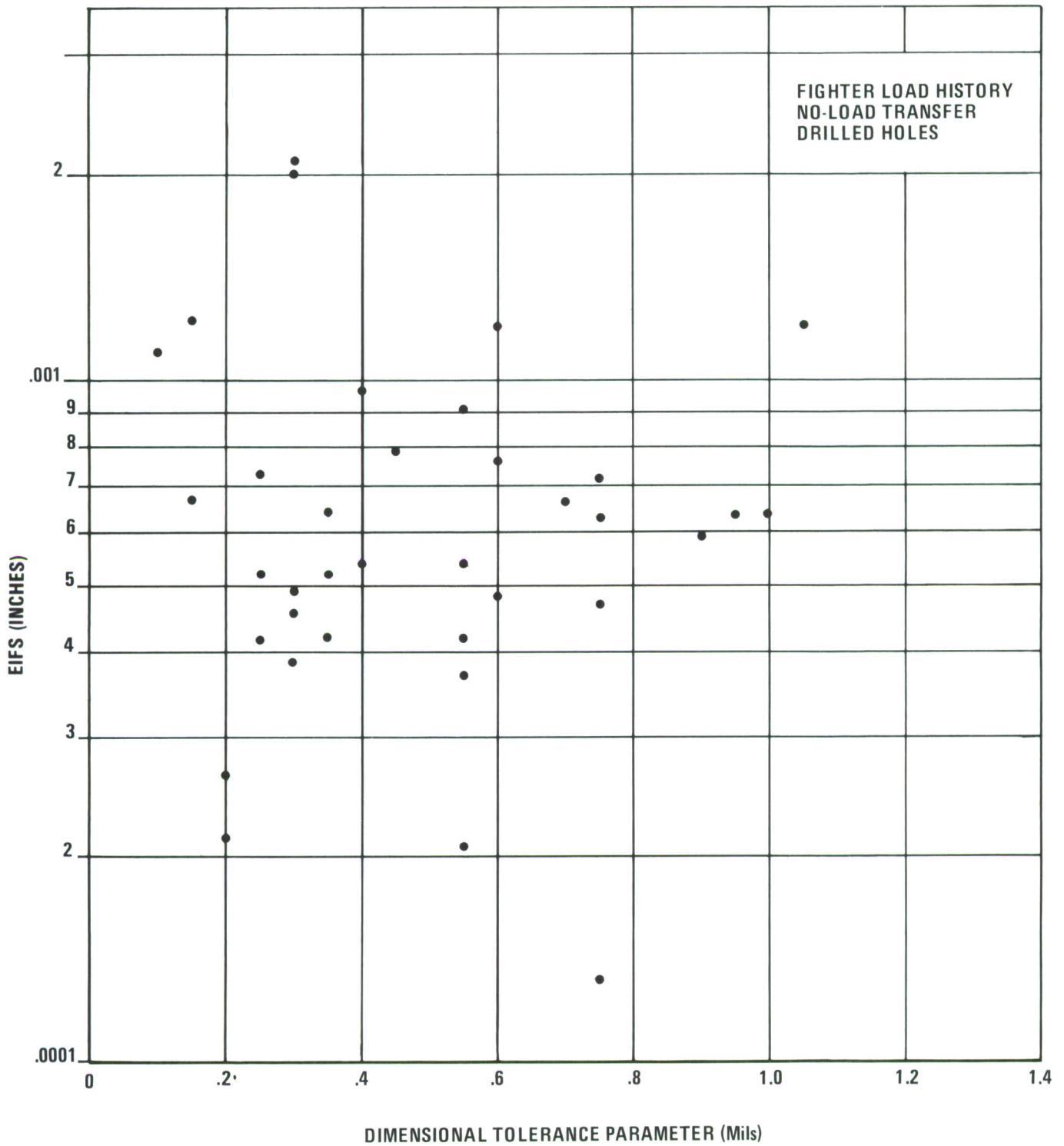
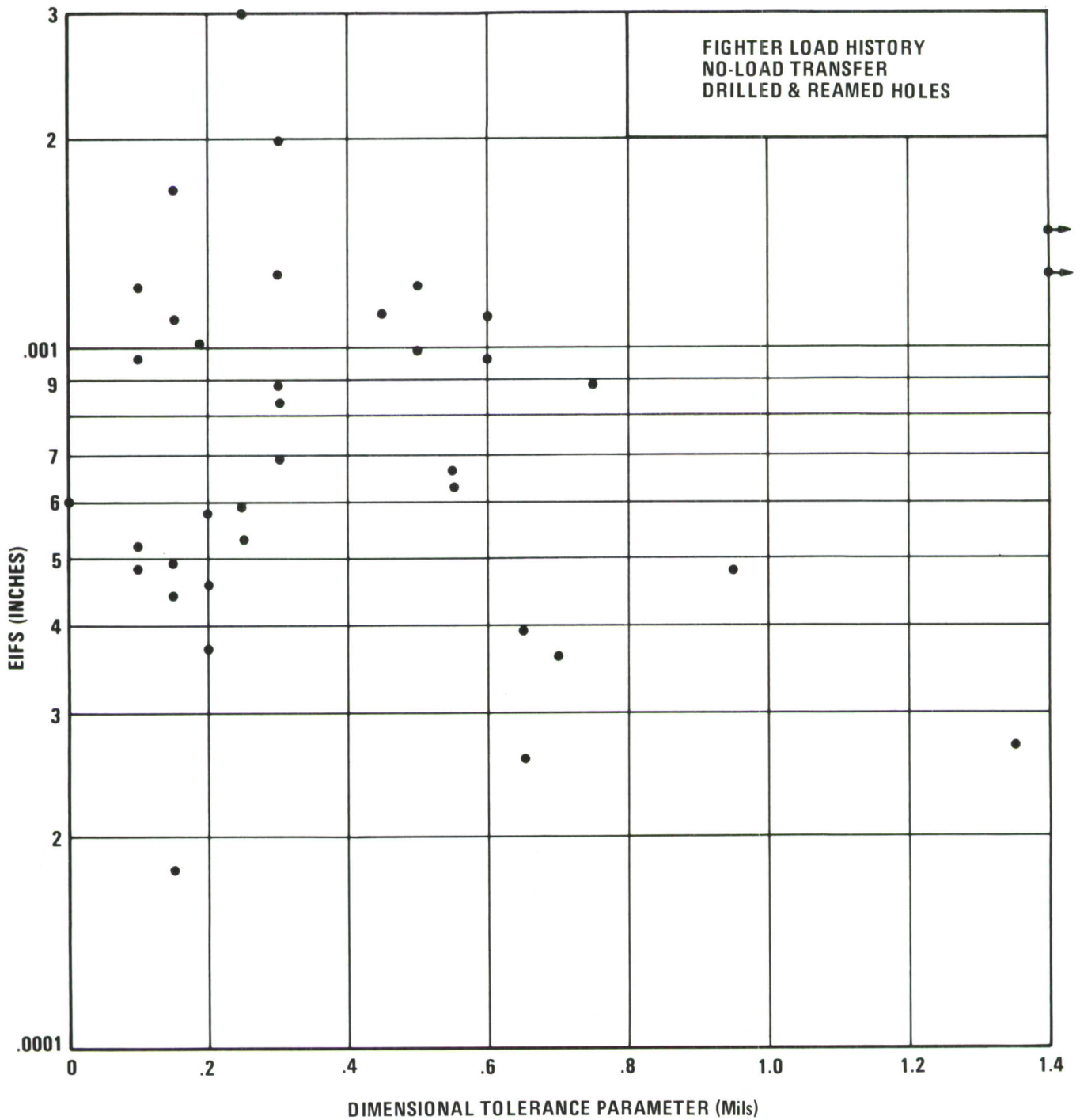


Figure 3-22 Dimensional Tolerance Parameter versus EIFS for Drilled Holes, Fighter Load History



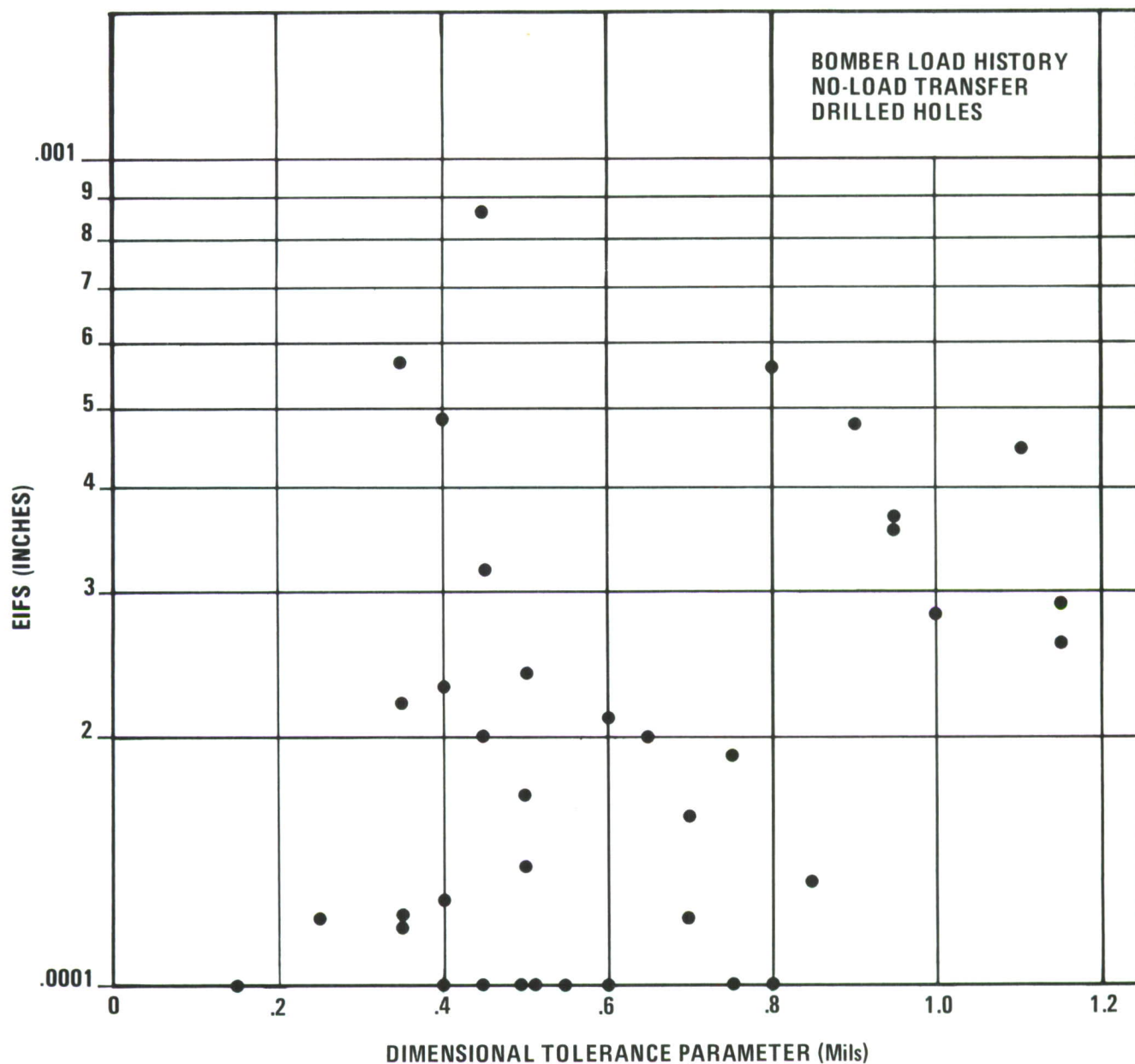


Figure 3-24 Dimensional Tolerance Parameter versus EIFS for Drilled Holes, Bomber Load History

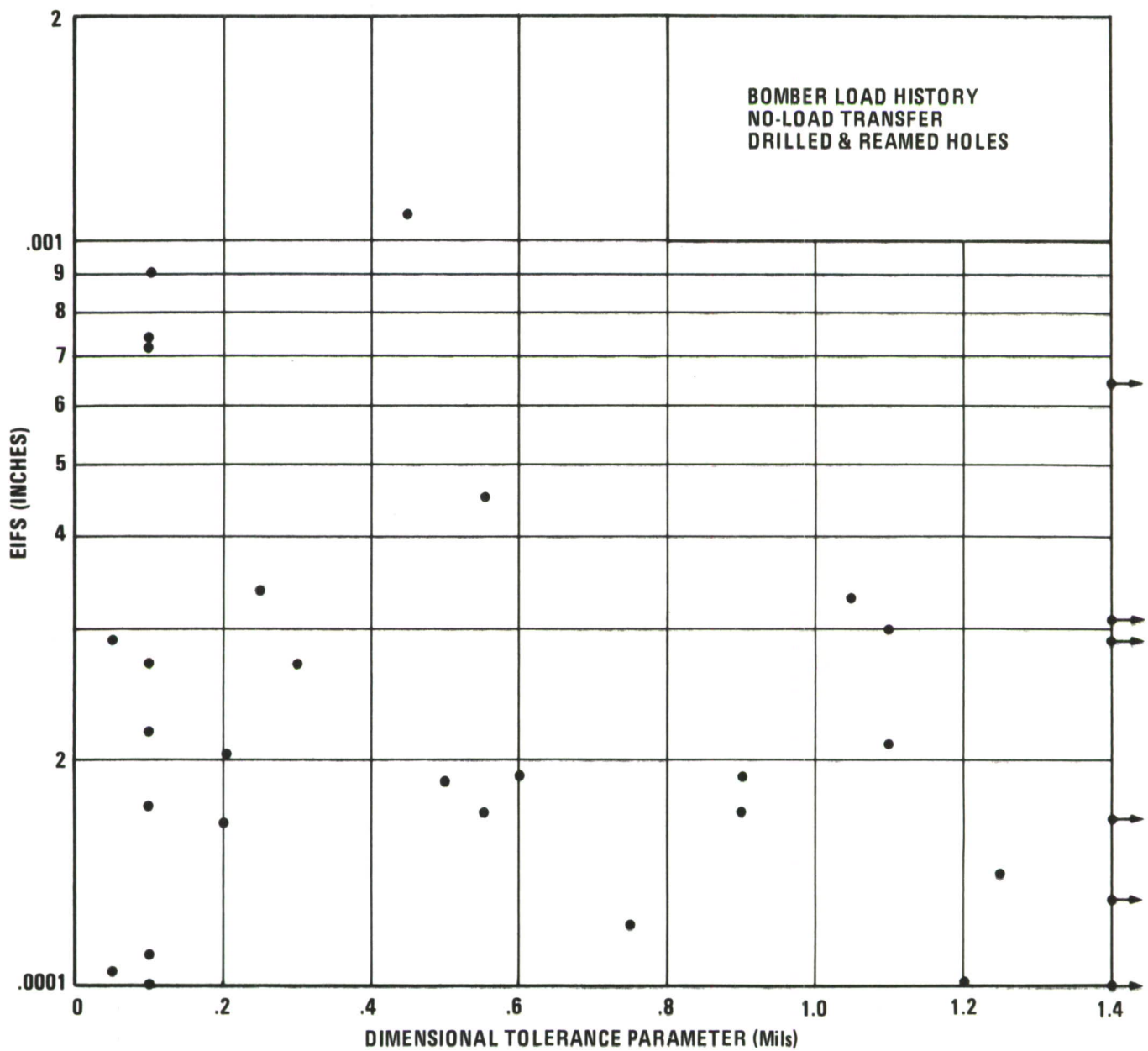


Figure 3-25 Dimensional Tolerance Parameter versus EIFS for Drilled and Reamed Holes, Bomber Load History

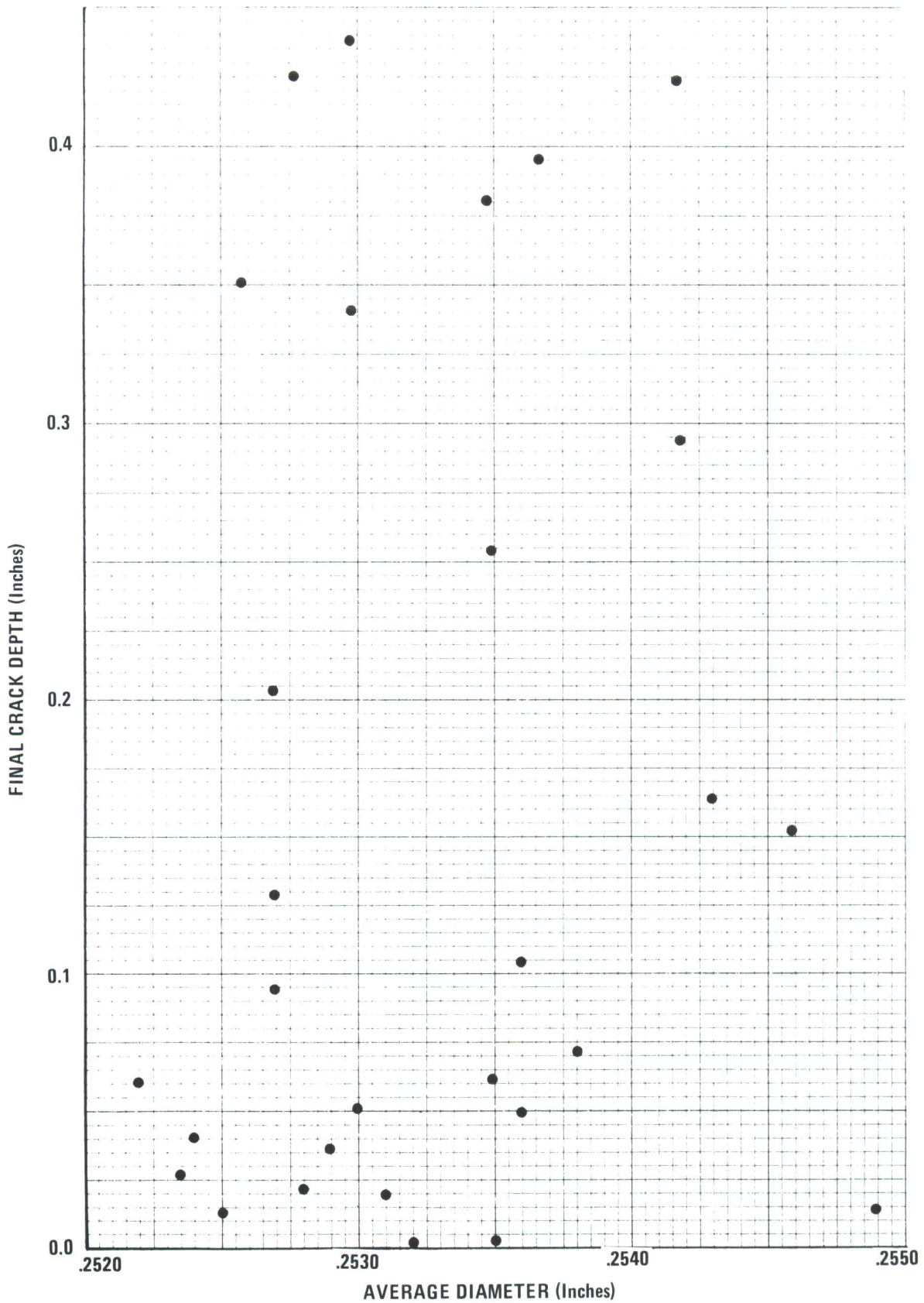
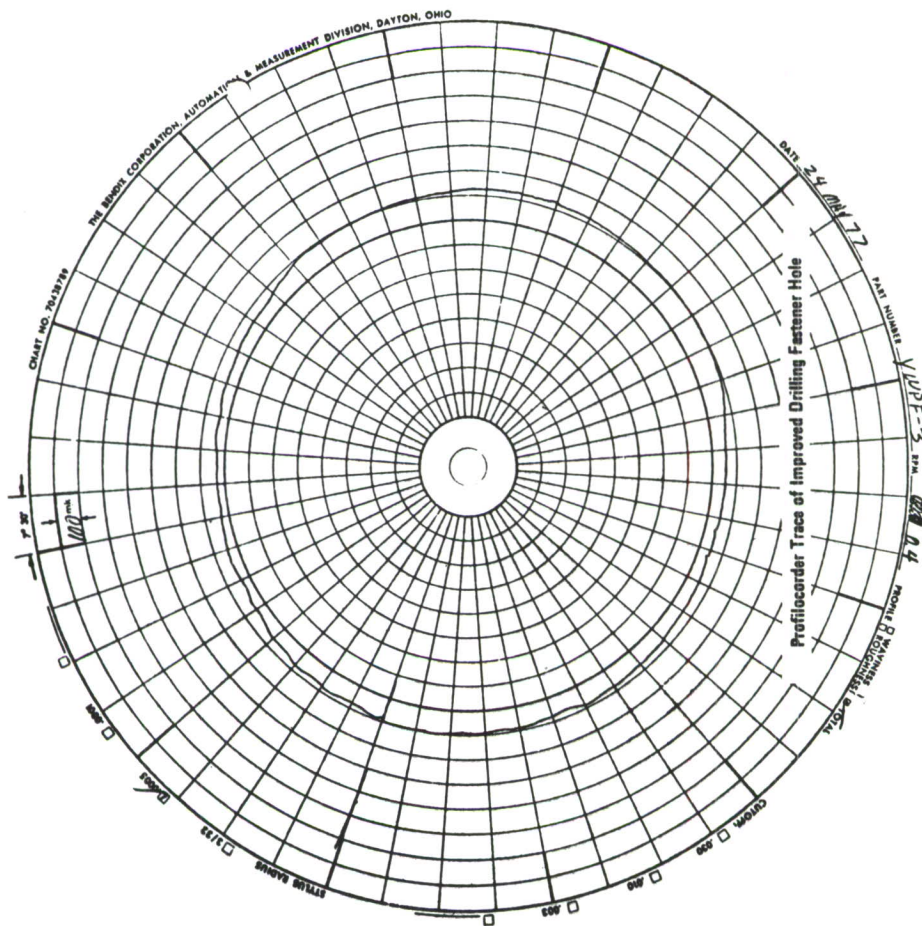


Figure 3-26 Final Crack Depth vs. Average Hole Diameter for Holes Drilled by the Winslow Technique



CHARACTERISTIC RANGE μ $\pm \sigma_T$	IMPROVED DRILLING	CONVENTIONAL DRILLING
	.2515" - .253" .2518" .0003"	.2515" - .256" .2524" .0007"

Figure 3-27 Typical Properties of Conventional and Improved Drilling

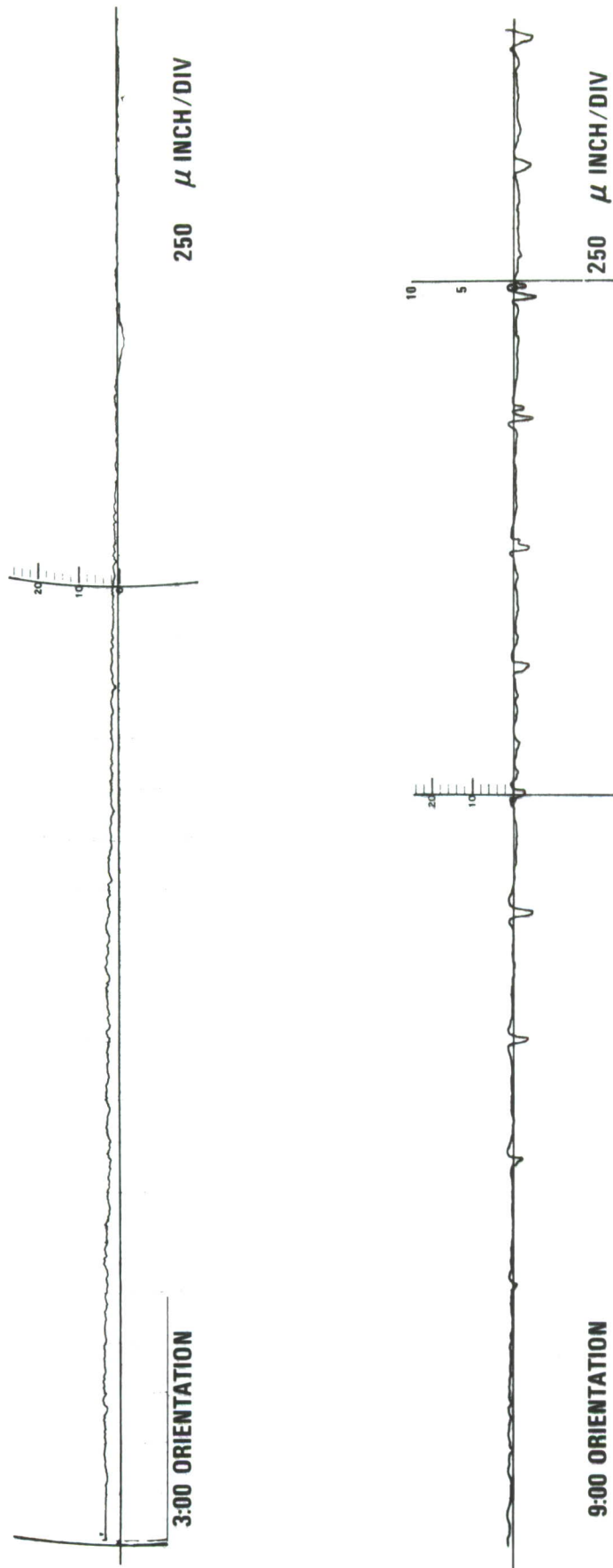


Figure 3-28 Linear Proficorder Scans Showing Total Surface Profile for Two Quackenbush Properly Drilled Holes

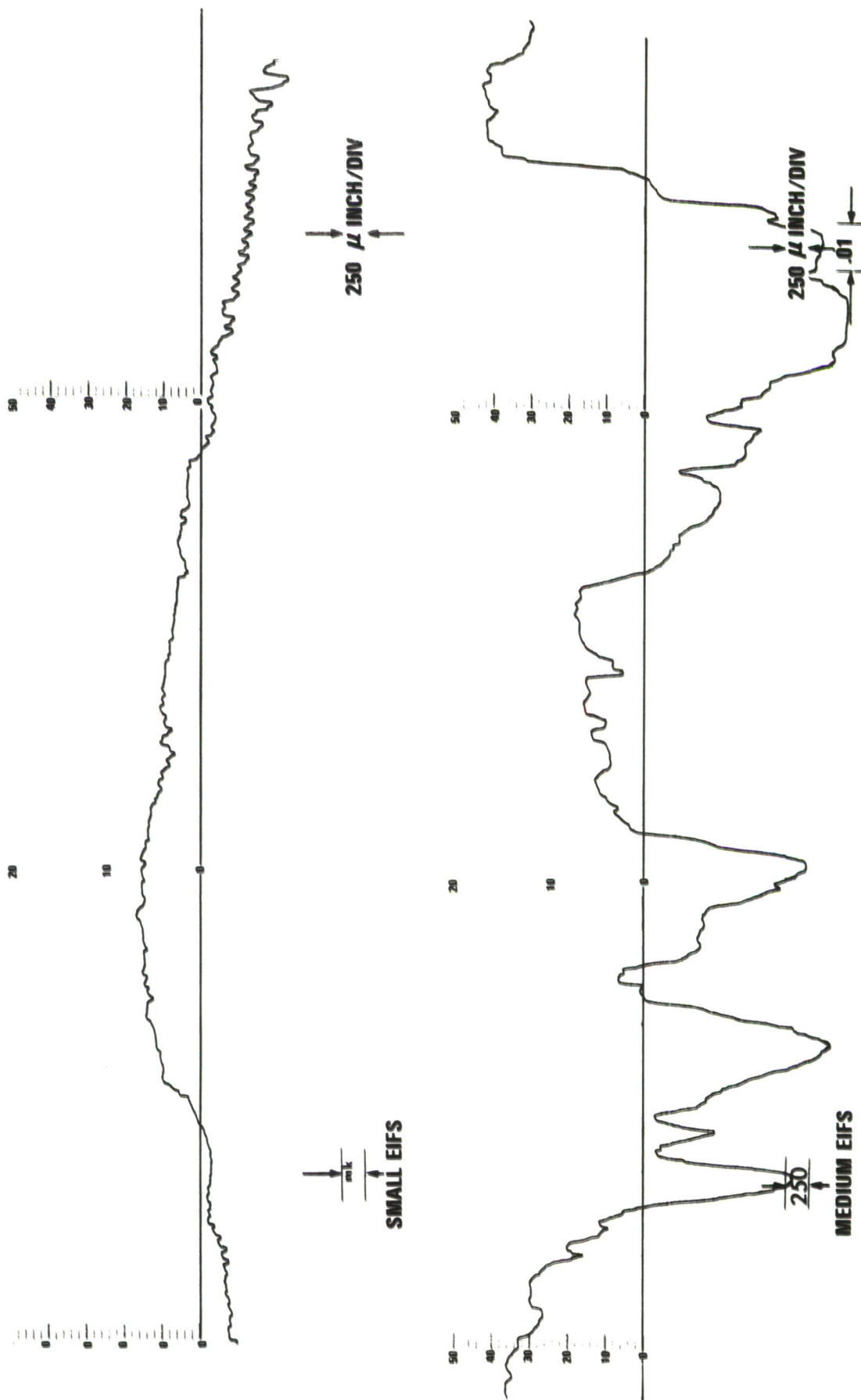


Figure 3-29 Linear Proficorder Scans Showing Total Surface Profile for Two Window Improperly Drilled Holes

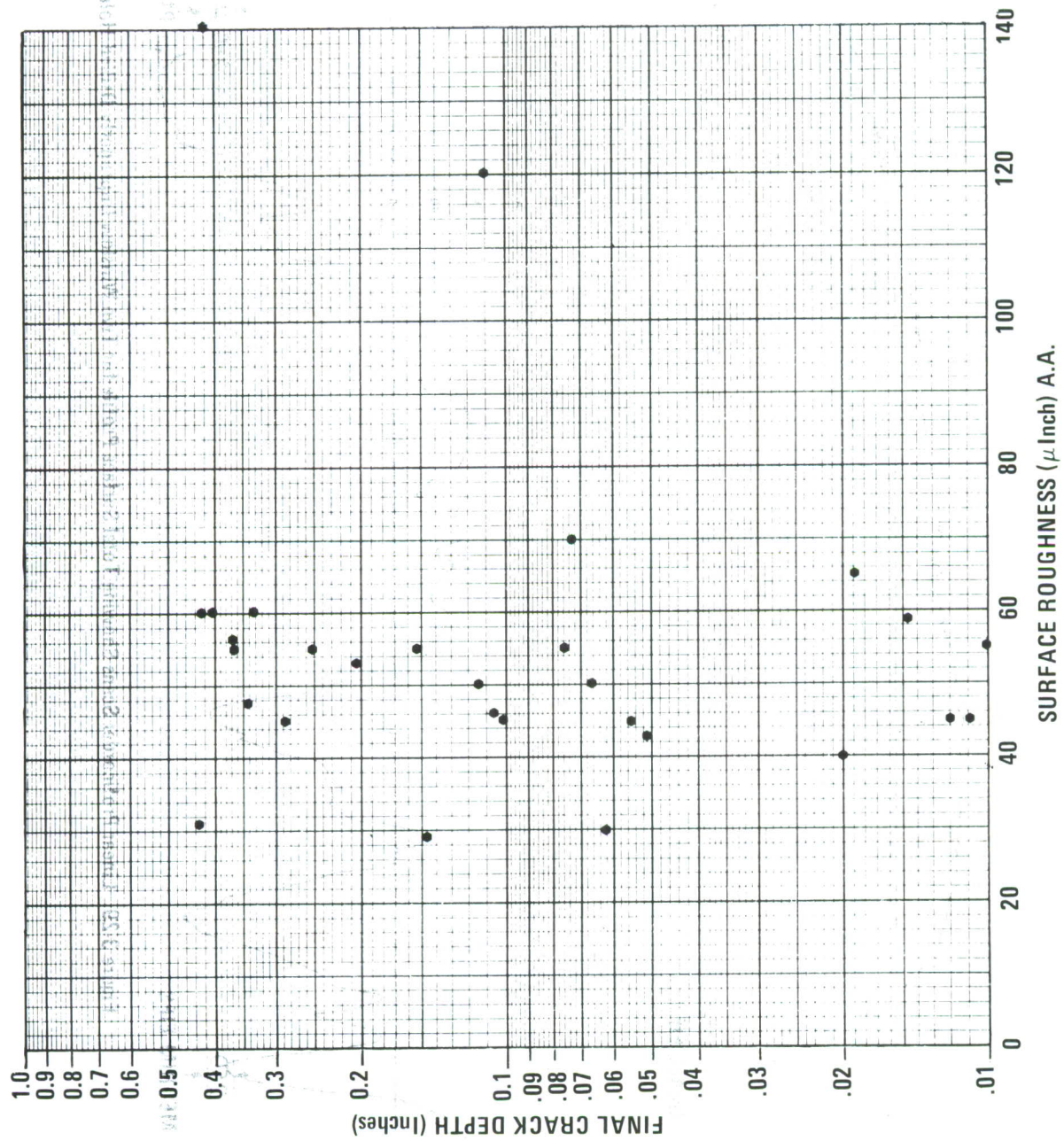


Figure 3-30 Surface Roughness As a Function of Crack Depth

correlation could be obtained between these defects and EIFS or surface roughness and EIFS, Figure 3-30. Good agreement was obtained by the different NDE techniques in identifying defects such as wide grooves, Figure 3-31. One of the disadvantages of the linear proficorder trace was that the scan was made parallel to the thickness in the 3 o'clock and 9 o'clock orientations. Consequently, small vertical scratches lying parallel to the direction of scanning were missed.

3.3.5 Ultrasonics

From the ultrasonics data, the reflected ultrasonic signal amplitude was used for correlation to the EIFS of the fastener holes. Shown in Figure 3-32 are the results obtained for no-load-transfer drilled specimens exposed to a fighter load history. Again, no correlation was obtained between the two parameters. Only the larger gross defects, such as found in a double-drilled hole, could be resolved with ultrasonics, Figure 3-33.

3.4 SCANNING ELECTRON MICROSCOPE INVESTIGATION

Original program objectives required hole quality to be monitored during manufacture by NDI-based techniques. As previously mentioned, there existed no correlation between EIFS or fatigue life with NDI results. There also existed unexplained anomalous behavior of transition-fit relative to clearance-fit fastener holes - mainly that the EIFS and crack-depth cumulative probability distributions were lower for clearance-fit than transition-fit fastener holes. This lack of correlation and the anomalous behavior precipitated the scanning electron microscope (SEM) investigation.

The presence of this defect served to explain the lack of correlation of NDI to fatigue behavior and the anomaly of longer life for drilled-and-drilled and reamed holes.

Figures 3-34 and 3-35 show the morphology of a scratch in the bore of a clearance-fit and transition-fit fastener holes, respectively. In both cases the fatigue crack initiated at axial scratches. The cause of the axial scratches was isolated and traced back to the actual hole production equipment.

The drilling equipment used to produce clearance-fit fastener holes was modified to alleviate the cause of the axial scratches. Results of these modifications are shown in Figure 3-36. There are two prominent features in these micrographs - the absence of axial scratches and point-source initiation of fatigue cracks.

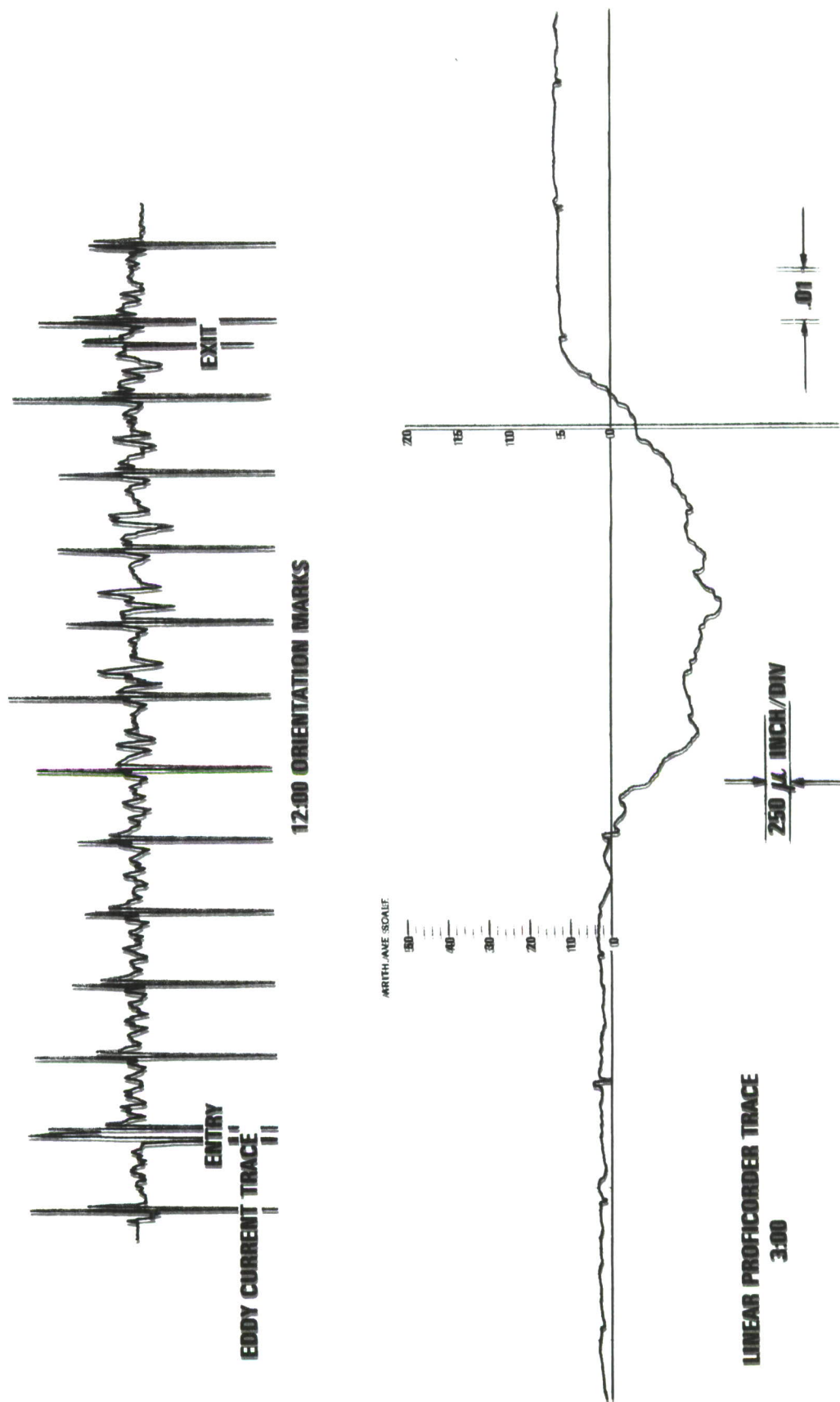


Figure 3-31 Eddy Current and Linear Proficorder Trace (Specimen QPF-10; Wide Groove at the 3:00 Orientation)

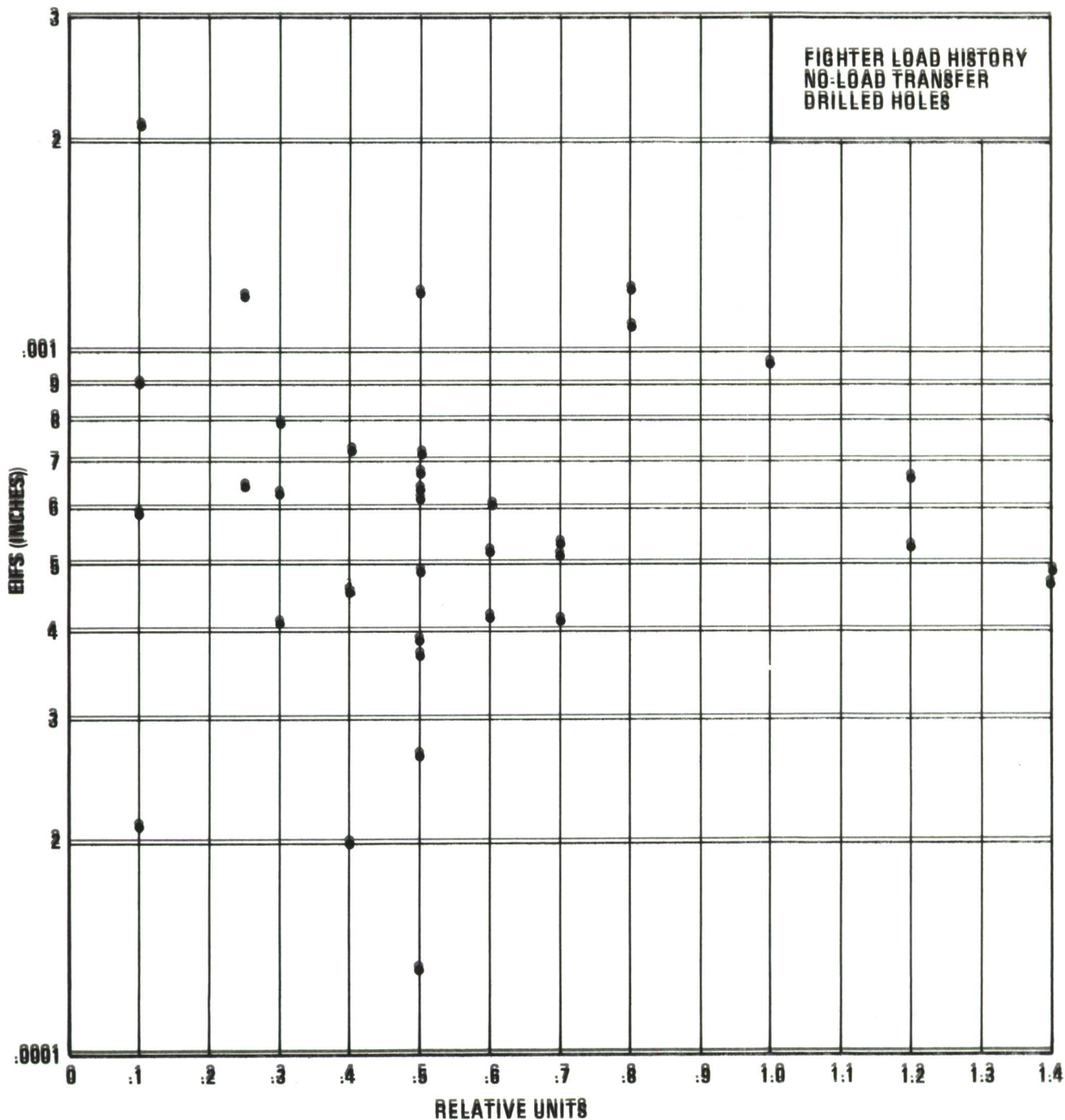


Figure 3-32 Reflected Ultrasonic Signal Amplitude versus EIFS

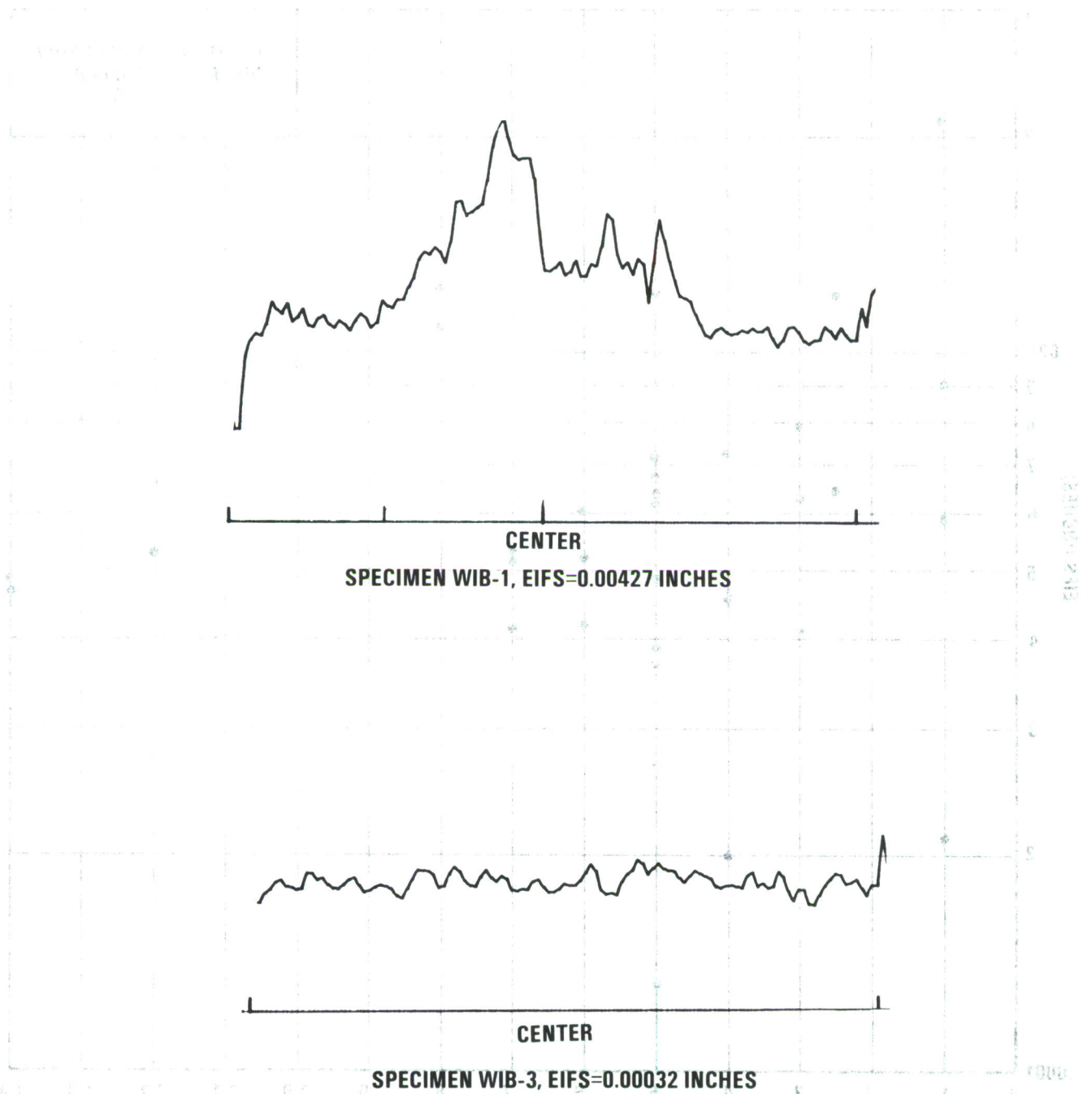


Figure 3-33 Reflected Ultrasonic Waveforms Showing the Effect of a Double-Drilled Hole on the Reflected Waveform

Figure 3-32 Fatigue Crack Initiating from a Scratch in a Drilled and Resin-Bonded Fastener Hole

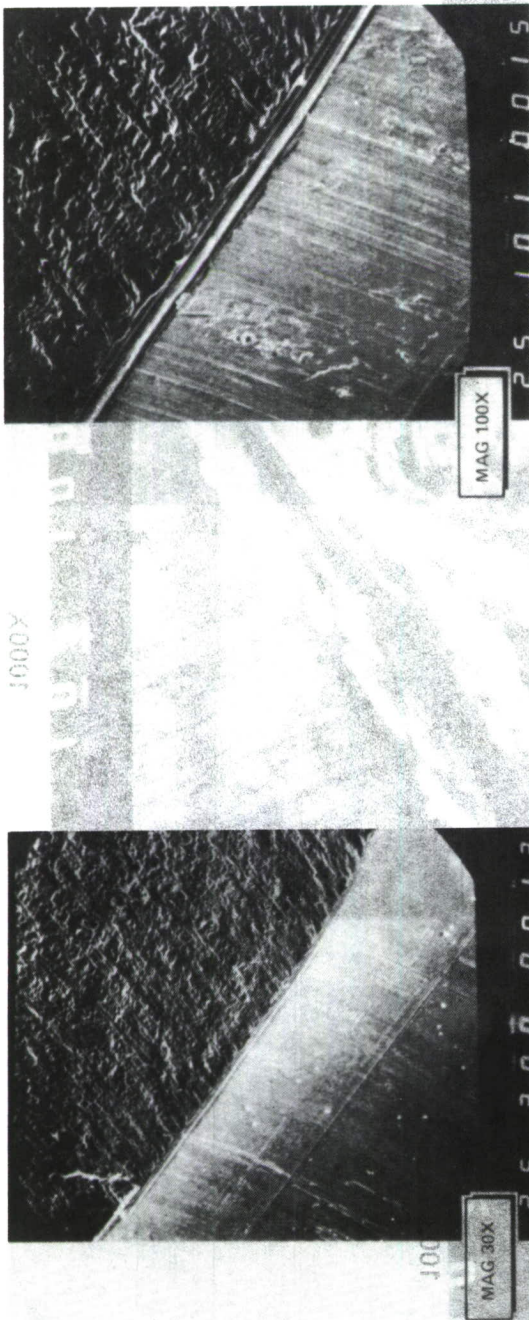


Figure 3-34 Morphology of a Scratch — Properly Drilled Fastener Hole (Large EIFS)

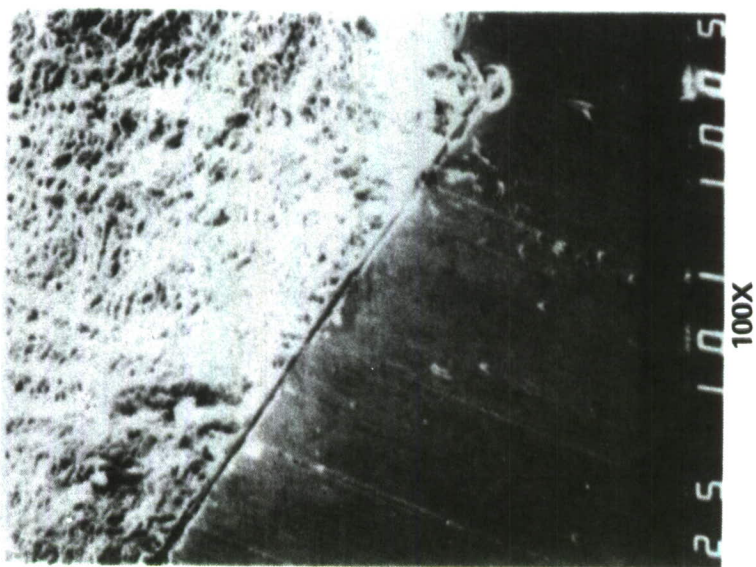
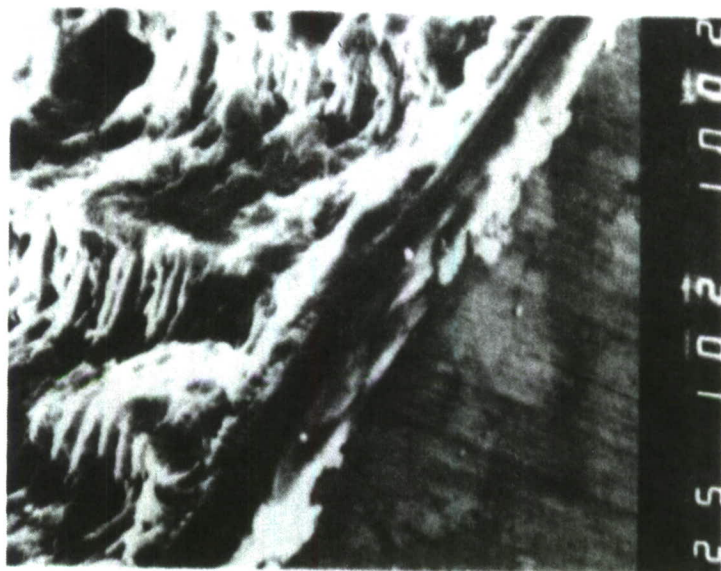
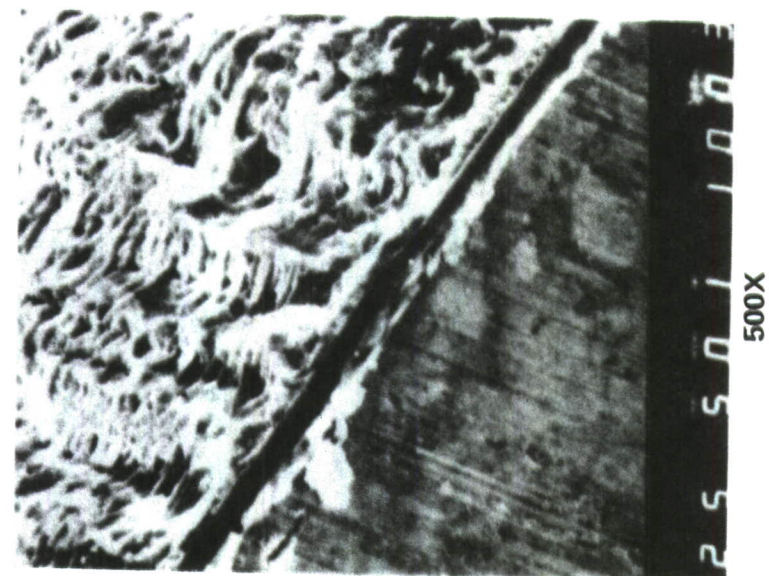


Figure 3-35 Fatigue Crack Initiating from a Scratch in a Drilled and Reamed Fastener Hole

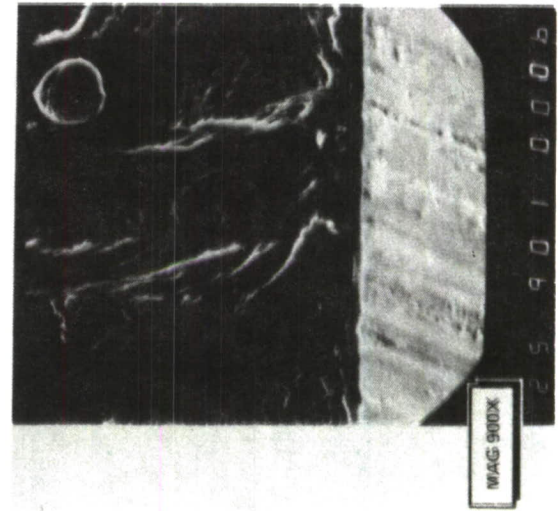
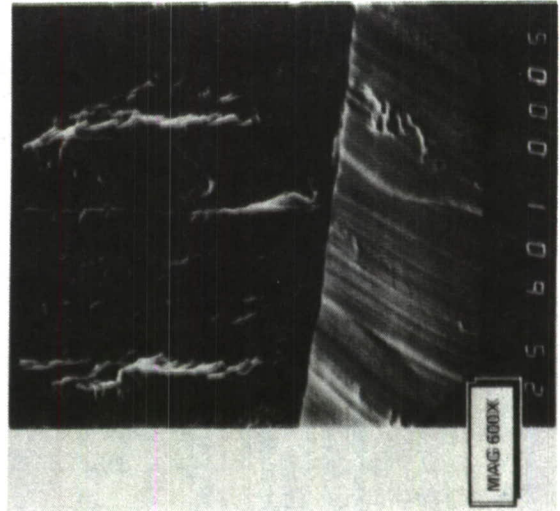
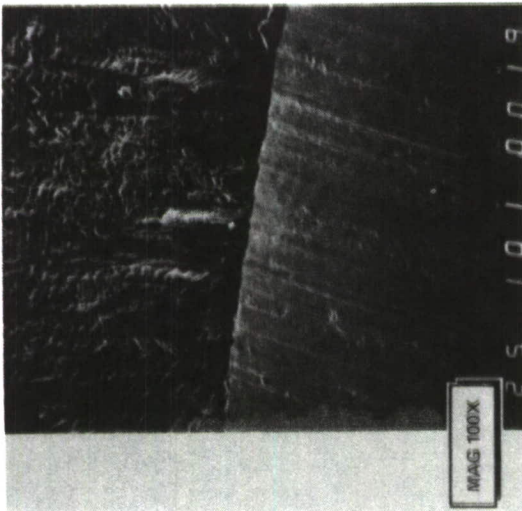


Figure 3-36 Morphology of a Crack Initiating from a Point Source, Improved Drilling Fastener Hole (Small EIFS)

3.5 IMPROVED DRILLING

Modifications made to the Winslow Spacematic drilling equipment were introduced into Task I. The objective to increase the fatigue life of a structure containing fastener holes was attempted through close control of the drilling process. The improved drilling specimens were tested using the most severe load history, i.e., the fighter spectrum.

The improvements in fatigue life for improved drilling are shown in Figures 3-37 and 3-38. EIFS cumulative probability distribution of Figure 3-37 reflects a three-fold decrease for improved drilling with respect to conventional drilling. A more dramatic effect is seen in Figure 3-38 where 90-percentile crack depth values for conventional drilling are five times those for improved drilling. A seven-fold decrease in crack depth at 1.5 lives is shown in Figure 3-39 for improved drilling versus conventional. The gains in fatigue life available through the implementation of improved drilling are tangible and realistic.

3.6 COMPARISON OF RESULTS

Table 3-3 contains 50- (mean) and 90-percentile EIFS and crack depths at one life for both hole production techniques and the fighter spectrum. In both cases of clearance-fit fastener holes for EIFS and crack depth, the improper drilling technique yielded larger values. Improper drilling can thus be assumed to be a process inferior to conventional drilling. On the other hand, the transition fit resulted in approximately the same values for proper and improper techniques. Thus, the transition-fit technique proved to be insensitive to those variables and conditions thought to be abusive. A comparison of the conventional clearance-versus transition-fit values is of interest. The less-expensive-to-produce clearance fit fastener hole is on all counts equal to or lower than the transition-fit fastener holes.

This somewhat anomalous behavior was explained through the SEM investigation. It was shown that the major topological difference between clearance- and transition-fit fastener holes was the morphology of the axial scratches found therein. In both cases, fatigue-crack initiation occurred at the scratches. Wide discontinuous scratches were the predominate morphology found in the clearance-fit holes, while long, narrow scratches were found in the transition-fit fastener holes. The relative behavior can be

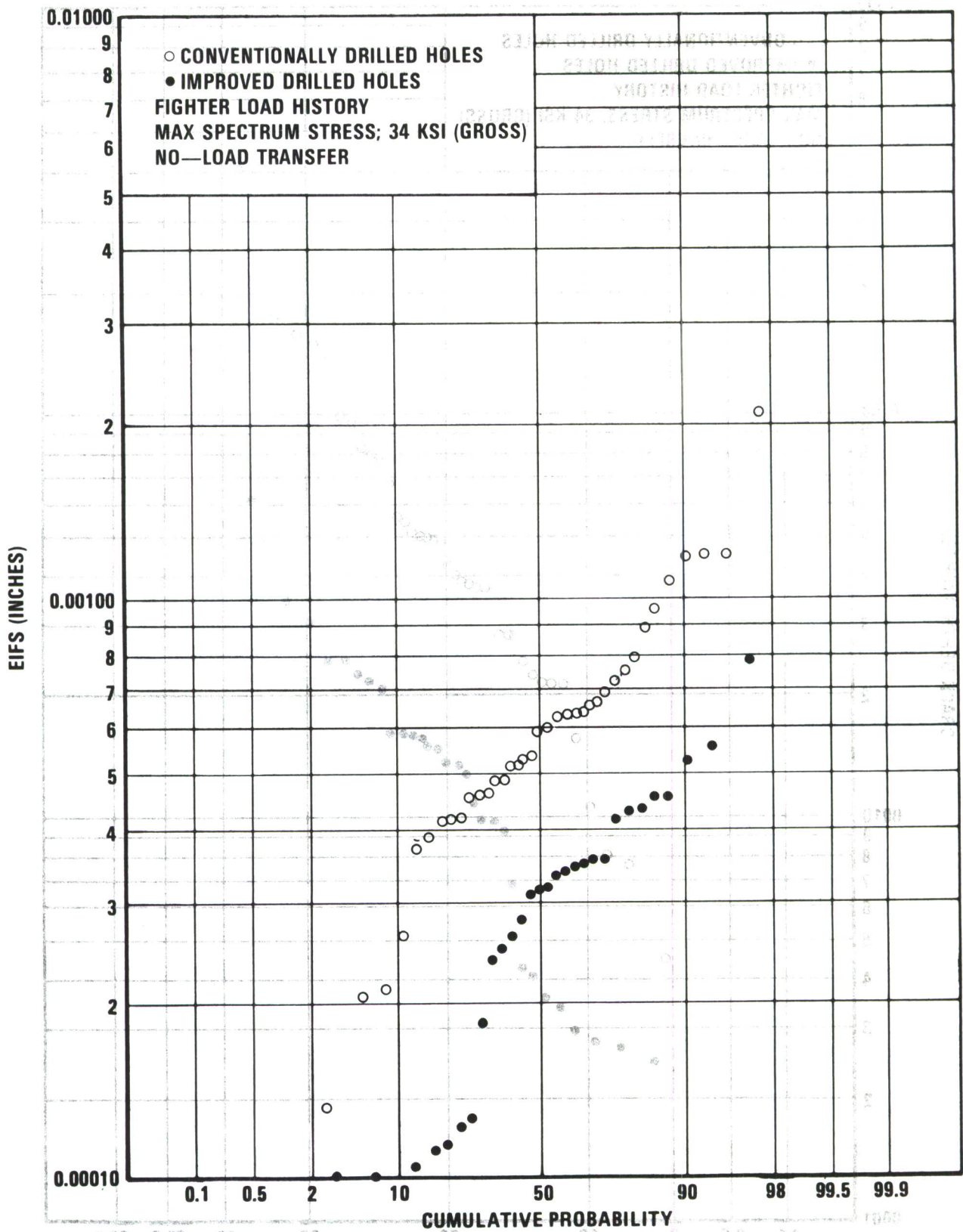


Figure 3-37. EIFS for Conventionally Drilled and Improved Drilled Holes

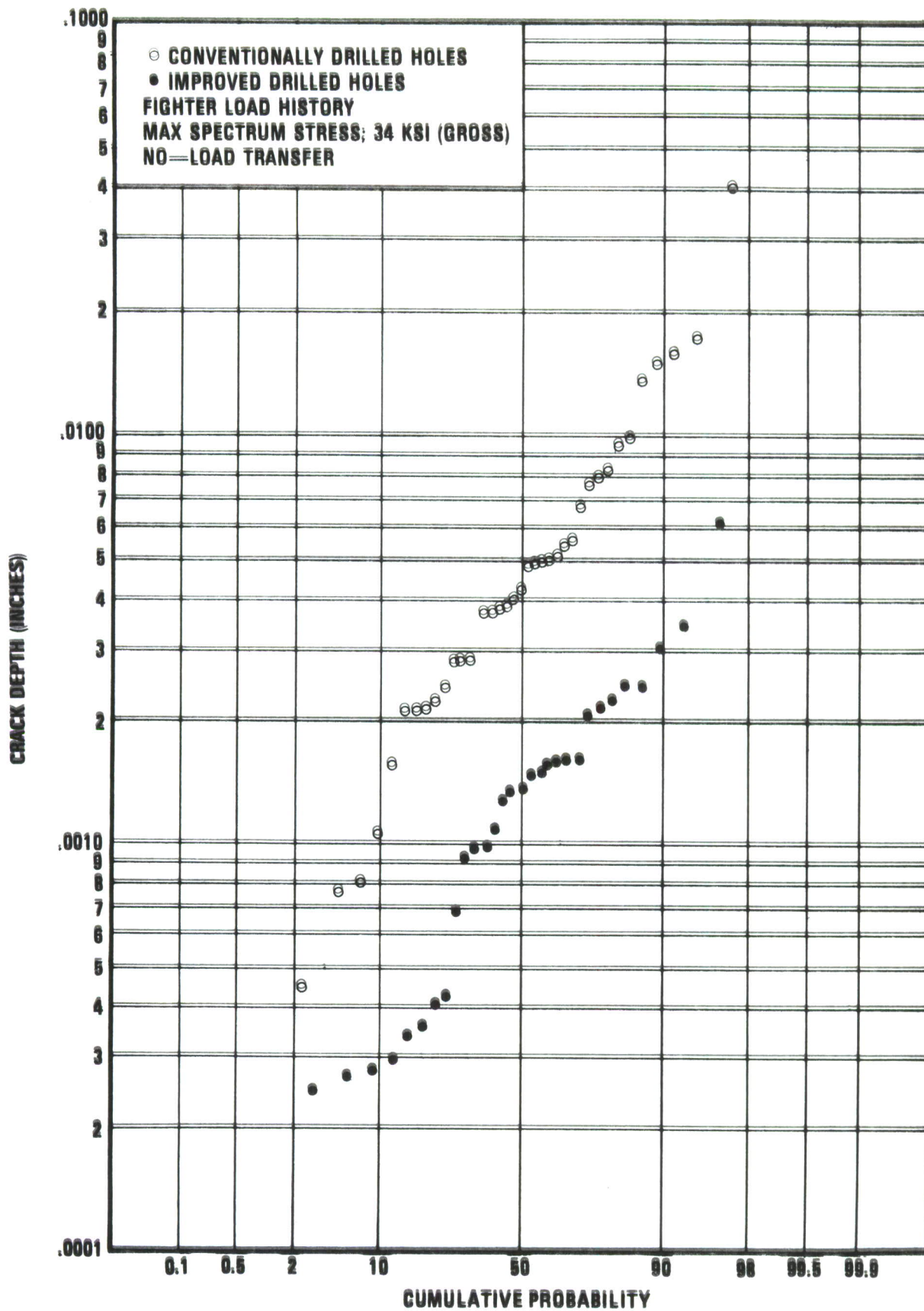


Figure 3-38 Crack Depth at One Life for Conventionally and Improved Drilled Holes

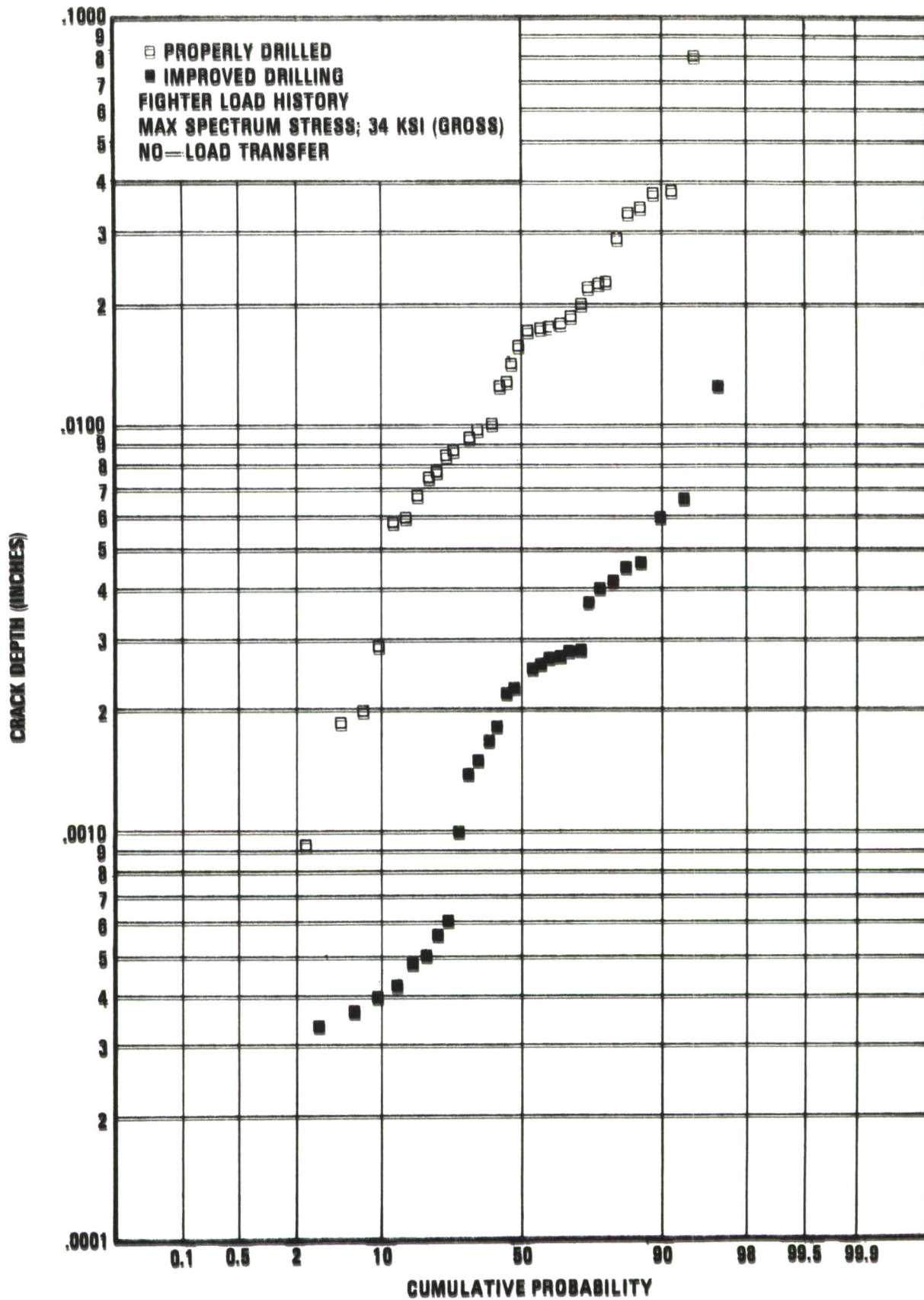


Figure 3-39 Crack Depth at 1.5 Lives

Table 3-3 CUMULATIVE PROBABILITY RESULTS FOR TASK I NO-LOAD TRANSFER, FIGHTER SPECTRUM

TASK	HOLE PRODUCTION TECHNIQUE	EIFS (INCHES)		CRACK DEPTH AT 1 LIFE (INCHES)	
		50 PERCENTILE (MEAN)	90 PERCENTILE	50 PERCENTILE (MEAN)	90 PERCENTILE
I	Conventional Drilling	0.0006	0.0012	0.0043	0.016
	Improper Drilling	0.0012	0.0019	0.017	0.025
IB	Improved Drilling	0.00032	0.00052	0.0014	0.003
	Conventional Drill & Ream	0.0007	0.0014	0.064	0.021
	Improper Drill & Ream	0.0007	0.0015	0.066	0.020

explained through fracture mechanics. The clearance-fit fastener holes showed a tendency to initiate fatigue cracks at point sources within the discontinuous scratches. This initiation mechanism is shown in Figure 3-40, where the initial $a/2c$ ratio is equal to 0.5 and fatigue-crack propagation occurs in a well-behaved manner. Crack fronts resulting from point-source initiation are seen in Figure 3-41. Transition-fit fastener holes with the continuous scratches tended to initiate multiple cracks simultaneously. This behavior is manifested in Figure 3-42, where multiple initiation yields an $a/2c$ ratio much less than 0.5. Crack growth is unstable, i.e., fast crack growth is in the "a" or depth direction until the 0.5 equilibrium ratio is achieved. Flat crack fronts resulting from this behavior are seen in Figure 3-43. Thus the fatigue cracks initiating in the bore of a transition -fit fastener hole, i.e., drilled and reamed, will have a greater propensity to grow more rapidly than a crack in a clearance-fit fastener hole.

Obviously the morphology of a scratch in a transition-fit fastener hole is narrower, smaller in radius, and more continuous than a scratch in a clearance-fit hole and, therefore, is a more severe condition in fatigue. Why a clearance-fit hole is affected less is a function of the dimensional tolerance. The clearance-fit tolerance range is 0.250 - 0.253 inch, leaving a maximum radial clearance of 0.0015 inch between the hole and tool. The corresponding values for transition-fit holes are 0.2500 - 0.2507 inch, yielding a maximum radial clearance of 0.00035 inch. The chips produced by the reaming process are much smaller, discontinuous in nature, and not removed by the straight flutes of the reamer. These relative radial clearances combined with the geometry of these chips best explains the source of the scratches, differences in scratch morphology, and severity in fatigue.

The major objective of this task, fatigue life extension through process control, was achieved through the use of improved drilling. EIFS and crack depth cumulative probability distributions were reduced significantly, as shown in Table 3-3 and Figures 3-37, -38, and -39. The driving force behind improvements to the drilling process was to remove those scratches observed to be caused by that process. The elimination of those scratches removed the cause for rapid crack growth following initiation at a scratch. The initiation behavior was that shown in Figure 3-40 basically point-source initiation followed by stable crack growth.

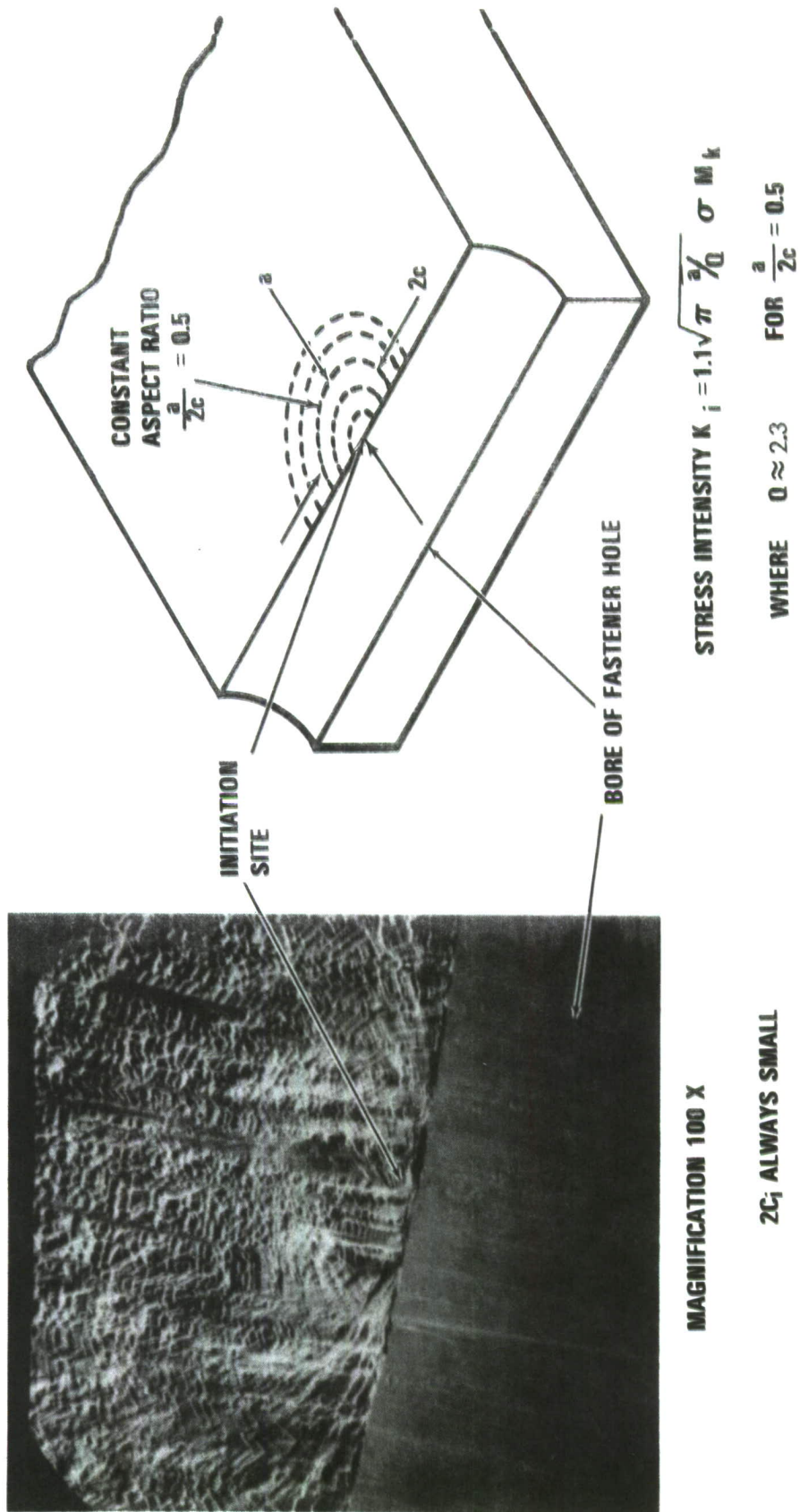
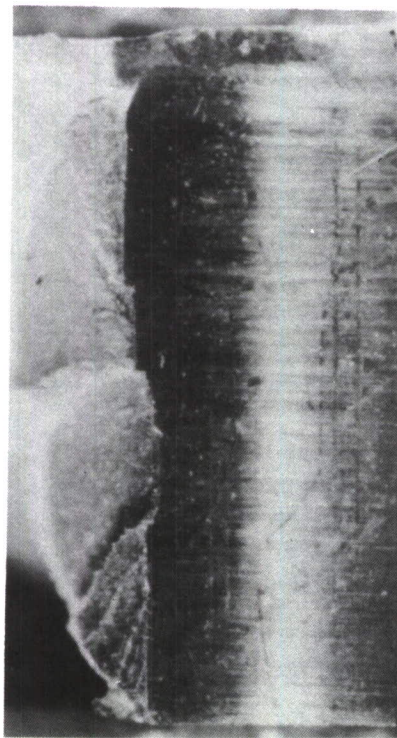
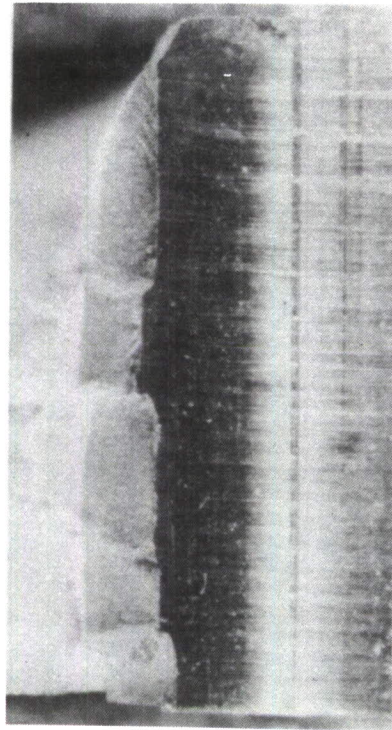


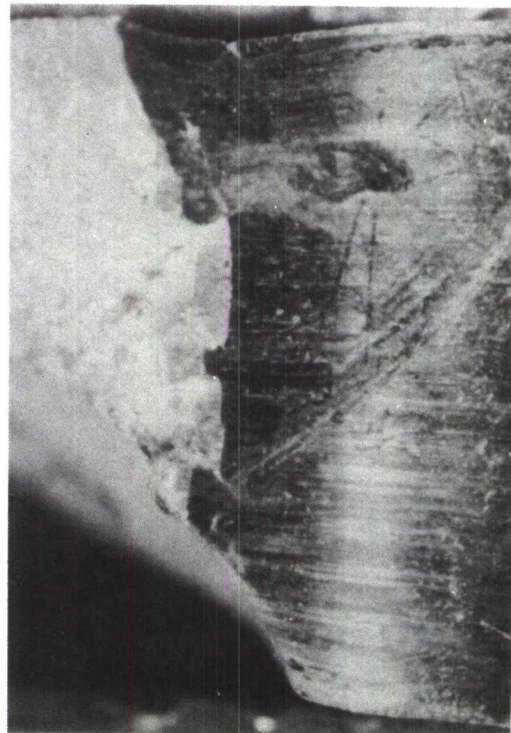
Figure 3-40 Behavior of Fatigue Crack Initiating at Point Source



— — — — —



— — — — —



— — — — —

Figure 3-41 Crack Front Morphology Due to Point Source Initiation

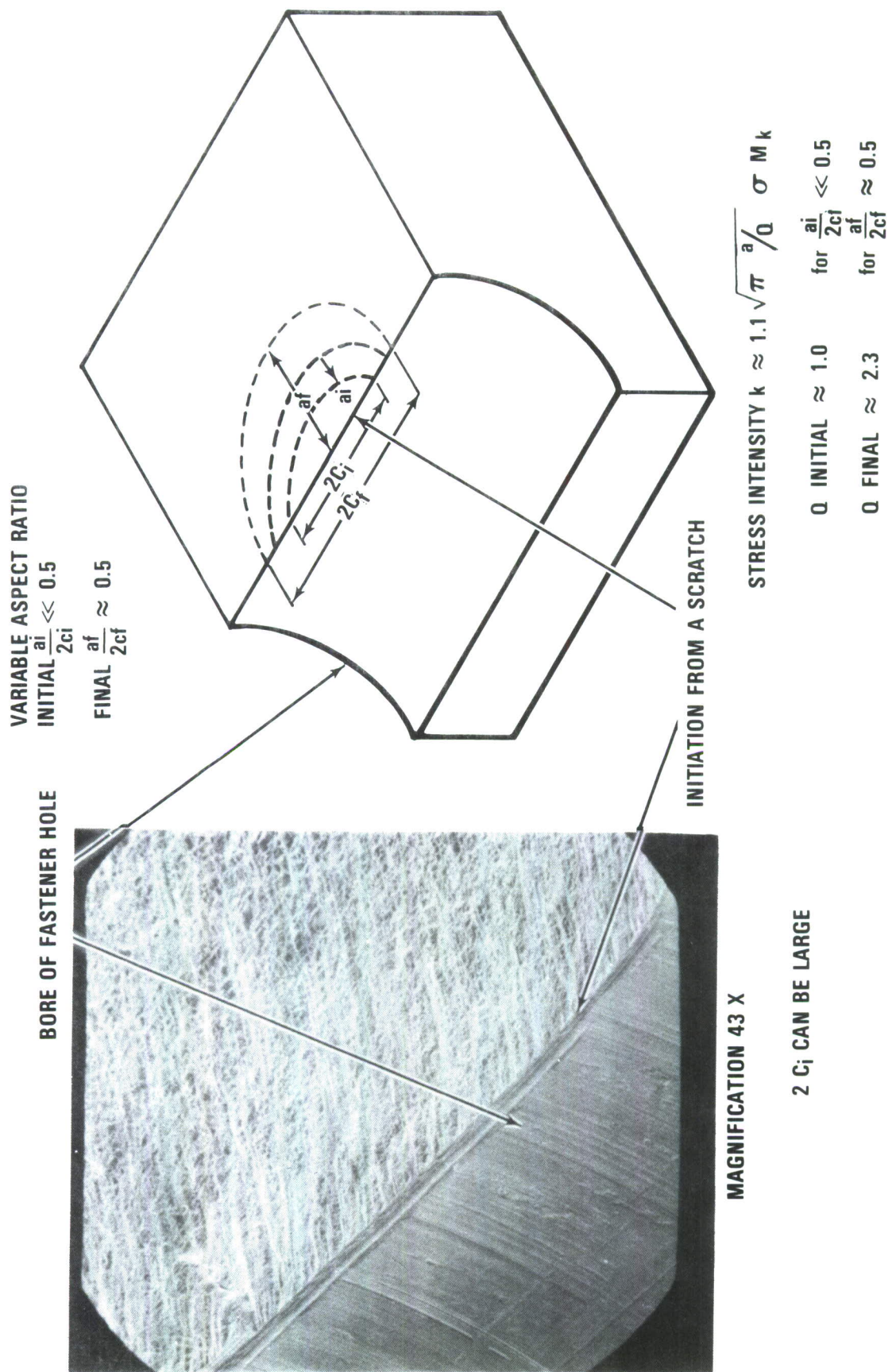
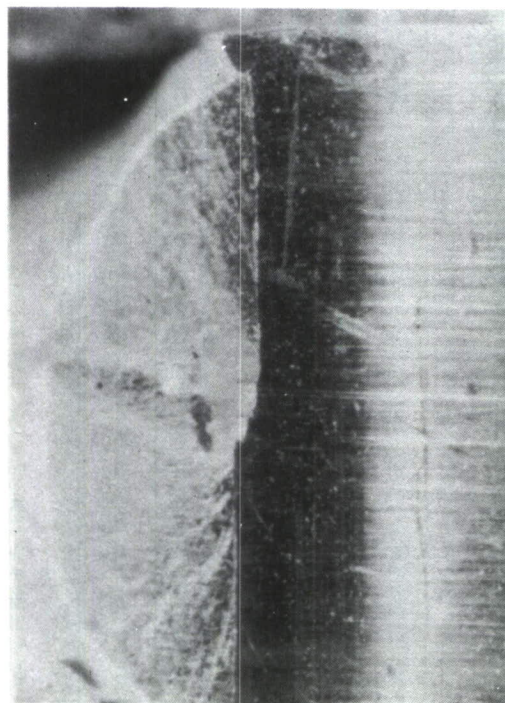
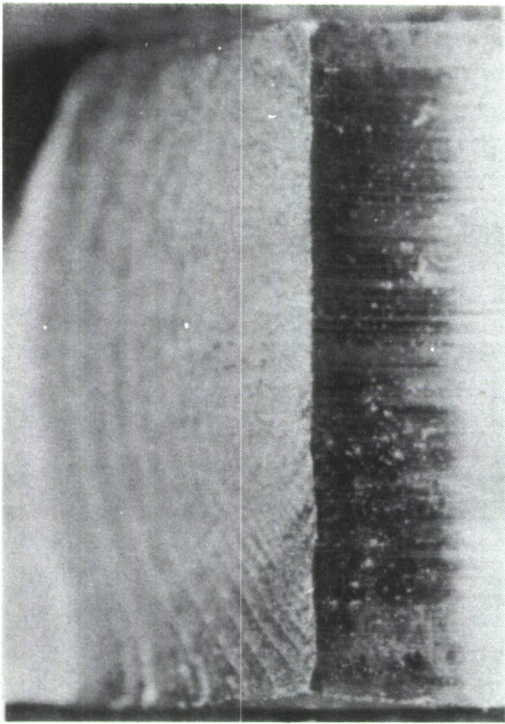
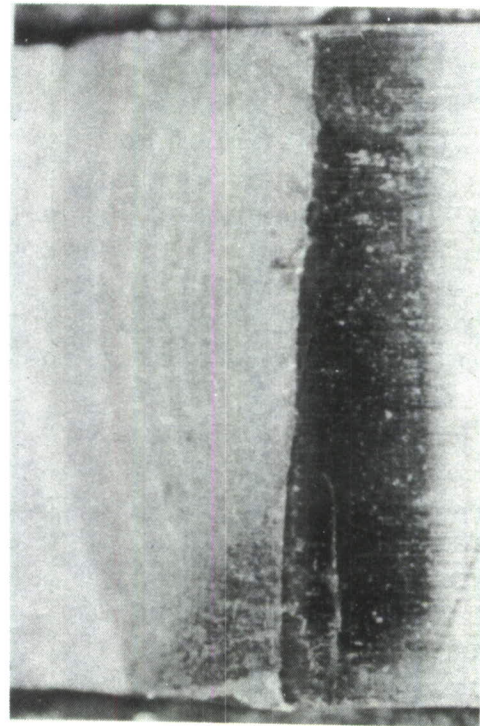


Figure 3-42 Behavior of Fatigue Crack Initiating from a Scratch



—

—



—

Figure 3-43 Initiation of a Line Source Yielding a Single Plane Crack

The analogy previously used to show the difference between crack-growth rates in clearance-and transition-fit holes should be modified at this point. Fatigue crack initiation in a clearance-fit hole, i.e., conventional techniques, is actually the same as in a transition-fit hole with the exception that the scratch is less severe and not continuous, thereby explaining the less-favorable fatigue behavior of a transition-fit hole relative to clearance- and improved clearance-fit holes.

In summary, the improved drilling produced a clearance-fit fastener hole with consistently superior fatigue behavior. This behavior was achieved by removing the major cause of early fatigue-crack initiation within fastener holes, i.e., long, narrow axial scratches, thus shifting the initiation mechanism to one that is a function of circumferential tool marks.

Cumulative probability results for coupon specimens tested using bomber load history are shown in Table 3-4. The EIFS values, both mean and 90 percentile, show no significant difference. Crack depths at one life tend to enhance any differences not seen in the EIFS values. The most significant result is that the crack depth at one life for conventionally produced clearance-fit holes are less than those of transition-fit holes.

EIFS values for bomber spectrum testing are less than those from fighter spectra testing as shown in Figure 3-7 and through comparison of Tables 3-3 and 3-4. This effect was due to the fighter spectrum being more severe than the bomber spectrum.

EIFS values from improved-drilling and fighter-spectra testing were approximately equal to EIFS values from bomber spectrum testing. A limited number of no-load transfer specimens precluded testing of improved drilling under the bomber spectrum.

Table 3-4 CUMULATIVE PROBABILITY RESULTS FOR TASK I NO-LOAD TRANSFER, BOMBER SPECTRUM

	HOLE PRODUCTION TECHNIQUE	EIFS (INCHES)		CRACK DEPTH AT ONE LIFE (INCHES)	
		50 PERCENTILE (MEAN)	90 PERCENTILE	50 PERCENTILE (MEAN)	90 PERCENTILE
Clearance Fit Holes	Conventional Drilling	0.00018	0.0005	0.0009	0.0052
	Improper Drilling	0.0002	0.0007	0.0052	0.023
Transition Fit Holes	Conventional Drill & Ream	0.00021	0.0007	0.0012	0.0075
	Improper Drill & Ream	0.0002	0.00078	0.0019	0.012

SECTION IV

TASK II LOW-LOAD TRANSFER RESULTS

The objective of Task II, testing with the low-load transfer, were the same as those established for Task I with only conventional and improper processes being used. A total of 150 specimens were tested, and as before were equally divided between clearance- and transition-fit processes tested with fighter and bomber spectra.

4.1 FIGHTER SPECTRUM

Cumulative probability plots of EIFS values for clearance- and transition-fit fastener holes are shown in Figure 4-1. The mean EIFS values for both processes are approximately equal, i.e., the two distributions cross at the 62 percentile point. Clearance-fit holes exhibit lower EIFS values at cumulative probabilities greater than 62% than do transition-fit fastener holes. The same trend is seen in crack depth behavior at one life for clearance- and transition-fit fastener holes in Figure 4-2. Thus at cumulative probabilities greater than 65%, the transition-fit holes will have the larger crack-depth values. It is of interest that in both Figures 4-1 and 4-2 that clearance-fit distributions have less spread, as reflected in their relative slopes, than the transition-fit distributions.

A noticeable difference between Task I and Task II can be detected through the slopes of the distributions. Task I distributions were characterized by roughly equivalent slopes, whereas Figures 4-1 and 4-2 each show two distinct slopes.

4.2 BOMBER SPECTRUM

Figures 4-3 and 4-4 show cumulative probability plots of EIFS and crack depth for load-transfer coupon specimens tested using the bomber spectrum. The result of these particular test variables i.e., load transfer, bomber load history, and 33 ksi stress levels, were totally opposite from all others tested. Figure 4-3 shows EIFS distributions for transition-fit holes three to four times lower than the same clearance-fit values. Crack depth values at one life, shown in Figure 4-4, repeat this trend, with clearance-fit values greater than transition-fit values. To avoid speculation no attempt will be made to explain this behavior.

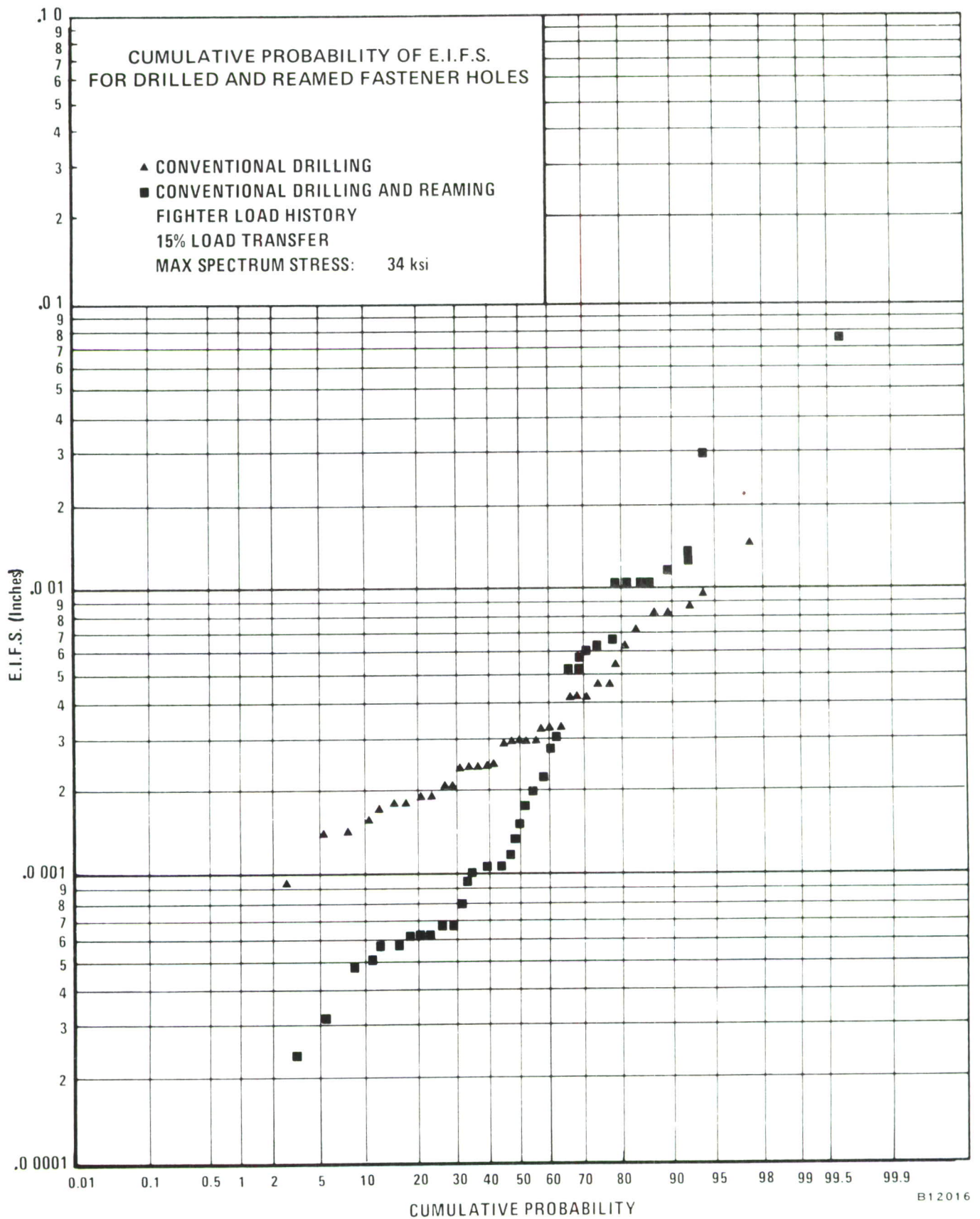


Figure 4-1 Cumulative Probability of EIFS for Drilled and Reamed Fastener Holes

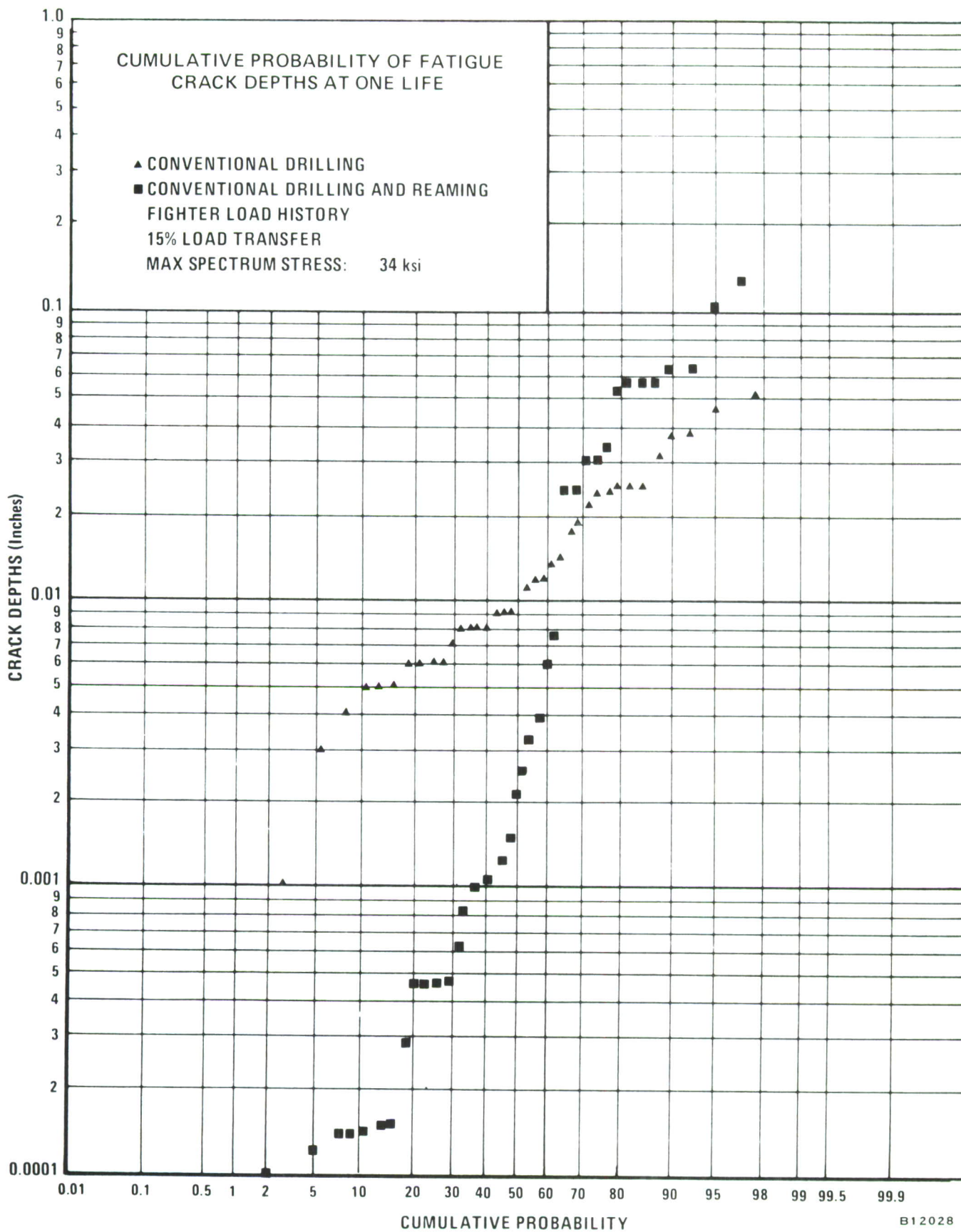


Figure 4-2 Cumulative Probability of Fatigue Crack Depths at One Life

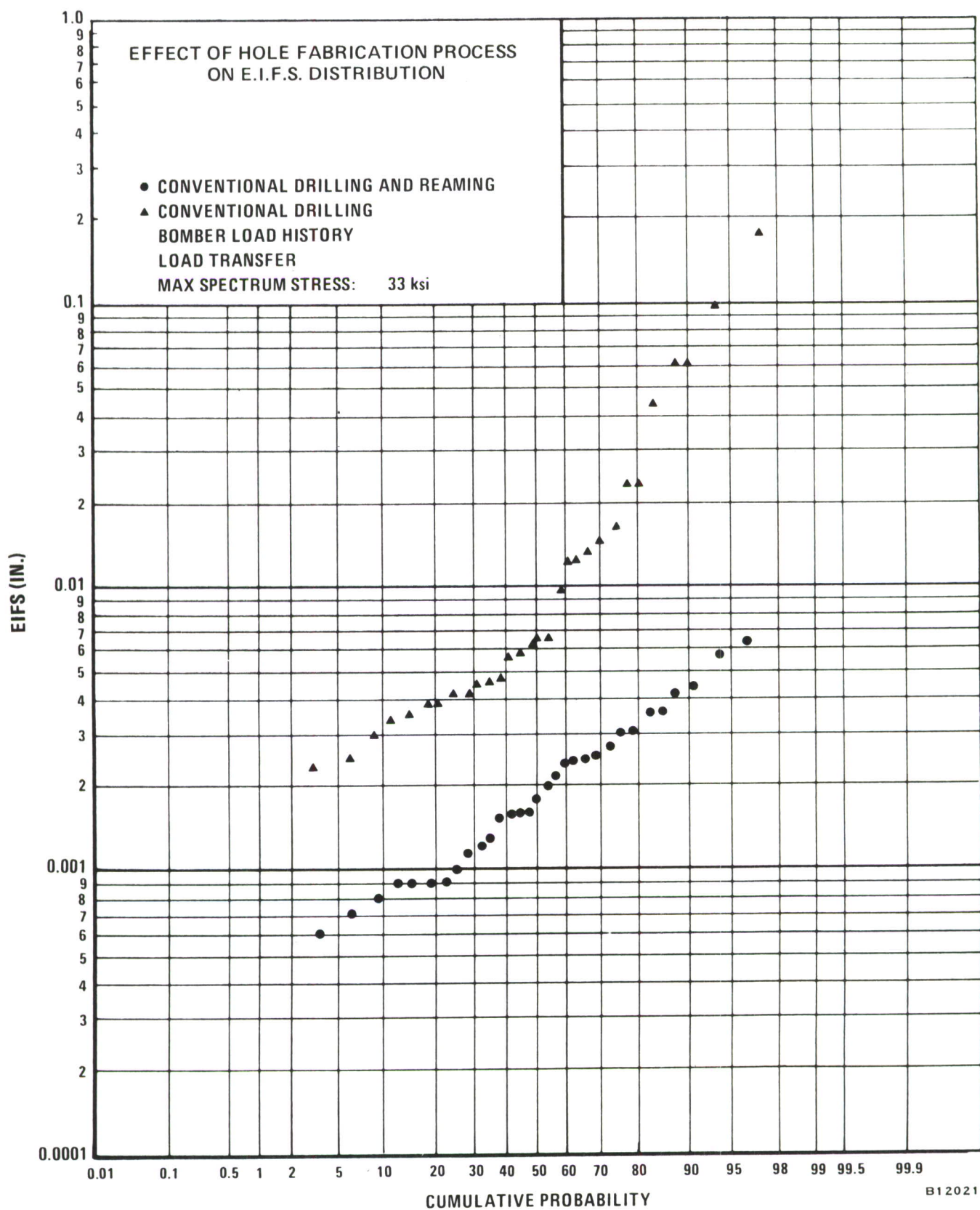


Figure 4-3 Effect of Hole Fabrication Process of EIFS Distributions

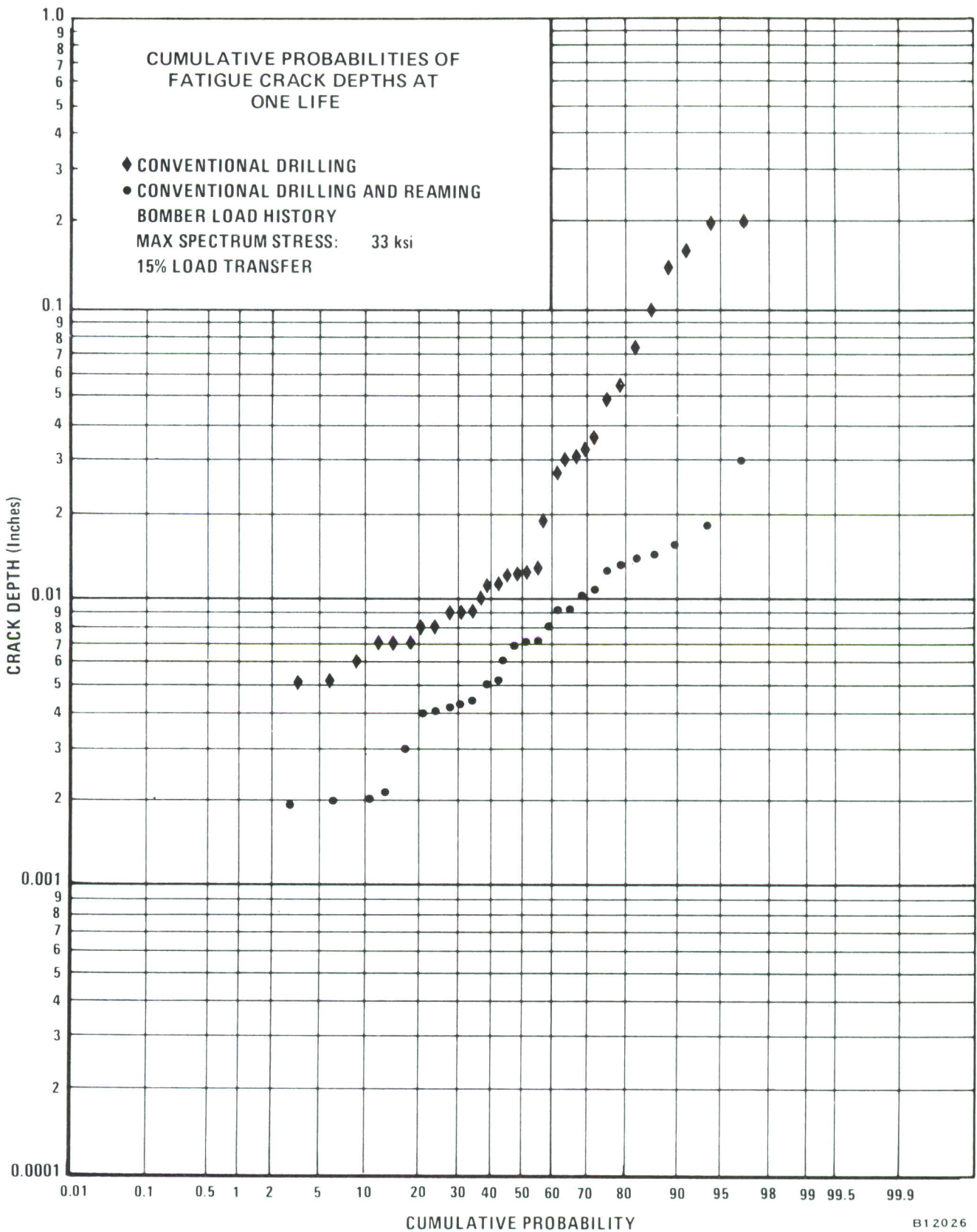


Figure 4-4 Cumulative Probabilities of Fatigue Crack Depths at One Life

Also of interest is the effect of stress level on EIFS and crack depth distributions. The EIFS distributions, Figure 4-5, do show a dependence on stress level, but this dependence is not fully understood. On the other hand, the effect of stress-level on crack depth, Figure 4-6, is as expected with crack depth directly proportional to stress level. To facilitate data presentation, the crack depth distribution for 40.8 ksi is shown at one-half life.

4.3 NDE RESULTS

Two of the NDE and surface-characterization techniques from Task I were used to identify surface topography in Task II. The two techniques selected were (1) eddy current and (2) rotary profiler combined with the dial bore gauge.

4.3.1 Eddy Current

Since the primary fatigue-crack origin in Task I was due to shallow vertical scratches, major emphasis in Task II was placed on increasing sensitivity and resolution with the eddy current technique. The Magnaflux ED-520 eddy current instrument was replaced by an Automation Industries EM3300 phase-amplitude unit. With this set-up, hole topography and fatigue cracks can be monitored by measurement of phase changes due to the eddy current response. The phase of the EM3300 was adjusted such that the initial lift-off had a purely horizontal component, and by only monitoring the vertical component, lift-off effects were minimized. The signal from the vertical output was then sent through a bandpass filter to reject the d.c. component of the signal and amplified. For in-lab inspection, this system was integrated with the HP2100 digital computer.

Conventional eddy current probes used in Task I were replaced by high-sensitivity probes (CREG Model 102, Reluxtrol Company). These probes have coils of approximately 0.050-inch diameters as compared to .125-inch diameters for the conventional probes, thus giving better resolution for small defects. An operating frequency of 1 MHz with the EM3300 was found to work quite well in detection of small cracks and scratches. The standard probes required an operating frequency as low as 50 KHz for normal usage. The higher-frequency signal used with the smaller probes allows less penetration depth of the eddy current signal and, thus, increased sensitivity to surface defects.

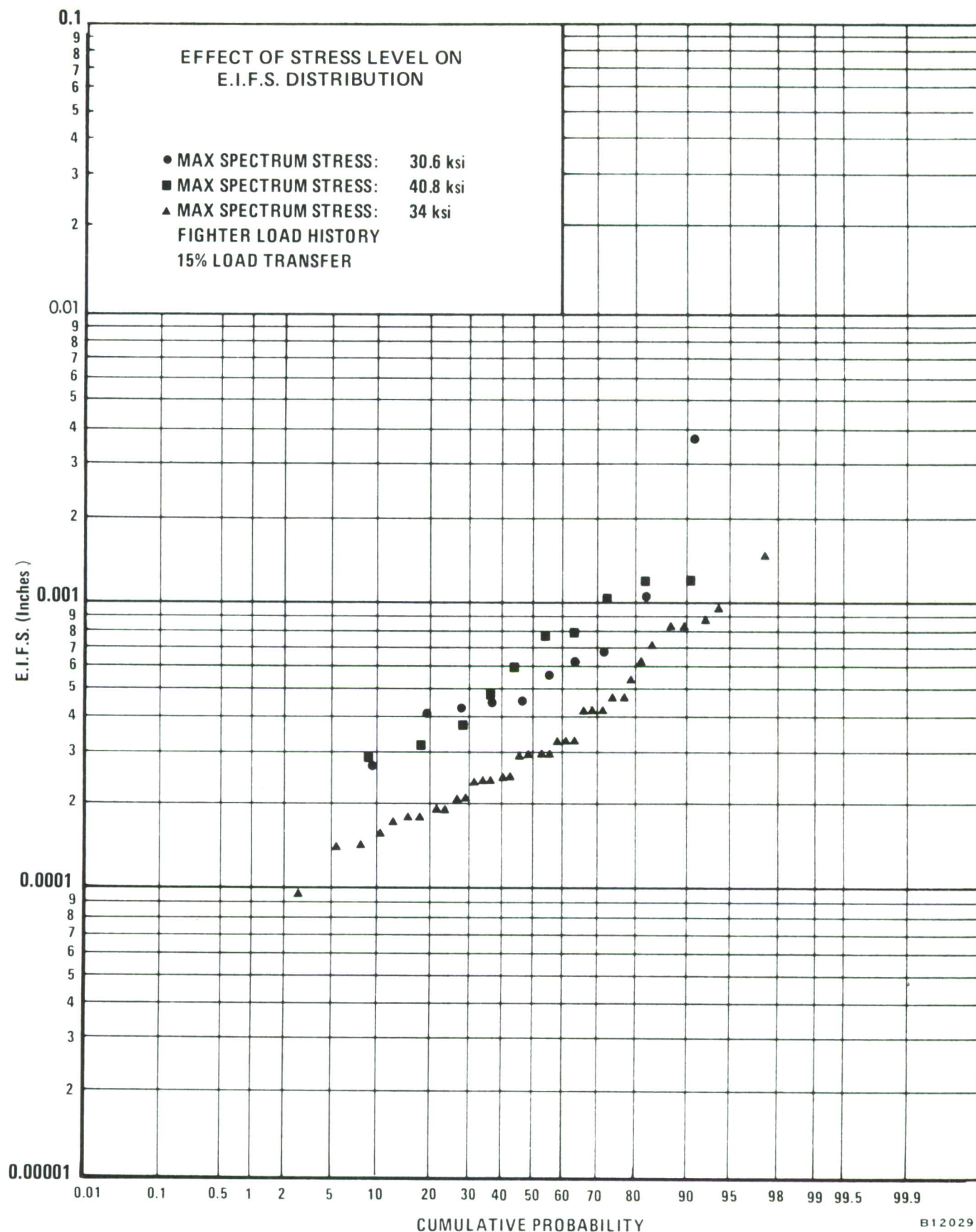


Figure 4-5 Effect of Stress Level on EIFS Distribution

B12029

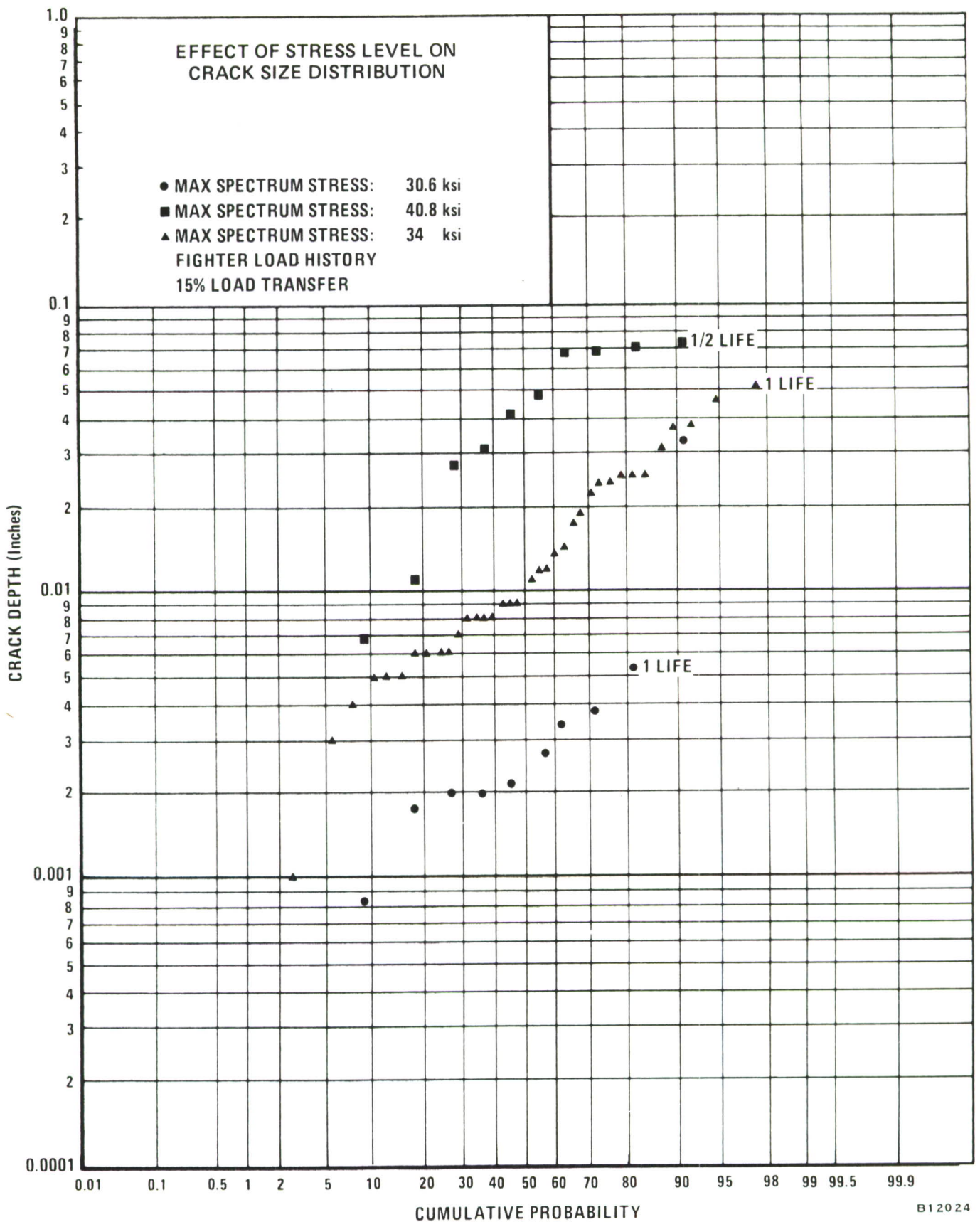


Figure 4-6 Effect of Stress Level on Crack Size Distribution

B1 2024

Figure 4-7 shows eddy current scans of a 0.025-inch-deep fatigue crack in a .250-inch-diameter 7475 aluminum fastener hole obtained through the use of both types of probes. The eddy current amplitude obtained with the CREG probe is shown to be nearly double that obtained with the conventional probe. The resolution obtained with the CREG probe is also better because of the smaller-diameter coil. The dual set of inductance change peaks obtained with the conventional probe resulted from the diameter of the coil being larger than the length of the fatigue crack. Most of the induced eddy currents will surround the crack when the probe is centered on the crack, causing a minimum in the amplitude of the recorded inductance change peaks.

By use of the higher-sensitivity probes, a study was conducted to determine the maximum sensitivity of eddy current to scratches. These measurements were made on Task II drilled specimens where crack depths were measured with the rotary attachment to the Bendix proficorder. These studies indicated minimum detectability of approximately 0.0004-inch depth in production-drilled holes, Figure 4-8. This minimum detectability limit is a function of other factors such as hole surface finish and out-of-roundness, which also can influence the eddy current signal. For instance, the minimum detectability in a polished hole (low surface roughness) should be improved over detectability obtained in the present experiments.

Even with the improved eddy current system, no correlation could be obtained between eddy current amplitudes and EIFS. All of the problems encountered in correlating NDI parameters and EIFS in Task II specimens were due to many of the primary crack-initiation sites being away from the bore of the hole, where no inspection had been done.

In general, the eddy current background in Task II, in which holes were conventionally drilled, was considerably higher than that obtained in the improved drilled holes, Figure 4-9. This is indicative of better hole quality when the improved drilling process is used.

4.3.2 Rotary Attachment to Proficorder Plus Dial Bore Gauge

Total surface profiles around the bore of the hole were obtained on all Task II specimens. Measurements were made on the bottom section at a depth of 0.050 inch from the top. The low-load drilled specimens contained larger surface irregularities than the holes

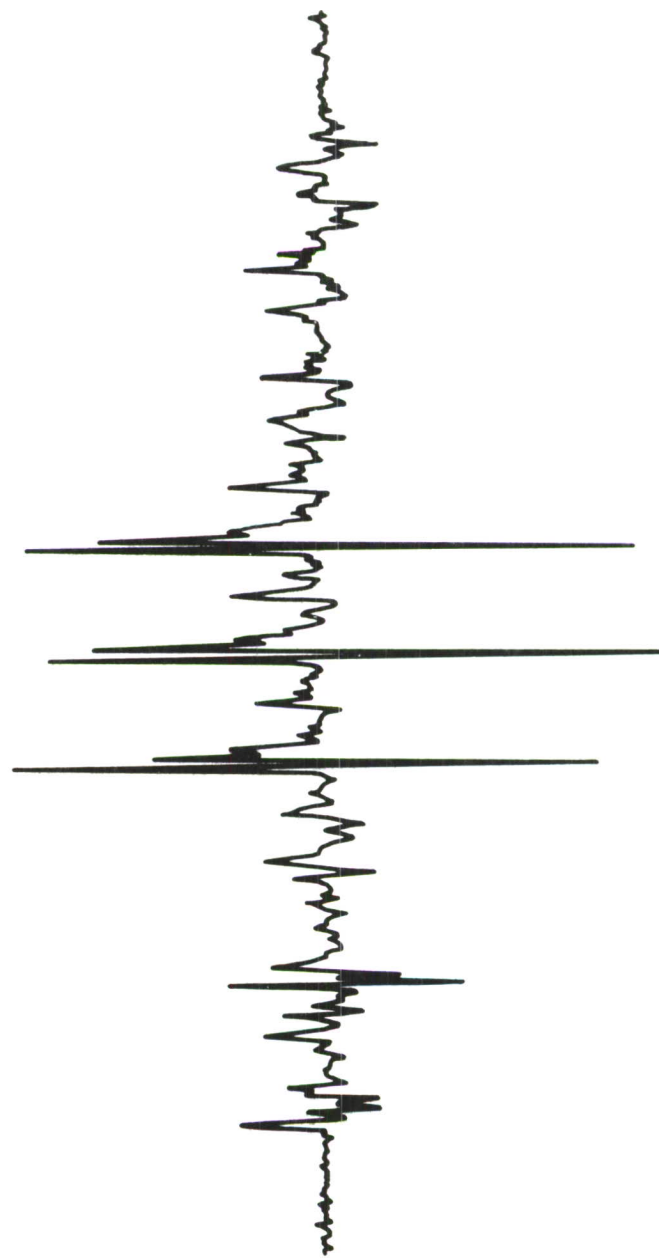
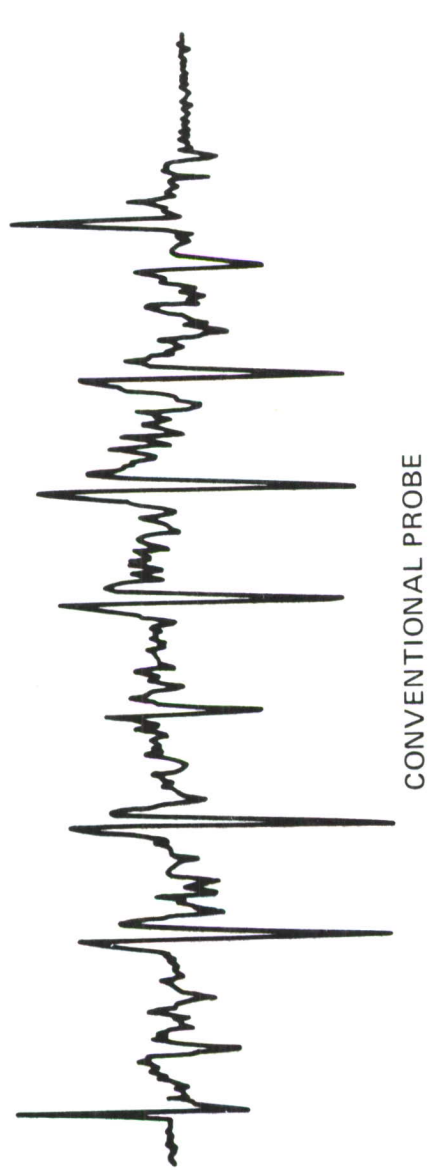


Figure 4-7 Resolution of 0.025-Inch-Deep Fatigue Crack

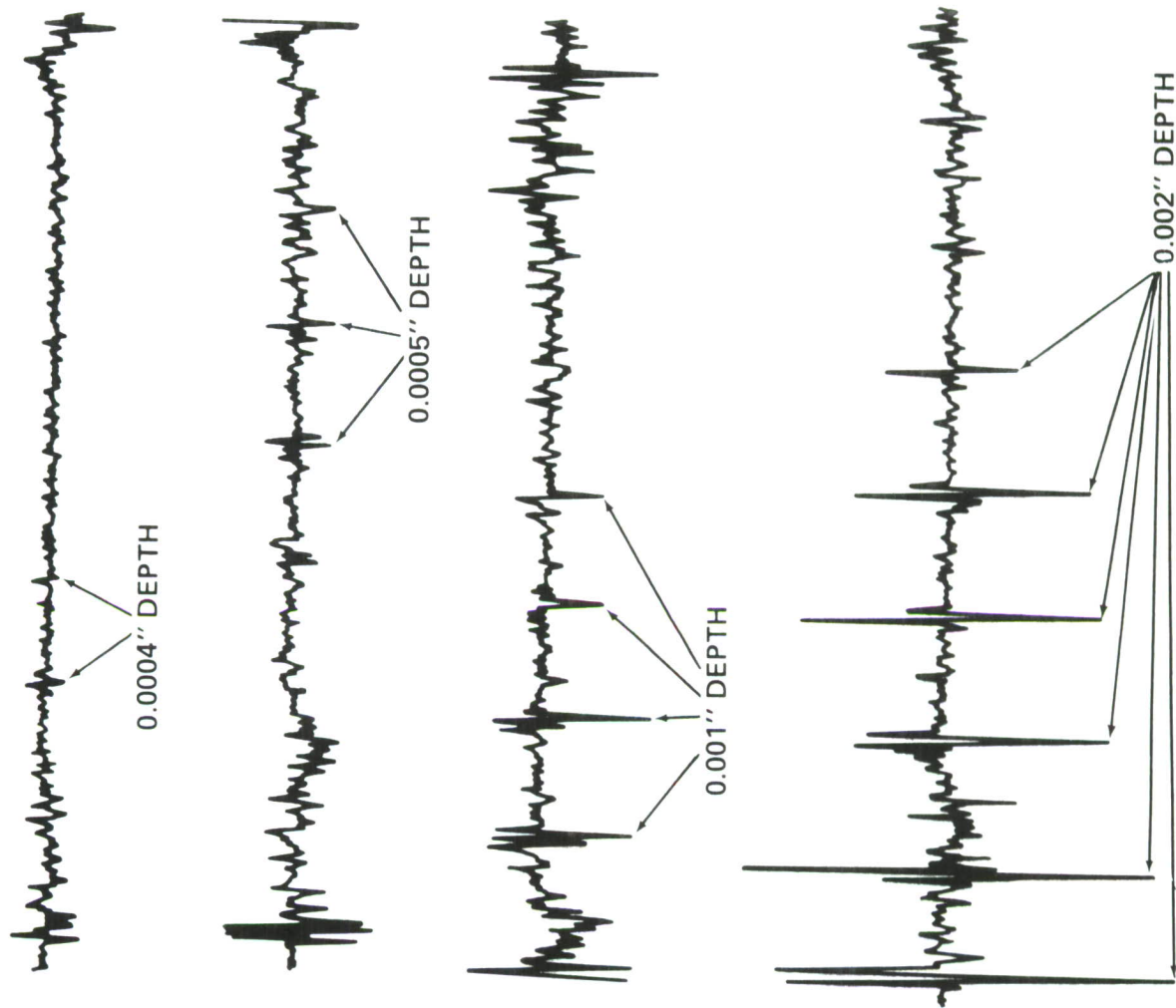


Figure 4-8 Sensitivity of Eddy Current to Surface Defects



CONVENTIONAL WINSLOW



IMPROVED WINSLOW

Figure 4-9 Typical Eddy Current Scans of Conventional and Improved Drilling Fastener Holes

drilled by use of improved techniques. A comparison of hole out-of-roundness between the two techniques is shown in Figure 4-10. Examples of scratches present in the conventionally drilled specimens are shown in Figure 4-11.

Dial bore gauge readings on Task II holes indicated a larger spread in diameters of the drilled holes compared to the reamed holes. For the smaller diameter holes, there was no correlation between the dimensional tolerance parameter or maximum diameter measured and the EIFS. However, in the drilled specimens, for maximum diameters measured greater than 0.253 inch, there was a general tendency of larger flaw size, Figure 4-12. For specimens where only one of the holes was oversized, the oversized hole caused the adjacent hole to fail early due to the increased load on the smaller hole.

4.4 SEM ANALYSIS

A general SEM analysis was performed on Task II specimens. Efforts were concentrated on initiation-site behavior since general topological features within the sites were consistent with those seen in Task I.

The major difference seen between Task I and Task II specimen failures was the location of fatigue crack initiation sites. Task I initiation occurred predominately within the bore of the fastener holes. In Task II the initiation sites tended to move to the faying-surface corner, i.e., fastener hole faying-surface intersection. Two typical examples are shown in Figures 4-13 and 4-14. Faying-surface initiation is seen in Figure 4-13, where the fatigue crack was growing parallel to the axis of the fastener hole until it became a full corner crack. The second type of typical initiation site behavior, Figure 4-14, is initiation at or very near the corner. In this case the actual initiation site was destroyed by compressive loads in the spectrum. Note should be made of the relatively flat crack front following axial scratches within the bore of the fastener hole.

We thus see two mechanisms at work in the Task II specimens. First, corner or faying-surface initiation, followed by flat crack fronts propagating along axial scratches within the fastener holes. These mechanisms will be further addressed in Task III.

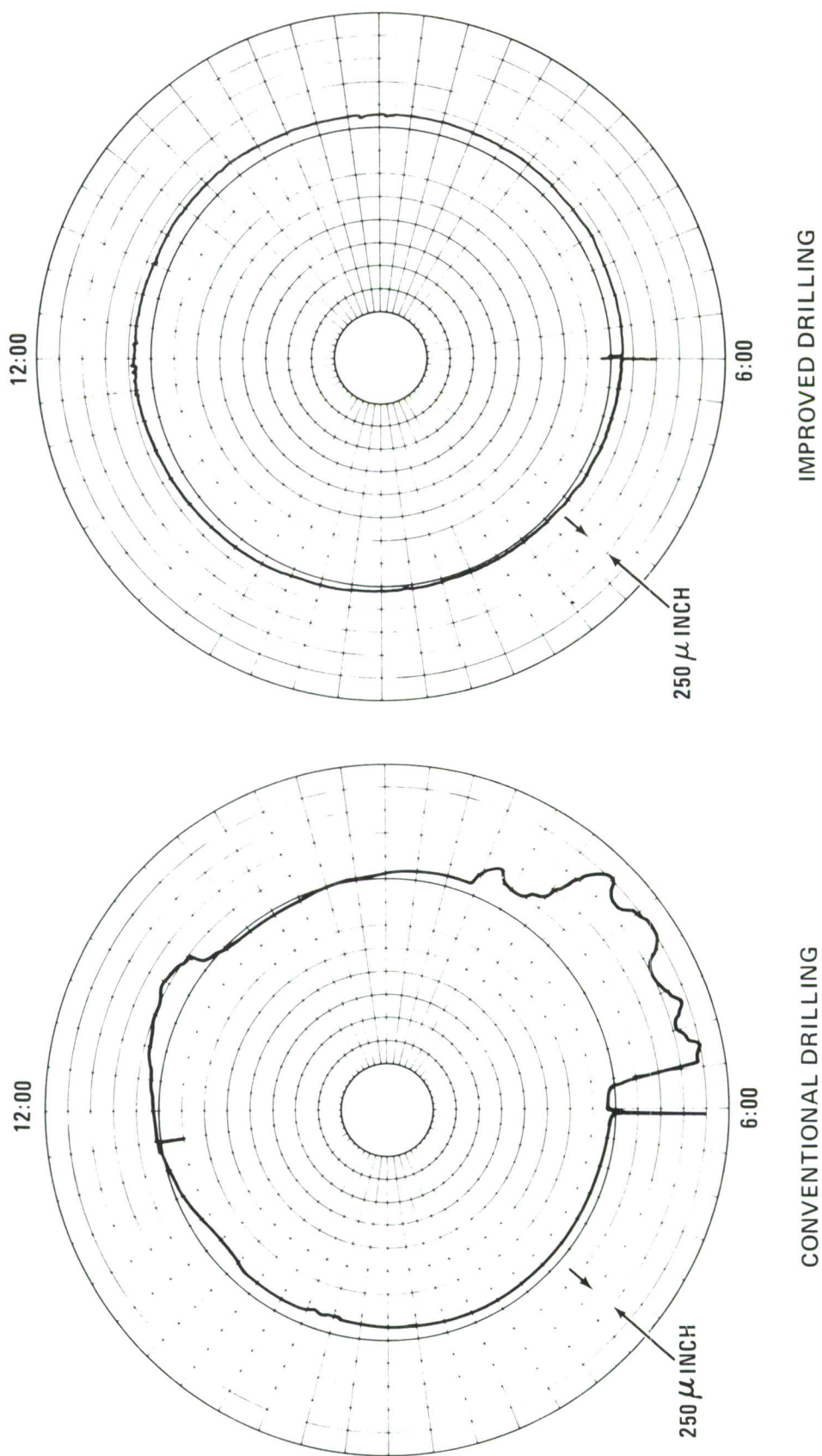


Figure 4-10 Comparison of Roundness for Conventional and Improved Drilling

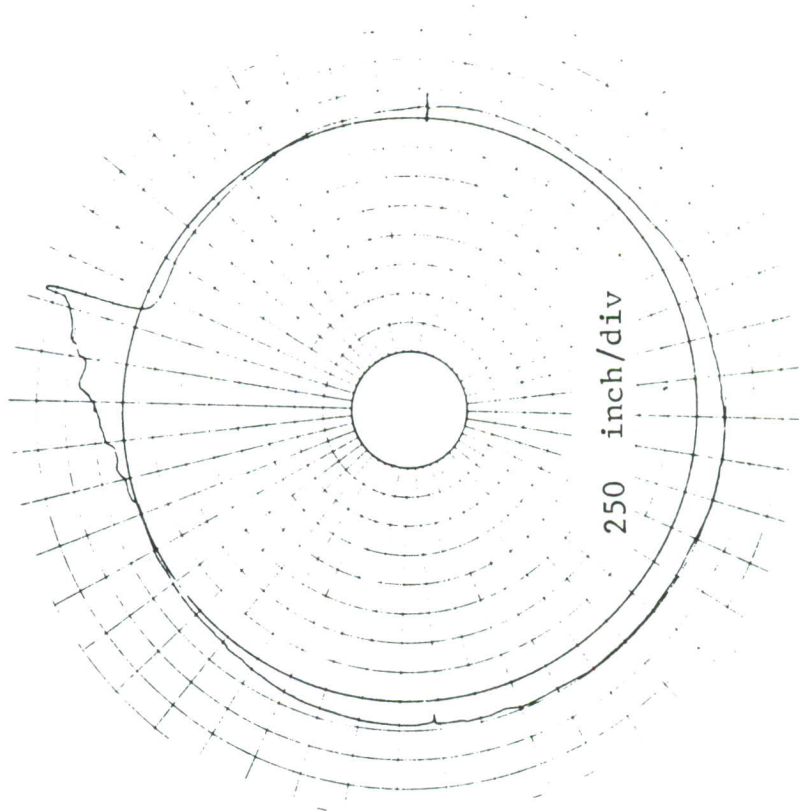
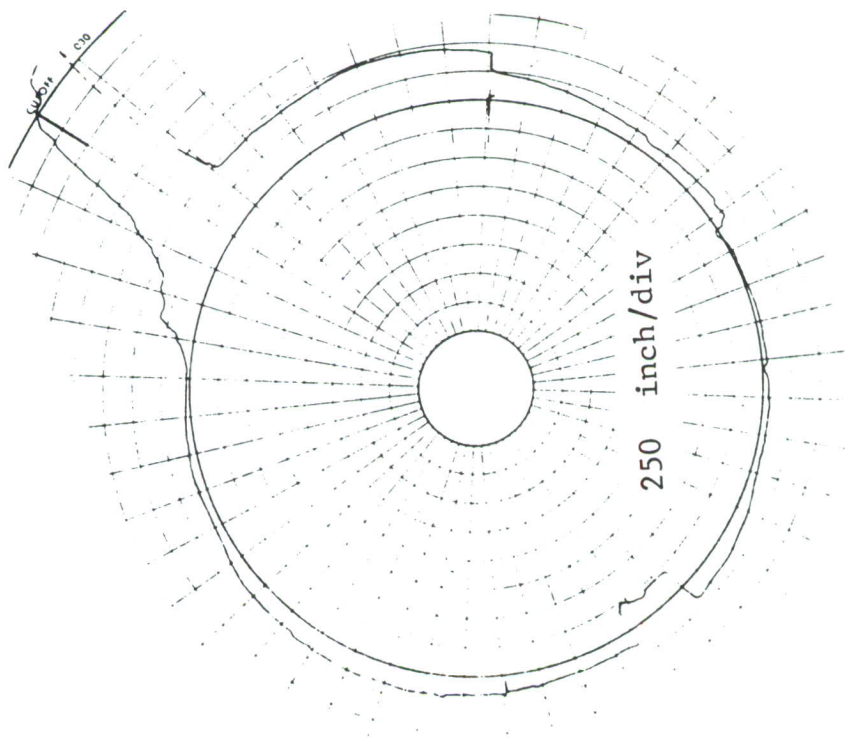


Figure 4-11 Polar Plots Showing (a) a Scratch 2.25 Mils Deep x 8.0 Mils Wide and (b) a Scratch .9 Mils Deep

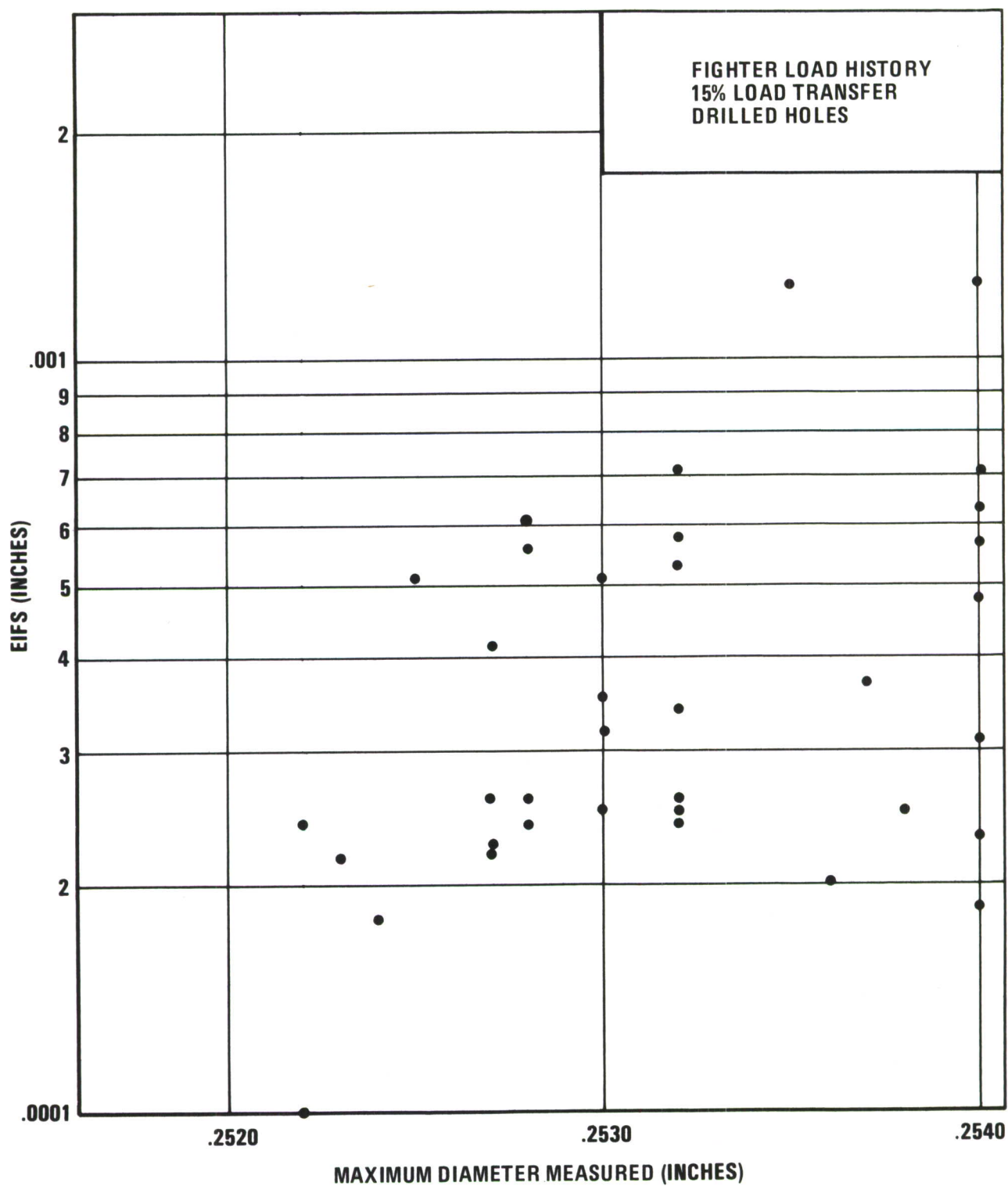


Figure 4-12 Maximum Diameter versus EIFS

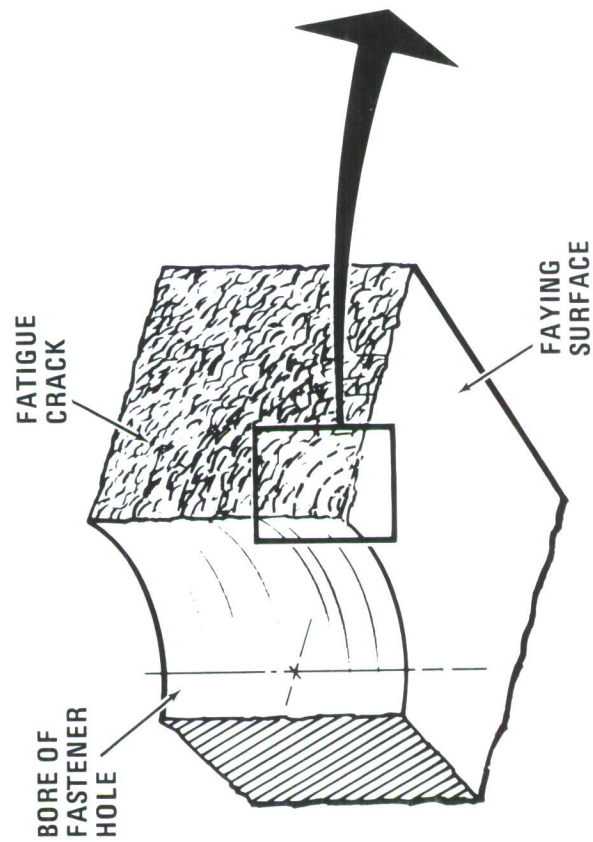
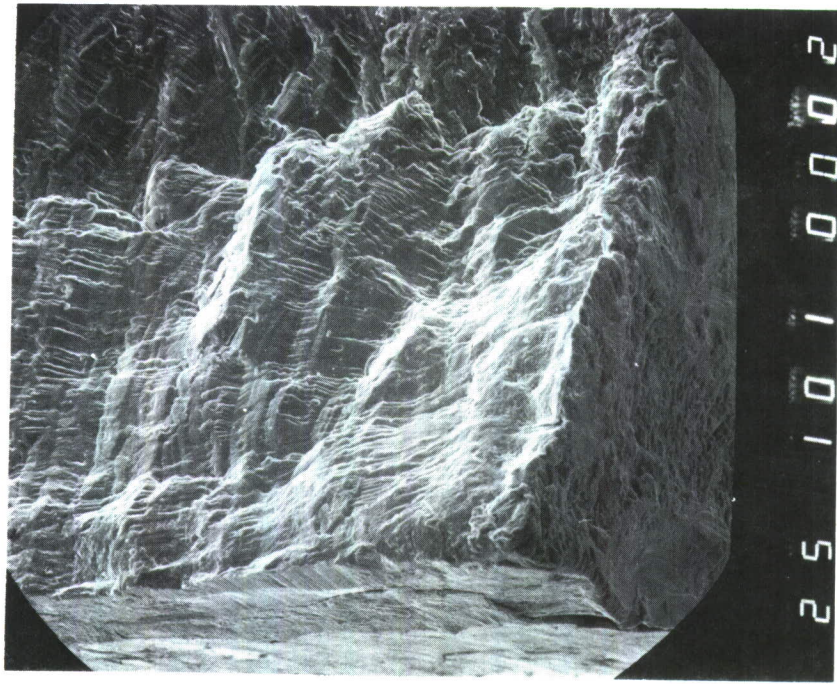


Figure 4-13 SEM Micrograph Showing Fatigue Crack Initiation from Faying Surface Near Fastener Hole for a Transition-Fit Hole (100X)

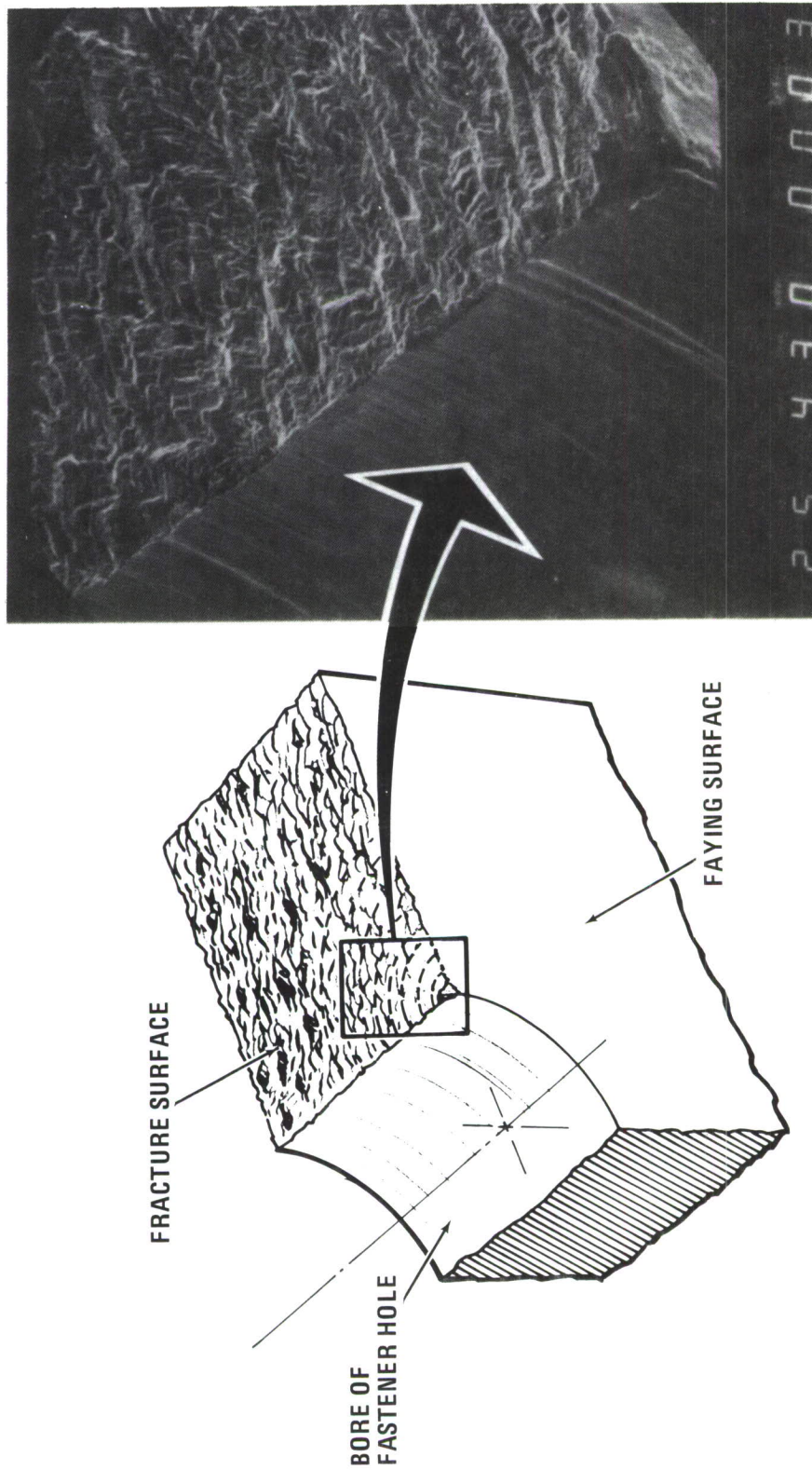


Figure 4-14 SEM Micrograph Showing "Near Corner" Crack Initiation at Faying Surface for a Transition-Fit Hole (43X)

4.5 COMPARISON OF RESULTS

Fighter spectrum results for Task II were consistent with the previous task, that is, at higher cumulative probabilities the clearance-fit EIFS and crack depth distributions were lower than the transition-fit distributions. These trends are summarized in Table 4-1. For the fighter spectrum the EIFS values are roughly equal in both task. The anticipated spread in the clearance- and transition-fit crack depth is seen at the 90-percentile values.

As previously mentioned, the bomber spectrum Task II results show no one-to-one correlation within this task or to Task I. These results are not fully understood and, therefore, no attempt will be made to explain them.

Table 4-1 SUMMARY OF RESULTS

	FIGHTER SPECTRUM				BOMBER SPECTRUM			
	EIFS (INCHES)		CRACK DEPTH (INCHES) AT 1 LIFE		EIFS (INCHES)		CRACK DEPTH (INCHES) AT 1 LIFE	
	50	90	50	90	50	90	50	90
NO-LOAD TRANSFER								
Drilled	0.0006	0.0012	0.0043	0.016	0.00018	0.0005	0.0009	0.0052
Drilled and Reamed	0.0007	0.0014	0.064	0.021	0.00021	0.0007	0.0012	0.0075
LOAD TRANSFER								
Drilled	0.0003	0.0008	0.0092	0.038	0.0065	0.06	0.013	0.15
Drilled and Reamed	0.00015	0.0012	0.0021	0.063	0.0018	0.0043	0.007	0.015

SECTION V

TASK III FASTENER HOLE QUALITY IMPROVEMENTS

The objectives of this task were to improve the fatigue behavior of fastener holes with the use of NDE techniques to eliminate test specimens with large EIFS in the fastener holes, and then, mechanically test only those specimens with acceptable EIFS as established by the results of the 400 test specimens of Task I and II.

5.1 DEFINITION AND IDENTIFICATION OF HOLE QUALITY

One of the first priorities of this task was to establish the criteria for fastener hole quality, i.e., fatigue behavior. Our initial guideline for hole quality was hole surface finish and morphology, i.e., roughness, scratches, and out-of-roundness, since fastener hole inspection rejection criteria as used by most of the major aerospace companies were based on hole finish and other geometry related details. However, it became quite evident when the results of Task I and II were examined that there were little, if any, correlation between NDE measurements and fastener hole fatigue behaviors. Task I results showed that there is no correlation between EIFS and final flaw sizes with hole diameter dimensions of 0.250 to 0.255 inch for drilled holes. Diameters greater than 0.253 are out of tolerance. Task I results also showed that there is no correlation between EIFS and final flaw sizes with hole roughness up to 150 RMS. Holes that have deep gouges and rifling marks (~ 1.25 mil) that were introduced by deviating from the normal drilling procedure also did not appear to effect the fatigue behavior. Upon closer examination of the fastener hole surface by SEM after the cracks were broken open, we found that fastener holes with large EIFS were mostly initiated from axial scratches. For the no-load transfer specimens, this was particularly true. Hole roughness as caused by rifling marks, gouges, etc., did not generate large EIFS or early fatigue failure. However, that is not to say that rifling marks, gouges, etc., do not initiate cracks. They do, and from fractography investigations they appear to initiate cracks as early as axial scratches. But, their growth rate is slower than those initiated from axial scratches.

Qualitatively, a crack initiated from an axial scratch has a small crack depth (a) and a large crack length ($2c$) or a small $a/2c$ ratio, as illustrated in Figure 3-40. The flaw shape parameter Q for $a/2c$ much less than 0.5 is, roughly speaking, unity. For $a/2c$ around 0.5, as a crack which was initiated from a rifling mark or other circumferential tool marks might be approximated, the Q value can be twice as large as unity. Thus, the stress intensity factor will be larger for a crack growing from an axial scratch ($a/2c \ll 0.5$) than a crack growing from a rifling mark ($a/2c \sim 0.5$). Quantitative stress intensity factors for a part-through or elliptical surface crack can be found in References 5 and 6. Figure 5-1 illustrated this case in point. Specimen A failed before the end of two service lives and the crack depth was traced to 0.6 mil by fractography. Specimen B, which was fabricated and tested in exactly the same manner as Specimen A, has a final flaw depth of 0.085 inch at the end of two service lives and the smallest crack depth was traced to 1.3 mil by fractography. Post-test scanning electron microscope examination showed that cracks in Specimen A were initiated from an axial scratch and it grew rapidly between zero and $3/4$ service life. At that point, the $a/2c$ ratio approaches 0.5 and the crack grew in a manner similar to the crack in Specimen B. Specimen A has an EIFS of about 5 mils as obtained by following the analytical procedure used to obtain EIFS. Specimen B has an EIFS of about 0.9 mil.

A second factor that contributes to faster crack growth with axial scratch initiation is multiple crack initiations that will grow together along the axial scratch to form a longer crack, as illustrated in Figure 5-2. Prior to joining together, each crack might have reached an $a/2c$ ratio of approximately 0.5, but when they grew together to form a single crack, this newly formed crack will now have an $a/2c$ ratio of less than 0.5. Thus, it will grow at a faster rate. Multiple crack initiations can occur in non-axial scratches, but the cracks are growing in separate planes and can not grow together to form one crack front.

These explanations are only intended to give a qualitative account of crack growth behavior as influenced by the manufacturing process to establish a criteria for fastener hole quality. These same qualitative explanations for drilled holes also apply to drilled and reamed holes. Thus, based on the results of Task I, which included 100 specimens tested with the F-16 randomized block spectrum and 100 specimens tested with the AMAVS (B-1) spectrum, axial scratches appeared to be the major mechanism contributing to the degradation of fastener hole fatigue behavior.

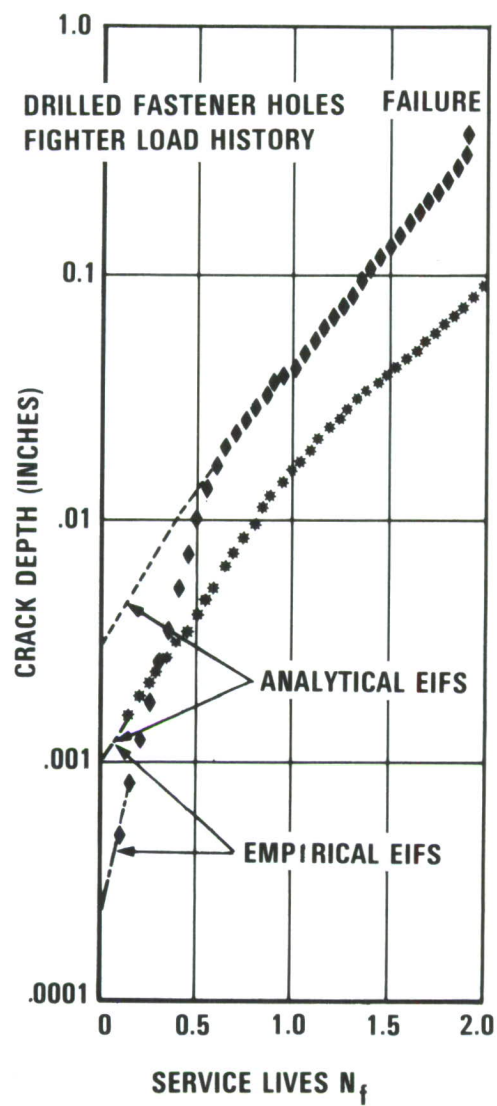


Figure 5-1 Effect of Flaw Shape Size on EIFS

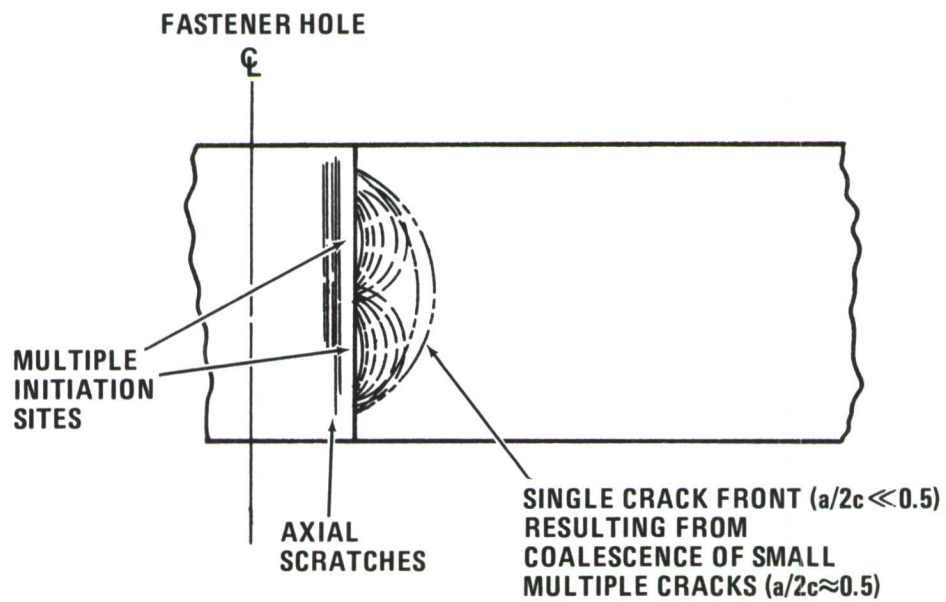


Figure 5-2 Coalescence of Multiple Cracks to Form a Single Large Crack

The criteria for fastener hole quality in the case of low-load transfer appears to be much more complex than the no-load transfer case. Post-test examination by SEM revealed that large EIFS fastener holes were initiated from axial scratches, localized yielding/fretting at the interface, and mismatch. Mismatch refers to the lack of concentricity of the two fastener holes. Our traditional concept of fastener hole quality consisting of hole roughness and geometric details, except for hole diameter tolerance, does not appear at all to be appropriate. A large majority of the Task II specimens initiated cracks at the interfaces and slightly away from the hole; but grew back toward the hole and eventually fail as a corner crack. This mode of crack initiation is referred to in this report as localized yielding or fretting. There were a few cracks initiated at the hole that appeared to be the result of localized yielding caused by the fastener and one of the plates. This mode of crack initiation is referred to in this report as mismatch. These two crack initiation modes dominate hole quality or lack of it along with axial scratches.

Localized yielding can not be detected by conventional production inspection procedures. Mismatch might or might not be detectable with production inspection procedures. Even if it is detectable, it might not be correctable without causing one of the holes to be out of tolerance. Axial scratches, unless they are deep and can easily be detectable with the human eye, are for the most part not detectable by conventional production inspection procedures. Fastener hole quality in the load transfer case can not in the large majority of the cases be controlled by inspection. It must be controlled by a combination of design and manufacturing processes, which will be discussed in the next subsection of this report.

5.2 LOW-LOAD TRANSFER RESULTS

Task III low-load transfer coupon fatigue testing was performed on 113 specimens. All fastener holes in this task were clearance-fit and produced with the modified equipment; thus, they were improved fastener holes. One group of 50 was tested with the fighter load history, and a second group tested with the bomber load history. Specimen testing was broken down into three basic levels, 100% baseline stress (30 specimens), 120% baseline stress (10 specimens) and 90% baseline stress (10 specimens). An additional 13 specimens were fabricated with the improved process using improper or abusive techniques and tested with the fighter load history.

5.2.1 Fighter Spectrum Results

Figure 5-3 shows a comparison of Task III load-transfer EIFS results and Task III abusively drilled improved-process EIFS results. The mean value for abusive drilling is approximately three times greater than the improved drilling values, but the 90-percentile values approach each other.

The behavior of EIFS distributions for improved drilling and conventional drilling is seen in Figure 5-4. These distributions are essentially inseparable from the 50-percentile values and greater. It should be pointed out that although these higher percentile values of both distributions are very nearly equal, the improved drilling produces a distribution with a steeper slope and, thus, less statistical spread.

5.2.2 Bomber Spectrum Results

The results of bomber spectrum testing are shown in Figures 5-5 and 5-6. EIFS values for improved drilling are seen to decrease with respect to conventional drilling. The same trend, although less apparent for the mean is seen in crack depth values at one life. EIFS values exhibit a slight decrease for improved drilling relative to conventional drilling, where no improvement was seen in the fighter spectrum data. There are obvious differences in the fighter and bomber spectra data, which will be addressed below.

5.2.3 Improved Drilling and Assembly

Since the fatigue behavior and EIFS distributions from Task II and Task III were very similar, most notably the fighter spectrum results, and did not provide a dramatic increase in fatigue life, the conventional assembly process was evaluated. The fatigue crack initiation sites for both Tasks II and III were of a "corner" mode and, except for Task III bomber test, improved drilling showed significant gain. Thus, assembly techniques were evaluated and modified to correct the major mechanisms thought to contribute to early corner initiation and rapid crack growth. These mechanisms were misalignment or mismatch of fastener holes and metal yielding at the faying surface.

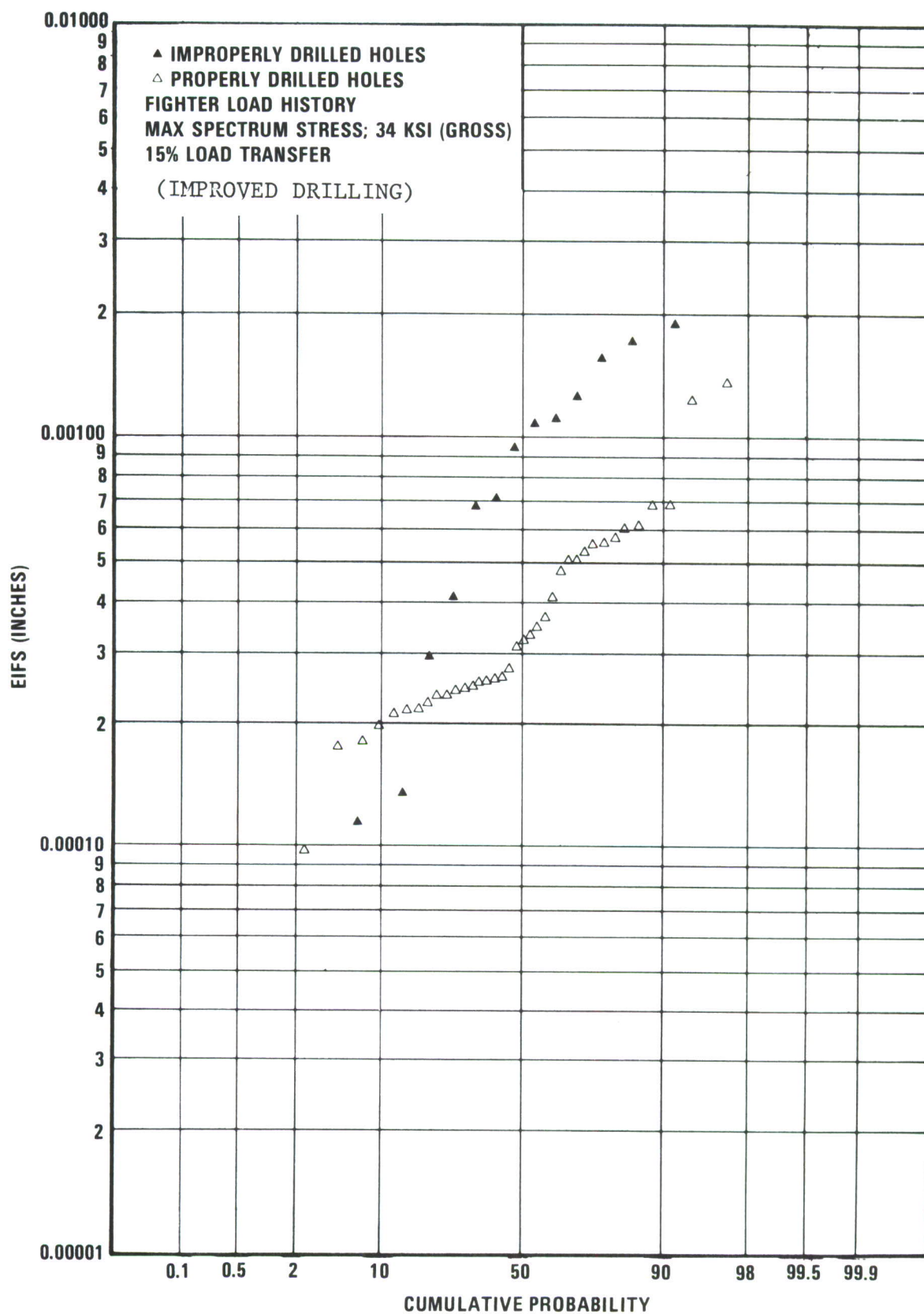


Figure 5-3 EIFS for Properly and Improperly Drilled 15%-Load Transfer Specimens

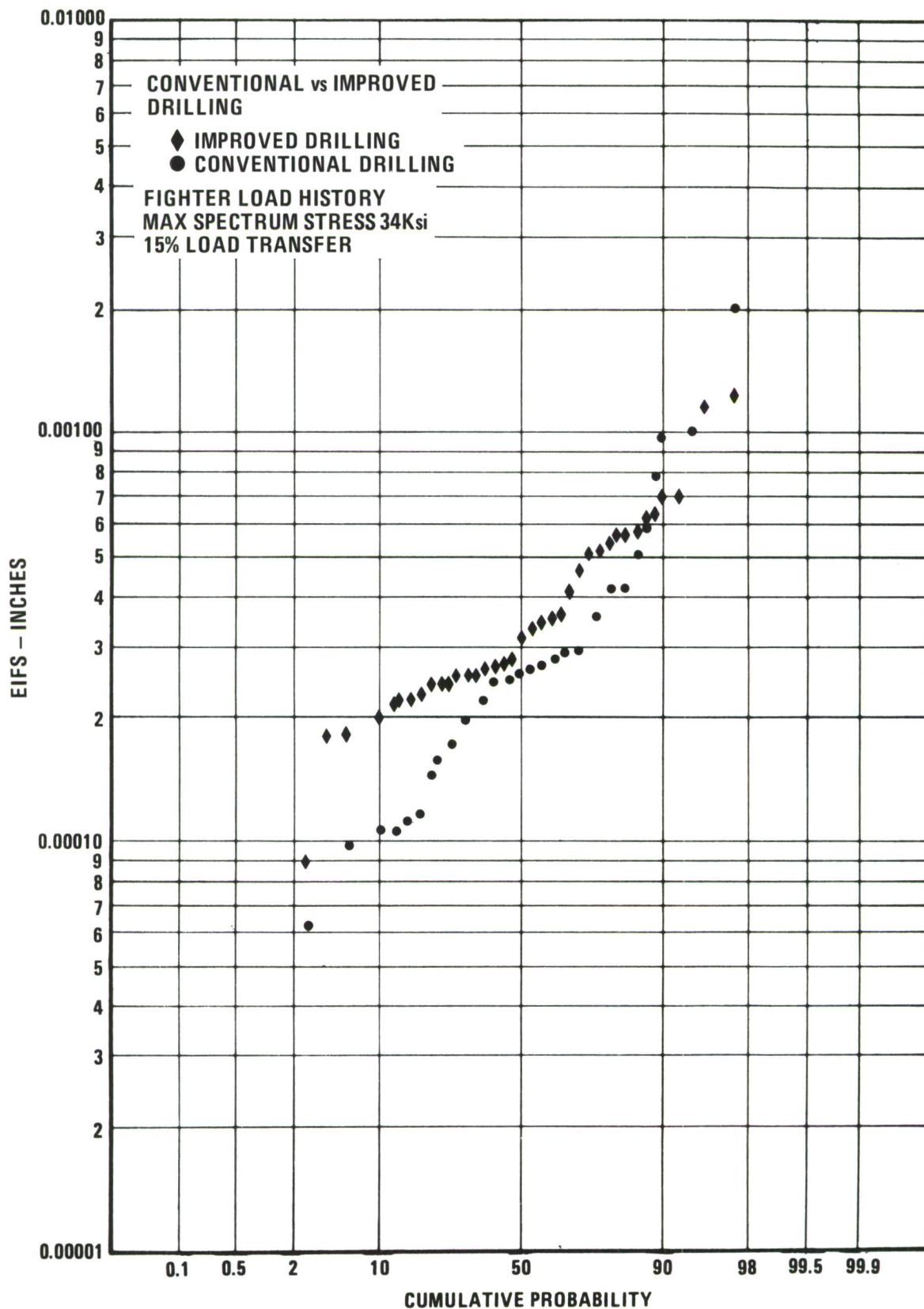


Figure 5-4 EIFS Distributions for Conventional and Improved Drilling, Fighter Load History and 15% Load Transfer

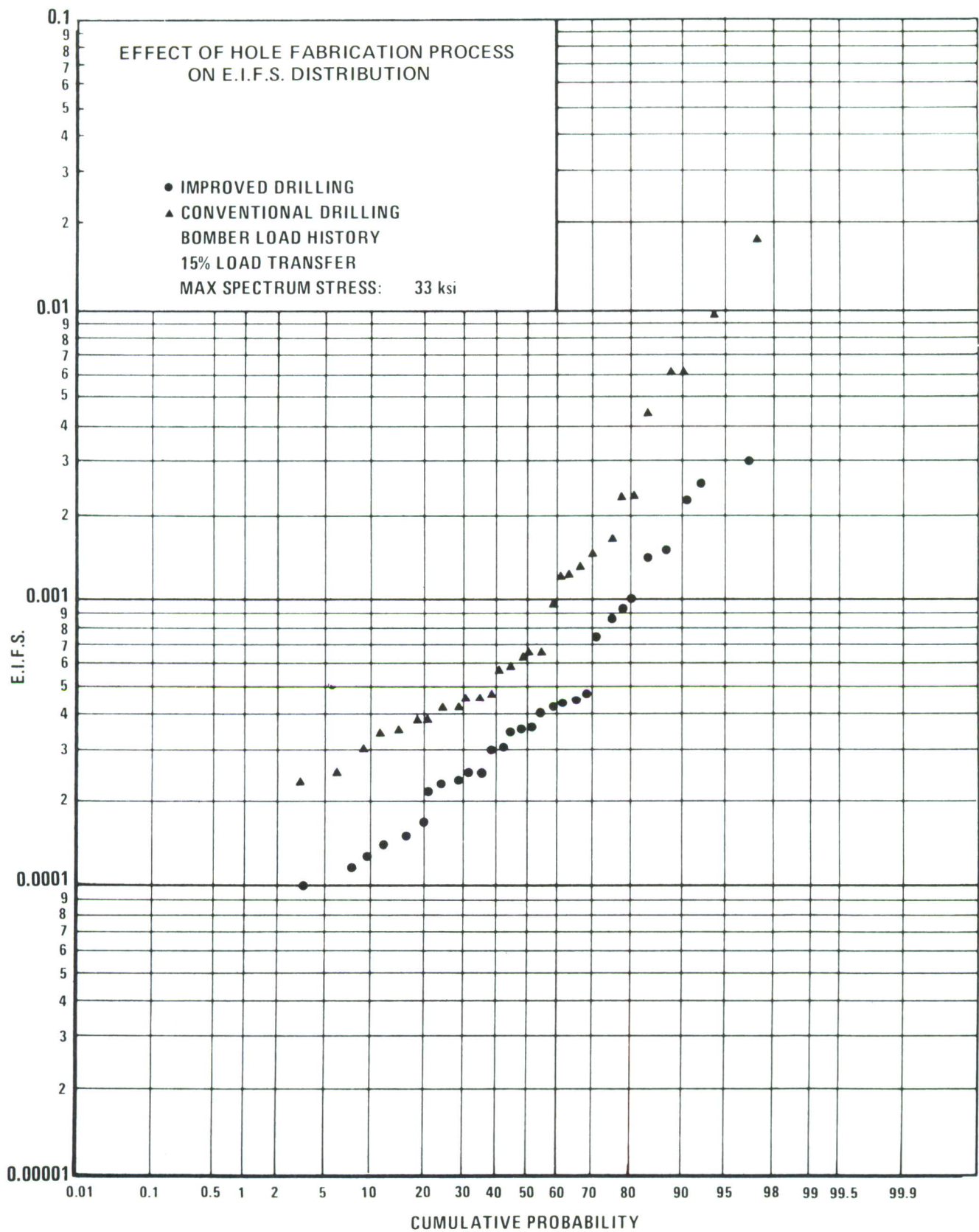


Figure 5-5 Effect of Hole Fabrication Process on EIFS Distributions

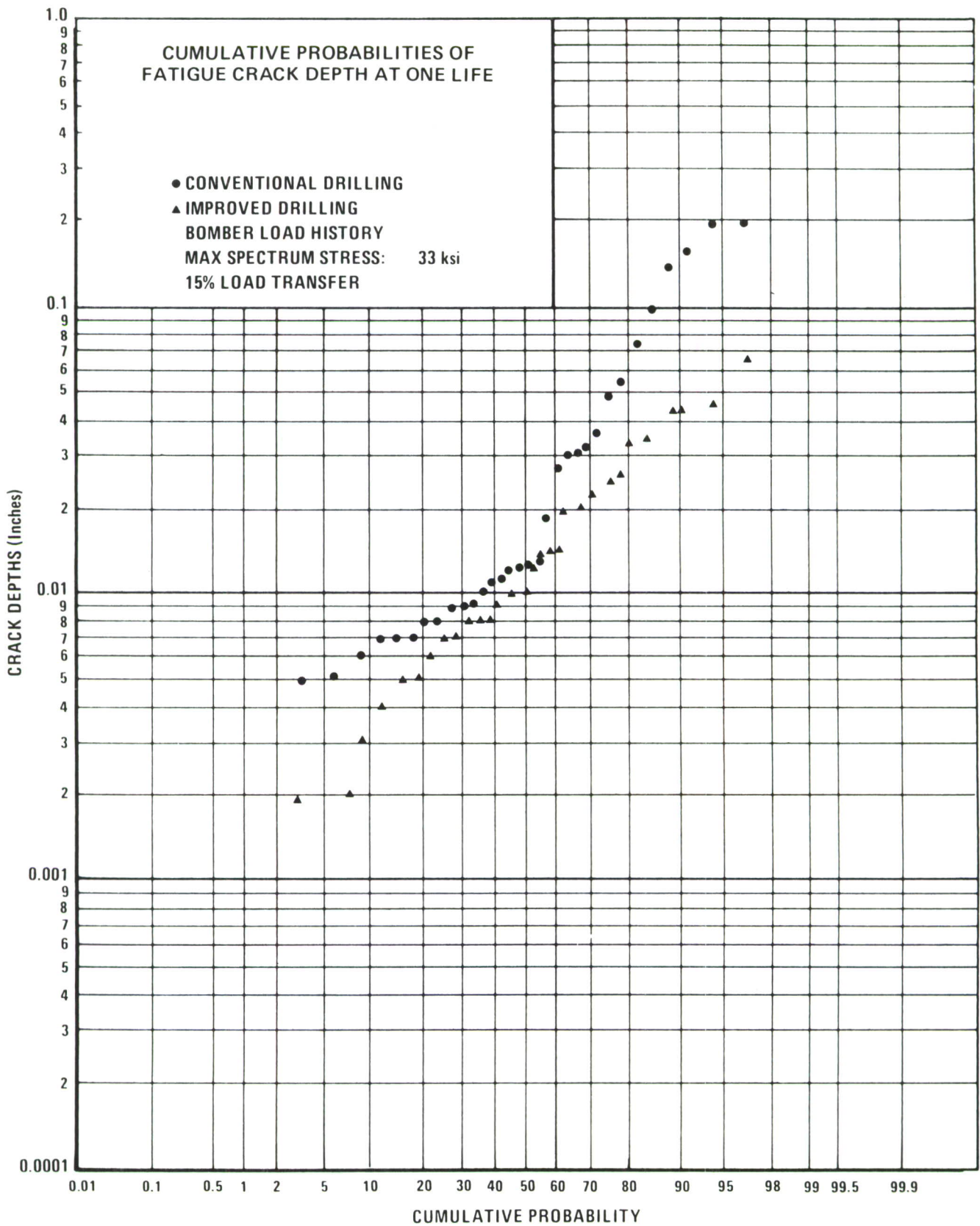


Figure 5-6 Cumulative Probabilities of Fatigue Crack Depths at One Life

Mismatch occurs when two plates, for example, are match drilled with several fastener holes, separated for some secondary operation, and remated for assembly. The probability of perfectly realigning all of the pre-drilled holes is very small. This probability will be decreased when a fastener or some other device is used to aid in the alignment process. Dimensional tolerance stack-ups of the hole and fastener will allow the holes to become "partially" aligned, and mismatch results. Mismatch becomes detrimental when load is transferred through the plate and some fasteners receive a larger proportion of the bearing load, causing the fatigue cracks to initiate and grow.

The deleterious effects of mismatch were minimized by never separating faying surfaces prior to assembly. All fastener holes were drilled in production-type tooling. Prior to removal from the tooling, fasteners were installed and torqued to required values.

The second and more detrimental mechanism was found to be "metal yielding", localized yielding at the circumference of the fastener holes on the faying surface. The cause is a combination of (1) compressive stresses from fastener preload and (2) cyclic testing loads. The compressive stress field resulting from fastener preload deteriorates rapidly in a radial direction (Reference 7). Since cyclic loads cannot be changed, the effect of preload was minimized in two ways. First, constant sealant thicknesses were maintained through the use of shims (0.004 inch). These tests confirmed the available extension in fatigue life.

Secondly, the faying surfaces were spot-faced prior to drilling to approximately 0.005 inch in depth by 0.5 inch in diameter. Spot-facing of the faying surface alleviated bearing forces and, thus, relieved the region of high compressive stress.

The combination of a spotface and the removal of mismatch produced significant increases in fatigue crack depth at one life and decreases in EIFS for the load-transfer condition. Figure 5-7 shows decreases in EIFS for improved drilling and assembly of four to seven times for mean and 90-percentile values, respectively. Crack depths at one life, Figure 5-8, graphically show a 20-fold decrease for mean values and a 25-fold decrease for 90-percentile values. These results, which speak for themselves, are significant steps toward increasing fatigue life in the load-transfer condition.

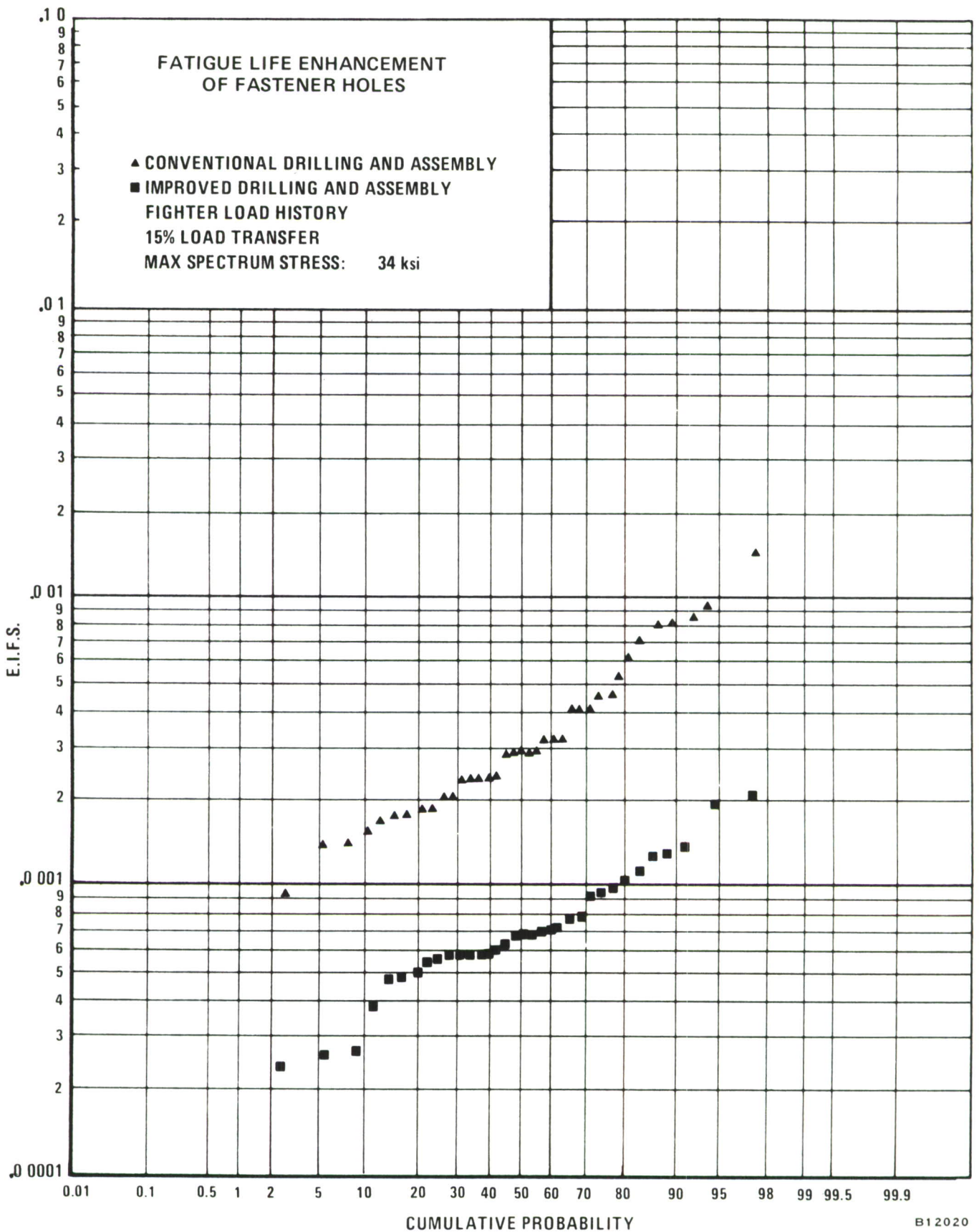


Figure 5-7 Cumulative Probabilities Showing Fatigue Enhancement of Fastener Holes

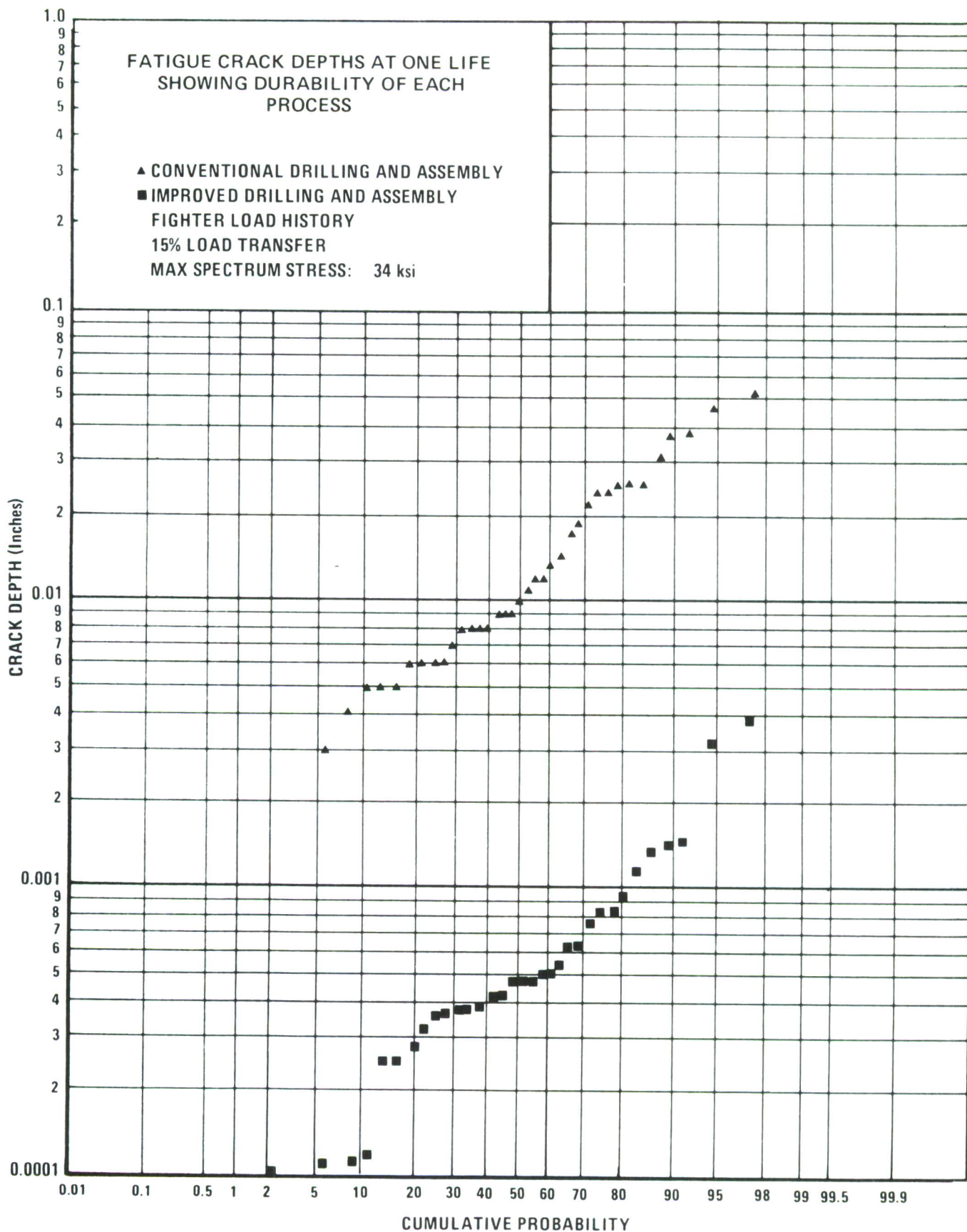


Figure 5-8 Cumulative Probabilities for Fatigue Crack Depths at One Life Showing Durability of Each Process

5.2.4 Comparison of Results

The variance of EIFS results from fighter to bomber spectrum testing is evident. These differences although not fully understood may well be products of maximum stress level and spectrum effects. The effect of maximum stress level on EIFS is seen in Figure 5-9 for the fighter load history. The 30.6-ksi and 34-ksi EIFS distributions are essentially inseparable, and the 40.8 ksi distribution falls into a range of larger EIFS values. The same trend, higher stress levels and higher distributions, does not hold for the bomber load history, seen in Figure 5-10. The effects on EIFS are not fully understood and, at a minimum, it must be assumed that EIFS is not only a function of stress level but also dependent upon spectra effects. These effects, although not fully understood, do not come as a surprise.

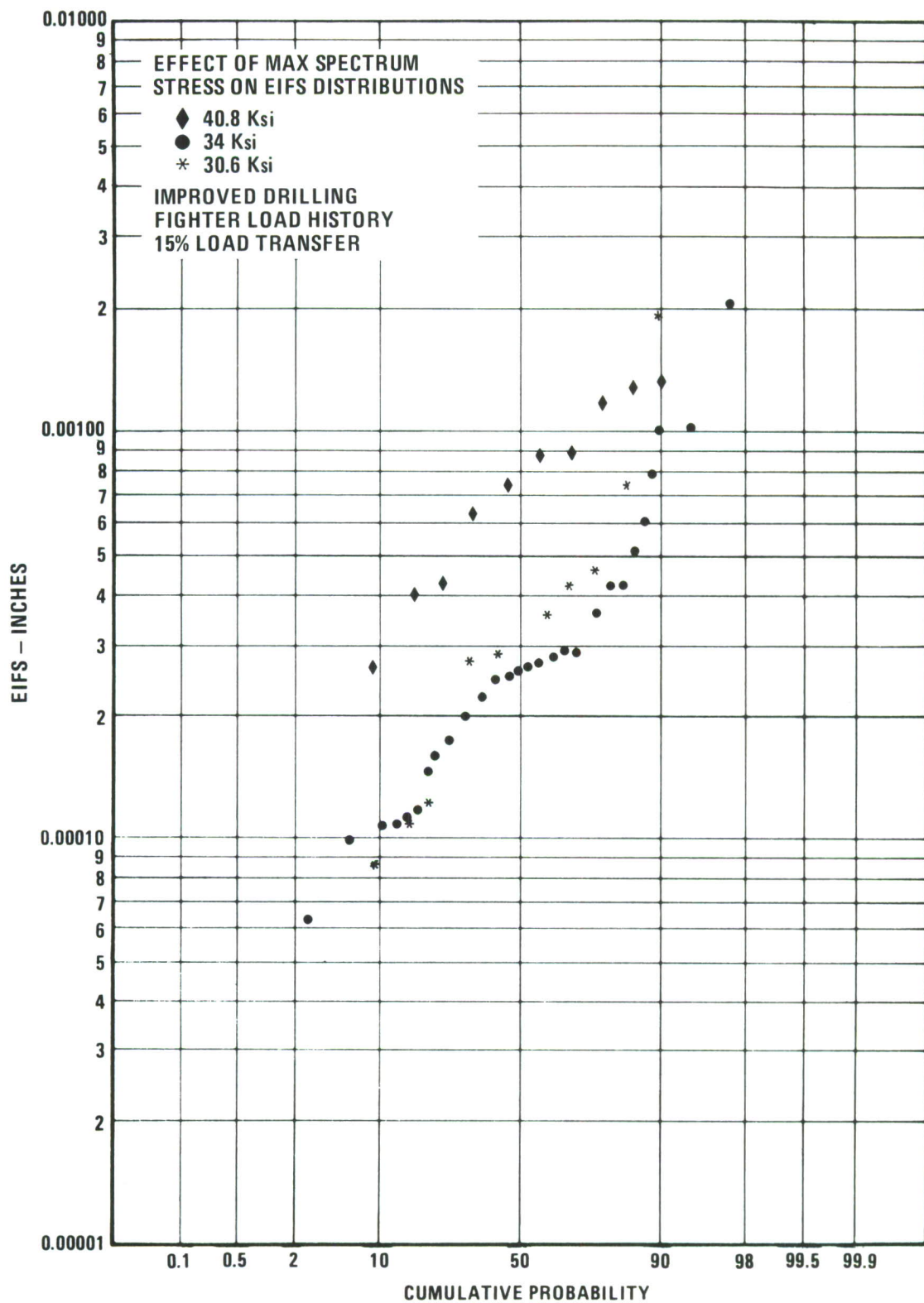


Figure 5-9 Effect of Max Fighter Spectrum Stress Level On EIFS Distribution for Improved Drilling of Load Transfer Specimens

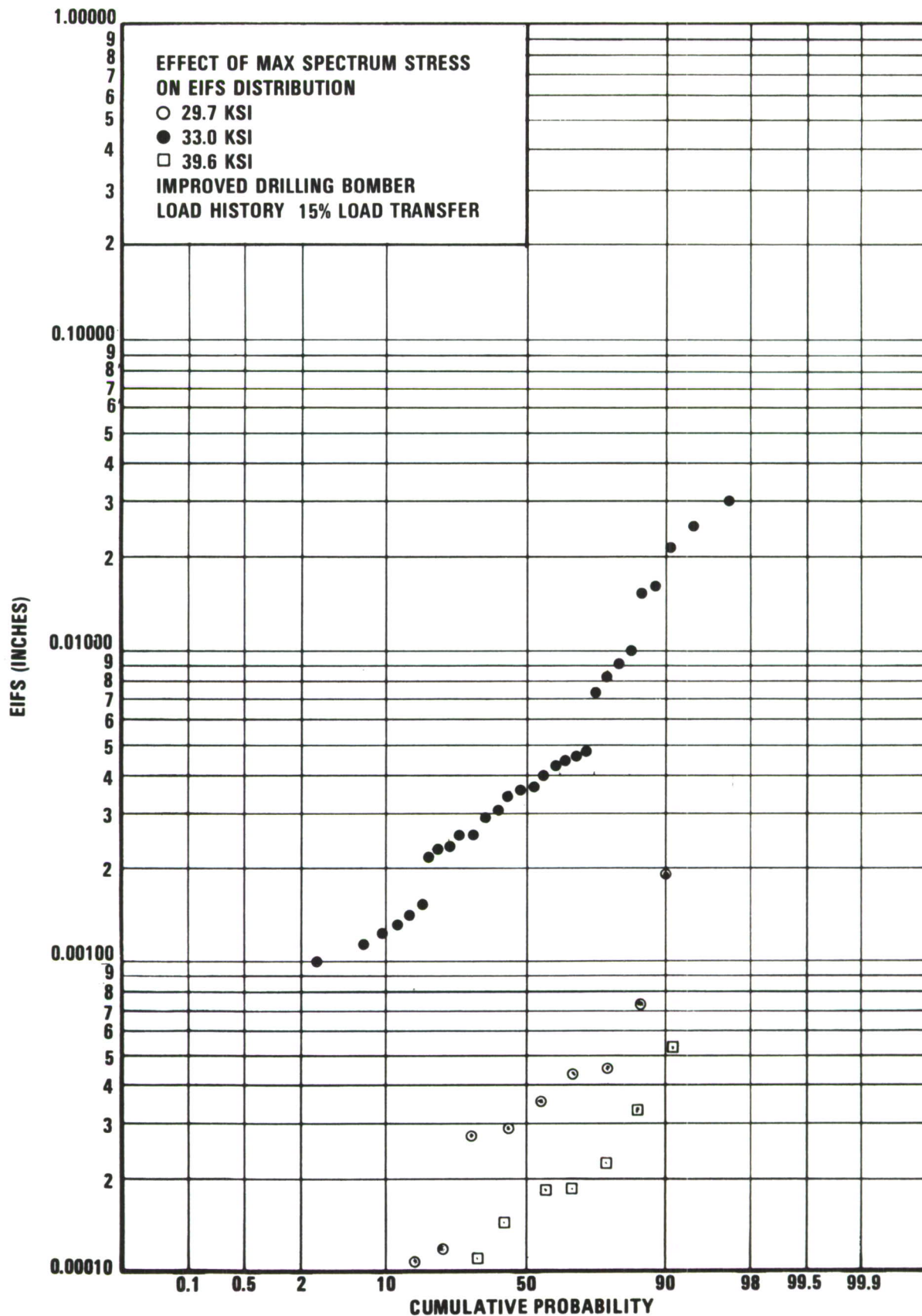


Figure 5-10 Effect of Maximum Spectrum Stress on EIFS Distribution

SECTION VI

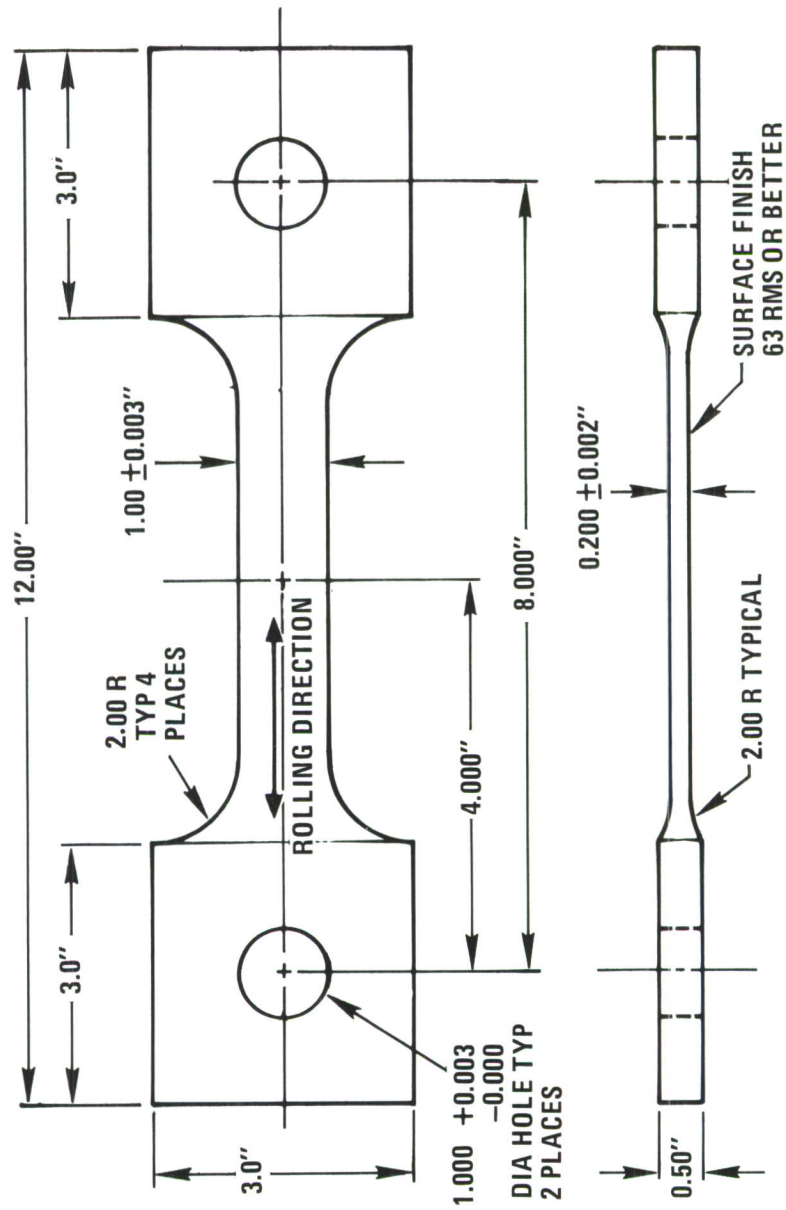
TASK IV EXTENSION TO STEEL AND TITANIUM

6.1 STEEL

In this phase of the program, 30 AF1410 steel no-load transfer specimens were cyclic-load tested using the fighter load sequence. AF 1410 steel was developed by General Dynamics (Reference 8) under a contract with the Air Force Materials Laboratory. This particular steel is similar in composition to HY 180 steel. Yield strength of the material as used in the program was approximately 224 ksi.

Specimen design is shown in Figure 6-1. The dimensions shown were to allow testing with the same load frames that were used for 7475-T7351 aluminum. The procedure for specimen manufacture is as follows:

1. Material will be shipped in a premachining, heat-treated condition (Rc 32 to 35 analogous to Ti-6Al-4V for machining properties).
2. Rough machine allowing 0.020 in. to 0.030 in. on all dimensions for clean up. Will be in blanks approximately 0.625 in. thick.
3. Double austenitize: (a) $1650^{\circ}\text{F} \pm 20^{\circ}\text{F}$ for 1 hour, oil quench
(b) $1525^{\circ}\text{F} \pm 20^{\circ}\text{F}$ for 1 hour, oil quench
4. Straighten if required
5. Age at $950^{\circ}\text{F} \pm 10^{\circ}\text{F}$ for five hours; air cool Rc 48 to 52
6. Final machine to following specifications and attached drawing.
 - (a) Grips will have a 125-rms minimum finish.
 - (b) Gage area will have a 63-rms minimum finish.
 - (c) Centerline symmetry must be strictly maintained from one edge.
 - (d) Tolerance on gage thickness will be ± 0.002 inch.
 - (e) Tolerance on 1.000-inch diameter pin holes will be -0.000 inch $+ 0.003$ inch.
 - (f) Material will be supplied as blanks 3 x 12 x 0.625 inches, having a saw-cut finish.



All holes in the AF 1410 steel specimens were drilled and reamed by the Quackenbush technique. Drilling speed and feed rates were identical to drilling parameters used for Ti 6Al-4V (drilling speed - 250 rpm, drilling rate - 0.001 inch/revolution). Dimensions of all holes were measured with a dial bore gauge. All diameters were within tolerance for drilling and reaming (.2500 - .2507 inch).

Maximum baseline stress used during testing was 125 ksi for a majority of the specimens, Table 6-1. Even at this stress level, most of the specimens failed before two lifetimes were completed. In many of the holes, cracks almost identical in size were found 180° from each other (at the location of maximum stress). The EIFS distribution is shown in Figure 6-2.

6.2 TITANIUM

Thirty Ti 6Al-4V no-load transfer specimens were cyclic-load tested using the fighter load sequence. This material was obtained from RMI Company, Niles, Ohio, and was made according to North American Rockwell Specification ST0170LB0032 Rev. E Cond. A (annealed). Microstructural examination of the plate indicated a nearly equiaxed alpha grain structure. Yield strength of the material in the as-received condition was approximately 130 ksi.

Specimen design was similar to that used for 7475-T7351 aluminum no-load transfer specimens, Figure 6-3. Since a much higher baseline stress was used as compared to the 7475-T7351 aluminum specimen, the cross-sectional area was decreased to allow testing with the same load frames. All holes in the Ti 6AL-4V specimens were drilled and reamed by the Quackenbush technique. Rate of drilling and reaming was 250 rpm. at a feed rate of 0.001 inch/revolution. After varying the maximum baseline stress between 75 ksi and 85 ksi on selected specimens, a stress of 82.5 ksi was established. A large variation was found in final crack depths Table 6-2. Crack growth rate was very rapid at these baseline stress levels.

Hole diameters were measured on all specimens using a dial bore gauge, Table 6-3. Except for four of the specimens, which were drilled and reamed under improper conditions, all hole dimensions were within tolerance (.2500-.2507 inch). The largest equivalent initial flaw size (EIFS) was found in a specimen (TYPF-2) where improper speeds, feeds, and lack of coolant had been used during the drilling and reaming process, Table 6-3. Eddy current signatures were nearly identical on all specimens except for TYPF-2, where, due to the oversized hole, large lift-off signals were present. The EIFS distribution for the Ti 6Al-4V specimens is shown in Figure 6-4.

**Table 6-1 FINAL CRACK DEPTHS FOR AF 1410 STEEL NO-LOAD TRANSFER SPECIMENS
(Fighter Load Sequence)**

<u>SPECIMEN NO.</u>	<u>FINAL CRACK DEPTH (IN.)</u>	<u>MAXIMUM BASELINE STRESS (KSI)</u>	<u>COMMENTS</u>
ST-1	.223	148.4	Failed after 3235 Flt-Hrs.
-2	.221	149.0	Failed after 3606 Flt-Hrs.
-3	.280	125	Failed after 5077 Flt-Hrs.
-4	.329	125	Failed after 9077 Flt-Hrs.
-5	.280	125	Failed after 10673 Flt-Hrs.
-6	.223	125	Failed after 10406 Flt-Hrs.
-7	.024	125	
-8	.220	125	Failed after 13206 Flt-Hrs.
-9	.071	125	Failed after 11600 Flt-hrs.
-10	.218	125	Failed after 13,235 Flt-Hrs.
-11	.232	125	Failed after 11,606 Flt-Hrs.
-12	.260	125	Failed after 6749 Flt-Hrs.
-13	.222	125	Failed after 9478 Flt-Hrs.
-14	.160	125	
-15	.232	125	Failed after 11235 Flt-Hrs.
-16	---	---	
-17	.267	125	Failed after 9606 Flt-Hrs.
-18	---	---	
-19	.258	125	Failed after 10006 Flt-Hrs.
-20	.303	125	Failed after 14671 Flt-Hrs.
-21	.328	125	Failed after 7067 Flt-Hrs.
-22	.281	125	Failed after 11606 Flt-Hrs.
-23	.228	125	Failed after 9773 Flt-Hrs.
-24	.262	125	Failed after 8455 Flt-Hrs.
-25	.234	125	Failed after 8502 Flt-Hrs.
-26	.287	125	Failed after 9635 Flt-Hrs.
-27	.298	125	Failed after 8806 Flt-Hrs.
-28	.326	125	Failed after 9144 Flt-Hrs.
-29	.353	125	Failed after 10677 Flt-Hrs.
-30	.300	125	Failed after 6348 Flt-Hrs.

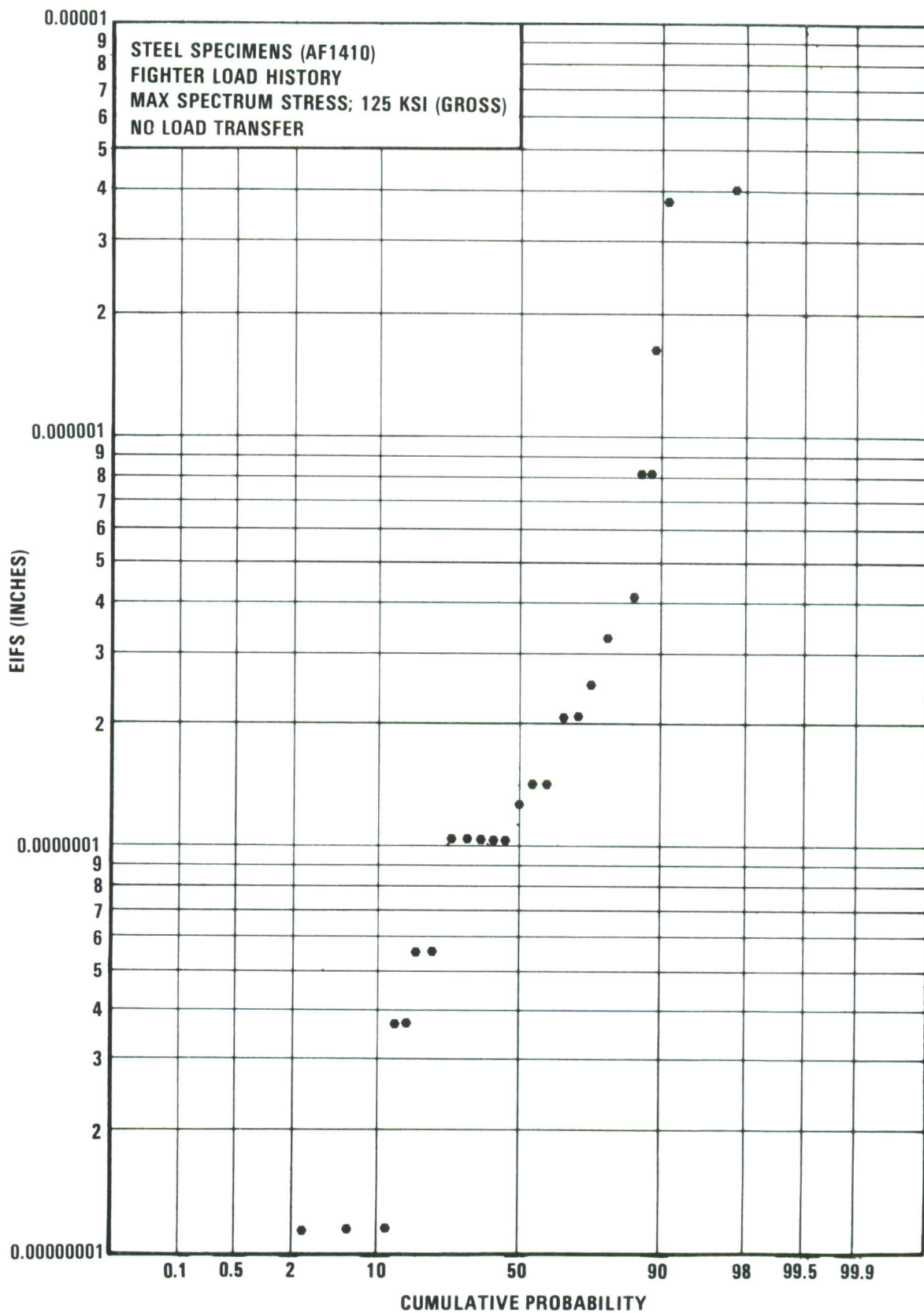
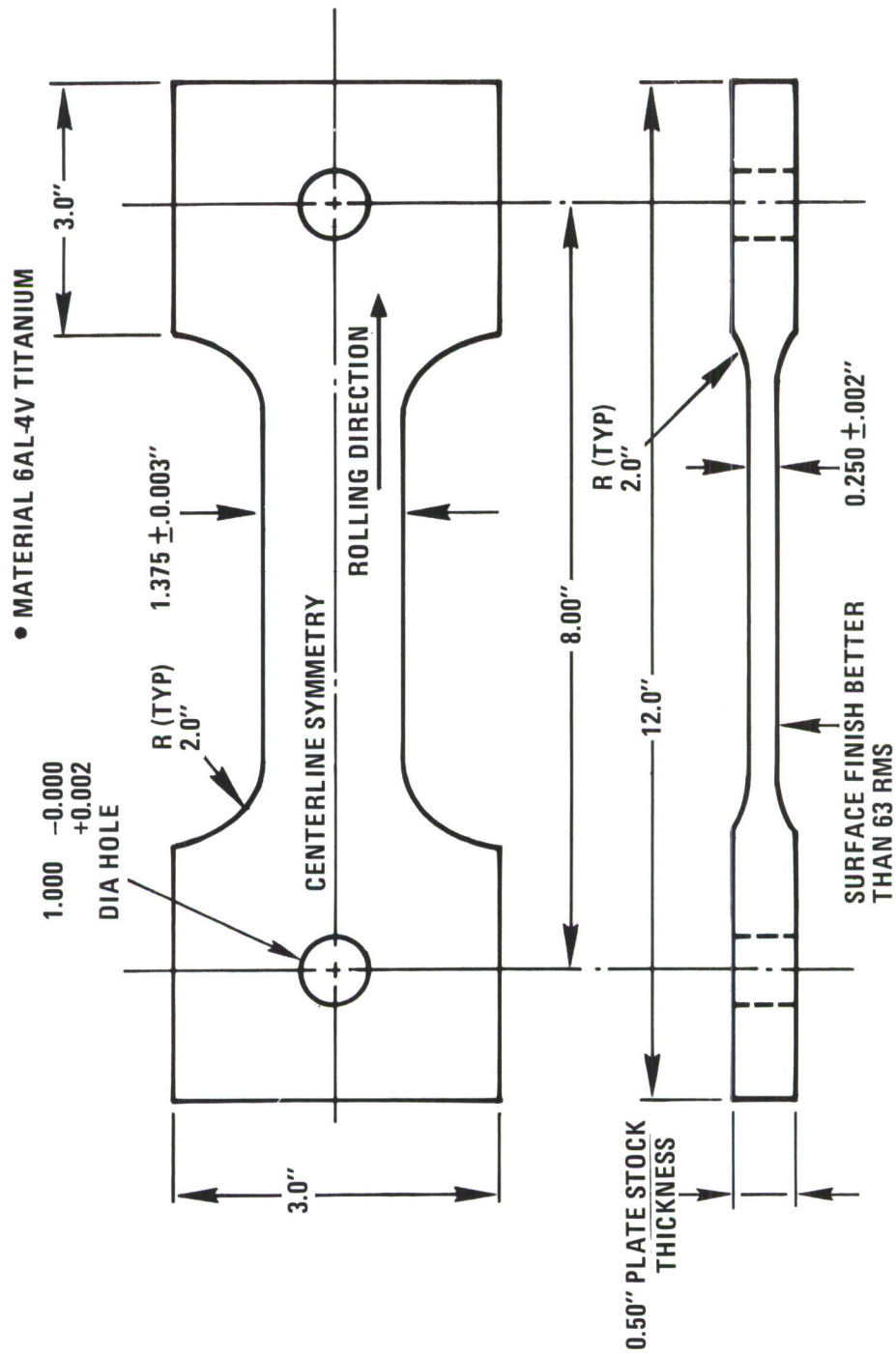


Figure 6-2 EIFS for Drilled and Reamed No-Load Steel Specimens



CENTERLINE SYMMETRY MUST BE MAINTAINED FROM ONE EDGE OF THE SPECIMENS

Figure 6-3 No-Load Transfer Specimen for Task IV

Table 6-2 FINAL CRACK DEPTHS FOR Ti 6A1-4V NO-LOAD TRANSFER SPECIMENS
(Baseline Stress = 82.5 ksi)

<u>SPECIMEN NO.</u>	<u>FINAL CRACK DEPTH (IN.)</u>	<u>COMMENTS</u>
TXPF-1	.392	Drilled and Reamed at Excessive Speed Failed after 10,000 Flt. Hrs.
-2	.002	No Coolant on Drill During Drill Process
-3	.003	
-4	.345	Failed after 11,077 Flt-Hrs.
-5	.003	
-6	.433	Failed after 15,635 Flt-Hrs.
-7	.058	
-8	.413	Failed after 13,478 Flt-Hrs.
-9	.004	
-10	.477	Failed after 14,806 Flt-Hrs.
-11	.017	
-12	.290	Failed after 10,835 Flt-Hrs.
-13	.282	Failed after 12,006 Flt-Hrs.
-14	.345	Failed after 12,806 Flt-Hrs.
-15	.196	Failed after 13,606 Flt-Hrs.
TYPF-1		
-2	.358	Improper Speeds, Feeds and Lack of Coolant During Drilling & Reaming. Failed after 6006 Flt-Hrs.
-3	.001	Run at Baseline Stress of 75KSI
-4	.366	Run at Baseline Stress of 85 KSI Failed After 15,467 Flt-Hrs.
-5	.009	Run at Baseline stress of 80 KSI
-6	.365	Failed after 12,035 Flt-Hrs.
-7	.354	Failed after 10,806 Flt-Hrs.
-8	.292	Failed after 15,606 Flt-Hrs.
-9	.017	
-10	.546	Failed after 11,547 Flt-Hrs.
-11	.351	Failed after 10,903 Flt-Hrs.
-12	.243	
-13	.206	Failed after 10,903 Flt-Hrs.
-14	.011	
-15	.363	Failed After 15,303 Flt-Hrs.

Table 6-3 EIFS AND HOLE DIAMETERS FOR Ti 6Al-4V NO-LOAD TRANSFER SPECIMENS

<u>SPECIMEN NO.</u>	<u>EIFS (IN.)</u>	<u>MAX, DIAMETER MEASURED (IN.)</u>
TXPF-1	.00190	.2516
-2	.00082	.2515
-3	.00067	.2505
-4	.00222	.2507
-5	.00067	.2507
-6	.00113	.2507
-7	.00110	.2507
-8	.00135	.2507
-9	.00066	.2507
-10	.00121	.2507
-11	.00090	.2507
-12	.00157	.2507
-13	.00189	.2507
-14	.00063	.2507
-15	.00081	.2507
 TYPF-1		.250
-2	.00312	.2535
-3		.2507
-4	.00106	.2506
-5	.00083	.2505
-6	.00145	.2507
-7	.00165	.2507
-8	.00103	.2507
-9	.00090	.2507
-10	.00157	.2507
-11	.00151	.2507
-12	.00110	.2507
-13	.00164	.2506
-14	.00084	.2505
-15	.00108	.2507

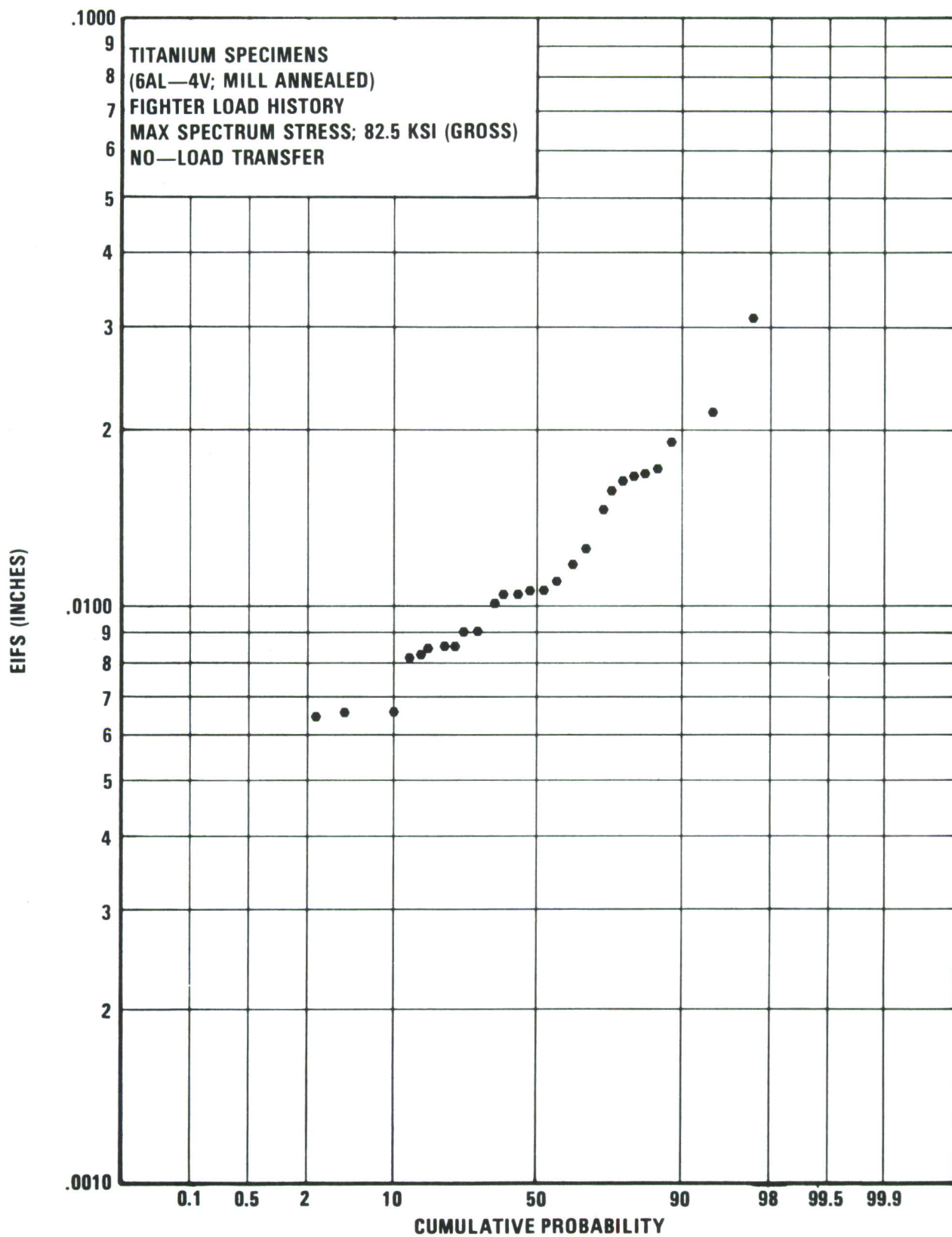


Figure 6-4 EIFS for Drilled and Reamed Titanium Specimens

SECTION VII

EXTENSION TO COLD-WORKED AND TAPER-LOK HOLES

7.1 COLD-WORKED HOLES

Thirty 7475-T7351 aluminum no-load transfer specimens were cold-worked by a method developed by the Boeing Company (Reference 9). The initial hole is drilled or reamed and a mandrel and split sleeve are inserted in the hole. The mandrel is pulled through the sleeve, which then is removed from the hole. The hole is finally reamed and is ready for fastener installation. The split-sleeve cold-working process specifications are controlled by an Industrial Wire and Metal Forming, Inc., document (Reference 10).

A mandrel for cold-working nominal 1/4-inch-diameter holes was not available; therefore, a mandrel for cold-working second oversize, 1/4-inch diameter holes (Mandrel No. 1WCMB-9-0-N-1) was used. The corresponding sleeve number was CBS-9-0-N-12-S.

All specimens were cyclic tested according to the F-16 wing root fighter spectrum. A maximum stress of 34 ksi was used. Specimens were cycled for two lifetimes before the crack depths and crack lengths of the largest fatigue cracks were measured, Table 7-1.

Original starting holes were drilled with diameters ranging from 0.2655 inch to 0.2710 inch. All diameters measured after cold-working and before final reaming were 0.274 inches. From these readings, values of permanent deformation in the diameter of the specimen were measured and plotted as a function of crack size after two lifetimes. These results are shown in Figures 7-1 and 7-2. No significant decrease in crack size was observed for specimens that had received the smaller percentage of permanent deformation.

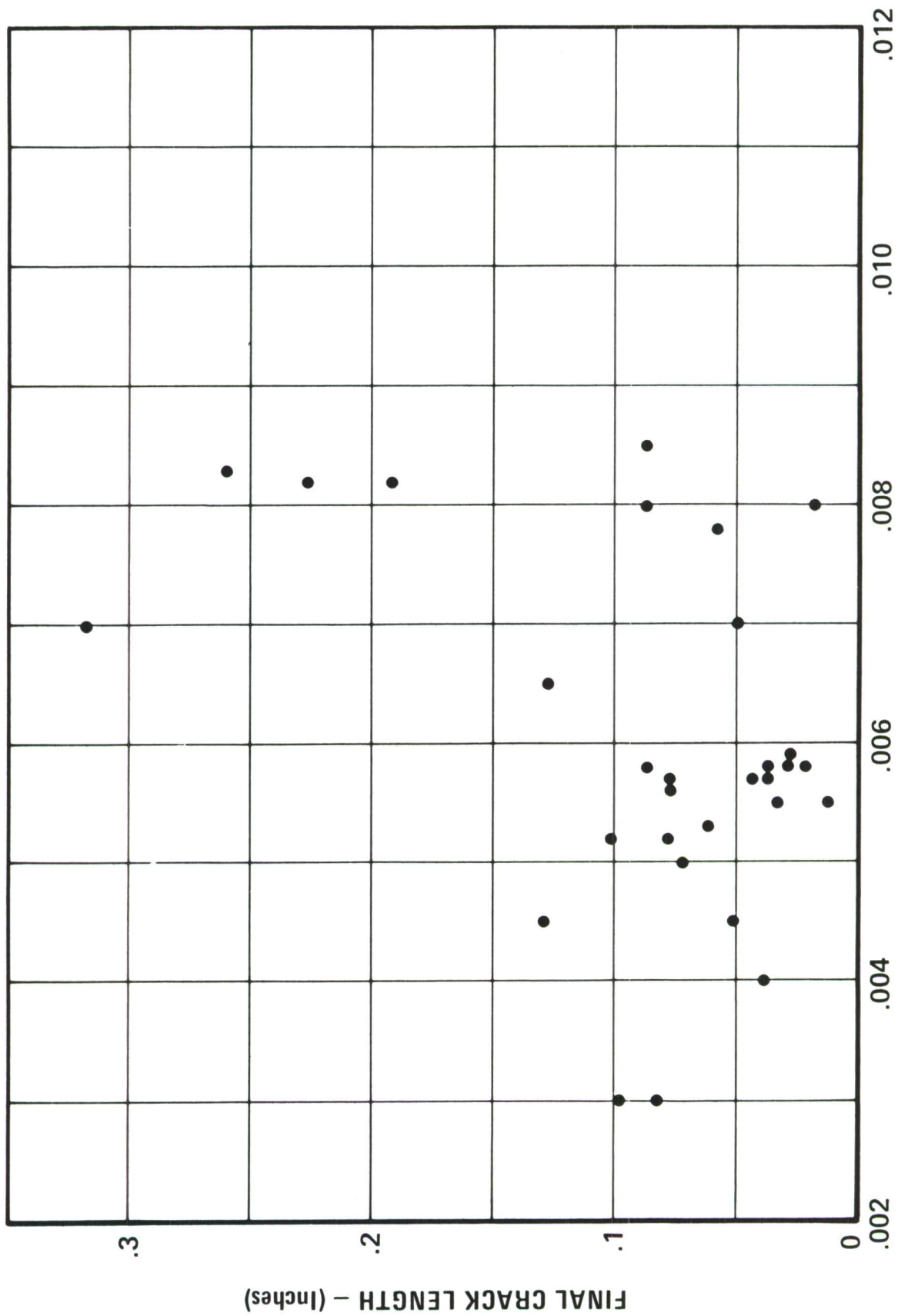
X-ray diffraction techniques were used to measure tangential residual stress around two of the cold-worked holes. Prior to cold-working, the plate surfaces on these specimens were polished such that no residual stresses were present prior to the cold-working process. Results of the residual stress measurements are shown in Table 7-2. Measurements were made adjacent to the hole on both the tool entry and exit sides at the critical orientations (3:00 and 9:00). Results indicate significantly higher compressive residual stress on the exit side compared to the entry side.

Table 7-1 FINAL CRACK SIZES FOR COLD-WORKED HOLES

SPECIMEN NUMBER	FINAL CRACK DEPTH (IN.)	FINAL CRACK LENGTH (IN.)	PERMANENT DEFORMATION OF DIAMETER (IN.)	ORIENTATION OF SPLIT IN SLEEVE
CW-1 *	.046	.260	.0083	8:00
-2	.023	.098	.0030	2:00
-3	.009	.088	.0080	5:00
-4	.006	.019	.0080	2:00
-5 +	.033	.317	.0070	3:00
-6	.021	.050	.0070	1:00
-7	.014	.228	.0082	10:00
-8	.015	.058	.0078	11:30
-9	.027	.199	.0082	7:00
-10	.017	.087	.0085	8:30
-11 +	.016	.129	.0045	9:00
-12	.014	.037	.0040	4:30
-13	.014	.101	.0052	3:00
-14	.014	.028	.0059	5:00
-15	.027	.079	.0057	1:30
-16	.015	.061	.0053	10:30
-17	.028	.028	.0058	8:00
-18	.016	.044	.0057	8:00
-19 +	.047	.077	.0052	1:30
-20	.016	.038	.0057	10:00
-21	.021	.073	.0050	5:00
-22	.019	.083	.0030	3:30
-23	.015	.128	.0065	10:30
-24	.040	.032	.0055	2:00
-25	.014	.051	.0045	7:30
-26	.009	.036	.0058	7:30
-27	.017	.086	.0058	8:00
-28	.008	.021	.0058	10:00
-29	.021	.077	.0056	12:30
-30	.014	.011	.0055	3:00
	.021 Avg.	.082 Avg.		

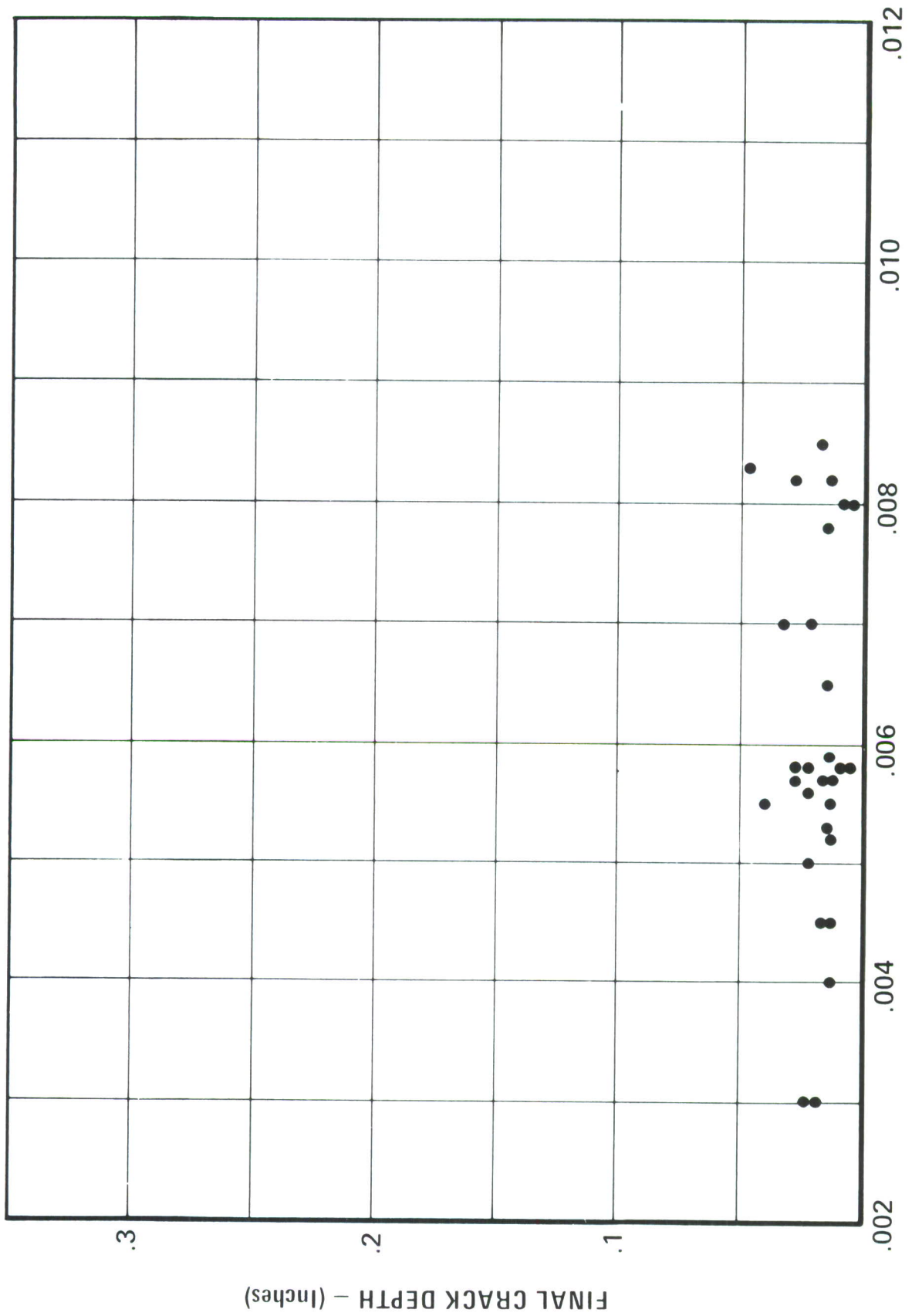
* Specimen run at maximum baseline stress of 38 ksi instead of 34 ksi

+ Specimens completed 6 lives



PERMANENT DEFORMATION IN DIAMETER – (Inches)

Figure 7-1 Final Crack Length versus Permanent Deformation for Cold-Worked Holes



PERMANENT DEFORMATION IN DIAMETER – (Inches)

Figure 7-2 Final Crack Depth versus Permanent Deformation for Cold-Worked Holes

Table 7-2 RESULTS OF RESIDUAL STRESS MEASUREMENTS

<u>HOLE NO.</u>	<u>LOCATION OF MEASUREMENT</u>	<u>MEASURED RESIDUAL STRESS (KSI)</u>
CW-6 (After Cold-Working)	Entry, 0° (9:00)	-12.8 (Compressive)
	Entry, 180° (3:00)	-17.1 "
	Exit, 0° (9:00)	-44.0 "
	Exit, 180° (3:00)	-48.0 "
CW-16 (After Cold-Working)	Entry, 0° (9:00)	-25.6 (Compressive)
	Entry, 180° (3:00)	-17.0 "
	Exit, 0° (9:00)	-42.0 "
	Exit, 180° (3:00)	-34.2 "

The orientation of the split in the sleeve was documented (Table 7-1) prior to cold-working to determine if the location of the split in the sleeve at a critical orientation might have an effect on fatigue life. No effect of orientation of the sleeve was observed.

Fractographic data were obtained on two cold-worked specimens. These results are shown in Figure 7-3, where the crack depth is plotted as a function of cycling. Crack growth was observed to be slower in the cold-worked holes as compared to growth in conventional drilled holes after cracks had grown to approximately 0.030 inch in depth.

7.2 TAPER-LOK HOLES

Thirty 7475-T7351 aluminum no-load transfer specimens were prepared for installation of tapered-bolt interference-fit fasteners. Standard-fit taper-lok bolts were used. The 1/4-inch taper-lok fastener produces an interference of 1 per 48 units in length.

Cyclic-load testing of all specimens was conducted using the fighter load sequence. In hopes of initiating fatigue cracks in all of the specimens during two lives, a higher baseline stress of 45 ksi was selected. Even at this higher stress level, many of the holes did not initiate fatigue cracks. In the few holes that initiated large cracks, the primary origin was on the specimen surface near the countersink and not in the bore of the hole. Primary crack depths after two lives are shown in Table 7-3.

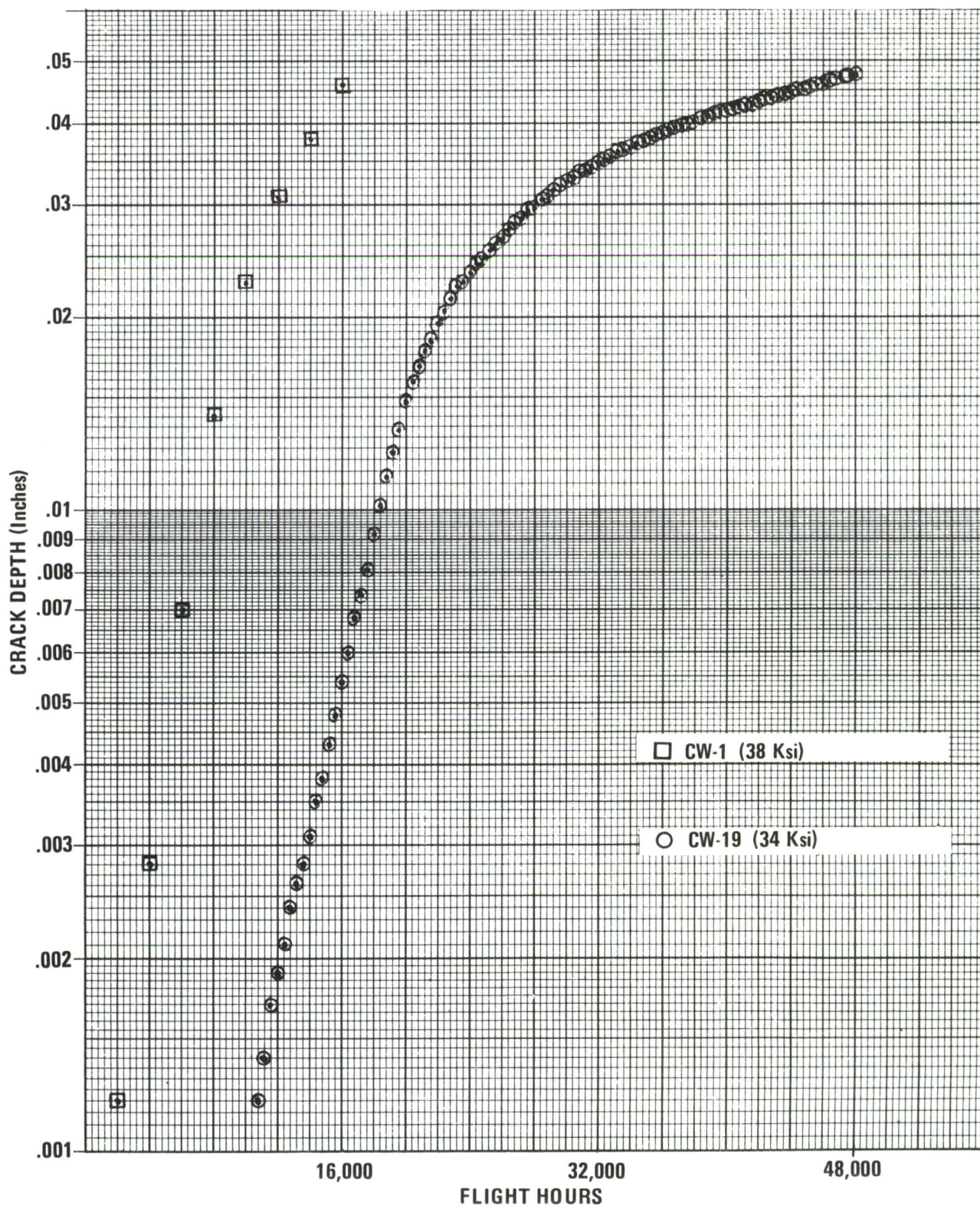


Figure 7-3 Crack Growth as a Function of Fatigue Cycling in No-Load Transfer Cold-Worked Holes

**Table 7-3 PRIMARY CRACK AFTER TWO LIVES FOR 7475-T7351 Al TAPER-LOK NO-LOAD
TRANSFER SPECIMEN, BASELINE STRESS = 45 ksi, FIGHTER SPECTRUM**

<u>SPECIMEN NO.</u>	<u>FINAL PRIMARY CRACK DEPTH (IN.)</u>	<u>FINAL PRIMARY CRACK LENGTH (IN.)</u>	<u>COMMENTS</u>
TL-1	-	-	
TL-2	-	-	
TL-3	.010	.007	
TL-4	.150	.200	primary origin lies on specimen surface near countersink
TL-5	.011	.094	
TL-6	.321	.254	primary origin lies on specimen surface near countersink
TL-7	Crack too small to measure		
TL-8	"		
TL-9	"		
TL-10	"		
TL-11	"		
TL-12	"		
TL-13	.363	.437	primary origin lies on specimen surface near countersink
TL-14	.033	.143	
TL-15	.037	.023	corner crack
TL-16	Crack too small to measure		
TL-17	"		
TL-18	"		
TL-19	"		
TL-20	.012	.074	
TL-21	Crack too small to measure		
TL-22	"		
TL-23	"		
TL-24	"		
TL-25	.006	.075	
TL-26	.020	.082	
TL-27	Crack too small to measure		
TL-28	.012	.068	
TL-29	.017	.125	
TL-30	Crack too small to measure		

SECTION VIII

CONCLUSIONS AND OBSERVATIONS

This program has investigated and developed an equivalent initial flaw size (EIFS) concept to quantitatively evaluate and compare the hole quality or fatigue performance of fastener holes and has identified and made improvements on several manufacturing and design parameters affecting fastener hole quality. The conclusions and observations that will be discussed in this section are based solely on the test results obtained with the parameters selected and tested by this program. Some of these same conclusions have been reached by the investigators of Reference 3 and 4, but with a different set of test parameters (i.e., material type, fastener/hole type, load spectrum, etc.). Although about half of the specimens tested in this program were conducted with the randomized 400-hour wing-root-bending load spectrum of the F-16 and the other half were tested with the AMAVS (B-1) wing pivot bending moment test spectrum, the program conclusions should be applicable to the general determination of fastener hole quality.

In reading the conclusions, one should keep in mind that it was not the intent of this program to perform a systematic study of hole roughness and other geometric details as a function of hole quality. Rather, it was to fabricate the test specimens using quality based on the distribution of production quality. However, 54 out of 613 specimens were fabricated with intentional deviation from standard production procedures i.e., dull drills, low speed, no coolant, etc. to produce holes that might not pass production inspection requirements and to compare their fatigue behavior with those fabricated by following standard production procedures.

Conclusions

1. Axial scratches are the key cause of early fatigue failure in no-load transfer fastener holes. These scratches were introduced by not maintaining drill bit rotation during retraction from the hole. Hole roughness as caused by rifling marks, gouges, drill tool chatter marks, etc., did not appear to degrade hole quality.
2. Hole diameters that were 0.002 inch out of tolerance did not appear to effect hole quality for the no-load transfer case.

3. Drilled and reamed holes are about equivalent, if not slightly worse, in fatigue behavior than drilled holes in the no-load-transfer case, with axial scratches caused by the reamer not rotating fast enough in relation to the rate of retraction from the fastener hole being the major contributor to early fastener hole failure.
4. Holes drilled by not using standard production procedures behaved only slightly worse than properly drilled holes in fatigue performance in the no-load transfer case.
5. Fastener hole quality in the low-load transfer case is much more difficult to determine, with several potential competing factors that could cause early fatigue failure. Localized yielding and/or fretting at the interfaces around the holes appeared to be the dominant factor in crack initiation and corner-crack growth leading to early fatigue failure. Mismatch is caused by the non-concentricity of the two holes appeared to be the second dominant factor that lead to early failure. The axial scratch, as in the no-load transfer case, is again a contributing factor that could lead to early fatigue failure. These conclusions are based on all the fastener-hole diameters within tolerance, namely, 0.250 ± 0.003 inch for drilled holes and 0.250 ± 0.0007 inch for drilled and reamed holes.
6. Burrs did not appear to affect the fatigue behavior of fastener holes, since no cracks were found to be initiated from burrs. With the exception of the first few specimens in the no-load transfer specimens, none of the holes were deburred.
7. Six state-of-the-art laboratory NDE techniques: eddy current, linear profilometer, rotary profilometer, dial bore gage, ultrasonics, and rubber cast, were evaluated, and little, if any, correlation has been found between inspection results and fatigue behavior of fastener holes.
8. A concept has been developed to ascertain EIFS that can be used with good accuracy to predict flaw size for some service time. The proof of the concept is in having the EIFS distribution (EIFSD) paralleling the flaw size distribution as determined by fractography. Using this concept, EIFSD has been obtained for the conditions shown in Table 3-1. However, the EIFS data for the cold-worked, taper-lok, and AF1410 steel holes still should be taken with a "grain of salt". In the case of cold-worked

and taper-lok holes, there was little, if any, crack growth to ascertain EIFS data. In the case of steel, a combination of small specimen size and high stress levels make it difficult to obtain a good analytical fit for EIFS determination.

Program Payoffs

- a. A Winslow Spacematic automatic drill was modified to maintain rotation during retraction to eliminate the introduction of axial scratches. The gain in fatigue behavior is summarized in Figure 8-1, where the data obtained with the improved drilling showed an approximately 40% improvement over those of the conventional Winslow drilling. General Dynamics, Fort Worth Division has ordered 170 modification kits for old Winslow drills and new drills with the modifications for the F-16 production program. The Lockheed-Georgia Company, Marietta, Georgia and the AVCO Corp., Nashville, Tennessee, have modified their drills to eliminate axial scratches in fastener holes for the USAF C5A-H Mod. program. The Fairchild Republic Corporation, Farmingdale, New York, has modified their drills on the USAF A-10 production line to eliminate the axial scratches.
- b. Improved assembly procedures were evaluated to eliminate or minimize mismatch and localized yielding to obtain improved fatigue behavior. By combining improved drilling and assembly, an approximately 100% improvement in the fatigue behavior was realized over the conventional case, as can be seen in Figure 8-2. The assembly improvements were made by either i) spot-facing 0.5 inch diameter by about 0.005 inch deep or ii) maintaining the sealant thickness between the two plates greater than 0.012 inch.
- c. Deburring requirements for the F-16 production program have been relaxed to eliminate the need for deburring of interface burrs and to remove the existing burrs with a flat plate rather than a conventional deburring tool, which could introduce notches for crack initiation sites.
- d. The implementation of elimination of mismatch for the F-16 production program is pending successful demonstration on a F-16 rear-fuselage component, where the destacking operation after the drilling operation will be eliminated.

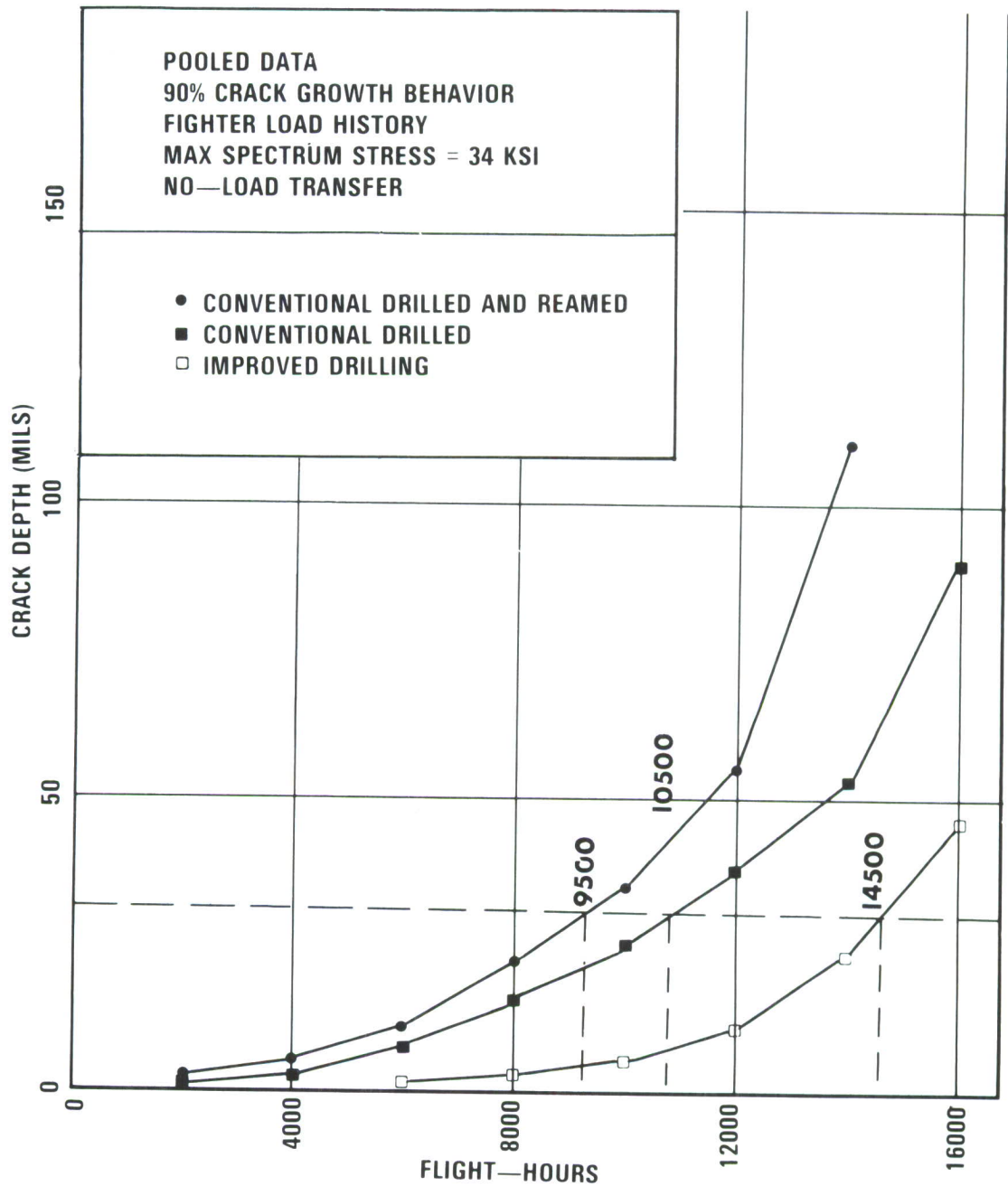


Figure 8-1 Ninety-Percentile Crack Growth Behavior for Conventionally Drilled and Reamed, Conventionally Drilled and Improved Drilling of Fastener Holes

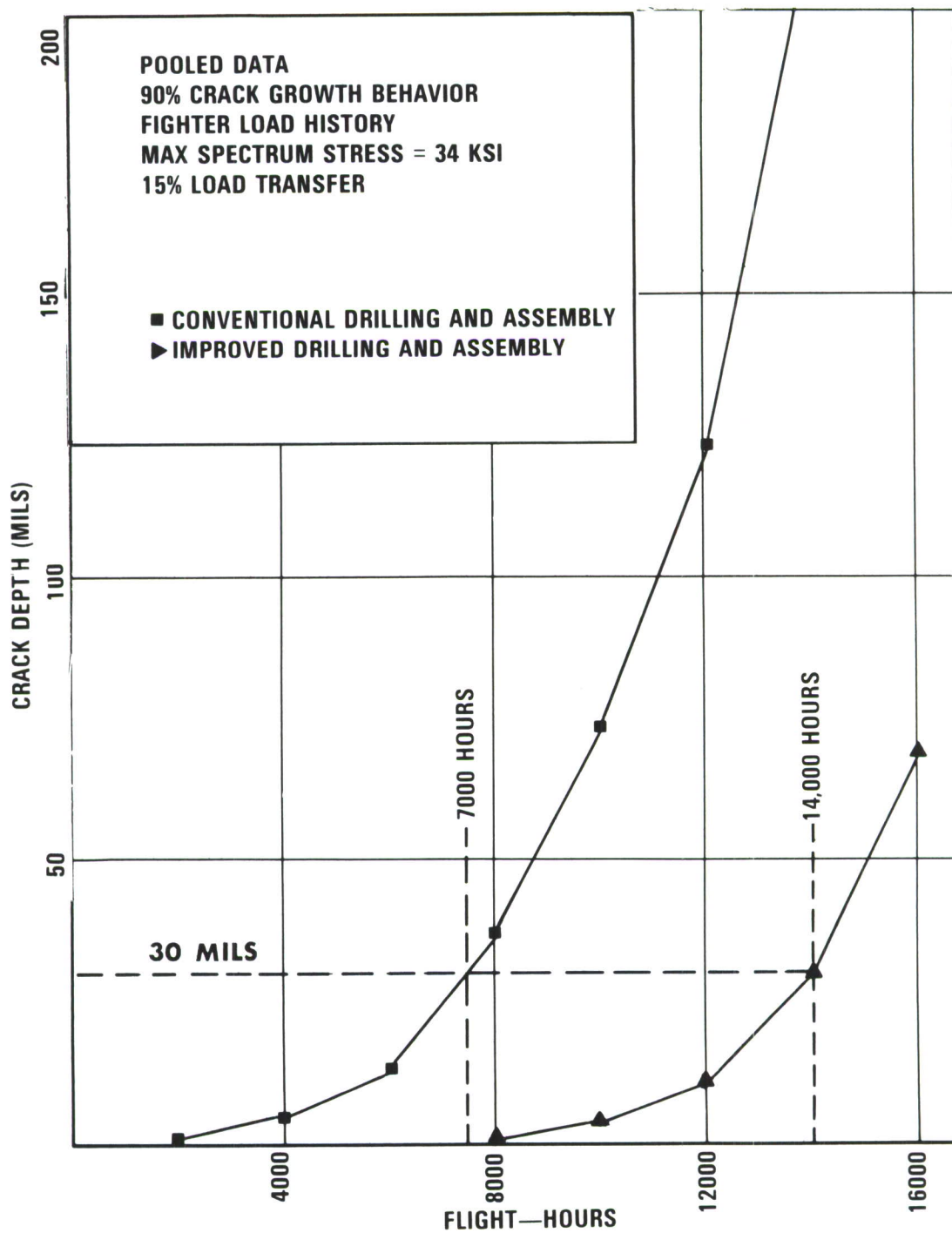


Figure 8-2 Ninety-Percentile Crack Growth Behavior for Conventional Drilling and Assembly and Improved Drilling and Assembly

SECTION IX

RECOMMENDATIONS

Based on the results and general outcome of this program, the following recommendations are made to: 1) further develop the EIFS concept as a routine design methodology, 2) evaluate new manufacturing and design concepts for fastener hole quality improvement, and 3) demonstrate the improved drilling and assembly procedures on aircraft structural components for improved durability and manufacturing cost reduction.

1. Conduct tests using counter-sunk and other commonly used aircraft fasteners for EIFS and fastener hole quality determination.
2. Conduct tests using specimens simulating fuselage construction which are drilled with hand-held drills for the determination of EIFS and fastener hole quality.
3. Determine the effects of manufacturing and design variables, i.e., stress level, load transfer, load spectrum, etc. on EIFS so it can be reduced to a generic dependence on material properties.
4. Conduct more tests with titanium and high strength steel to enlarge the EIFS data base and prove the EIFS concept on these aircraft structural alloys.
5. Conduct tests to determine the effects of simulated service environments on EIFS and fastener hole quality.
6. Conduct component demonstrations using the improved drilling and assembly procedures that were evaluated in this program in conjunction with some improved design concept for structural durability improvement.

APPENDIX A

NDE TECHNIQUES

All eddy current measurements in Task I were made with an automated eddy current inspection unit, Figure A-1. This unit consists of a Magnaflux ED-520 eddy current tester, a Gulton TR-711 high-speed recorder, and a variable drivespeed mini-scanner head. This inspection system was computer automated by the addition of a Hewlett-Packard HP5610A analog-to-digital converter, an HP2100 digital computer, and a HP7210 digital plotter.

The addition of the HP5610A analog-to-digital converter, which samples the Magnaflux ED-520 output, makes it possible to digitize eddy current signatures and store them in the memory of an HP2100 digital computer. The wave form is typically sampled by up to 5000 digitized values, $R(n)$, as the eddy current probe rotates its way through the fastener hole. The sampling time can be varied from 1 second to several minutes by a time-wasting calculation programmed into the computer software. Once digitized in the computer, the eddy current traces may be signal processed and displayed on an HP7210 digital plotter.

Software capabilities of this system consist of (1) filtering analytically, (2) data rectification, (3) data read-in, (4) data storage and retrieval, (5) zero read-in, (6) variable read-in times, (7) scale expansion, (8) computing correlation coefficients, (9) plotting out signal noise, (10) adjustable gain, (11) computing means and standard deviations, and (12) Fourier transforms. Several capabilities were used in this program.

Eddy current probes used were standard 1/4 inch diameter fastener hole probes, which give high signal-to-noise ratios. The coil diameter of these probes is approximately 1/8 inch. The probes contained axial relief slots, which were filled with rubber to give a fairly tight fit in the holes investigated. This has been found to increase the signal-to-noise ratio at the expense of greater probe wear.

Typical eddy current scans of holes with different types of defects are shown in Figure A-2. Chamfers, burrs, scratches and cracks can all be catalogued according to their different eddy current signatures. The probe rotates through the hole at a linear rate of probe travel, which is approximately .025 inch per revolution.

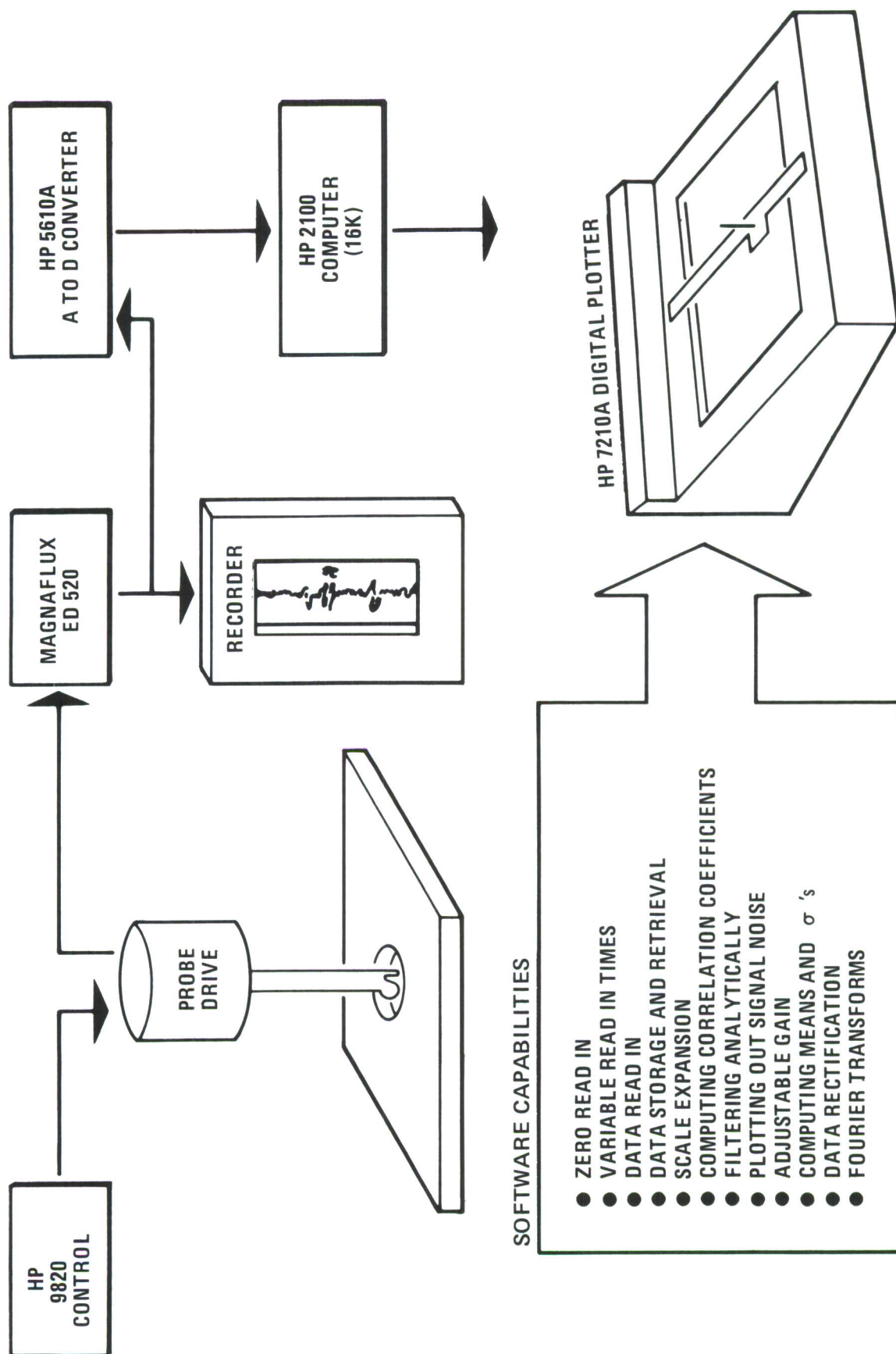


Figure A-1 Eddy Current Inspection Scheme

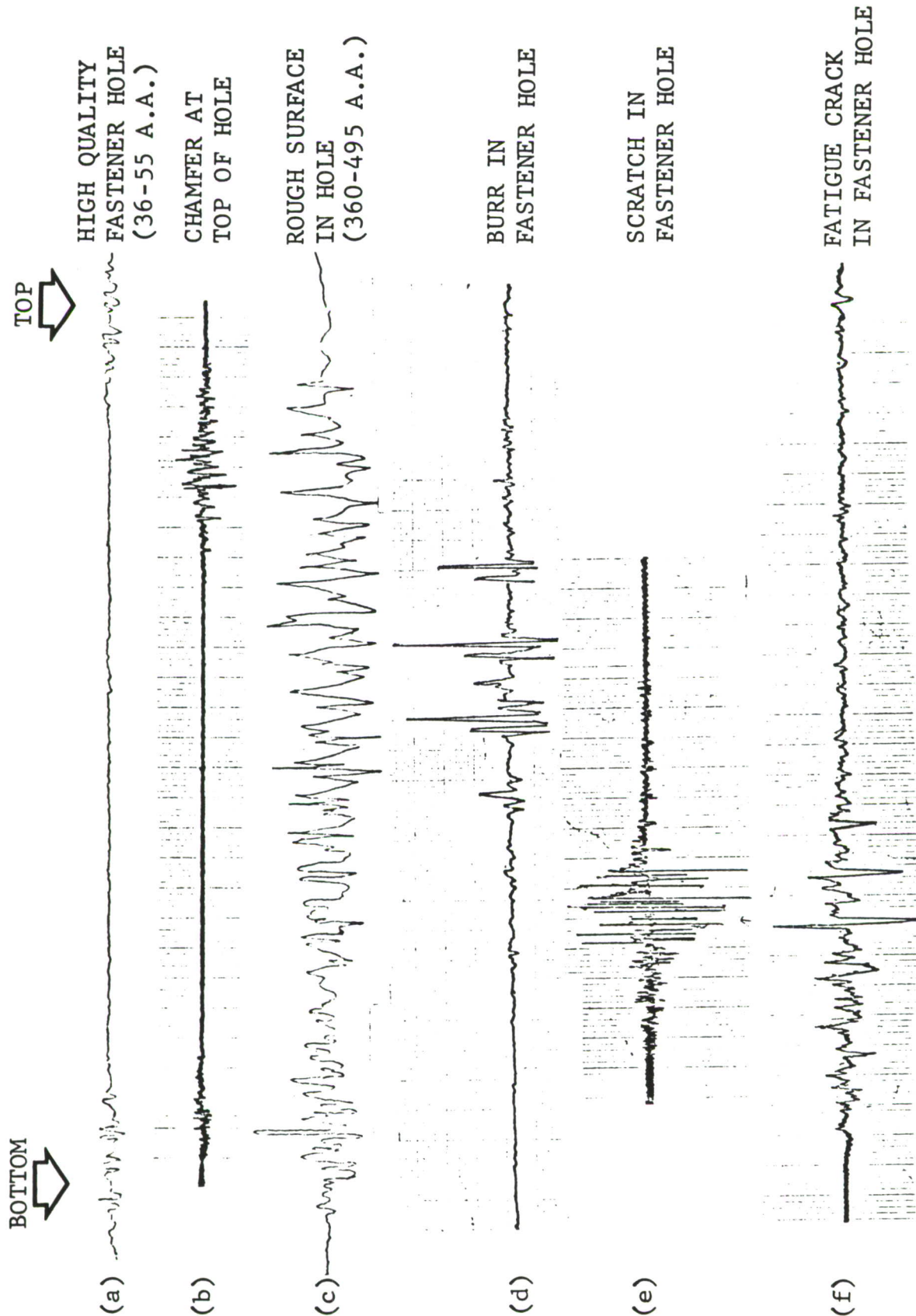


Figure A-2 Automatic Eddy Current Traces of Various Flaw Types in Fastener Holes

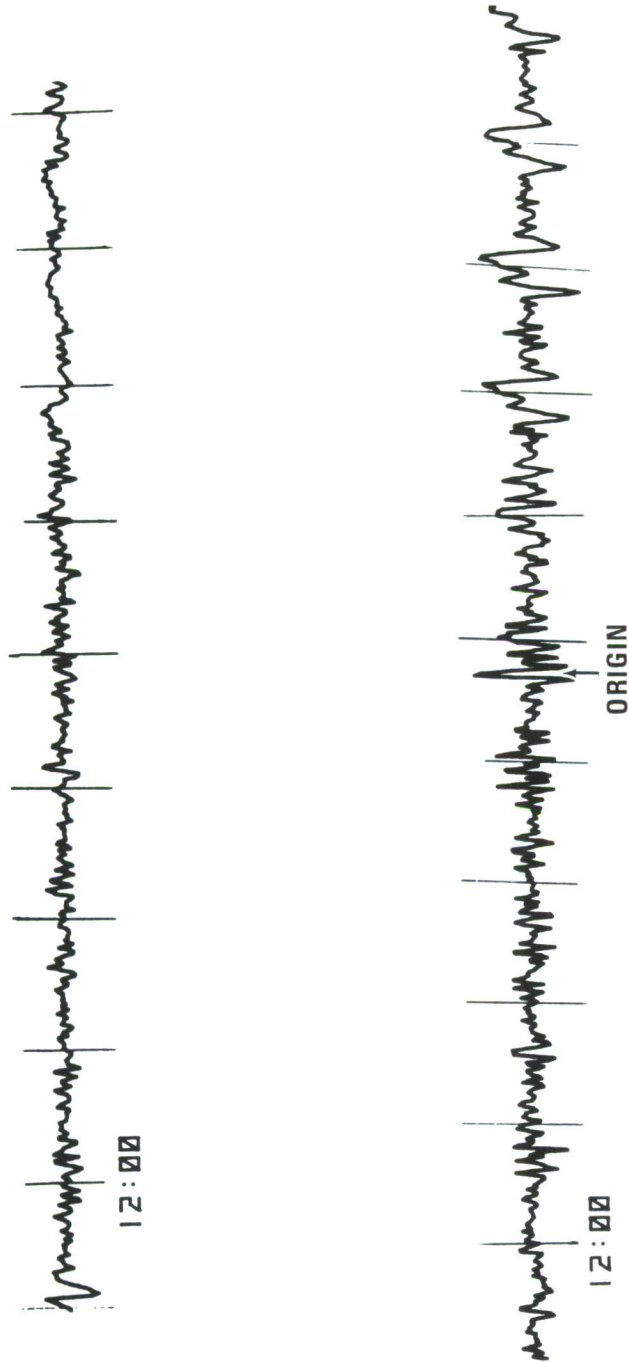


Figure A-3 Eddy Current Signatures for Two Winslow Properly Drilled Holes

The depth of the surface defects are related to the eddy current amplitude, while the length is related to the number of peaks (deflections) observed. Defect orientation in the hole can be determined also by use of the marker on the strip chart in conjunction with the orientation of a known defect in a reference part. Eddy current signatures of two Winslow (clearance fit) properly drilled holes along with the orientation in the hole are shown in Figure A-3. Each marker corresponds to the 12:00 o'clock* orientation, and each mark corresponds to one revolution in the hole.

A computer program was written for the HP2100 computer that calculated the (1) maximums, (2) minimums, (3) means, and (4) standard deviation of the eddy current signal at the critical orientations (2:00 to 4:00 and 8:00 to 10:00). This information was displayed in the form of a table (Table A-1) and, thus, eddy current parameters could be related to EIFS.

Rotary Proficorder

A Bendix proficorder with a rotary piloter was used to measure a total surface profile around the bore of the hole. Measurements were taken midway through the depth of the hole. A diamond stylus with a 0.0005-inch radius was used. A typical polar plot is shown with scans in Figure A-4, with scans originating at approximately 9:00 orientation. Both 250 μ inch/division and 1000 μ inch/division ranges were used. The total surface profile obtained includes both surface roughness and waviness. The orientation and dimensions of surface irregularities can be determined by this technique. For example, scratches are denoted by outward deflections shown in Figure A-4. The depth, width, and orientation of these scratches can be measured from a typical polar plot. On the other hand, smears are denoted as inward deflections. Their dimensions can also be obtained from polar plots.

The polar plot also gives a measure of out-of-roundness in the specimen. Shown in Figure A-5 are total surface profiles indicating the difference in out-of-roundness between two holes drilled and reamed by the Quackenbush technique. These out-of-roundness readings are more accurate than those obtained with a dial bore gauge but are much more time consuming to obtain.

* By the clock designation for the test specimens, 9:00 and 3:00 are the critical orientations or the location of maximum stress.

Table A-1 EDDY CURRENT TABULATION SHOWING (1) MAXIMUMS, (2) MINIMUMS, (3) MEANS AND (4) STD. DEV. OF THE EDDY CURRENT SIGNAL AT THE CRITICAL ORIENTATIONS (2:00 - 4:00, 8:00 - 10:00)

	MIN.	MAX.	MEAN	STAND.	DEV.
33	-.003516	.016797	-.007656	.015707	
65	-.194531	.035547	-.049902	.087072	
93	.000000	.021494	.010230	.006564	
117	-.332422	.195703	-.059352	.196379	
144	-.013156	.039375	-.002127	.006732	
163	-.351172	.183594	-.075365	.190593	
194	-.012109	.014844	.000365	.009084	
213	-.207812	.083594	-.052648	.112973	
244	-.019531	-.000731	-.008311	.005438	
268	-.073047	.055359	.000304	.048999	
294	-.024219	-.001172	-.010327	.007321	
310	-.012109	.024219	.004470	.013838	
344	-.021375	.005859	-.009418	.008230	
368	-.023828	.019141	.000420	.013834	
394	-.045313	-.005273	-.013238	.012741	
418	-.141406	.020703	-.032422	.059279	
445	-.116797	.012500	-.052691	.049429	
469	-.133672	.012109	-.043186	.053570	
495	-.110547	.043750	-.057899	.047458	
519	-.138934	-.016797	-.054942	.032217	
547	-.092600	.043359	-.034896	.048845	
571	-.100344	-.023433	-.055903	.026683	
597	-.130013	.053125	.000911	.057956	
621	-.038281	.010391	-.035592	.036833	
648	-.094531	.052344	.004774	.052693	
672	-.045703	.002344	-.025998	.015953	
698	-.117138	.003281	.001910	.070023	
722	-.074609	-.005859	-.044358	.025493	
747	-.037109	.045313	-.007335	.029218	
771	-.007109	.007422	-.015625	.032542	
797	-.007109	.060933	-.004687	.057274	
821	-.004375	.019531	-.016316	.035435	
848	-.006719	.035938	-.011241	.050032	
872	-.002234	.017969	-.047396	.037548	
899	-.029297	.032422	-.000087	.020343	
923	-.074219	.010547	-.033333	.026695	
950	-.039363	.013231	-.006858	.018046	
974	-.044531	.000734	-.017274	.017069	

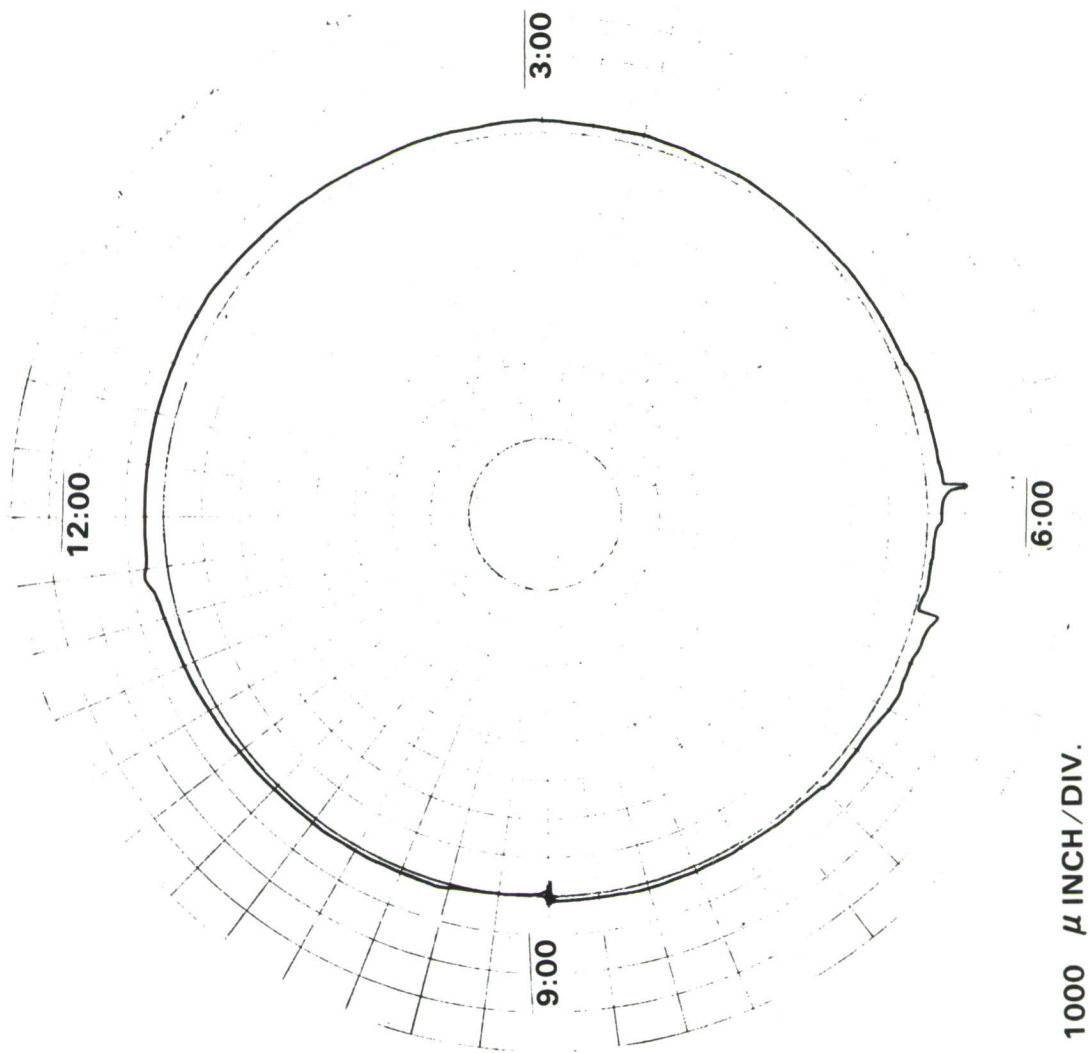
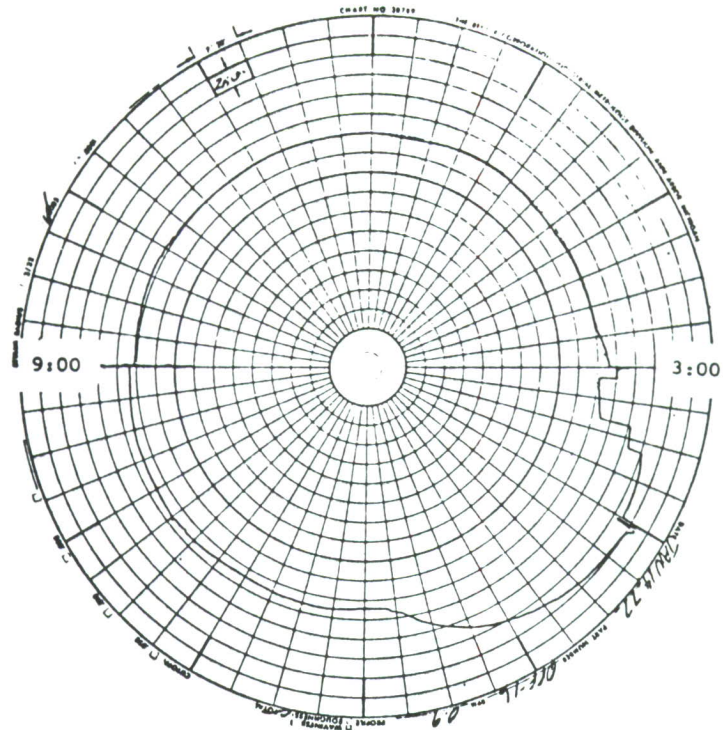
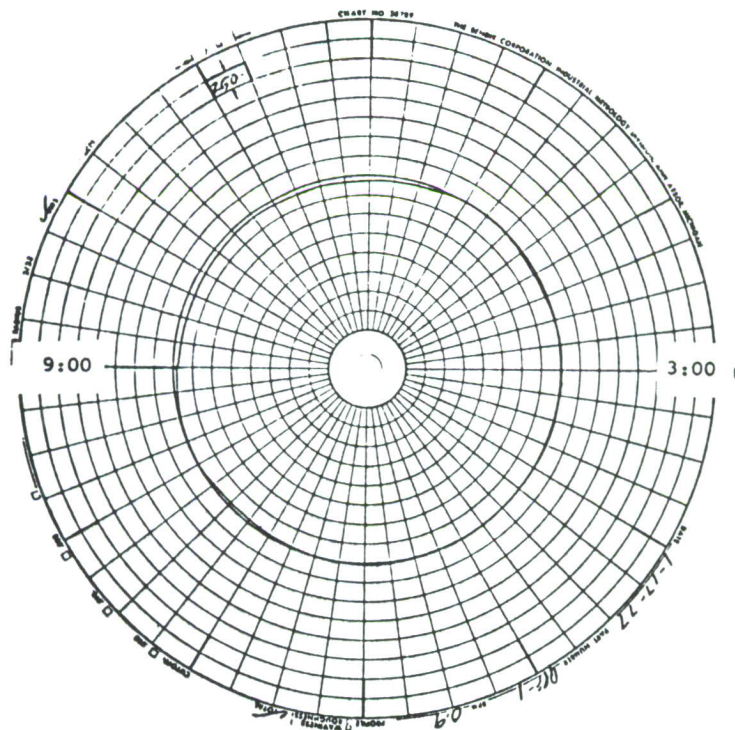


Figure A-4 Scratches at Non-Critical Orientations in a Drilled Hole



250 μ inch/div.



250 μ inch/div.

Figure A-5 Polar Plots Showing the Difference in Out-of-Roundness Between Two Holes Drilled By the Quackenbush Technique

APPENDIX A

NDE TECHNIQUES

All eddy current measurements in Task I were made with an automated eddy current inspection unit, Figure A-1. This unit consists of a Magnaflux ED-520 eddy current tester, a Gulton TR-711 high-speed recorder, and a variable drivespeed mini-scanner head. This inspection system was computer automated by the addition of a Hewlett-Packard HP5610A analog-to-digital converter, an HP2100 digital computer, and a HP7210 digital plotter.

The addition of the HP5610A analog-to-digital converter, which samples the Magnaflux ED-520 output, makes it possible to digitize eddy current signatures and store them in the memory of an HP2100 digital computer. The wave form is typically sampled by up to 5000 digitized values, $R(n)$, as the eddy current probe rotates its way through the fastener hole. The sampling time can be varied from 1 second to several minutes by a time-wasting calculation programmed into the computer software. Once digitized in the computer, the eddy current traces may be signal processed and displayed on an HP7210 digital plotter.

Software capabilities of this system consist of (1) filtering analytically, (2) data rectification, (3) data read-in, (4) data storage and retrieval, (5) zero read-in, (6) variable read-in times, (7) scale expansion, (8) computing correlation coefficients, (9) plotting out signal noise, (10) adjustable gain, (11) computing means and standard deviations, and (12) Fourier transforms. Several capabilities were used in this program.

Eddy current probes used were standard 1/4 inch diameter fastener hole probes, which give high signal-to-noise ratios. The coil diameter of these probes is approximately 1/8 inch. The probes contained axial relief slots, which were filled with rubber to give a fairly tight fit in the holes investigated. This has been found to increase the signal-to-noise ratio at the expense of greater probe wear.

Typical eddy current scans of holes with different types of defects are shown in Figure A-2. Chamfers, burrs, scratches and cracks can all be catalogued according to their different eddy current signatures. The probe rotates through the hole at a linear rate of probe travel, which is approximately .025 inch per revolution.

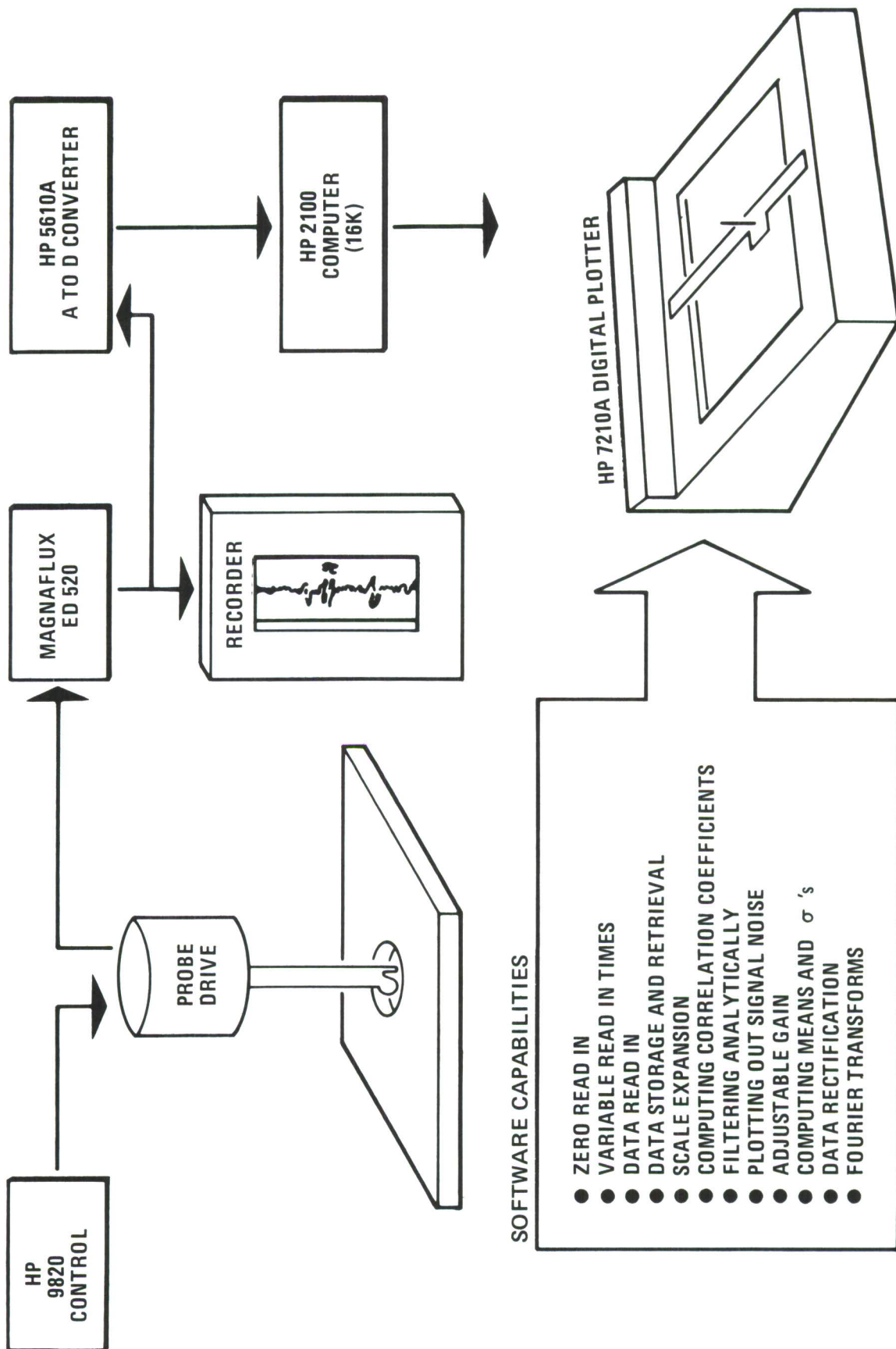


Figure A-1 Eddy Current Inspection Scheme

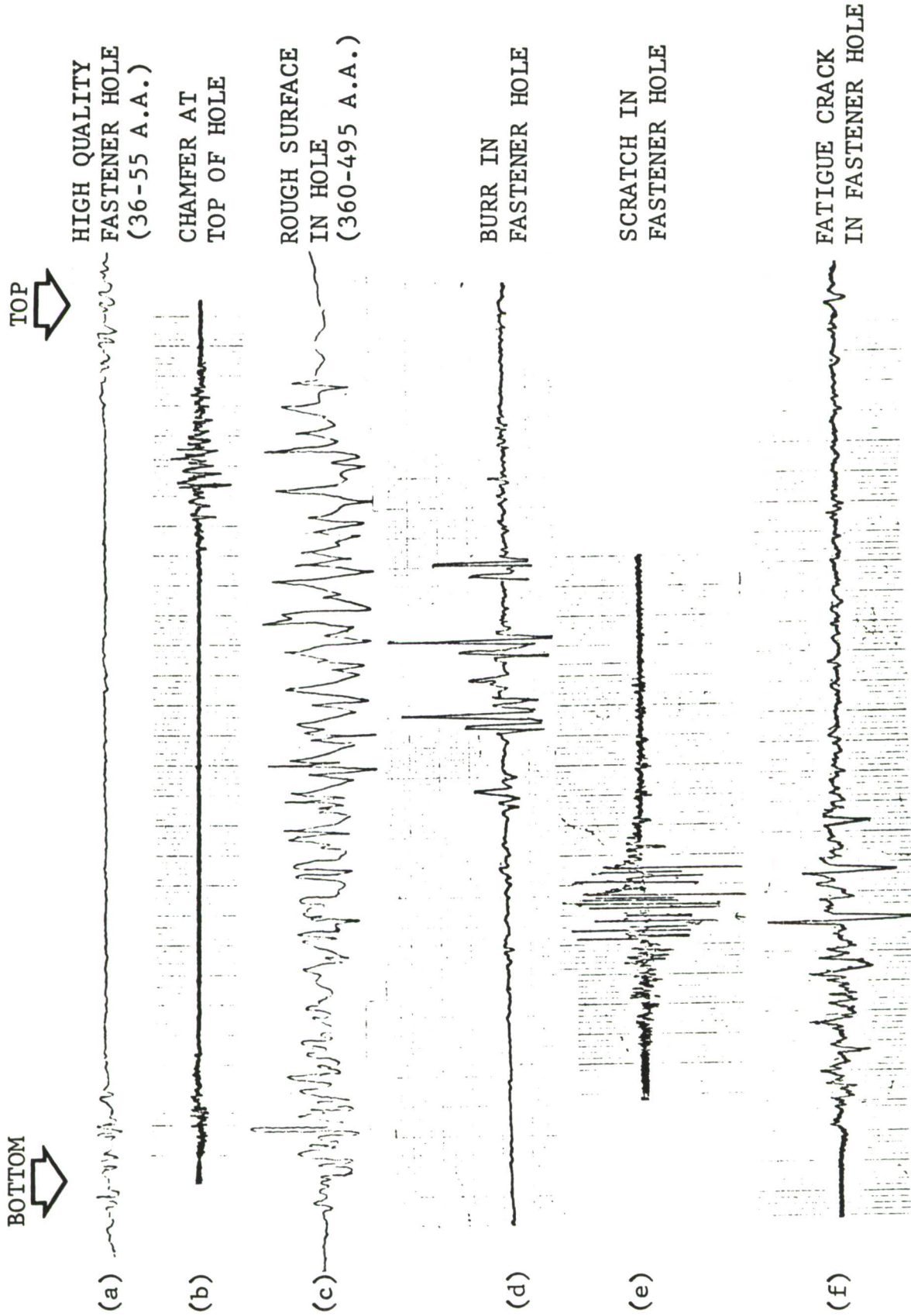


Figure A-2 Automatic Eddy Current Traces of Various Flaw Types in Fastener Holes



Figure A-3 Eddy Current Signatures for Two Winslow Properly Drilled Holes

The depth of the surface defects are related to the eddy current amplitude, while the length is related to the number of peaks (deflections) observed. Defect orientation in the hole can be determined also by use of the marker on the strip chart in conjunction with the orientation of a known defect in a reference part. Eddy current signatures of two Winslow (clearance fit) properly drilled holes along with the orientation in the hole are shown in Figure A-3. Each marker corresponds to the 12:00 o'clock* orientation, and each mark corresponds to one revolution in the hole.

A computer program was written for the HP2100 computer that calculated the (1) maximums, (2) minimums, (3) means, and (4) standard deviation of the eddy current signal at the critical orientations (2:00 to 4:00 and 8:00 to 10:00). This information was displayed in the form of a table (Table A-1) and, thus, eddy current parameters could be related to EIFS.

Rotary Proficorder

A Bendix proficorder with a rotary piloter was used to measure a total surface profile around the bore of the hole. Measurements were taken midway through the depth of the hole. A diamond stylus with a 0.0005-inch radius was used. A typical polar plot is shown with scans in Figure A-4, with scans originating at approximately 9:00 orientation. Both 250 μ inch/division and 1000 μ inch/division ranges were used. The total surface profile obtained includes both surface roughness and waviness. The orientation and dimensions of surface irregularities can be determined by this technique. For example, scratches are denoted by outward deflections shown in Figure A-4. The depth, width, and orientation of these scratches can be measured from a typical polar plot. On the other hand, smears are denoted as inward deflections. Their dimensions can also be obtained from polar plots.

The polar plot also gives a measure of out-of-roundness in the specimen. Shown in Figure A-5 are total surface profiles indicating the difference in out-of-roundness between two holes drilled and reamed by the Quackenbush technique. These out-of-roundness readings are more accurate than those obtained with a dial bore gauge but are much more time consuming to obtain.

* By the clock designation for the test specimens, 9:00 and 3:00 are the critical orientations or the location of maximum stress.

Table A-1 EDDY CURRENT TABULATION SHOWING (1) MAXIMUMS, (2) MINIMUMS, (3) MEANS AND (4) STD. DEV. OF THE EDDY CURRENT SIGNAL AT THE CRITICAL ORIENTATIONS (2:00 - 4:00, 8:00 - 10:00)

	MIN.	MAX.	MEAN	STAND.	DEV.
33	-.003516	.016797	-.007656	.015727	
65	-.194531	.035547	-.049902	.087372	
93	.003427	.021494	.012230	.026564	
117	-.332422	.195702	-.259352	.196879	
144	-.013156	.039375	-.002127	.026732	
163	-.351172	.183594	-.075365	.193593	
194	-.012109	.014844	.002865	.009084	
213	-.207812	.083594	-.352648	.112973	
244	-.019531	-.000751	-.008311	.005438	
268	-.073247	.055359	.000304	.048999	
294	-.024219	-.001172	-.010827	.027321	
310	-.012109	.024219	.004472	.013838	
344	-.021375	.005859	-.009418	.008230	
363	-.023828	.019141	.008420	.013834	
394	-.045313	-.005273	-.013238	.012741	
418	-.141406	.020703	-.032422	.059279	
445	-.116797	.012500	-.052691	.049429	
469	-.138672	.012139	-.043186	.053572	
495	-.110547	.043753	-.057899	.047458	
519	-.138934	-.016797	-.054942	.032217	
547	-.099610	.043359	-.034896	.048845	
571	-.100344	-.023433	-.055923	.026683	
597	-.130313	.053125	.000911	.057956	
621	-.038281	.010391	-.035592	.036833	
648	-.094531	.052344	.004774	.052693	
672	-.045703	.002344	-.025998	.015253	
693	-.117133	.008281	.001910	.070003	
722	-.074639	-.005859	-.044358	.025493	
747	-.037139	.045313	-.007335	.029218	
771	-.057109	.007422	-.015625	.032542	
797	-.007139	.060933	-.004687	.057274	
821	-.004375	.019531	-.016316	.035435	
848	-.006719	.035938	-.011241	.052832	
872	-.092234	.017969	-.047396	.037548	
899	-.029297	.032422	-.000087	.020343	
923	-.074219	.010547	-.033333	.026695	
950	-.039063	.013231	-.006858	.018046	
974	-.044531	.000734	-.017274	.017369	

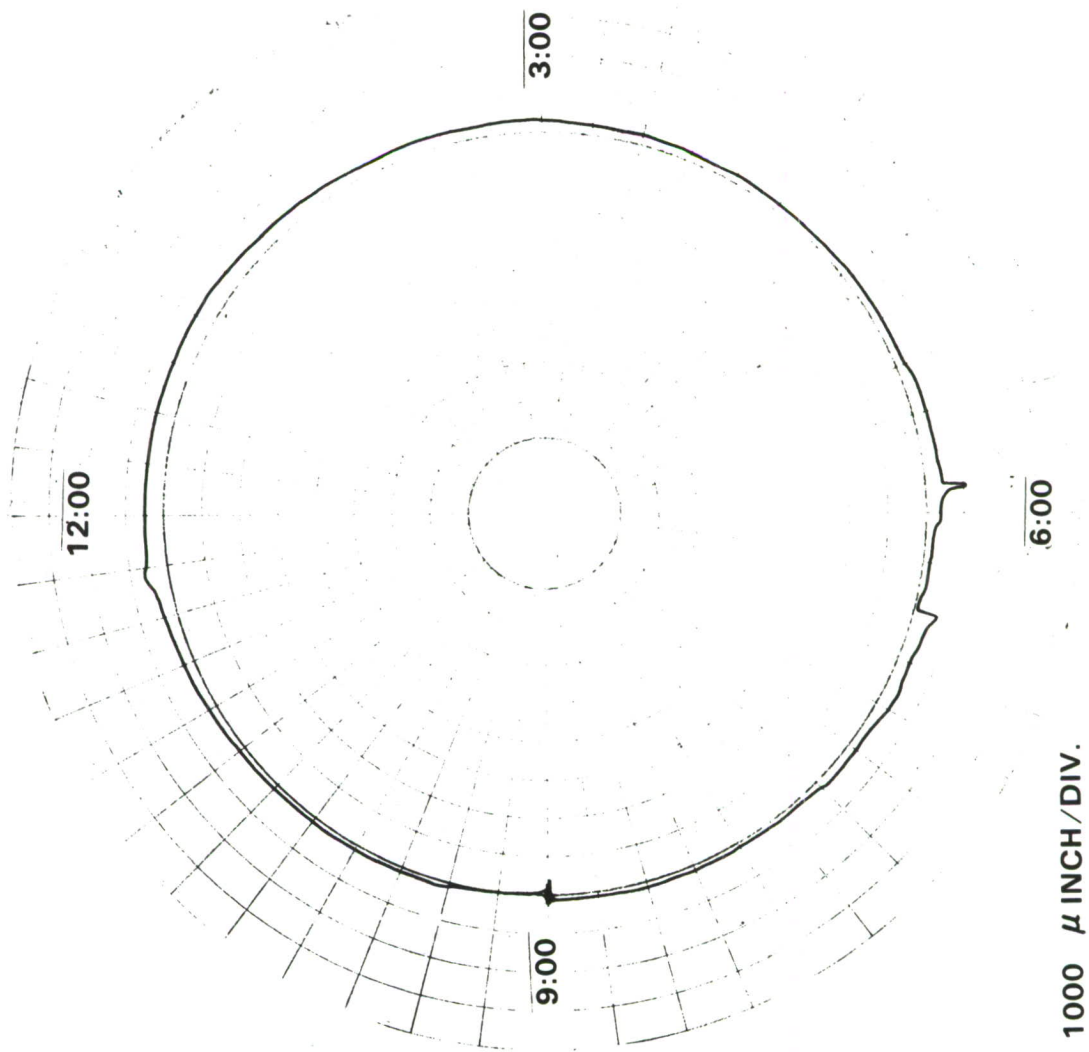
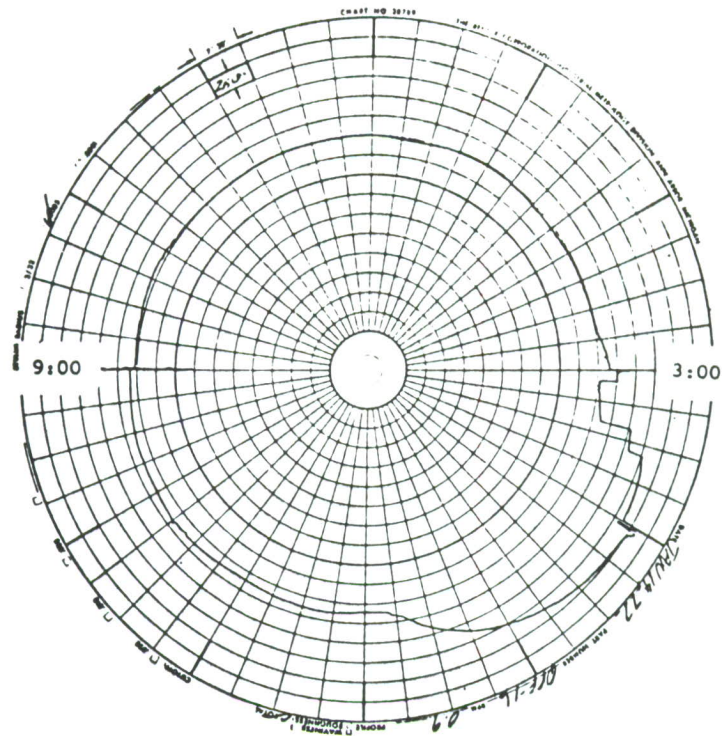
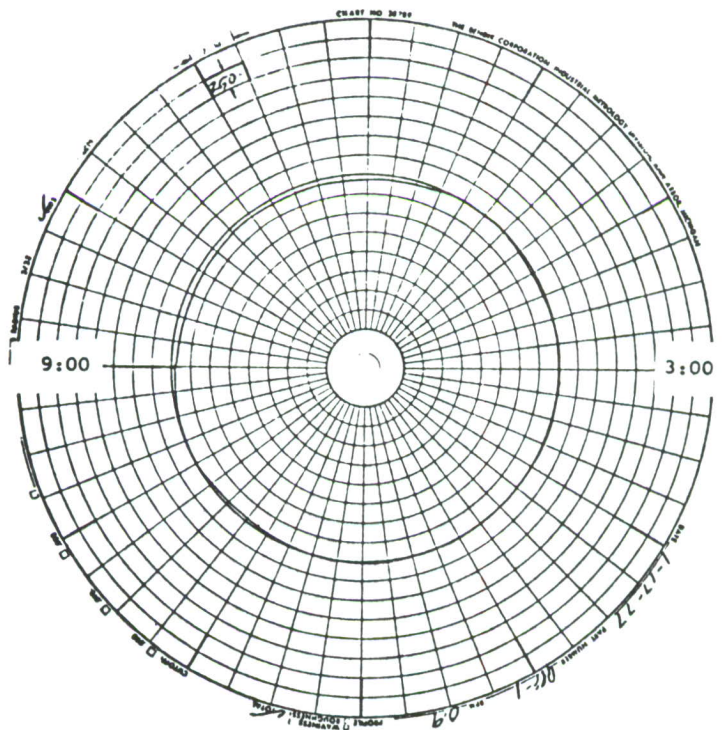


Figure A-4 Scratches at Non-Critical Orientations in a Drilled Hole



250 μ inch/div.



250 μ inch/div.

Figure A-5 Polar Plots Showing the Difference in Out-of-Roundness Between Two Holes Drilled By the Quackenbush Technique

Linear Proficorder (Task I)

A Bendix proficorder with a linear piloter was used in Task I. The diamond stylus used had a radius of .0005 inch. Scans were made along the surface of the bore of the hole parallel to the thickness. A typical scan is shown in Figure A-6. Most of the scans were taken at the 3:00 orientation. A total surface profile, which includes both surface roughness and waviness, was obtained. A vertical scale of 250 μ inches/division while a horizontal scale of .010 inch/division was used.

A scratch shows as a downward deflection on the linear proficorder trace, while a smear is represented by an upward deflection. A small scratch is shown in Figure A-6. From these scans, the depth and width of the surface irregularity can be determined.

Dial Bore Gauge (Task II)

A dial bore gauge (Boice, Model No. 1) was used to measure the diameter of the fastener holes at four different orientations, Figure A-7, and, thus, give a relative measure of out-of-roundness (OOR). Measurements were taken at three different depth, A, B, and C, in the hole, Figure A-7. From these readings, the average out-of-roundness was obtained.

$$(\text{OOR})_{\text{average}} = \frac{(\text{OOR})_A + (\text{OOR})_B + (\text{OOR})_C}{3} \quad (1)$$

From dial bore gauge measurements, the degree of hole tapering can also be determined. This value is obtained by subtracting the average diameter at Position C from the average diameter at Position A. This can be written as

$$\text{Hole Tapering} = (\Delta \text{dia.})_{A-C} = (\text{dia.})_A - (\text{dia.})_C \quad (2)$$

A parameter was defined to include both the effects of out-of-roundness and hole tapering. This parameter is called the dimensional tolerance parameter, written as

$$\text{Dimensional Tolerance Parameter} = (\text{OOR})_{\text{ave.}} + (\Delta \text{dia.})_{A-C} \quad (3)$$

This composite dimensional tolerance parameter was used for correlation to the EIFS of the fastener holes.

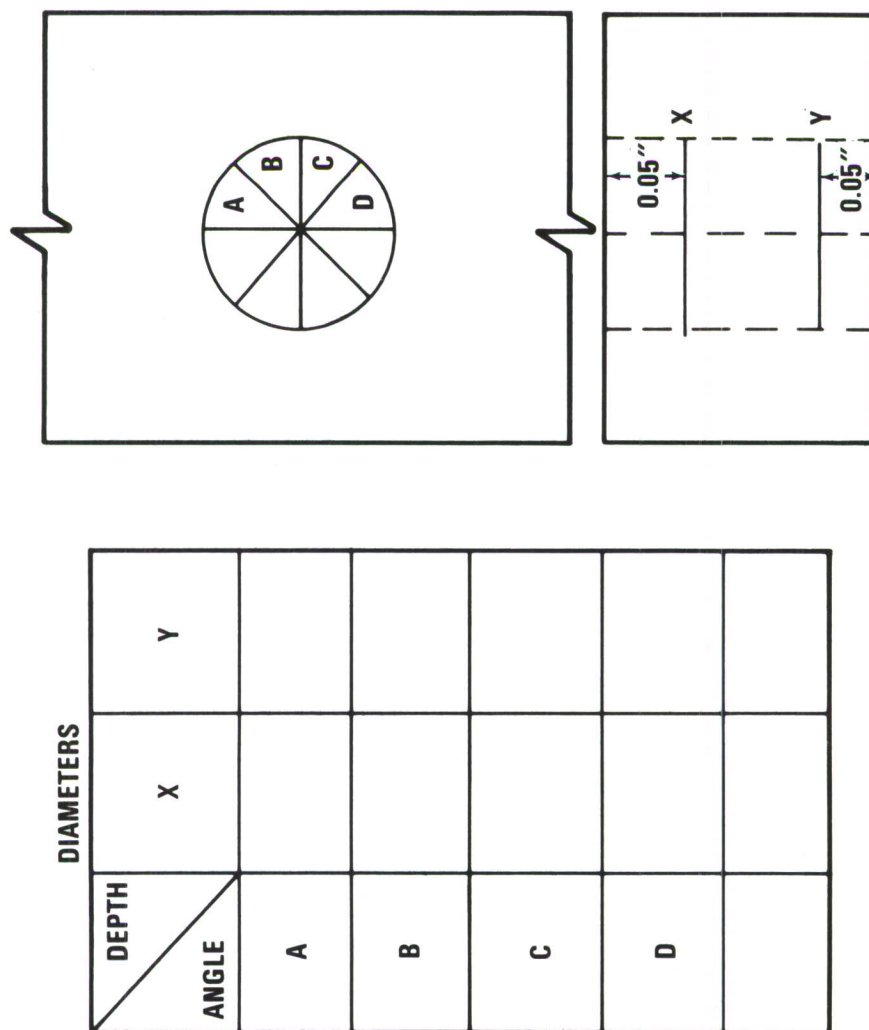


Figure A-7 Dial Bore Gauge Inspection Scheme

Ultrasonics

An ultrasonic system was developed by General Dynamics for the scanning and detection of cracks under installed fasteners for the F-111 (Reference 11). This system is very similar to the Boeing rotor scanner for detection of cracks under installed fasteners, except that a digital computer, HP2100A, has been integrated with the system for the control of the scanner and to digitize, analyze, and store the received ultrasonic signal. As with eddy current waveforms, discussed previously, ultrasonic waveforms can be digitized with the computer, rectified, filtered, and then processed to remove symmetrical signals from nonsymmetrical signals for potential EIFS correlation. Unlike the application for detection of cracks under installed fasteners, where a mode-converted shear wave is propagated tangent to the edge of the hole, the present application calls for the propagation of a mode-converted shear wave toward the hole as shown in Figure A-8. The ultrasonic shear wave transducer was attached to a teflon rod that could be inserted into the hole to form a tight fit. The transducer is driven by a digital stepping motor in the manner shown in Figure A-8. The received ultrasonic signal is digitized and recorded every five degrees.

A typical reflected waveform from a specimen containing a 0.050 inch deep saw-cut at the top corner at 6:00 orientation is shown in Figure A-9. This specimen was used as a standard before scanning any of the Task I specimens. Oscilloscope settings were made such that separate reflected waveforms were obtained from the top, middle, and bottom of the specimen.

In a manner similar to the data analysis of eddy current data, a computer program was written for the HP2100 computer that calculated the (1) maximums, (2) minimums, (3) means, and (4) standard deviation of the ultrasonic signal at the critical orientations (2:00 - 4:00, 8:00 - 10:00). This information was displayed in the form of a table, Figure A-9.

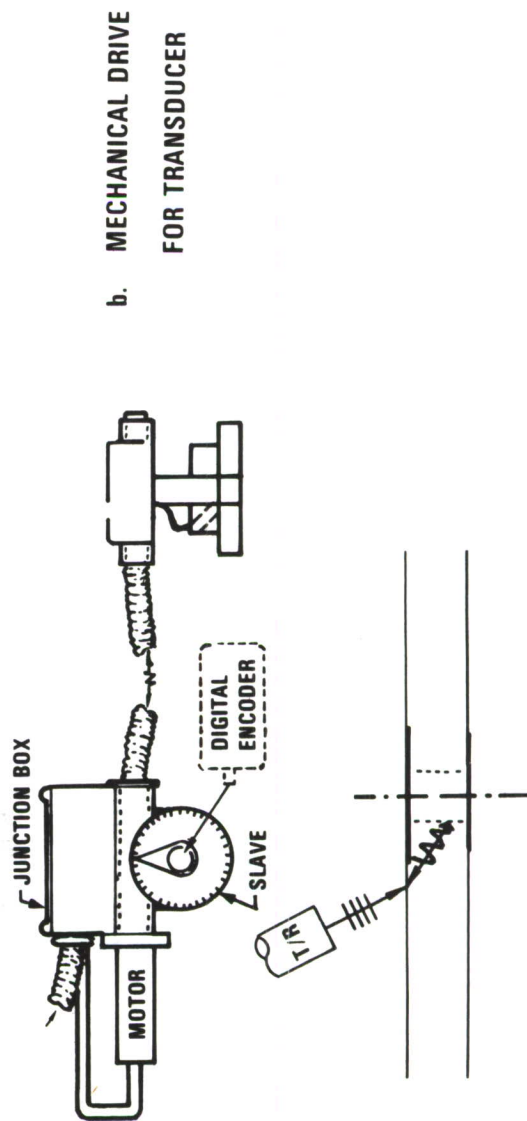
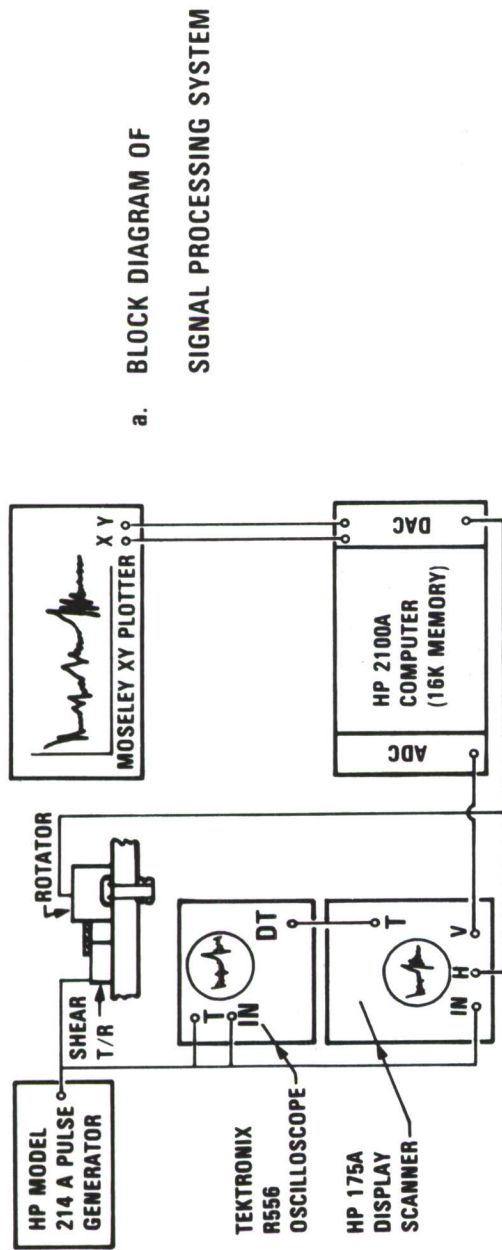


Figure A-8 Ultrasonic Inspection Scheme

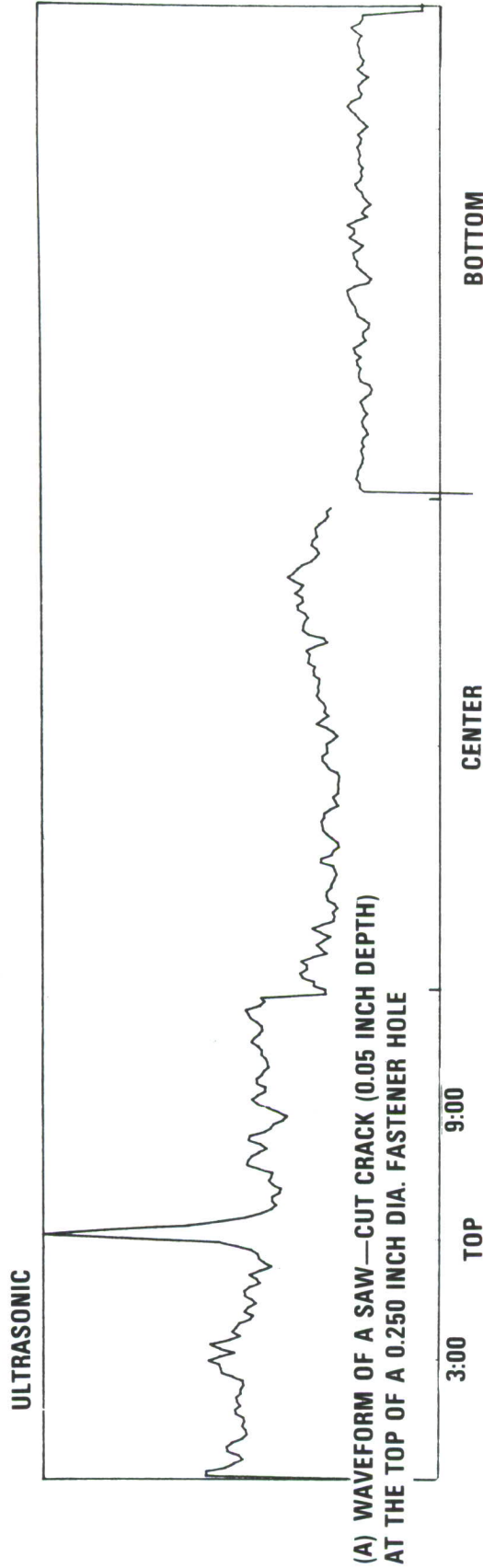


Figure A-9 Total Reflected Ultrasonic Waveform Analysis

APPENDIX B

EQUIVALENT INITIAL FLAW SIZE CONCEPT

The following procedures, to determine the EIFS, will pertain only to a specific test condition. Each case was generally made up of thirty-eight specimens. At the conclusion of fatigue testing, i.e., termination by time or specimen failure, the exact load sequence was known and stored in the computer, which monitored and controlled the test. All fatigue cracks were exposed, if that specimen had not failed during testing, by a single tensile overload. Fractography was performed on each crack from the crack length at the time of failure, specified by the computer, to crack depths generally 0.001 inch or less. Each fatigue crack was thus accompanied by its own particular crack growth curve.

The fastest-growing crack from a given test condition was then matched with analytical data, as closely and as conservatively as possible. This procedure is shown in Figure B-1. The crack growth analysis variables used to grow the analytical curves are listed in Table 2-1. Once the "master" analytical curve was generated for a specific test condition, i.e., load transfer, stress level, etc., it was regressed to extremely small crack sizes (~ 0.00005 inch).

For an illustration of the generation of a "master" curve from the analytical curve, first consider the analytical curve (Figure B-2(a)) plotted as a standard crack growth curve whose abscissa is dimensioned from time zero to some service life or number of test blocks. The ordinate crosses the abscissa at time zero with dimensions of crack length. To transform this analytical curve, the abscissa now becomes nondimensional, Figure B-2(b). The actual fitting of the master curve to the empirical curve is performed by sliding the master curve from side-to-side until a "best" fit is achieved over the specified range of crack length, generally 0.01 - 0.05 inch, Figure B-2(c). The fitting of a crack growth curve to the master curve or template is shown in Figure B-3. Since the master was regressed to very small crack lengths it will cross the ordinate of the empirical crack growth curve. The crack length at this crossing of time zero for the empirical crack growth curve is the EIFS for that specific specimen. Basic instructions and assumptions are shown in Figure B-4, with curve-fitting guidelines listed in Figure B-5.

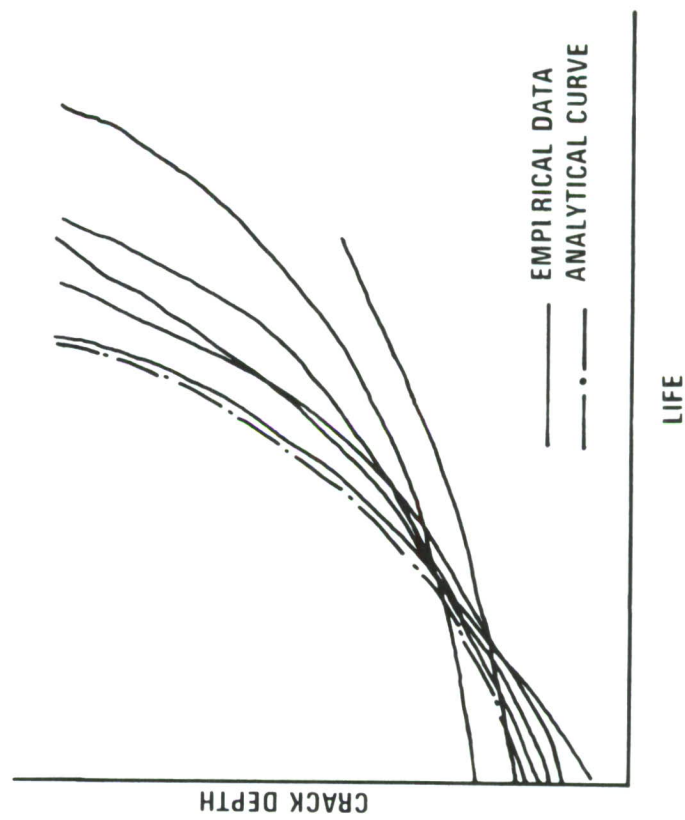


Figure R-1 Selection of a "Master" Analytical Curve

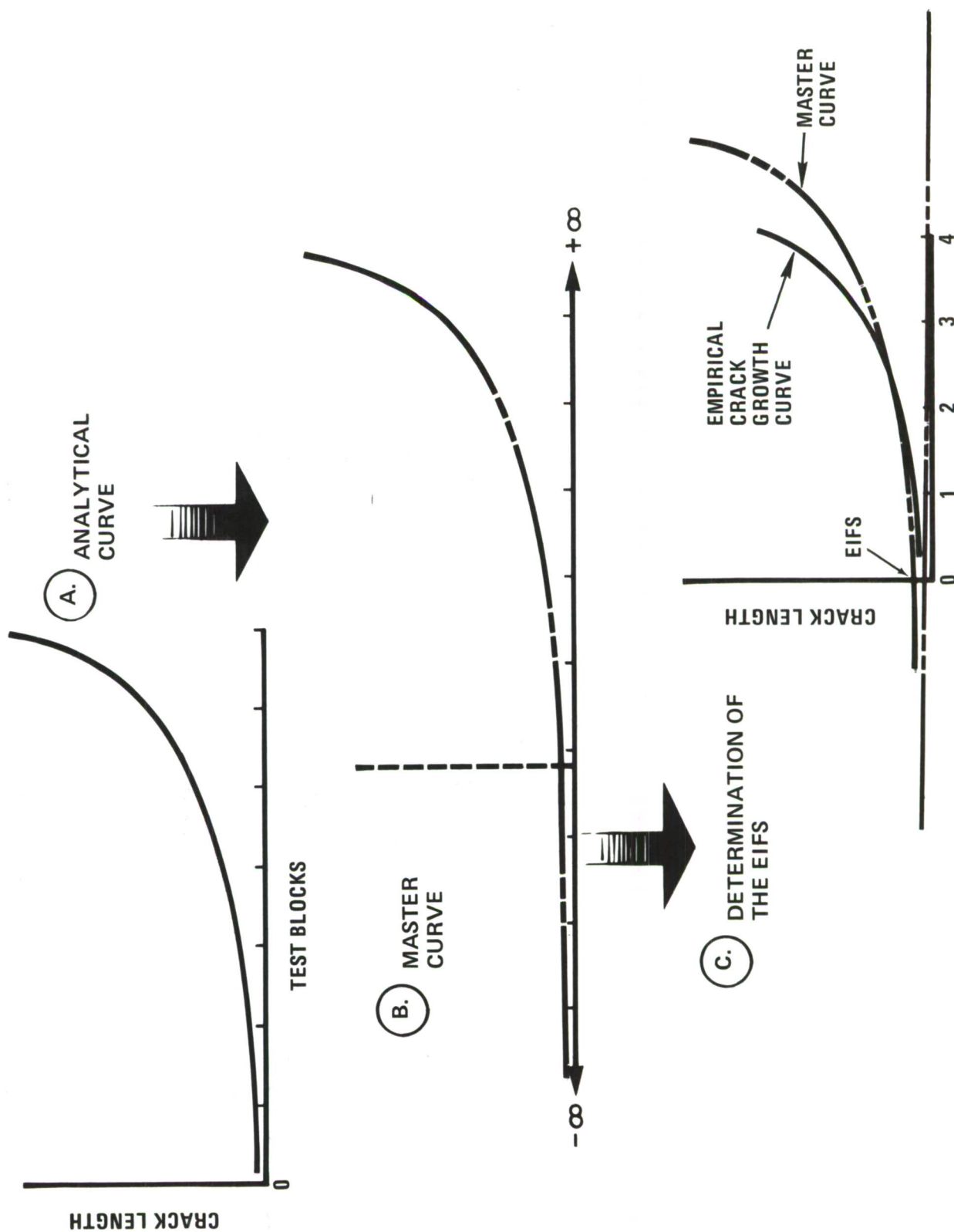


Figure B-2 The Development of a Master Curve

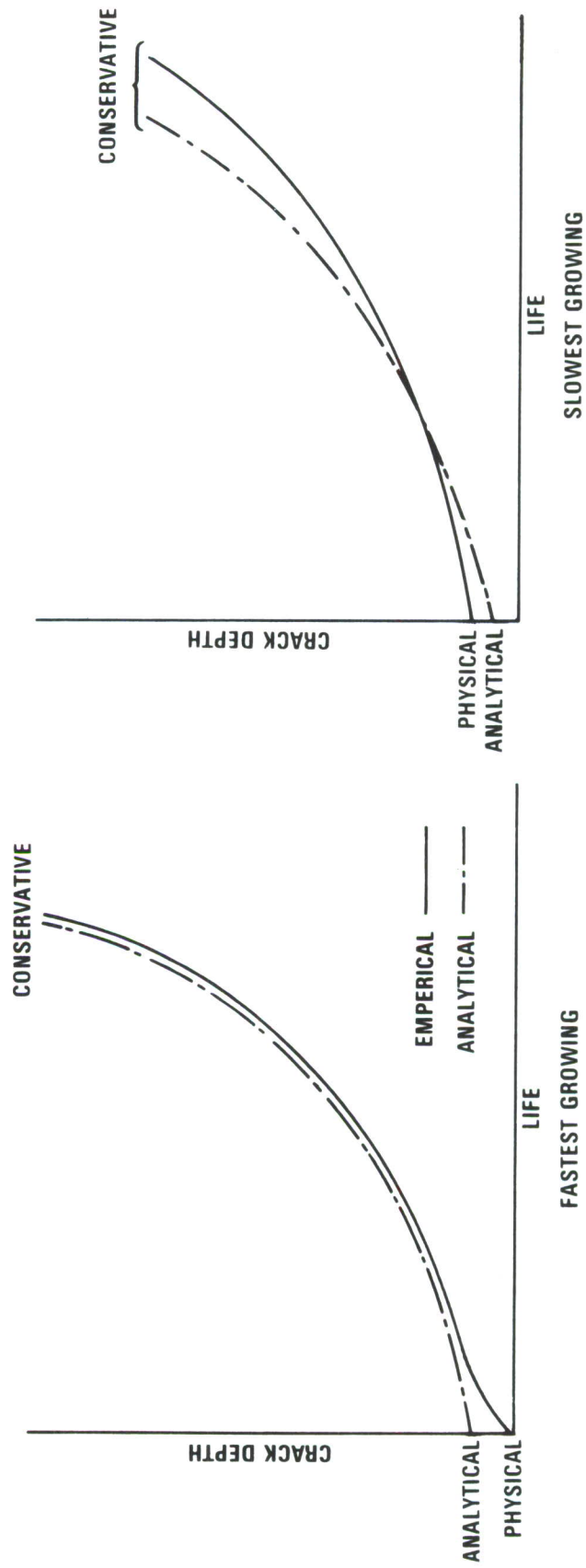


Figure B-3 Curve Fitting to Obtain the EIFS Using a Simple Template

I. ELIMINATE LINE SOURCE AND CORNER (INTERFACE) CRACK INITIATION (IF POSSIBLE)

II. IGNORE ANOMOLIES IN GROWTH OCCURING SHORTLY AFTER INITIATION AND SELECT ONE MASTER CURVE.

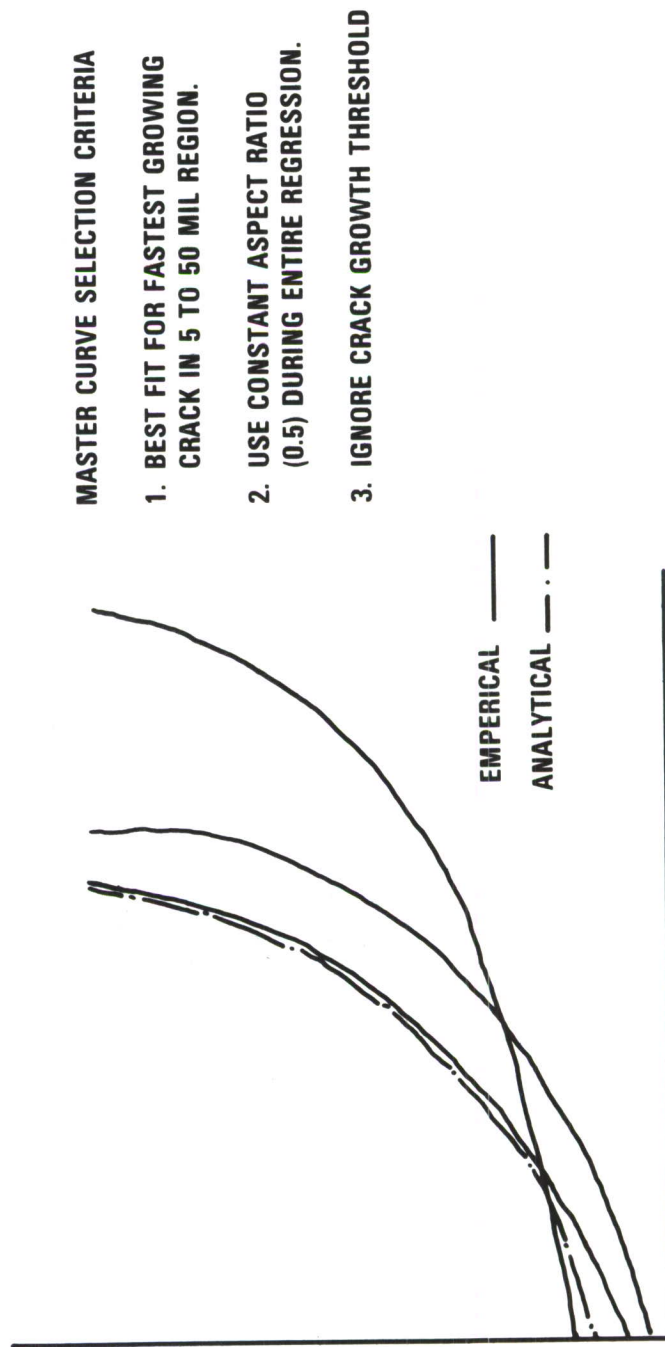


Figure B-4 The Solution to EIFS Determination

- (i) CURVE FITTING BETWEEN 5 AND 50 MILS PRODUCES EIFS VALUES THAT ARE CONSISTENT WITH DEFINITION.
- (ii) IGNORE ACTUAL PHYSICAL DIMENSIONS (DEPTH) OF INITIATING DEFECT
- (iii) IGNORE CRACK GROWTH VARIATIONS BELOW 5 MILS
- (iv) LIFE PREDICTION FROM EIFS VALUES ARE ALWAYS CONSERVATIVE
- (v) AMOUNT OF CONSERVATISM INCREASES FOR SLOWER GROWING CRACKS

Figure B-5 Guidelines for Curve Fitting

As pointed out in Figure B-5, the actual physical dimensions of the fatigue-crack initiating defect should be ignored. EIFS values are artificial with respect to any actual physical defect found within the fastener hole. The EIFS value has meaning only with respect to the crack growth analyses used to produce the template, or when compared to other EIFS values produced from testing with identical conditions. That is, the EIFS distribution for a clearance-fit process is directly comparable to that of a transition-fit process tested with the same spectra stress level, specimen geometry, etc.

REFERENCES

1. Hall, L. R., Shah, R. C., and Engstrom, W. L., Fracture and Fatigue Crack Growth Behavior of Surface Flaws and Flaws Originating at Fastener Holes, AFFDL-TR-74-47, Vol. I, Air Force Flight Dynamics Laboratory, Wright-Patterson Air Force Base, Ohio, May 1979.
2. Wood, H. A., Engle, R. M., Gallagher, J., and Potter, J. M., Current Practice on Estimating Crack Growth Damage Accumulation with Specific Application to Structural Safety Durability and Reliability, AFFDL-TR-75-32, Air Force Flight Dynamics Laboratory, Wright-Patterson Air Force Base, Ohio, January 1976.
3. Koster, W. P., et al, Verification of Production Hole Quality, AFML-TR-77-185, Vol. I, Air Force Materials Laboratory, Wright-Patterson Air Force Base, Ohio, November 1977.
4. Moore, Col. Dr. Thomas K., "The Influence of Hole Processing and Joint Variables on the Fatigue Life of Shear Joints," Ph.D. Dissertation, Ohio State University, 1977.
5. Masters, J. N., Hease, W. P., and Finger, R. W., "Investigation of Deep Flaws in Thin Walled Tanks," NASA DR-726-6.
6. Tiffany, C. F., and Master, J. N., "Applied Fracture Mechanics," ASTM STP 381, 1974, pp. 249-278.
7. Urzi, R. B., Standardization of Fastener Test, Lockheed California Company Report No. LR 24328, December 1970.
8. Little, C. D., and Machmeier, P. M., Development of a Weldable High Strength Steel, AFML-TR-75-148, Air Force Materials Laboratory, Wright-Patterson Air Force Base, Ohio, September 1975.
9. The Boeing Company, Renton, Washington, Report No. D6-25215, July 1979.
10. Sleeve Cole-Expansion of Fastener Holes Process Instructions, Industrial Wire & Metal Forming, Inc., IWMF-1-75, 1975.
11. Couchman, J. C., Yee, B. G. W, Chang, F. H., and Bell, J. R., NDE of Aerospace Metals - Ultrasonic Methods for the Detection of Cracks Under Fasteners in Metallic Components, ERR-FW-1559, December 1974.